Advances
in Clinical and Experimental Medicine

MONTHLY ISSN 1899-5276 (PRINT) ISSN 2451-2680 (ONLINE) www.advances.umw.edu.pl

2021, Vol. 30, No. 9 (September)

Impact Factor (IF) – 1.727
Ministry of Science and Higher Education – 40 pts.
Index Copernicus (ICV) – 152.95 pts

Wroclaw
Medical University

Advances
in Clinical and Experimental
Medicine

Advances
in Clinical and Experimental Medicine

ISSN 1899-5276 (PRINT) ISSN 2451-2680 (ONLINE) www.advances.umw.edu.pl

MONTHLY 2021
Vol. 30, No. 9
(September)

Advances in Clinical and Experimental Medicine (*Adv Clin Exp Med*) publishes high quality original articles, research-in-progress, research letters and systematic reviews and meta-analyses of recognized scientists that deal with all clinical and experimental medicine.

Editorial Office
ul. Marcinkowskiego 2–6
50-368 Wrocław, Poland
Tel.: +48 71 784 11 36
E-mail: redakcja@umw.edu.pl

Publisher
Wroclaw Medical University
Wybrzeże L. Pasteura 1
50-367 Wrocław, Poland

Online edition is the original version of the journal

Editorial Policy

Advances in Clinical and Experimental Medicine (Adv Clin Exp Med) is an independent multidisciplinary forum for exchange of scientific and clinical information, publishing original research and news encompassing all aspects of medicine, including molecular biology, biochemistry, genetics, biotechnology and other areas. During the review process, the Editorial Board conforms to the "Uniform Requirements for Manuscripts Submitted to Biomedical Journals: Writing and Editing for Biomedical Publication" approved by the International Committee of Medical Journal Editors (www.ICMJE.org/). The journal publishes (in English only) original papers and reviews. Short works considered original, novel and significant are given priority. Experimental studies must include a statement that the experimental protocol and informed consent procedure were in compliance with the Helsinki Convention and were approved by an ethics committee.

For all subscription-related queries please contact our Editorial Office:
redakcja@umw.edu.pl

For more information visit the journal's website:
www.advances.umw.edu.pl

Pursuant to the ordinance No. 134/XV R/2017 of the Rector of Wroclaw Medical University (as of December 28, 2017) from January 1, 2018 authors are required to pay a fee amounting to 700 euros for each manuscript accepted for publication in the journal Advances in Clinical and Experimental Medicine.

Indexed in: MEDLINE, Science Citation Index Expanded, Journal Citation Reports/Science Edition, Scopus, EMBASE/Excerpta Medica, Ulrich's™ International Periodicals Directory, Index Copernicus

Typographic design: Piotr Gil, Monika Kolęda
DTP: Wydawnictwo UMW
Cover: Monika Kolęda
Printing and binding: Soft Vision Mariusz Rajski

Advances
in Clinical and Experimental Medicine

MONTHLY 2021, Vol. 30, No. 9 (September)

ISSN 1899-5276 (PRINT)
ISSN 2451-2680 (ONLINE)
www.advances.umw.edu.pl

Contents

Editorials

Original papers

Research letter

The RANKL/RANK system in female reproductive organ tumors: A preclinical and clinical overview

Ana Monzó-Miralles[1,2,A,E,F], Víctor Martín-González[3,A,E,F], Sara Smith-Ballester[4,A,E,F], Victoria Iglesias-Miguel[4,A,E,F], Antonio Cano[4,A,D–F]

[1] Service of Obstetrics and Gynecology "La Fe", Hospital Universitari i Politècnic La Fe, Valencia, Spain
[2] Department of Pediatrics, Obstetrics and Gynecology, University of Valencia, Spain
[3] Service of Obstetrics and Gynecology, Hospital Clínico Universitario-INCLIVA, Valencia, Spain
[4] University of Valencia and Service of Obstetrics and Gynecology, Hospital Clínico Universitario-INCLIVA, Spain

A – research concept and design; B – collection and/or assembly of data; C – data analysis and interpretation; D – writing the article; E – critical revision of the article; F – final approval of the article

Advances in Clinical and Experimental Medicine, ISSN 1899–5276 (print), ISSN 2451–2680 (online) *Adv Clin Exp Med*. 2021;30(9):879–883

Address for correspondence
Antonio Cano
E-mail: Antonio.cano@uv.es

Funding sources
This research received funding from the Project EURODIET, jointly funded by the action Impact of Diet, Food Components and Food Processing on Body Weight Regulation and Overweight Related Metabolic Diseases (METADIS 2019) of the European Union's H2020 Research and Innovation Program (grant No. 696300), and Health Institute Carlos III, Spain (Project AC19/00084), with the support of the European Regional Development Fund (ERDF).

Conflict of interest
None declared

Received on July 16, 2021
Accepted on July 21, 2021

Published online on August 24, 2021

Cite as
Monzó-Miralles A, Martín-González V, Smith-Ballester S, Iglesias-Miguel V, Cano A. The RANKL/RANK system in female reproductive organ tumors: A preclinical and clinical overview. *Adv Clin Exp Med*. 2021;30(9):879–883. doi:10.17219/acem/140422

DOI
10.17219/acem/140422

Abstract

The receptor activator of nuclear factor-κB (RANK) and its ligand RANKL are members of the tumor necrosis factor (TNF) super-family of cytokines with a role in progestogen-associated malignancies in breast. Basic and clinical data support the participation of the cytokine pathway in metastatic disease and as poor prognosis markers. The value of RANK/RANKL as prognostic indicators in endometrial and ovarian tumors, as well as the data suggesting a potential role of RANK/RANKL in hormone dependent tumorigenesis in the endometrium, have been described. The D-CARE study could not confirm benefit in the modulation of RANKL in breast cancer.

Key words: RANK, RANKL, cancer, breast, genital tract

Background

Cancers of the reproductive tissues have a particularly predominant place in the global burden of cancer in women. According to the American Cancer Society, the 6 most frequently diagnosed tumors in women are breast cancer (30%), lung and bronchus (13%), colon and rectum (8%), uterine corpus (7%), skin melanoma (5%), and non-Hodgkin lymphoma (4%).[1] The picture changes for mortality, in which lung and bronchus ranks 1st (22%), breast 2nd (15%), followed by colon and rectum (8%), pancreas (8%), ovary (5%), and uterine corpus (4%). Accordingly, 3 reproductive organ-related cancers, breast, uterus and ovary, are among the 6 most prevalent and deadliest tumors in women.

There is a well-established role for ovarian steroids in the genesis of tumors affecting the female reproductive organs. Associations have been shown not only in epidemiological data, but also via clear biological mechanisms. For example, the proliferative role of estrogens in the endometrial epithelium has been confirmed under different experimental conditions, including cell lines and animal models, and in humans.

Molecular background

Estrogen and the endometrium

Estrogen receptors (ER) are highly expressed in both epithelium and stroma in the human endometrium, and ER activation leads to a proliferative effect, as shown throughout the physiological menstrual cycle and in classic studies in the human endometrium.[2,3]

Considerable advances have also been made by studying the molecular mechanisms underlying these observations.[4] Indeed, the ER transcription apparatus has been linked to the activation of a long list of genes that control multiple cellular pathways. These include mitogenic actions matching those of human cancer, including rapidly increased *c-Myc* and *cyclin D1* expression. Angiogenesis, a crucial mechanism linked to tumor progression, is also promoted by estrogen; although its action, if any, is limited to inducing metastasis.[4] Consistent with these actions, estrogen-only use has been associated with an increased risk of endometrial cancer in clinical studies of menopausal women.[5] The association is less clear in the breast;[6] although, limiting estrogen exposure with aromatase inhibitors[7] or ER blockade with selective estrogen receptor modulators (SERMs)[8] have been shown to reduce breast cancer risk.

Early work confirmed that progesterone receptors (PR) are a product of ER gene activation,[9] which was followed by finding that PR activation in the endometrium limited the mitogenic effect of estrogens.[3] This anti-proliferative action of progestogens is the reason behind recommending progestogen use in combination with estrogen in women who have not undergone hysterectomy.[10] There is consistent clinical evidence showing that adding progestogens to estrogens in hormonal therapy reduces endometrial cancer risk to similar rates as in untreated women.[5]

Progestogens and the breast

A series of findings prompted the hypothesis that the anti-proliferative action of progestogens observed in the endometrium might not be replicated in the breast. Proliferation was increased in breast epithelium during the luteal phase, a finding that contrasted with its quiescent status in the endometrium.[11] Observational studies and clinical trials subsequently confirmed that progestogens and estrogens combined result in a higher risk than is associated with estrogen-only treatment.[6] These findings have also been observed for progestogen-only treatments in hormonal contraceptive users.[12] The molecular mechanism underlying the proliferative effect of progestogens seen in breast but not endometrium has remained elusive for several years.

RANK/RANKL and hormone-linked tumorigenesis

Studies in recent years have contributed pivotal data on the oncogenic role of progestogens and the involvement of the receptor activator of nuclear factor-κB (RANK) and its ligand, RANKL. RANK and RANKL are members of the tumor necrosis factor (TNF) super-family of cytokines. RANK was identified in 1997 in the T cell membrane, where it showed a modulating role in the interaction of T cells and dendritic cells.[13] RANK/RANKL have emerged as key elements in various immune response processes, as well as in mechanisms linked to inflammation, organogenesis and apoptosis.[14,15] A fundamental role has also been found in bone metabolism regulation, in which they act mainly by promoting the differentiation and activation of osteoclast progenitors.[16]

The RANKL ligand participates in the growth and differentiation of the epithelial component in mammary ducts and lobes during puberty and the phases of the menstrual cycle[17], as shown in both animal and human research. Likewise, RANK/RANKL have been proposed as key mediators in the proliferative action of progestogens in the breast.[18,19]

RANK/RANKL and breast tumorigenesis as a model

The current understanding concerning the role of RANK/RANKL in tumorigenesis stems largely from studies in the breast. Mapping studies showed that RANKL expression increases during gestation, expressed mainly in the ductal luminal area and in developing alveoli, while RANK is expressed in the basal layers of the ductal epithelium.[17] Experiments in transgenic animals clearly showed the role of RANK/RANKL in proliferative and anti-apoptotic mechanisms.[20]

RANK/RANKL involvement in hormonal tumorigenesis is suggested by various findings: i) ER and PR are co-expressed with RANKL in luminal epithelium; ii) there is a confirmed correlation between RANKL expression and circulating levels of progesterone in humans, in both normal and malignant cells[21,22]; iii) the induction of mammary tumors by progestogens is accompanied by a striking overexpression of RANKL in PR-positive luminal cells[19,23]; and iv) RANK blockade is associated with tumor differentiation and reduced propensity for recurrence.[24]

Molecular mechanisms of RANKL/RANK in breast tumorigenesis

Animal models have revealed a perfectly coordinated apparatus involving progesterone-induced proliferation and synthesis of RANKL in luminal cells expressing PR, and paracrine-induced proliferation by RANKL in neighboring cells lacking PR (Fig. 1). In the presence of susceptibility

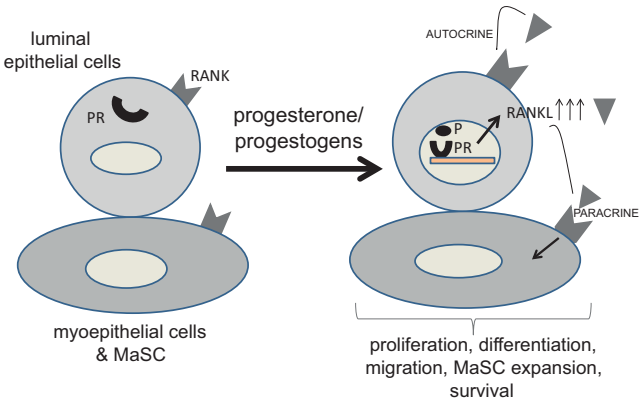

Fig. 1. The image shows RANK expressed in luminal, myoepithelial, and mammary stem cells (MaSC). Luminal cells also express progesterone receptors (PR), which upon stimulation induce RANKL synthesis. In an autocrine or paracrine form, RANKL activates RANK to promote proliferation, migration, MaSC expansion and cell survival[18]

agents like carcinogens or genetic lesions, persistent proliferative stimuli may lead to hyperplasia and neoplastic transformation.

Data from human studies have reinforced findings from preclinical studies. For example, malignant mammary cells express RANK and RANKL,[23] and more intriguingly, RANK expression has been correlated with tumor aggressiveness in women.[25] A crucial notion in this regard is whether RANK/RANKL overexpression following malignancy onset feeds cellular machinery involved in dedifferentiation and aggressive tumor behavior, or rather represents a mere epiphenomena associated with the malignant phenotype.

RANK/RANKL and tumor aggressiveness

Beyond data confirming a role for RANK/RANKL in channeling the oncogenic role of progestogens, other findings suggest that these cytokines could constitute preferential pathways to cancer, independently of their relationship with these steroids.

Along these lines, interesting results were derived from studies in carriers of the susceptibility genes *BRCA1* and *BRCA2*, which confer increased risk for more aggressive mammary tumor patterns, often ER- and PR-negative tumors. A multicenter study compared circulating levels of osteoprotegerin (OPG), which exhibits affinity and acts as a blocking agent of RANKL, between *BRCA1/2* carriers (n = 391) and non-carriers (n = 782). *BRCA 1/2* carriers had lower serum free levels of OPG, implying that RANKL activity was probably higher.[26] Of particular interest, the levels of OPG were inversely correlated with the detection of germ mutations known to confer a higher risk for breast cancer in BRCA carriers.[26]

Other research has found that the RANK/RANKL system plays a role in malignant drift in cancers in *BRCA 1/2* carriers, in both experimental models[27] and clinical studies.[28] These findings have fueled interest in a proposal of RANKL blockade with anti-RANKL antibodies, such as denosumab, as a possible way to reduce cancer risk in *BRCA1* carriers.[29]

Another key feature ascribed to RANK/RANKL is their value as indicators of poor tumor prognosis. In this regard, increased RANK expression has been found in hormone receptor-negative mammary tumors.[30] There are also some indications of metastatic potential, another feature related to tumor aggressiveness. Treatment with OPG reduced bone metastases in a mouse model of melanoma metastasis; although, the effect seemed limited to bone, without extending to other organs.[31]

Endometrium as a new scenario

The human menstrual cycle clearly reflects the opposing actions of estrogen and progesterone on the proliferative response of endometrial epithelium. A rapid proliferative response during the follicular phase is soon downregulated by progesterone, which is synthesized by the corpus luteum after ovulation. Progesterone therefore has an anti-proliferative effect in endometrium, in contrast to reported findings in the breast. While the molecular details underlying these opposing actions are not well understood, the question has arisen as to whether RANKL/RANK participate in endometrial proliferative events.

A first step has been taken to investigate whether RANK/RANKL are expressed in human endometrium. Recent work identified RANK in human endometrial sections by immunohistochemistry (Fig. 2).[32] Moreover, estrogens are associated with an increased risk of type I endometrial tumors, and also type II tumors, albeit to a lesser extent.[33] However, and against what has been observed in the breast, it is unclear in the endometrium whether RANKL/RANK is involved in the process of estrogen-mediated tumorigenesis.

More data have been published concerning the roles of RANK/RANKL as prognostic indicators in endometrial cancer. Analysis of data obtained by immunohistochemistry in a series of tumors has shown that, as for the breast, RANK expression is associated with indicators of poor prognosis, such as grade of differentiation or tumor stage,[32] and also with myometrial invasion, lymph node metastasis, and lymphovascular space involvement.[34] Remarkably, RANK activation with RANKL reproduced findings similar to the aforementioned cell proliferation; although, in this case, in an endometrial tumor cell line. This effect was downregulated by medroxyprogesterone acetate (MPA), a progestogen repeatedly shown to limit the progression of PR-positive endometrial cancers.

The conclusion drawn from these experiments is that, in endometrial cancer cell lines, RANKL reproduced the proliferative and anti-apoptotic effect observed in the breast. However, and against the observations

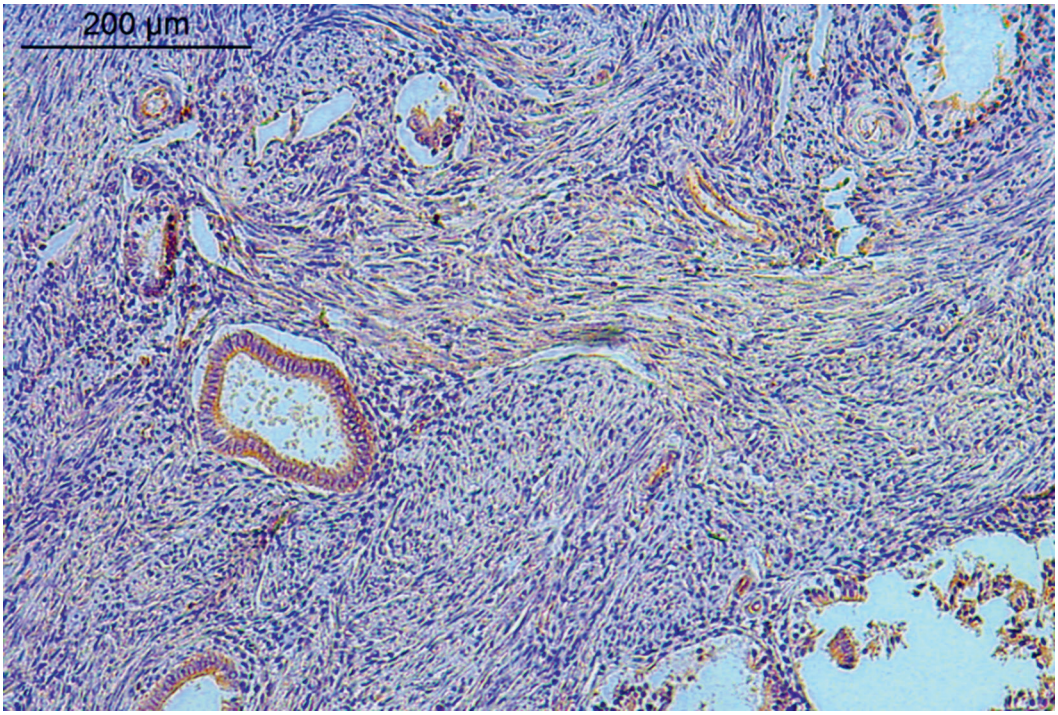

Fig. 2. The receptor activator of nuclear factor-κB (RANK) immunohistochemical staining (brown) in normal endometrium. Faint positive staining was found across luminal and glandular epithelium and stroma. The density of RANK staining increases in malignant endometrial tumors (not shown) and the signal increases with tumor de-differentiation; ×100 magnification[32]

in the breast, the progestogen (MPA) limited the expansive effects mediated by RANKL in the endometrial tumor. The molecular basis for the opposite action of progestogens in breast and endometrium is unknown.

Ovarian cancer

Studies have been published linking hormonal therapy use with risk of ovarian cancer,[35] yet the potential involvement of RANKL/RANK in ovarian tumorigenesis is still unclear, and data are still very sparse. Interestingly, as shown in endometrium and breast, increased RANKL expression has been found in ovarian cancer, where higher expression was associated with poor prognosis indicators, specifically with reduced progression-free and overall survival.[36]

Conclusions

A wealth of data has accumulated over recent years implicating RANKL/RANK in both tumorigenesis and prognosis in several reproductive system cancers, including breast and endometrium. The only confirmed role in both endometrial and ovarian cancer is that of prognostic indicator, which may involve either RANK or RANKL depending on the study. Experiments with endometrial cancer cell lines have shown that, in parallel with findings in breast cancer, RANK/RANKL are involved in proliferation and migration mechanisms.

These data have aroused interest in the potentially beneficial effect of blocking RANKL to improve prognosis in women with any of the cancer types studied. Unfortunately, available studies are inconclusive. The D-CARE study randomized 4509 women with stage II or III breast cancer to denosumab or placebo. The primary endpoint was bone metastasis-free survival, for which no between-group differences were found.[37] However, time to first skeletal-related effect and time to bone metastasis progression were significantly lower in women with metastatic breast cancer, receiving denosumab when they expressed RANK on circulating tumor cells.[38] Consequently, further research is needed to better define the role of RANK/RANKL in tumors of the reproductive organs. Only through enhanced understanding will appropriate strategies utilizing modulators such as denosumab be designed.

ORCID iDs

Ana Monzó-Miralles https://orcid.org/0000-0003-4509-0065
Víctor Martín-González https://orcid.org/0000-0002-2989-4883
Sara Smith-Ballester https://orcid.org/0000-0003-4117-7454
Victoria Iglesias-Miguel https://orcid.org/0000-0002-9334-3920
Antonio Cano https://orcid.org/0000-0001-8046-0303

References

1. Siegel RL, Miller KD, Fuchs HE, Jemal A. Cancer statistics, 2021. *CA Cancer J Clin*. 2021;71(1):7–33. doi:10.3322/caac.21654
2. Lessey BA, Killam AP, Metzger DA, Haney AF, Greene GL, McCarty KS Jr. Immunohistochemical analysis of human uterine estrogen and progesterone receptors throughout the menstrual cycle. *J Clin Endocrinol Metab*. 1988;67(2):334–340. doi:10.1210/jcem-67-2-334
3. Whitehead MI, Townsend PT, Pryse-Davies J, Ryder TA, King RJ. Effects of estrogens and progestins on the biochemistry and morphology of the postmenopausal endometrium. *N Engl J Med*. 1981; 305(27):1599–1605. doi:10.1056/NEJM198112313052701
4. Liang J, Shang Y. Estrogen and cancer. *Annu Rev Physiol*. 2013;75: 225–240. doi:10.1146/annurev-physiol-030212-183708

5. Beral V, Bull D, Reeves G; Million Women Study Collaborators. Endometrial cancer and hormone-replacement therapy in the Million Women Study. *Lancet*. 2005;365(9470):1543–1551. doi:10.1016/S0140-6736(05)66455-0
6. Vinogradova Y, Coupland C, Hippisley-Cox J. Use of hormone replacement therapy and risk of breast cancer: Nested case-control studies using the QResearch and CPRD databases. *BMJ*. 2020;371:m3873. doi:10.1136/bmj.m3873
7. Cuzick J, Sestak I, Forbes JF, et al. Use of anastrozole for breast cancer prevention (IBIS-II): Long-term results of a randomised controlled trial. *Lancet*. 2020;395(10218):117–122. Erratum in: Lancet. 2020 Feb 15; 395(10223):496. Erratum in: Lancet. 2021 Feb 27;397(10276):796. doi:10.1016/S0140-6736(19)32955-1
8. Vogel VG, Costantino JP, Wickerham DL, et al. Effects of tamoxifen vs raloxifene on the risk of developing invasive breast cancer and other disease outcomes: The NSABP study of tamoxifen and raloxifene (STAR) P-2 trial. *JAMA*. 2006;295(23):2727–2741. Erratum in: JAMA. 2006 Dec 27;296(24):2926. Erratum in: JAMA. 2007 Sep 5;298(9):973. doi:10.1001/jama.295.23.joc60074
9. Sumida C, Lecerf F, Pasqualini JR. Control of progesterone receptors in fetal uterine cells in culture: Effects of estradiol, progestins, antiestrogens, and growth factors. *Endocrinology*. 1988;122(1):3–11. doi:10.1210/endo-122-1-3
10. National Institute for Health and Care Excellence. *Menopause: diagnosis and management: 2019*. London, UK: National Institute for Health and Care Exellence; 2019. PMID:31940155
11. Zolfaroli I, Tarín JJ, Cano A. The action of estrogens and progestogens in the young female breast. *Eur J Obstet Gynecol Reprod Biol*. 2018;230:204–207. doi:10.1016/j.ejogrb.2018.03.057
12. Zolfaroli I, Tarín JJ, Cano A. Hormonal contraceptives and breast cancer: Clinical data. *Eur J Obstet Gynecol Reprod Biol*. 2018;230:212–216. doi:10.1016/j.ejogrb.2018.03.058
13. Anderson DM, Maraskovsky E, Billingsley WL, et al. A homologue of the TNF receptor and its ligand enhance T-cell growth and dendritic-cell function. *Nature*. 1997;390(6656):175–179. doi:10.1038/36593
14. Walsh MC, Choi Y. Biology of the RANKL-RANK-OPG system in immunity, bone, and beyond. *Front Immunol*. 2014;5:511. doi:10.3389/fimmu.2014.00511
15. Ahern E, Smyth MJ, Dougall WC, Teng MWL. Roles of the RANKL-RANK axis in antitumour immunity – implications for therapy. *Nat Rev Clin Oncol*. 2018;15(11):676–693. doi:10.1038/s41571-018-0095-y
16. Lacey DL, Timms E, Tan HL, et al. Osteoprotegerin ligand is a cytokine that regulates osteoclast differentiation and activation. *Cell*. 1998;93(2):165–176. doi:10.1016/s0092-8674(00)81569-x
17. Gonzalez-Suarez E, Branstetter D, Armstrong A, Dinh H, Blumberg H, Dougall WC. RANK overexpression in transgenic mice with mouse mammary tumor virus promoter-controlled RANK increases proliferation and impairs alveolar differentiation in the mammary epithelia and disrupts lumen formation in cultured epithelial acini. *Mol Cell Biol*. 2007;27(4):1442–1454. doi:10.1128/MCB.01298-06
18. González Ricarte M, de Castro Pérez A, Tarín JJ, Cano A. Progestogens and risk of breast cancer: A link between bone and breast? *Gynecol Endocrinol*. 2016;32:6–8. doi:10.3109/09513590.2015.1078304
19. Gonzalez-Suarez E, Jacob AP, Jones J, et al. RANK ligand mediates progestin-induced mammary epithelial proliferation and carcinogenesis *Nature*. 2010;468(7320):103–107. doi:10.1038/nature09495
20. Sigl V, Penninger JM. RANKL/RANK – from bone physiology to breast cancer. *Cytokine Growth Factor Rev*. 2014;25(2):205–214. doi:10.1016/j.cytogfr.2014.01.002
21. Hu H, Wang J, Gupta A, et al. RANKL expression in normal and malignant breast tissue responds to progesterone and is up-regulated during the luteal phase. *Breast Cancer Res Treat*. 2014;146(3):515–523. doi:10.1007/s10549-014-3049-9
22. González-Suárez E. RANKL inhibition: A promising novel strategy for breast cancer treatment. *Clin Transl Oncol*. 2011;13(4):222–228. doi:10.1007/s12094-011-0646-5
23. Schramek D, Leibbrandt A, Sigl V, et al. Osteoclast differentiation factor RANKL controls development of progestin-driven mammary cancer. *Nature*. 2010;468(7320):98–102. doi:10.1038/nature09387
24. Yoldi G, Pellegrini P, Trinidad EM, et al. RANK signaling blockade reduces breast cancer recurrence by inducing tumor cell differentiation. *Cancer Res*. 2016;76(19):5857–5869. doi:10.1158/0008-5472.CAN-15-2745
25. Park HS, Lee A, Chae BJ, Bae JS, Song BJ, Jung SS. Expression of receptor activator of nuclear factor kappa-B as a poor prognostic marker in breast cancer. *J Surg Oncol*. 2014;110(7):807–812. doi:10.1002/jso.23737
26. Widschwendter M, Burnell M, Fraser L, et al. Osteoprotegerin (OPG), the endogenous inhibitor of receptor activator of NF-kappaB ligand (RANKL), is dysregulated in BRCA mutation carriers. *EBioMedicine*. 2015;2(10):1331–1339. doi:10.1016/j.ebiom.2015.08.037
27. Sigl V, Owusu-Boaitey K, Joshi PA, et al. RANKL/RANK control Brca1 mutation-driven mammary tumors. *Cell Res*. 2016;26(7):761–774. doi:10.1038/cr.2016.69
28. Odén L, Akbari M, Zaman T, et al. Plasma osteoprotegerin and breast cancer risk in BRCA1 and BRCA2 mutation carriers. *Oncotarget*. 2016;7(52):86687–86694. doi:10.18632/oncotarget.13417
29. Kotsopoulos J, Singer C, Narod SA. Can we prevent BRCA1-associated breast cancer by RANKL inhibition? *Breast Cancer Res Treat*. 2017;161(1):11–16. doi:10.1007/s10549-016-4029-z
30. Pfitzner BM, Branstetter D, Loibl S, et al. RANK expression as a prognostic and predictive marker in breast cancer. *Breast Cancer Res Treat*. 2014;145(2):307–315. doi:10.1007/s10549-014-2955-1.
31. Jones DH, Nakashima T, Sanchez OH, et al. Regulation of cancer cell migration and bone metastasis by RANKL. *Nature*. 2006;440(7084):692–696. doi:10.1038/nature04524
32. Gómez R, Castro A, Martínez J, et al. Receptor activator of nuclear factor kappa B (RANK) and clinicopathological variables in endometrial cancer: A study at protein and gene level. *Int J Mol Sci*. 2018;19(7):1848. doi:10.3390/ijms19071848
33. Mørch LS, Kjaer SK, Keiding N, Løkkegaard E, Lidegaard Ø. The influence of hormone therapies on type I and II endometrial cancer: A nationwide cohort study. *Int J Cancer*. 2016;138(6):1506–1515. doi:10.1002/ijc.29878
34. Wang J, Sun X, Zhang H, Wang Y, Li Y. MPA influences tumor cell proliferation, migration, and invasion induced by RANKL through PRB involving the MAPK pathway in endometrial cancer. *Oncol Rep*. 2015;33(2):799–809. doi:10.3892/or.2014.3651
35. Shi LF, Wu Y, Li CY. Hormone therapy and risk of ovarian cancer in postmenopausal women: a systematic review and meta-analysis. *Menopause*. 2016;23(4):417–424. doi:10.1097/GME.0000000000000550
36. Wieser V, Sprung S, Tsibulak I, et al. Clinical impact of RANK signalling in ovarian cancer. *Cancers (Basel)*. 2019;11(6):791. doi:10.3390/cancers11060791
37. Coleman R, Finkelstein DM, Barrios C, et al. Adjuvant denosumab in early breast cancer (D-CARE): an international, multicentre, randomised, controlled, phase 3 trial. *Lancet Oncol*. 2020;21(1):60–72. doi:10.1016/S1470–2045(19)30687-4
38. Pantano F, Rossi E, Iuliani M, et al. Dynamic changes of receptor activator of nuclear factor-κB expression in circulating tumor cells during denosumab predict treatment effectiveness in metastatic breast cancer. *Sci Rep*. 2020;10(1):1288. doi:10.1038/s41598-020-58339-2

Effect of histological examination on the diagnosis of pancreatic mass using endoscopic ultrasound fine-needle aspiration

Seong Ji Choi[1,A,C,D], Jae Min Lee[2,A,C,F], Kang Won Lee[2,B,C], Hyuk Soon Choi[2,B,C], Eun Sun Kim[2,B,C], Bora Keum[2,C,D], Jai Hoon Yoon[1,C,D], Yoon Tae Jeen[2,E,F], Hoon Jai Chun[2,E,F], Hong Sik Lee[2,E,F], Ho Soon Choi[1,C,F]

[1] Department of Internal Medicine, College of Medicine, Hanyang University, Seoul, South Korea
[2] Division of Gastroenterology and Hepatology, Department of Internal Medicine, Korea University College of Medicine, Seoul, South Korea

A – research concept and design; B – collection and/or assembly of data; C – data analysis and interpretation; D – writing the article; E – critical revision of the article; F – final approval of the article

Advances in Clinical and Experimental Medicine, ISSN 1899–5276 (print), ISSN 2451–2680 (online) *Adv Clin Exp Med*. 2021;30(9):885–891

Address for correspondence
Jae Min Lee
E-mail: jmlee1202@gmail.com

Funding sources
None declared

Conflict of interest
None declared

Acknowledgements
This study was supported by the Korea University grant (No. K1824371); 2018 Weolbong grant from the Korean Gastrointestinal Endoscopy Research Foundation; and the National Research Foundation of Korea (NRF) grant funded by the Korea government Ministry of Science and ICT – MSIT (No. NRF-2021M3E5D1A01015177).

Received on February 26, 2021
Reviewed on March 21, 2021
Accepted on April 29, 2021

Published online on August 18, 2021

Cite as
Choi SJ, Lee JM, Lee KW, et al. Effect of histological examination on the diagnosis of pancreatic mass using endoscopic ultrasound fine-needle aspiration. *Adv Clin Exp Med*. 2021;30(9):885–891. doi:10.17219/acem/136278

DOI
10.17219/acem/136278

Abstract

Background. Endoscopic ultrasound-guided fine-needle aspiration (EUS-FNA) is a well-established method for the diagnosis of solid pancreatic lesions. However, the diagnostic yield of EUS-FNA for pancreatic lesions varies at around 70–90%. Samples from EUS-FNA consist of cells and tissues that can be analyzed separately, and the results can be combined for a final diagnosis.

Objectives. To investigate the effect of cytological and histological analysis of EUS-FNA samples on the final diagnosis, and identify factors that may affect the accuracy of the cytological, histological, and overall analysis.

Materials and methods. A single-center prospective observational study was conducted at a tertiary university hospital from July 2018 to June 2019. Patients who underwent EUS-FNA for pancreatic solid lesions with a 22-gauge EUS-FNA needle were included in our study. Liquid-based cytological analysis of the specimen and histological analysis of the whitish core were performed, and factors that affected the diagnostic accuracy of each analysis were evaluated.

Results. In 63 EUS-FNA samples, the overall diagnostic accuracy was 87.3%, which was significantly higher than the cytological accuracy of 73.8% ($p = 0.031$) and the histological accuracy of 69.8% ($p = 0.001$). Factors that affected the results differed in each group: 1) cytological analysis: size, location, and approach method; 2) histological analysis: specimen weight; and 3) overall analysis: size, location, and approach method.

Conclusions. Histologic evaluation of core material obtained from EUS-FNA improved diagnostic accuracy, and factors that affected each result were analyzed. Further studies with prospective randomized trials are recommended to support our data.

Key words: endosonography, diagnosis, pancreatic neoplasms, endoscopic ultrasound-guided fine-needle aspiration

Background

Endoscopic ultrasound-guided fine-needle aspiration (EUS-FNA) is a well-established and safe method for tissue acquisition from solid pancreatic lesions. Ever since Vilmann et al. first reported the use of EUS-FNA in a solid pancreatic lesion, it has become one of the most important endoscopic procedures in the diagnosis of benign and malignant tumors, as well as in the staging of malignancies of the gastrointestinal tract and adjacent structures, including the pancreas.[1] However, the diagnostic yield of the procedure varies at around 70–90%, and is affected by several factors such as lesion location or size, characteristics of the target lesion, various procedural techniques and devices, tissue-processing method, the availability of cytology staff or rapid on-site evaluation (ROSE), and the experience of the endosonographer.[2,3] The fact that the diagnostic yield is sometimes as low as 70% in expert hands can result in high medical costs from extra procedures and/or imaging studies, and the uncertainty in diagnosis can also cause treatment delay.

Many studies have been performed to overcome the limitations of EUS-FNA and improve diagnostic yield. The development of diagnostic techniques, such as the fanning technique and the slow-pull technique, and new endoscopic ultrasound-guided fine-needle biopsy (EUS-FNB), have brought a certain degree of success in this regard.[2,4,5] Even though recent meta-analysis results have not been consistent enough to confirm the superiority of EUS-FNB over EUS-FNA, its ability to provide core tissue specimens with preserved architecture provides advantages, especially in diagnosing lymphoma, gastrointestinal stromal tumors (GIST) and autoimmune pancreatitis, as well as in molecular and genetic analyses for precision medicine.[2,6,7] However, the EUS-FNB needle has several technical disadvantages compared to the EUS-FNA needle due to its stiffness and targeting difficulties, especially during the transduodenal approach, and an ideal technique for EUS-FNB has not yet been established.[8,9]

Although it is easy to think otherwise due to the nomenclature, biopsy specimens can also be obtained from EUS-FNA, and several articles have shown no difference between EUS-FNA and EUS-FNB in histologic core procurement.[6,10,11] In EUS-FNA without ROSE, the number of EUS-FNA passes and the end of the procedure are decided by the endosonographer on the basis of macroscopic evaluation of the FNA specimen.[11]

Objectives

In this study, we aimed to compare the results of liquid-based preparation (LBP) cytology alone and LBP cytology with histopathological study, to assess whether histologic evaluation of core tissue obtained from EUS-FNA using a 22-gauge needle could improve the diagnostic accuracy of EUS-FNA for solid pancreatic lesions in the absence of ROSE. The influence of the characteristics of the lesion and core tissue derived from EUS-FNA on diagnostic yield was also evaluated.

Materials and methods

Patient eligibility

In this prospective observational study, we collected data from 70 consecutive patients who underwent EUS-FNA for solid pancreatic lesions from July 2018 to June 2019. Eligible individuals were patients older than 20 years with a suspected solid pancreatic tumor measuring ≥10 mm. Exclusion criteria were as follows: 1) previous history of intra-abdominal surgery or cancer; 2) bleeding tendency (platelet count ≤50,000, prothrombin time-international normalized ratio (PT-INR) ≥1.8); 3) no confirmed final diagnosis; 4) cystic lesion on EUS; 5) repeated procedures due to inadequate samples; 6) pregnancy; and 7) refusal to participate. Patient demographics, laboratory test results and follow-up clinical data were collected. The lesion size and location (head/body/tail), approach method (transduodenal/transgastric), needle device, number of needle passes, depth of the needle from the margin, suction technique (syringe/slow-pull), the weight of the specimen, cytology results, histology results, and the final diagnosis were recorded with regard to the procedure. The study was conducted in accordance with the Declaration of Helsinki and was approved by the Korea University Anam Hospital Institutional Review Board (approval No. 2019AN0406). Written informed consent was obtained from all patients before the procedure.

EUS-FNA procedure and sample handling

The EUS-FNA procedures were performed by 2 experienced endosonographers at Korea University Anam Hospital, Seoul, South Korea, from July 2018 to June 2019. The procedures were performed using an electronic curvilinear echoendoscope (GF-UCT 240; Olympus Corp., Tokyo, Japan), a standard endoscopic system (EVIS LUCERA ELITE CV-260/CLV-260, CV-290/CLV-290SL; Olympus Medical Systems, Co. Ltd.) and the ProSound α10 premier (ALOKA, Co. Ltd., Tokyo, Japan). The EUS-FNA needles used for the procedure were either 22-gauge Expect™ Slimline FNA needles (Boston Scientific, Boston, USA) or 22-gauge EchoTip® Ultra FNA needles (Cook Medical, Bloomington, USA), as per the preference of the endosonographer. The precision balance used in our study was the FX-200i Precision Balance (A&D Medical, Chicago, USA). Endoscopic procedures were

performed under a moderate degree of procedural sedation using intravenous injection of propofol.

The lesion and the surrounding structures were closely reviewed under EUS and color Doppler mode. All lesions at the head were approached in a transduodenal manner, and all lesions in the body and tail were approached in a transgastric manner. Under real-time EUS imaging, the EUS-FNA needle was inserted through the working channel of the echoendoscope, where it punctured the target lesion. The mean lesion diameter and the maximum puncture depth of the needle from the surface of the lesion were measured. Once the needle was advanced into the target lesion, a suction technique, either application of a 10-milliliter syringe with negative pressure or slow withdrawal of the stylet, was decided by the endosonographer. An assistant nurse applied the suction and 10 to-and-fro movements using a fanning technique, with a maximum of 3 passes, for sample collection were performed under the endosonographer's discretion.

After the sampling procedure, the whole needle was removed from the echoendoscope, and the content inside the needle was directly placed into a translucent bottle with a cellular preservative fluid (CytoRichRed; Becton Dickinson, Franklin Lakes, USA) for primary rinsing, inspection, weight measurement, and subsequent LBP cytology. The specimen obtained from the procedure was slowly pushed out of the needle, using a needle stylet. Before the placement of the specimen, the precision balance was rescaled to zero with the preservative bottle, so only the weight of the specimen was measured. The endosonographer carefully assessed the specimen macroscopically, and if thread-like, tan-pink/red, thick, and granular material was observed, it was considered a visible histologic core, which was harvested and placed into a formalin bottle for subsequent histologic evaluation. For the confirmation of adequate sampling, macroscopic examination of the specimen was performed by the endosonographer who performed the procedure, along with another endosonographer who had not participated in the procedure. The ROSE was not available in any of the cases.

Cytologic and histologic analyses

The collected remnant samples in the cellular preservative fluid were sent for LBP cytology and preparation of a cell block. The slide was prepared by a completely automated preparation technique for LBP cytology, and cell blocks were prepared using residual samples. The sections were stained with hematoxylin and eosin (H&E), and both slides were reviewed by a pathologist for cytological analysis. The core specimens transferred from the preservative fluid into the 20% buffered formalin bottle were embedded in paraffin, and these sections were also stained with H&E, which were reviewed by a pathologist for histologic analysis.

Data analyses

The adequacies of both samples were determined by pathologists. Overall, samples were considered adequate if either the cytology or histology was considered adequate. Both cytologic and histologic results were reported as: 1) definite malignancy; 2) suspicious of malignancy; 3) atypical cells present; 4) benign cytology/histology; or 5) inadequate. We considered patients as having a malignancy when their results were either 1) or 2).[12] The final diagnosis was confirmed according to the following criteria: 1) positive cytologic or histologic results of EUS-FNA with compatible clinical features; 2) histologic diagnoses from other sources like surgery or biopsy; or 3) negative EUS-FNA results with clinical follow-up of at least 6 months with compatible benign clinical features.

Statistical analyses

Descriptive statistics for continuous variables are presented as means and standard deviations (SD) or medians and ranges. Categorical variables are presented as counts and percentages. Continuous and categorical variables were analyzed using the Student's t-test and χ^2 test, respectively. The diagnostic sensitivity, specificity, accuracy, positive predictive value (PPV), and negative predictive value (NPV) were measured, and the diagnostic accuracies of the samples were compared using McNemar's test. Potential factors that might have affected the diagnostic accuracy were evaluated. A p-value <0.05 was considered statistically significant. The IBM SPSS Statistics for Windows v. 21.0 (IBM Corp., Armonk, USA) was used for all analyses.

Results

Among the 70 patients who were eligible for our study, 7 were excluded: 3 patients with cystic lesions, 2 patients without confirmation of final diagnosis, and 2 patients with re-study. After the exclusion, 63 patients who underwent EUS-FNA for pancreatic solid lesions were analyzed. Thirty-three males (52.4%) were included in the study, and the mean age of patients was 70.2 ±10.7 years. The mean lesion size was 3.9 ±1.6 cm, and the lesions were located in the head (n = 21, 35.9%), body (n = 30, 47.6%) or tail (n = 20, 33.3%). The final diagnoses included 2 focal chronic pancreatitis and 61 adenocarcinomas. Table 1 shows the baseline characteristics of the participants. Procedure-related characteristics are listed in Table 2. Twenty-one procedures were performed using the transduodenal approach and 42 procedures were performed using the transgastric approach. Two different needle devices were used: Expect™ Slimline (n = 35, 55.6%) and EchoTip® Ultra (n = 28, 44.4%). The median number of needle passes was 2 (range 1–3), and the mean needle depth was 15.6 ±4.1 mm. Two suction techniques were used: negative

Table 1. Baseline characteristics of the participants

Variables	FNA (n = 63)
Age [years], mean ±SD	70.2 ±10.7
Lesion size [cm], mean ±SD	3.9 ±1.6
Sex	
Male, n (%)	33 (52.4)
Female, n (%)	30 (47.6)
Location	
Head, n (%)	21 (35.9)
Body, n (%)	22 (30.8)
Tail, n (%)	20 (33.3)
Final diagnosis	
Benign, n (%)	2 (3.2)
Adenocarcinoma, n (%)	61 (96.8)

FNA – fine-needle aspiration; SD – standard deviation.

Table 2. Procedure-related characteristics

Variables	FNA (n = 63)
Approach method	
Transduodenal, n (%)	21 (33.3)
Transgastric, n (%)	42 (66.7)
Needle device	
Expect™ Slimline, n (%)	35 (55.6)
EchoTip® Ultra, n (%)	28 (44.4)
Needle passes, n	2.4 ±0.5
Needle depth [mm], mean ±SD	15.6 ±4.1
Suction technique	
Syringe, n (%)	29 (46.0)
Slow-pull, n (%)	34 (54.0)
Specimen weight [mg], mean ±SD	183.5 ±120.0

FNA – fine-needle aspiration; SD – standard deviation.

suction with a 10-mL syringe (n = 29, 46.0%) and the slow-pull technique (n = 34, 54.0%). The mean specimen weight was 183.5 ±120.0 mg.

Positive results were seen in 47 cytologic samples and 44 histologic samples, and 55 patients showed positive results on the final diagnosis. For evaluation, 96.8% of cytology samples, 85.7% of histology samples and 98.4% of the overall samples were adequate. Most diagnostic discrimination values for the cytologic analysis were slightly higher than those for the histologic analysis: sensitivity 73.8% compared to 68.9%; specificity 100% compared to 100%; accuracy 74.6% compared to 69.8%; PPV 100% compared to 100%; and NPV 11.1% compared to 9.5%. Overall results were the combined cytologic and histologic analyses showing: sensitivity 86.9%; specificity 100%; accuracy 87.3%; PPV 100%; and NPV 20.0% (Table 3).

Table 4 summarizes the comparison of the diagnostic accuracies; the overall accuracy was significantly higher than the accuracy of cytology (p = 0.031) and that of histology (p = 0.001). The accuracy of cytology was higher than the accuracy of histology, but the difference was not significant (p = 0.332).

Univariate analysis was performed to evaluate the factors affecting the results in different specimen types (Table 5). With cytology, the positive group was significantly larger than the negative group (p = 0.02), and there were differences related to the location (p = 0.02), such that the diagnostic accuracy was in the following order: body (86.4%), tail (75.5%), and head (52.4%). The approach method was also significant (p = 0.00). With histology, specimens that showed positive results tended to weigh more than those with negative results (199.8 ±129.6 mg compared to 145.7 ±85.5 mg; p = 0.04). Overall, the size and location of the lesion significantly affected obtaining positive results from EUS-FNA (both p = 0.04).

Discussion

Because pancreatic cancer has a dismal prognosis, accurate diagnosis is crucial for patients to receive adequate treatment without delay. The EUS-FNA is a safe, accurate

Table 3. Cytology, histology and overall outcomes of endoscopic ultrasound-guided fine-needle aspiration (EUS-FNA)

Samples	Positive, n	Negative, n	Adequacy (%)	Sensitivity (%)	Specificity (%)	Accuracy (%)	PPV (%)	NPV (%)
Cytology	47	16	96.8 (61/63)	73.8 (45/61)	100.0 (2/2)	74.6 (47/63)	100.0 (45/45)	11.1 (2/18)
Histology	44	19	85.7 (54/63)	68.9 (42/61)	100.0 (2/2)	69.8 (44/63)	100.0 (42/42)	9.5 (2/21)
Overall	55	8	98.4 (62/63)	86.9 (55/61)	100.0 (2/2)	87.3 (55/63)	100.0 (53/53)	20.0 (2/10)

PPV – positive predictive value; NPV– negative predictive value.

Table 4. Comparison of the diagnostic yield of cytology and histology with overall result

Result		Cytology		p-value	Result	Histology		p-value
		positive, n	negative, n			positive, n	negative, n	
Overall	positive	47	8	0.031*	positive	44	11	0.001*
	negative	0	8		negative	0	8	

* statistically significant (McNemar's test).

Table 5. Univariate analysis of factors affecting the results in different types of specimen

Variables	Cytology			Biopsy			Overall		
	positive (n = 47)	negative (n = 16)	p-value	positive (n = 44)	negative (n = 19)	p-value	positive (n = 5)	negative (n = 8)	p-value
Sex male, n female, n	 25 22	 8 8	0.83	 23 21	 10 9	0.98	 29 26	 4 4	0.89
Age [years], mean ±SD	70.7 ±9.3	68.9 ±12.8	0.53	69.6 ±11.1	71.8 ±7.8	0.43	70.1 ±10.3	71.5 ±10.0	0.72
Size [mm], mean ±SD	40.7 ±16.4	31.3 ±9.7	0.03	37.9 ±16.1	39.4 ±14.3	0.71	39.8 ±15.8	28.3 ±8.4	0.04
Location, n (head/body/tail)	11/19/17	10/3/3	0.02*	12/17/15	9/5/5	0.34*	15/21/19	6/1/1	0.04*
Approach method, n (transduodenal/transgastric)	11/36	10/6	0.00	12/32	9/10	0.15	15/40	6/2	0.05
Needle device, n (Expect™/EchoTip®)	28/19	7/9	0.28	23/21	12/7	0.43	30/25	5/3	0.76
Needle passes, n, median (range)	2 (1–5)	2 (1–5)	1.00	2 (1–5)	2 (1–5)	1.00	2 (1–5)	2 (1–5)	1.00
Needle depth [mm], mean ±SD	15.6 ±4.7	16.1 ±2.8	0.64	15.2 ±4.5	16.7 ±3.4	0.24	15.5 ±4.2	16.5 ±3.0	0.40
Suction technique, n (syringe/slow-pull)	22/25	7/9	0.84	19/25	10/9	0.50	25/30	4/4	0.81
Specimen weight [mg], mean ±SD	189.6 ±103.9	181.4 ±126.0	0.82	199.8 ±129.6	145.7 ±85.5	0.04	180.0 ±120.3	202.0 ±122.8	0.55

SD – standard deviation; * statistically significant.

and cost-effective diagnostic modality for pancreatic tumors, especially in providing specimens for cytological evaluation. However, it is sometimes difficult to distinguish adenocarcinoma from reactive changes on cytologic evaluation because of their overlapping features.[13] It is widely accepted that the presence of ROSE during EUS-FNA improves diagnostic yield, but the total procedure time and costs increase, and more importantly, this method is not available in many centers.[14] Special needles for biopsy were developed and they showed promising results in many studies by obtaining adequate histologic cores. Yet, they have limitations, including the tip hardness, cost and the lack of any set standard technique. We conducted a prospective observational study of EUS-FNA to evaluate the effects of cytological and histological examination on diagnostic accuracy, and the factors that affected each sample.

In our study, the diagnostic accuracy of cytology was higher than that of histology but the difference was not significant (74.6% compared to 69.8%), and the diagnostic accuracy of the final result of combined cytology and histology was significantly higher than that of cytology or histology alone. Even though the histologic evaluation alone yielded fewer results than cytologic evaluation, both cytology and histology specimens were important in EUS-FNA, as their results were complementary towards the diagnosis of the lesion. These results are consistent with those of previous studies.[15,16]

Because acquiring cytohistologic specimens is critical for diagnosis, many studies have been performed to evaluate the factors that affect the diagnostic accuracy of EUS-FNA. Though there is a lack of consensus over the findings of the reports, the presence of ROSE and size and location of the tumor are widely accepted factors that influence diagnostic accuracy.[2,9,17–20] In our study, tumor size, location and the approach method were significant factors that affected the rendering of positive cytologic results, and the specimen weight was a significant factor for positive histologic results. With combined analysis, the tumor size and location of the lesion were significant factors for a positive diagnosis.

Even though the tumor size was important, the mean needle depth from the margin of the lesion was not significantly greater in the positive group, and was even slightly lesser. The larger the tumor size, the more possible it is to insert the needle from various angles avoiding nearby vascular structures. Alternatively, more vigorous fanning techniques could be applied, and these factors might be the cause of this result. Regardless of specimen, in our study, diagnostic accuracy was the highest in the body, followed by the tail and then, the head. This was largely affected by the approach method. The transduodenal approach showed a significantly lower positive rate for cytology, and this may be due to disruption of the needle from its original arrangement.[21] Further research is needed in this regard.

Among the 16 and 19 negative results from cytology and histology, respectively, the ratio of atypical cells was higher with histology (n = 15, 78.9%) than cytology (n = 10, 62.5%). Atypical cells do not contribute to a definite diagnosis for malignancy; however, they can help clinicians suspect malignancy in false-negative cases and plan further more aggressive diagnostic procedures or approaches, rather than observation.[12]

The length of the tissue core is reported to be a significant factor for diagnosis in several studies, and our study is the first to analyze the sample weight and its correlation with diagnostic accuracy.[11,22] The weight of cytologic samples might not be accurate because of factors such as blood contamination or tissue fragments, and the result was not significant. The weight of the histologic core was also measured and was significantly higher in the positive group ($p = 0.04$). In particular, patients who underwent the slow-pull technique for suction showed significantly higher histologic core weight compared to those who underwent the negative syringe technique (201.3 ±138.6 mg compared to 130.1 ±61.8 mg; $p = 0.04$). This result suggests that although the slow-pull technique does not significantly improve the accuracy of EUS-FNA, positivity of histologic results can be predicted in advance through the weight of the sample in cases of EUS-FNA with the slow-pull technique. Further validation and study of thresholds are needed to confirm our suggestion.

Our study evaluated cytology with LBP and cellblock-processed samples. In our institute, the entire specimen is placed in cellular preservative fluid for better visualization of the core after rinsing. Although the diagnostic outcome of the conventional smear method is reported to be better than that of LBP cytology, it is not applicable in some hospitals because of pathologists' preferences and hospital settings.[23,24] However, our study results were similar to those of a previous study using the smear method.[15] To exclude the effects of various factors that are still controversial in their influence on the diagnostic accuracy of EUS-FNA, variables such as needle caliber (22-gauge), tissue acquisition method (fanning technique) and presence of stylet were controlled in our study.

Our study suggests that vigorous collection of tissue core and its analysis would be a method of increasing the diagnostic yield in cases of pancreatic head lesions without ROSE. In addition, EUS-FNA for collecting tissue samples may be helpful, but further studies are needed, considering the poor maneuverability of the needle in a bent, torqued position.

Limitations

Our study has several limitations. First, the study was performed in a single tertiary center. In addition, the weight of the specimen may not exactly correlate with the quantity of the specimen because of blood contamination or fibrosis, that may have been included. Other solid pancreatic lesions, such as neuroendocrine tumors or cystic pancreatic lesions were not evaluated. Also, the number of true-negative lesions was small, resulting in a low NPV. A larger prospective multicenter study is needed to provide more evidence for our results.

Conclusions

Our findings suggest that histologic evaluation of core material obtained from EUS-FNA improved diagnostic sensitivity, accuracy and NPV. Previous studies have focused on improving diagnostic accuracy by analyzing its factors, but our study shows that the factors influencing the results of cytology and histology are slightly different. Thus, overall diagnostic accuracy can be improved by improving each factor. Measuring the weight of the sample could be a method of obtaining sufficient samples during EUS-FNA, along with the slow-pull technique to increase histologic accuracy and, thus, the overall accuracy. Follow-up studies with prospective randomized trials are recommended to support our data.

ORCID iDs

Seong Ji Choi https://orcid.org/0000-0002-1969-516X
Jae Min Lee https://orcid.org/0000-0001-9553-5101
Kang Won Lee https://orcid.org/0000-0002-5902-9700
Hyuk Soon Choi https://orcid.org/0000-0002-4343-6950
Eun Sun Kim https://orcid.org/0000-0003-1820-459X
Bora Keum https://orcid.org/0000-0003-0391-1945
Jai Hoon Yoon https://orcid.org/0000-0003-3194-5149
Yoon Tae Jeen https://orcid.org/0000-0003-0220-3816
Hoon Jai Chun https://orcid.org/0000-0002-5539-361X
Hong Sik Lee https://orcid.org/0000-0001-9726-5416
Ho Soon Choi https://orcid.org/0000-0003-3746-8742

References

1. Vilmann P, Jacobsen GK, Henriksen FW, Hancke S. Endoscopic ultrasonography with guided fine needle aspiration biopsy in pancreatic disease. *Gastrointest Endosc*. 1992;38(2):172–173. doi:10.1016/s0016-5107(92)70385-x
2. Khan MA, Grimm IS, Ali B, et al. A meta-analysis of endoscopic ultrasound-fine-needle aspiration compared to endoscopic ultrasound-fine-needle biopsy: Diagnostic yield and the value of onsite cytopathological assessment. *Endosc Int Open*. 2017;5(5):E363–E375. doi:10.1055/s-0043-101693
3. Itoi T, Sofuni A, Itokawa F, Irisawa A, Khor CJ, Rerknimitr R. Current status of diagnostic endoscopic ultrasonography in the evaluation of pancreatic mass lesions. *Dig Endosc*. 2011;23(Suppl 1):17–21. doi:10.1111/j.1443-1661.2011.01132.x
4. Bang JY, Magee SH, Ramesh J, Trevino JM, Varadarajulu S. Randomized trial comparing fanning with standard technique for endoscopic ultrasound-guided fine-needle aspiration of solid pancreatic mass lesions. *Endoscopy*. 2013;45(6):445–450. doi:10.1055/s-0032-1326268
5. Lee JM, Lee HS, Hyun JJ, et al. Slow-pull using a fanning technique is more useful than the standard suction technique in EUS-guided fine needle aspiration in pancreatic masses. *Gut Liver*. 2018;12(3):360–366. doi:10.5009/gnl17140
6. Bang JY, Hawes R, Varadarajulu S. A meta-analysis comparing ProCore and standard fine-needle aspiration needles for endoscopic ultrasound-guided tissue acquisition. *Endoscopy*. 2016;48(4):339–349. doi:10.1055/s-0034-1393354
7. Larsen MH, Fristrup CW, Detlefsen S, Mortensen MB. Prospective evaluation of EUS-guided fine needle biopsy in pancreatic mass lesions. *Endosc Int Open*. 2018;6(2):E242–E248. doi:10.1055/s-0043-124078
8. Panic N, Larghi A. Techniques for endoscopic ultrasound-guided fine-needle biopsy. *Gastrointest Endosc Clin N Am*. 2014;24(1):83–107. doi:10.1016/j.giec.2013.08.010
9. Attili F, Fabbri C, Yasuda I, et al. Low diagnostic yield of transduodenal endoscopic ultrasound-guided fine needle biopsy using the 19-gauge Flex needle: A large multicenter prospective study. *Endosc Ultrasound*. 2017;6(6):402–408. doi:10.4103/eus.eus_54_17

10. Bang JY, Hebert-Magee S, Trevino J, Ramesh J, Varadarajulu S. Randomized trial comparing the 22-gauge aspiration and 22-gauge biopsy needles for EUS-guided sampling of solid pancreatic mass lesions. *Gastrointest Endosc*. 2012;76(2):321–327. doi:10.1016/j.gie.2012.03.1392
11. Iwashita T, Yasuda I, Mukai T, et al. Macroscopic on-site quality evaluation of biopsy specimens to improve the diagnostic accuracy during EUS-guided FNA using a 19-gauge needle for solid lesions: A single-center prospective pilot study (MOSE study). *Gastrointest Endosc*. 2015;81(1):177–185. doi:10.1016/j.gie.2014.08.040
12. Layfield LJ, Schmidt RL, Hirschowitz SL, Olson MT, Ali SZ, Dodd LL. Significance of the diagnostic categories "atypical" and "suspicious for malignancy" in the cytologic diagnosis of solid pancreatic masses. *Diagn Cytopathol*. 2014;42(4):292–296. doi:10.1002/dc.23078
13. Kato K, Kamada H, Fujimori T, Aritomo Y, Ono M, Masaki T. Molecular biologic approach to the diagnosis of pancreatic carcinoma using specimens obtained by EUS-guided fine needle aspiration. *Gastroenterol Res Pract*. 2012;2012:243524. doi:10.1155/2012/243524
14. Ganc RL, Carbonari AP, Colaiacovo R, et al. Rapid on-site cytopathological examination (ROSE) performed by endosonagraphers and its improvement in the diagnosis of pancreatic solid lesions. *Acta Cir Bras*. 2015;30(7):503–508. doi:10.1590/S0102-865020150070000009
15. Yang L, Iwai T, Kida M, et al. Analysis of the diagnostic yield of endoscopic ultrasonography-guided fine-needle aspiration in patients with a suspected pancreatic malignancy. *Rev Esp Enferm Dig*. 2018; 110(9):544–550. doi:10.17235/reed.2018.5455/2017
16. Moller K, Papanikolaou IS, Toermer T, et al. EUS-guided FNA of solid pancreatic masses: High yield of 2 passes with combined histologic-cytologic analysis. *Gastrointest Endosc*. 2009;70(1):60–69. doi:10.1016/j.gie.2008.10.008
17. Crino SF, Conti Bellocchi MC, Bernardoni L, et al. Diagnostic yield of EUS-FNA of small (≤15 mm) solid pancreatic lesions using a 25-gauge needle. *Hepatobiliary Pancreat Dis Int*. 2018;17(1):70–74. doi:10.1016/j.hbpd.2018.01.010
18. Li HZ, Peng CY, Shen SS, et al. Factors affecting the accuracy of endoscopic ultrasound-guided fine needle aspiration for the diagnosis of small (≤20 mm) pancreatic lesions. *J Dig Dis*. 2020;21(7):416–421. doi:10.1111/1751-2980.12875
19. Polkowski M, Jenssen C, Kaye P, et al. Technical aspects of endoscopic ultrasound (EUS)-guided sampling in gastroenterology: European Society of Gastrointestinal Endoscopy (ESGE) Technical Guideline – March 2017. *Endoscopy*. 2017;49(10):989–1006. doi:10.1055/s-0043-119219
20. Hwang CY, Lee SS, Song TJ, et al. Endoscopic ultrasound guided fine needle aspiration biopsy in diagnosis of pancreatic and peripancreatic lesions: A single center experience in Korea. *Gut Liver*. 2009; 3(2):116–121. doi:10.5009/gnl.2009.3.2.116
21. de Nucci G, Petrone MC, Imperatore N, et al. Feasibility and accuracy of transduodenal endoscopic ultrasound-guided fine-needle aspiration of solid lesions using a 19-gauge flexible needle: A multicenter study. *Clin Endosc*. 2021;54(2):229–235.doi:10.5946/ce.2020.056
22. Iglesias-Garcia J, Dominguez-Munoz E, Lozano-Leon A, et al. Impact of endoscopic ultrasound-guided fine needle biopsy for diagnosis of pancreatic masses. *World J Gastroenterol*. 2007;13(2):289–293. doi:10.3748/wjg.v13.i2.289
23. Lee JK, Choi ER, Jang TH, et al. A prospective comparison of liquid-based cytology and traditional smear cytology in pancreatic endoscopic ultrasound-guided fine needle aspiration. *Acta Cytol*. 2011; 55(5):401–407. doi:10.1159/000330811
24. Biermann K, Lozano Escario MD, Hebert-Magee S, Rindi G, Doglioni C. How to prepare, handle, read, and improve EUS-FNA and fine-needle biopsy for solid pancreatic lesions: The pathologist's role. *Endosc Ultrasound*. 2017;6(Suppl 3):S95–S98. doi:10.4103/eus.eus_71_17

High irisin and low BDNF levels in aqueous humor of high myopia

Xijuan Wang[1,2,3,A–F], Mingwu Li[2,B,C,E,F], Ruimao Zheng[4,B,C,E,F], Ting Cui[2,B,C,F], Jiayin Qin[2,B,C,F], Zhijie Su[4,C,F], Meng Shang[2,F], Yongzhen Bao[1,3,B,F]

[1] Department of Ophthalmology, Peking University People's Hospital, China
[2] Department of Ophthalmology, Peking University International Hospital, China
[3] Beijing Key Laboratory of Diagnosis and Therapy of Retinal and Choroid Diseases, China
[4] Department of Anatomy, Histology and Embryology, Health Science Center, Peking University, China

A – research concept and design; B – collection and/or assembly of data; C – data analysis and interpretation;
D – writing the article; E – critical revision of the article; F – final approval of the article

Advances in Clinical and Experimental Medicine, ISSN 1899–5276 (print), ISSN 2451–2680 (online) Adv Clin Exp Med. 2021;30(9):893–904

Address for correspondence
Yongzhen Bao
E-mail: drbaoyz@sina.com

Funding sources
National Natural Science Foundation of China (grant No. 21173012).

Conflict of interest
None declared

Received on April 23, 2020
Reviewed on April 24, 2020
Accepted on July 16, 2020

Published online on June 23, 2021

Cite as
Wang X, Li M, Zheng R, et al. High irisin and low BDNF levels in aqueous humor of high myopia. *Adv Clin Exp Med*. 2021;30(9):893–904. doi:10.17219/acem/125428

DOI
10.17219/acem/125428

Abstract

Background. The pathogenesis of myopia remains unclear. Both genetic and environmental factors play a role in the disease progression. Reasons including reduced physical activity (PA) and low-grade intraocular inflammation may be involved in the development of myopia.

Objectives. To analyze the levels of irisin, brain-derived neurotrophic factor (BDNF) and other intraocular cytokines in aqueous humor of high myopia patients, and to evaluate the roles of PA and inflammation in developing myopia.

Materials and methods. We collected aqueous humor samples from patients with axial length (AL) over 26 mm ($n = 35$) or shorter than 25 mm ($n = 38$) during cataract extraction surgery. Samples were assayed using the enzyme-linked immunosorbent assay (ELISA) kit for irisin and a multiplex immunoassay kit for BDNF, interleukin (IL)-6, IL-8 and IL-10, and tumor necrosis factor alpha (TNF-α).

Results. Irisin levels in the aqueous samples of the highly myopic eyes were significantly higher than in the control group ($p = 0.027$). The BDNF levels of the highly myopic group were significantly lower than in the control group ($p = 0.043$). Median level of leukemia inhibitory factor (LIF) for highly myopic group (2.035 pg/mL) was statistically significantly higher than in the control group (0.750 pg/mL) ($U = 210.5$, $Z = -4.495$, $p < 0.001$). Interleukin 1 receptor antagonist (IL-1ra) level in the aqueous samples of the highly myopic group was significantly lower than in the shorter AL group ($p = 0.049$). Interleukin 6, IL-8 and IL-10 levels were not significantly different between the 2 groups ($p = 0.501$, $p = 0.059$ and $p = 0.192$, respectively). Tumor necrosis factor α levels could only be detected in 30 samples and median levels in the 2 groups were not statistically significantly different ($U = 99$, $Z = -0.482$, $p = 0.650$). No correlation was found between IL-6, IL-8, IL-10 and TNF-α, and the AL ($p > 0.05$). Irisin was positively correlated with AL ($p = 0.028$, $r = 0.287$). The BDNF was negatively correlated with AL ($p = 0.040$, $r = -0.246$). Interleukin 1ra was negatively correlated with AL ($p = 0.038$, $r = -0.276$). There was also a correlation between LIF and AL ($p < 0.001$, $r = 0.486$).

Conclusions. Higher irisin level in high myopia group opens a new direction to discover the relationship between PA and myopia. The decreased BDNF in high myopia group probably demonstrates the connection between myopia and neurodegenerative disease.

Key words: physical activity, brain-derived neurotrophic factor, myopia, irisin, neurodegenerative disease

Background

Myopia is one of the leading causes of visual impairment worldwide. There are many patients with myopia who experience a progressive change over their entire lifetime, including elongation of the axial length (AL), and degenerative changes of the retina and choroid. Many population-based studies have shown that high myopia is the 2nd reason for visual disability in Asia.[1,2] The prevalence of myopia is predicted to increase to 49.8% by 2050, with 9.8% suffering from high myopia.[3] The risk increases along with the increased diopters of myopia.[4]

Currently, the pathogenesis of this disorder remains unclear. Both genetic and environmental factors play a role in the disease progression. It has been speculated that lifestyle changes such as reduced physical activity (PA), reduced time spend outdoors and more indoor work might be the reason of myopia progression.[5] Irisin,[6] as an exercise-induced myokine, is secreted into the circulation after proteolytic cleavage from fibronectin-type III domain containing 5 (FNDC5). The physiological function of irisin is to convert white adipose tissue to brown, which increases energy expenditure.[6] Physical activity is well-known as a protective lifestyle feature against type 2 diabetes mellitus (T2DM), cardiovascular diseases, cancer, dementia, and depression.[7] The protective role of PA against myopia has also been an area of interest in recent years. The mechanism of the positive effect of PA has not been discovered, but theories include increased choroidal blood flow and thickness.[8] We hypothesized that irisin, as an exercise-induced myokine, may be involved in the relationship of PA and myopia progression.

Although irisin was first found in skeletal muscles,[6] recent studies have proved it exists in various tissues, including smooth muscle tissue.[9] As early as the 1980s, close-up work was considered to be one of the important risk factors for the development of myopia. The ciliary muscle is related to the occurrence and development of myopia according to the ocular accommodation mechanism. Study of the relationship between irisin level and axial myopia may help to understand whether the ciliary muscle is involved in this pathological process and its mechanism.

Physical activity has also been shown to improve brain-related outcomes, in particular neurodegenerative disorders, such as Parkinson's disease (PD)[10] and Alzheimer's disease (AD).[11] High myopia-related retinal atrophy is known as a type of neurodegenerative change. Neurotrophins play a major role in the growth and development of neurons. One of these neurotrophic factors is brain-derived neurotrophic factor (BDNF). In addition, Young et al.[12] identified FNDC5 as an important regulator of BDNF. The goal of our study was to shed light on FNDC5/irisin and its role in the beneficial effects of PA on myopia prevention and its potential application in neurodegenerative disorders deregulating BDNF.

On the other hand, several studies showed that sclera stretching or staphyloma development can be monitored during treatment and follow-up of some inflammatory ocular disease such as Vogt–Koyanagi–Harada disease.[13] According to those studies, it is possible that chronic inflammation in the retina or choroid could induce stretching of the sclera and axial elongation. It has been demonstrated that the levels of drugs or cytokines are positively correlated between the aqueous and vitreous fluid.[14,15] In order to prove that there is a connection among myopia, PA and subclinical inflammation, we decided to collect aqueous humor from senile cataract extracts in normal and long AL eyes in our hospital from March to October 2019.

Objectives

To analyze the levels of irisin, brain-derived neurotrophic factor (BDNF) and other intraocular cytokines in aqueous humor of high myopia patients, and to evaluate the roles of PA and inflammation in developing myopia.

Materials and methods

Study design

Seventy-three eyes from 73 senile patients with cataract were studied from March to October 2019. The inclusion criterion was an uneventful cataract surgery. Eyes with glaucoma, uveitis, zonular weakness, previous trauma, previous intraocular surgery, or fundus pathology were excluded from the study. Patients with diabetes mellitus, using glucocorticoids and patients with autoimmune diseases were excluded. We used the IolMaster 500 (Carl Zeiss AG, Jena, Germany) to exam the AL, so that we could recruit patients and divide them into 2 groups (longer AL group with AL > 26 mm (35 eyes, 35 patients) and shorter AL group with AL < 25 mm (38 eyes, 38 patients)).

Sample collection

We administered to the patients Oxybuprocaine Hydrochloride Eye Drop (Santen Pharmaceutical Co., Ltd., Osaka, Japan) 4 times every 5 min before the surgery for local anesthesia. Eyelids and the surrounding skin were swabbed with povidone iodine. Samples of aqueous humor (90–120 μL) were aspirated by inserting a 29-gauge needle through the corneal paracentesis into the anterior chamber before surgery. Samples were immediately stored at −80°C until sample analysis.

Irisin analysis

Samples were harvested and assayed using enzyme-linked immunosorbent assay (ELISA) kit for irisin (Irisin ELISA Kit; Beijing Dongge Boye Biotechnology Co. Ltd., Beijing, China), and were measured according to the manufacturer's instructions. The stop solution changes the color from

blue to yellow and the intensity of the color is measured at 450 nm using a spectrophotometer. In order to measure the concentration of irisin in the sample, the Irisin ELISA Kit includes a set of calibration standards. The calibration standards are assayed at the same time as the samples and allow the operator to produce a standard curve of optical density (OD) compared to irisin concentration (Fig. 1). The concentration of irisin in the samples is then determined by comparing the OD of the samples to the standard curve.

Other cytokines analysis

We simultaneously analyzed a selection of 7 cytokines (BDNF, interleukin (IL)-10, IL-8, IL-6, leukemia inhibitory factor (LIF), interleukin 1 receptor antagonist (IL-1ra), and tumor necrosis factor alpha (TNF-α)), using a multiplex immunoassay kit (ProcartaPlex; Thermo Fisher Scientific, Waltham, USA). ProcartaPlex immunoassays are based on the principles of a ELISA, using 2 highly specific antibodies binding to different epitopes of 1 protein to quantitate all protein targets simultaneously using a Luminex 200™ System instrument (Luminex Corp., Austin, USA). The assays were performed according to the manufacturer's instructions. The standard curve was based on five-parameter nonlinear regression (Fig. 1). Each cytokine concentration was then calculated by the curve.

Statistical analysis

The data was processed and statistically analyzed using IBM SPSS Statistics for Mac, v. 26.0 (IBM Corp., Armonk, USA). All data are presented as means ± standard deviations

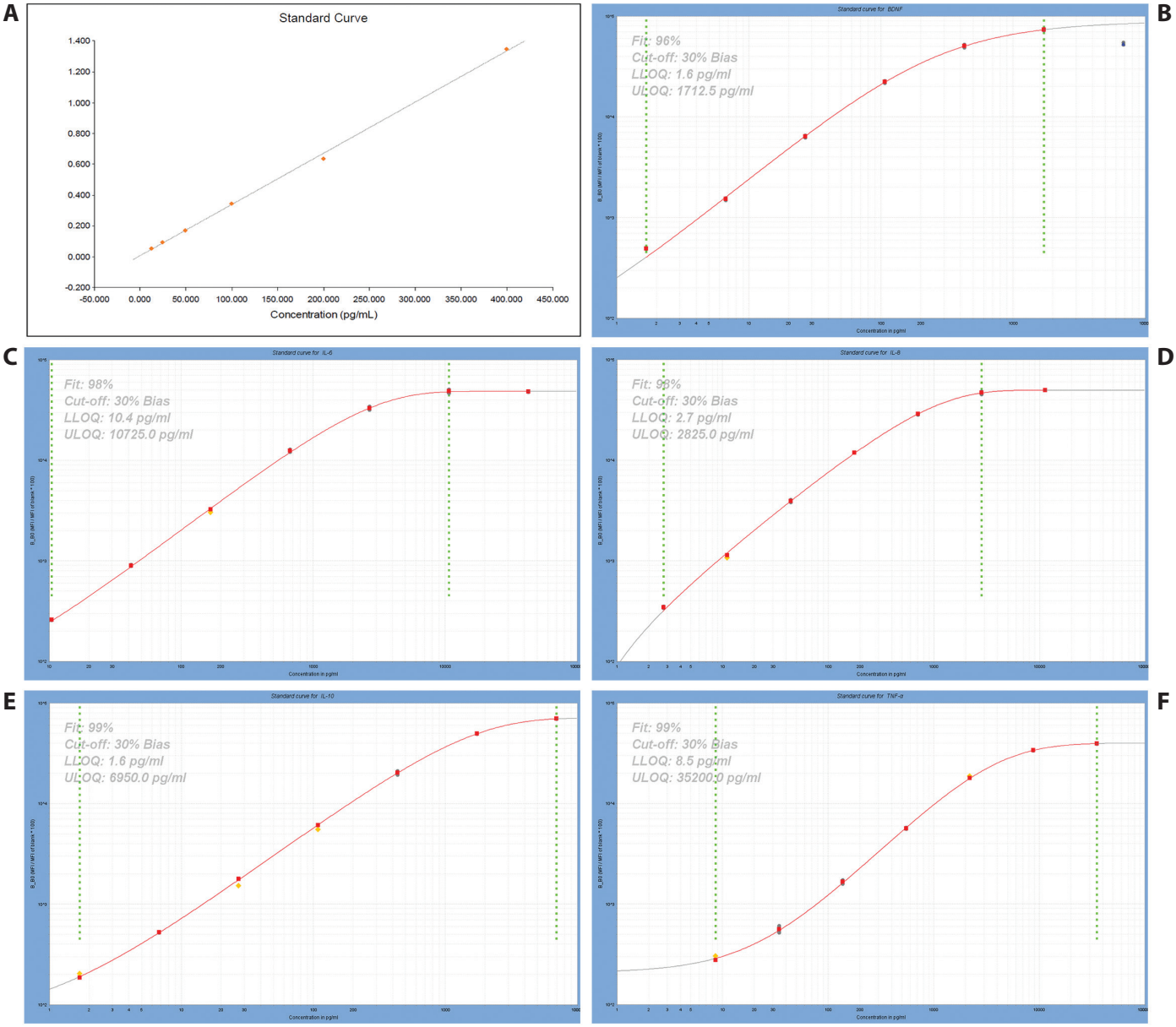

Fig. 1. Standard curve of cytokines. A. Standard curve of irisin based on linear regression; B–F. Standard curve of BDNF, IL-6, IL-8, IL-10, and TNF-α

(SD). Categorical data was compared between groups using χ^2 test. Student's t-test and Mann–Whitney U test were used to detect differences between the long AL group and normal group. Pearson's correlation analysis was adopted to analyze the relations among the cytokines and the AL in our study. Values of $p < 0.05$ were considered statistically significant.

Results

Baseline characteristics of the participants

The preoperative distributions of age, gender and AL are summarized in Table 1. There was a significant difference of gender and no significant difference of age in the 2 groups. The globe AL of highly myopic eyes was significant longer (5.6 mm longer) than the control eyes (28.4 ±2.4 mm compared to 22.8 ±1.0 mm, $p < 0.0001$ (t-test)).

Irisin levels in the aqueous humor of the study eyes

Student's t-test revealed that irisin level in the aqueous samples of the highly myopic eyes was significantly higher than in the control group ($p = 0.027$). Mean values of irisin in the samples were 118.76 ±9.6 pg/mL in the AL > 26 mm group compared to 113.45 ±8.99 pg/mL in the AL < 25 mm group (Table 2). Furthermore, positive correlation was found between irisin and the AL ($p = 0.028$, $r = 0.287$) (Fig. 2).

BDNF levels in the aqueous humor of the study eyes

Student's t-test revealed that BDNF level in the aqueous samples of the highly myopic eyes was significantly lower than in the control group ($p = 0.043$). Mean values of BDNF in the samples were 1.42 ±0.80 pg/mL in the AL > 26 mm group compared to 1.88 ±1.02 pg/mL in the AL < 25 mm group (Table 2). In addition, negative correlation was found between BDNF level and the AL ($p = 0.040$, $r = -0.246$) (Fig. 3).

Interleukin 6 levels in the aqueous humor of the study eyes

Median level of IL-6 for AL > 26 mm group (21.94 pg/mL) and AL < 25 mm group (14.29 pg/mL) was not statistically significantly different ($U = 338$, $Z = -0.674$, $p = 0.501$) (Table 3). No correlation was found between IL-6 level and the AL ($p = 0.209$, $r = 0.172$) (Fig. 4).

Interleukin 8 levels in the aqueous humor of the study eyes

Student's t-test showed that IL-8 level in the aqueous samples of the 2 groups presented no significant difference ($p = 0.059$). Mean values of IL-8 in the samples were 4.32 ±1.78 pg/mL in the AL > 26 mm group compared to 5.21 ±1.87 pg/mL in the AL < 25 mm group (Table 2). No correlation was found between IL-8 level and the AL ($p = 0.235$, $r = -0.153$) (Fig. 5).

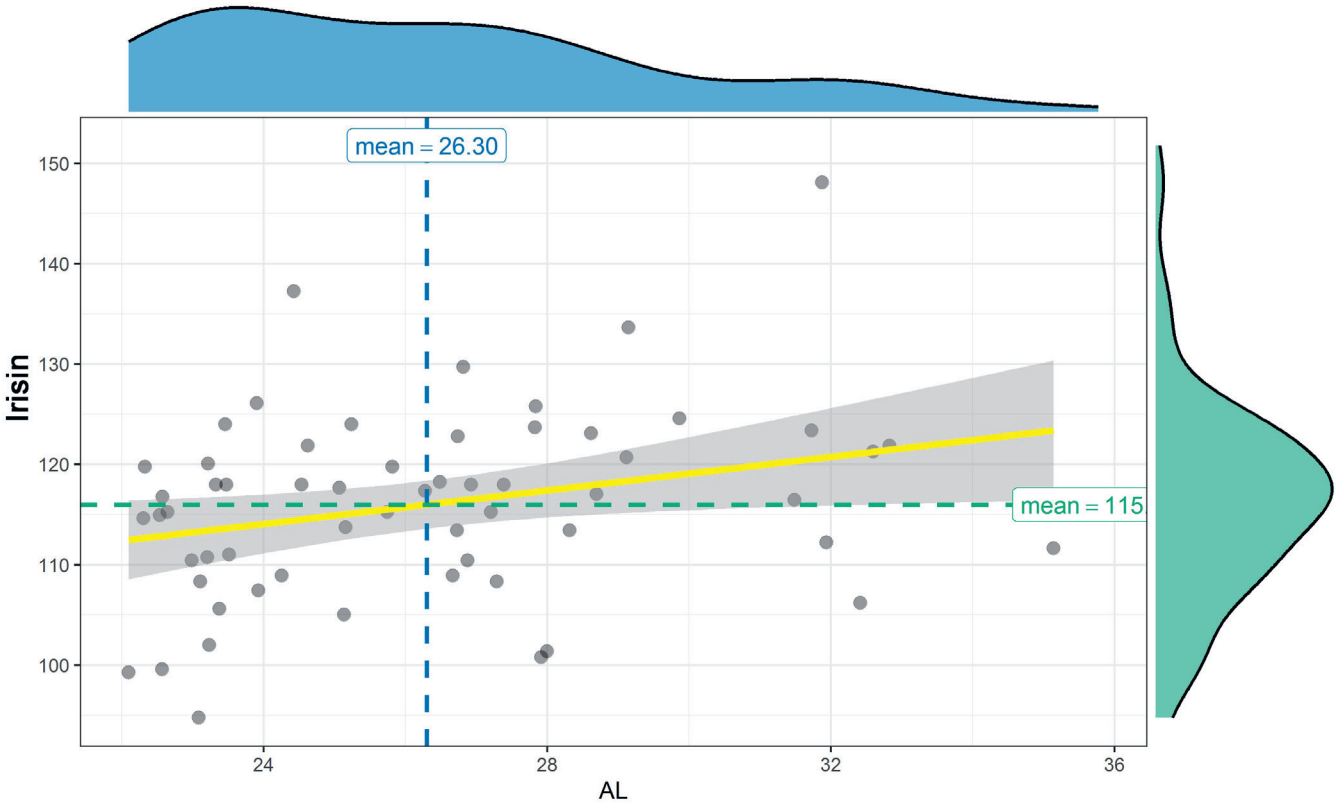

Fig. 2. Correlation between the irisin level and the axial length (AL)

Table 1. Baseline characteristics of the patients in respective groups

Group (n = 73)	Age	Gender	AL [mm]	Postoperative BCVA [logMAR]
AL > 26 mm (n = 35)	68.7 ±8.0	male (n = 14) 40% female (n = 21) 60%	28.4 ±2.4	0.34 ±0.24
AL < 25 mm (n = 38)	70.0 ±7.9	male (n = 4) 10.5% female (n = 34) 89.5%	22.8 ±1.0	0.15 ±0.12
p-value	0.48	0.004	<0.0001	<0.0001

AL – axial length of the eye globe; BCVA – best corrected visual acuity. The differences of age and AL between the 2 groups were tested using Student's t-test. The difference of the gender distribution between the 2 groups was tested using χ^2 test.

Table 2. The levels of irisin, BDNF, IL-8, IL-10 and IL-1ra in 2 groups

Group	Irisin	BDNF	IL-8	IL-10	IL-1ra
AL > 26 mm (n = 35)	118.76 ±9.68	1.42 ±0.80	4.32 ±1.78	1.21 ±0.54	111.01 ±46.51
Al < 25 mm (n = 38)	113.45 ±8.99	1.88 ±1.02	5.21 ±1.87	1.41 ±0.57	147.22 ±86.60
p-value*	p = 0.027	p = 0.043	p = 0.059	p = 0.192	p = 0.049

BDNF – brain-derived neurotrophic factor; IL – interleukin; IL-1ra – interleukin 1 receptor agonist; AL – axial length. Data is expressed as the means ± standard deviations (SD), in pg/mL. The differences of cytokines between the 2 groups were tested using Student's t-test.

Table 3. The levels of IL-6, LIF and TNF-α in 2 groups

Group	IL-6	LIF	TNF-α
AL > 26 mm (n = 35)	21.94 (3.29–90.84)	2.035 (0.01–19.39)	13.28 (1.10–88.90)
Al < 25 mm (n = 38)	14.29 (3.02–85.10)	0.750 (0.01–4.47)	16.86 (0.19–74.83)
p-value	p = 0.501	p < 0.001	p = 0.650
U-value	338	210.5	99
Z-value	–0.674	–4.495	–0.482

IL – interleukin; LIF – leukemia inhibitory factor; TNF-α – tumor necrosis factor alpha. The differences of cytokines between the 2 groups were tested using Mann–Whitney U test.

Interleukin 10 levels in the aqueous humor of the study eyes

Student's t-test revealed that IL-10 level in the aqueous samples of the highly myopic eyes was not significantly different than in the control eyes (p = 0.192). Mean values of IL-10 in the samples were 1.21 ±0.54 pg/mL in the AL > 26 mm group compared to 1.41 ±0.57 pg/mL in the AL < 25 mm group (Table 2). In addition, no correlation was found between IL-10 and the AL (p = 0.351, r = –0.125) (Fig. 6).

Leukemia inhibitory factor levels in the aqueous humor of the study eyes

Median level of LIF for longer AL group (2.035 pg/mL) was statistically significantly higher than in the shorter AL group (0.750 pg/mL) (U = 210.5, Z = –4.495, p < 0.001; Table 3). There was a correlation between LIF and AL (p < 0.001, r = 0.486) (Fig. 7).

Interleukin 1ra levels in the aqueous humor of the study eyes

Mean values of IL-1ra level were 111.01 ±46.51 pg/mL in the longer AL group compared to 147.22 ±86.60 pg/mL in the shorter AL group. Interleukin 1ra level in the aqueous samples of the longer AL group was significantly lower than in the shorter AL group (p = 0.049). Interleukin 1ra level was negatively correlated with AL (p = 0.038, r = –0.276) (Fig. 8).

Tumor necrosis factor α levels in the aqueous humor of the study eyes

Tumor necrosis factor α levels could only be detected in 30 samples (n = 30, n_{AL} > 26 group = 13, n_{AL} < 25 group = 17). Its median level for AL > 26 group (13.28 pg/mL) and AL < 25 group (16.86 pg/mL) was not statistically significantly different (U = 99, Z = –0.482, p = 0.650; Table 3). No correlation was found between TNF-α level and the AL (p = 0.687, r = –0.077) (Fig. 9).

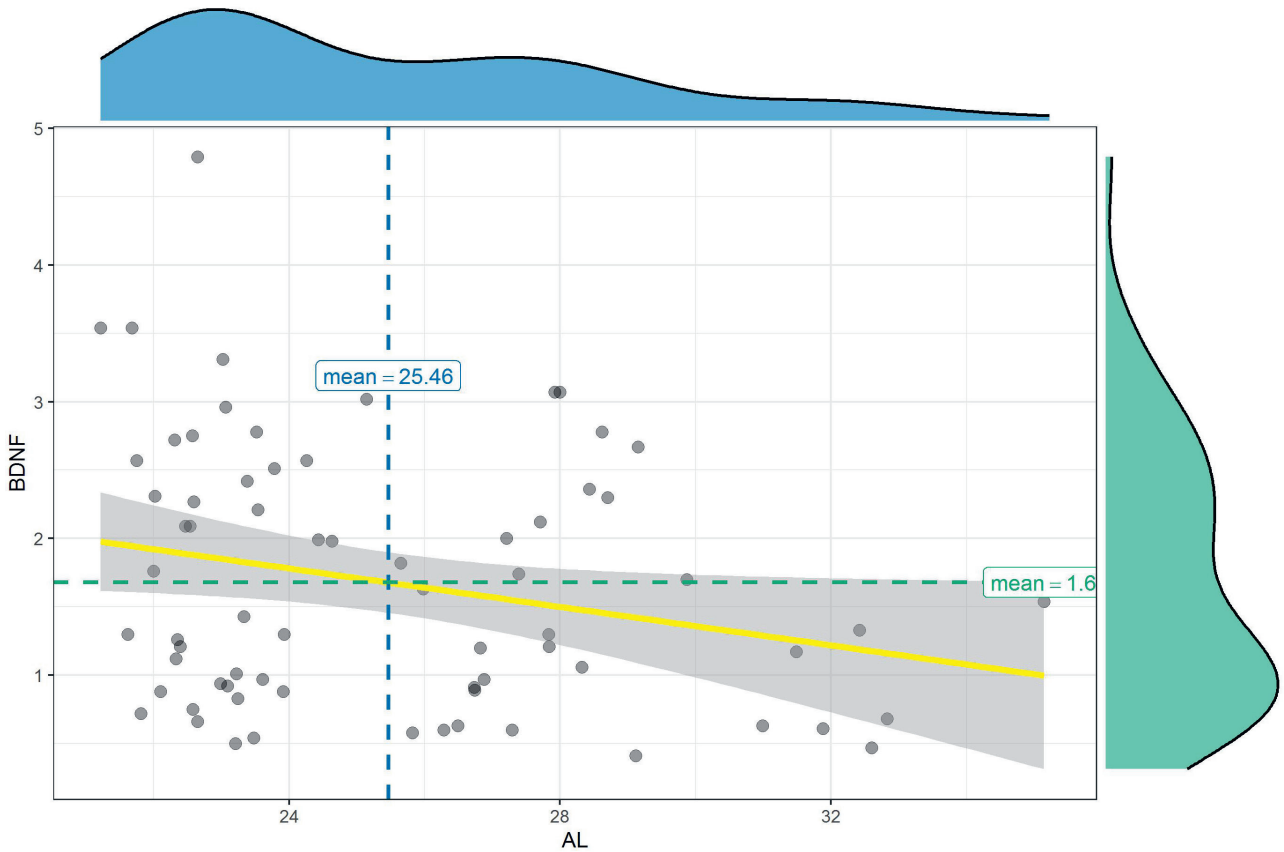

Fig. 3. Correlation between brain-derived neurotrophic factor (BDNF) and the axial length (AL)

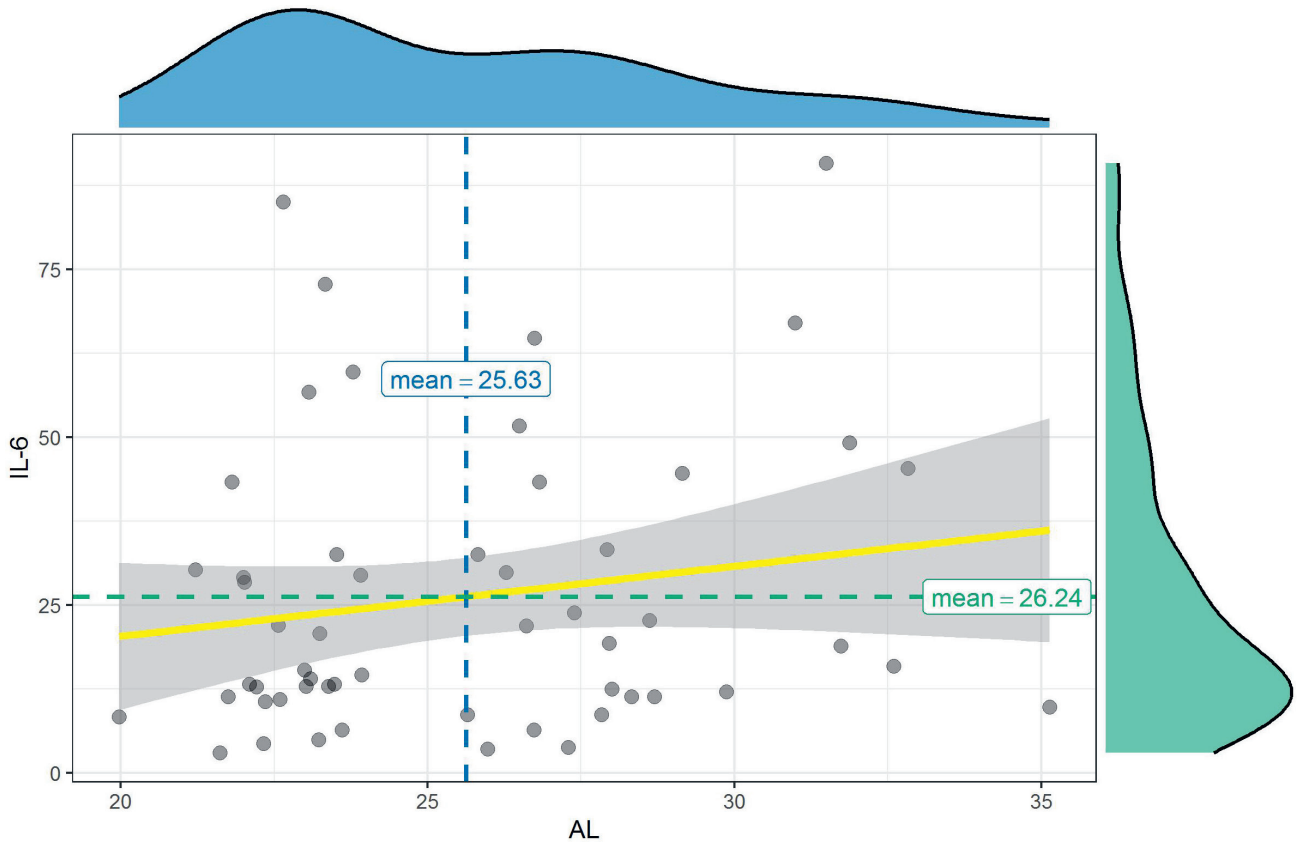

Fig. 4. Correlation between interleukin 6 (IL-6) level and the axial length (AL)

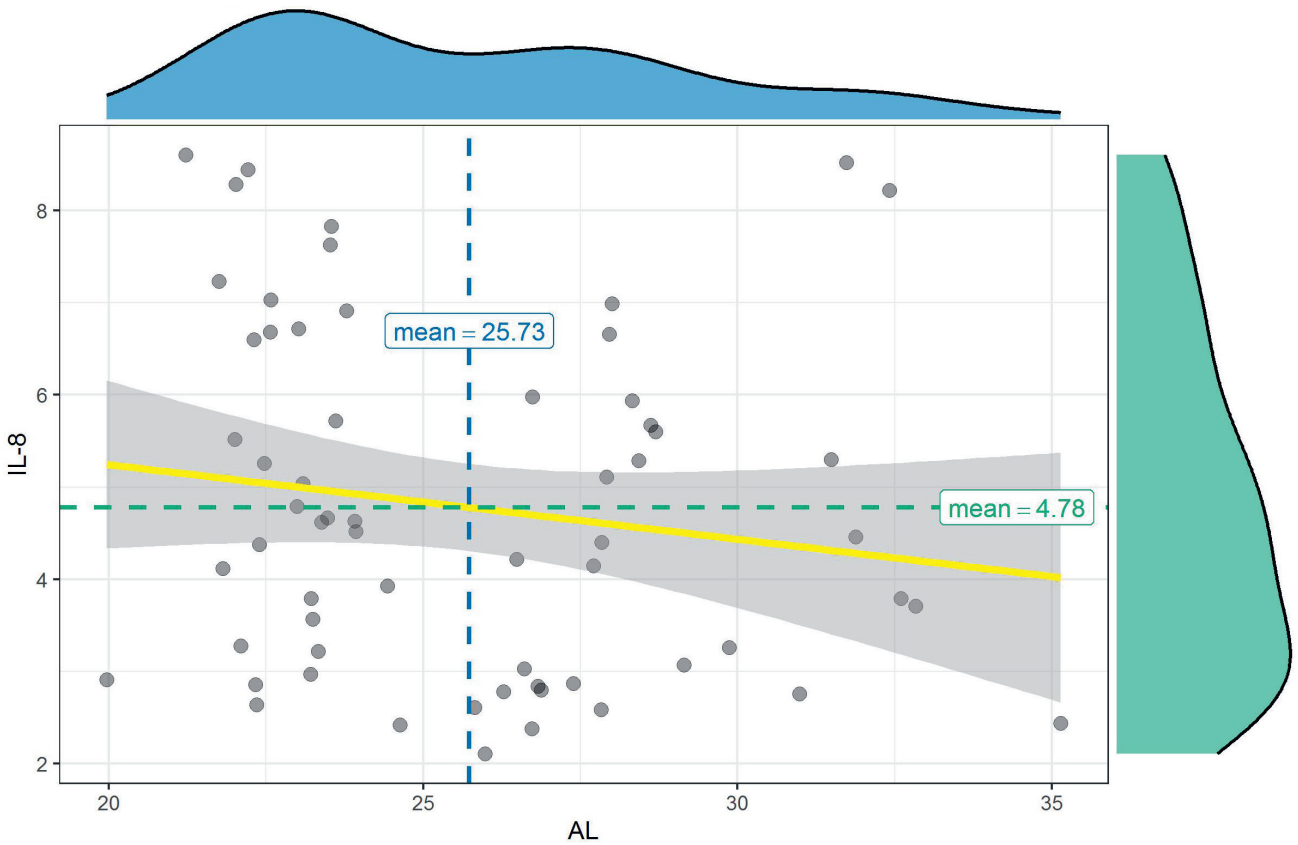

Fig. 5. Correlation between interleukin 8 (IL-8) level and the axial length (AL)

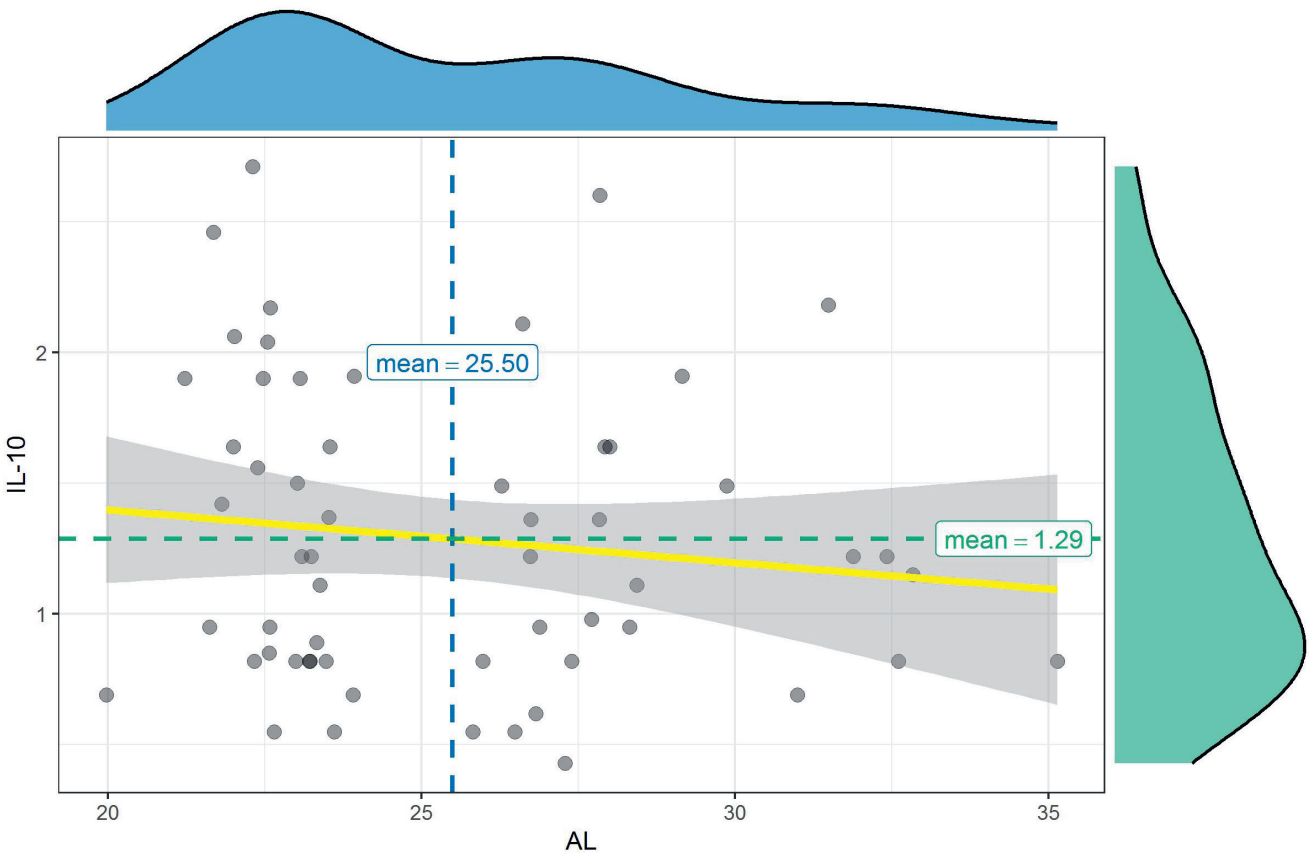

Fig. 6. Correlation between interleukin 10 (IL-10) level and the axial length (AL)

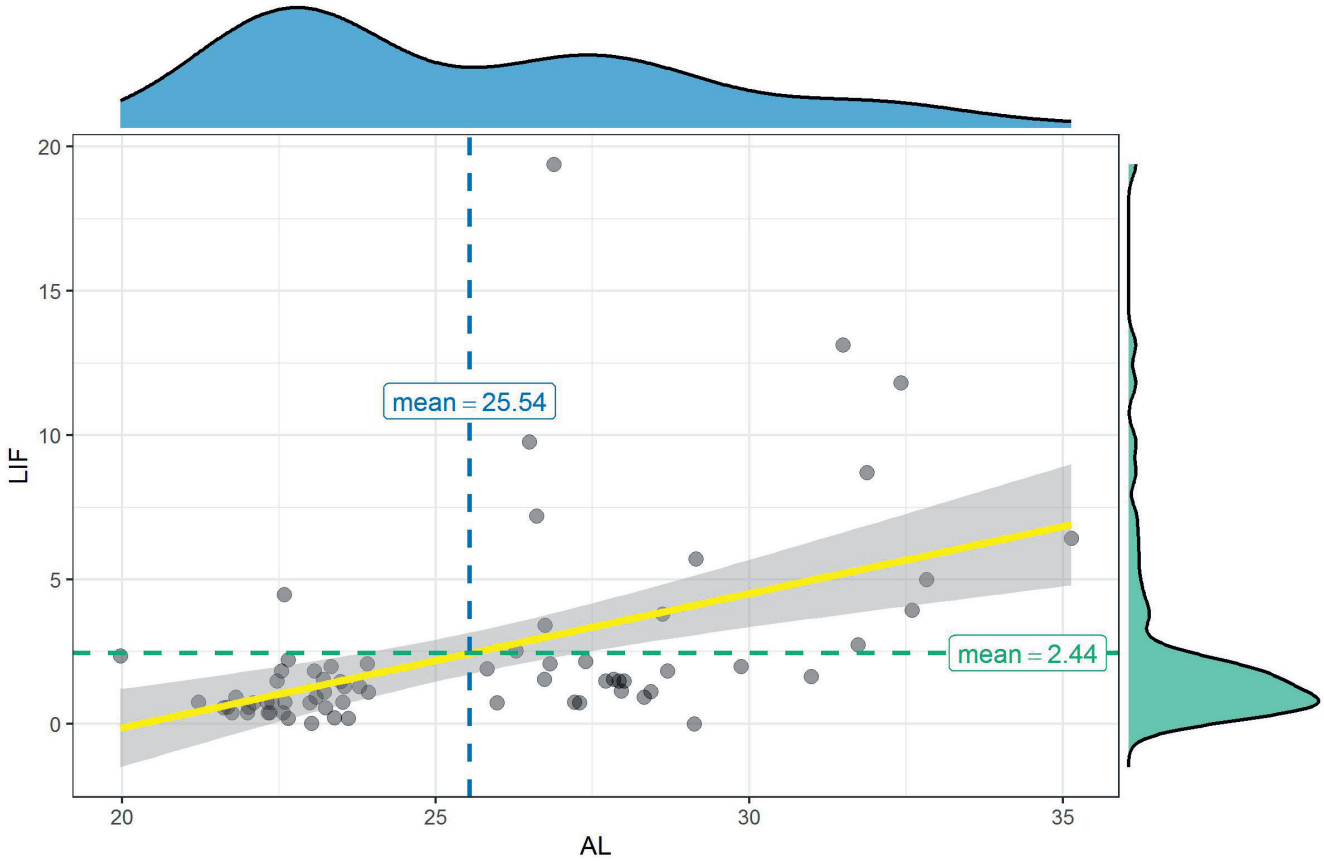

Fig. 7. Correlation between leukemia inhibitory factor (LIF) level and the axial length (AL)

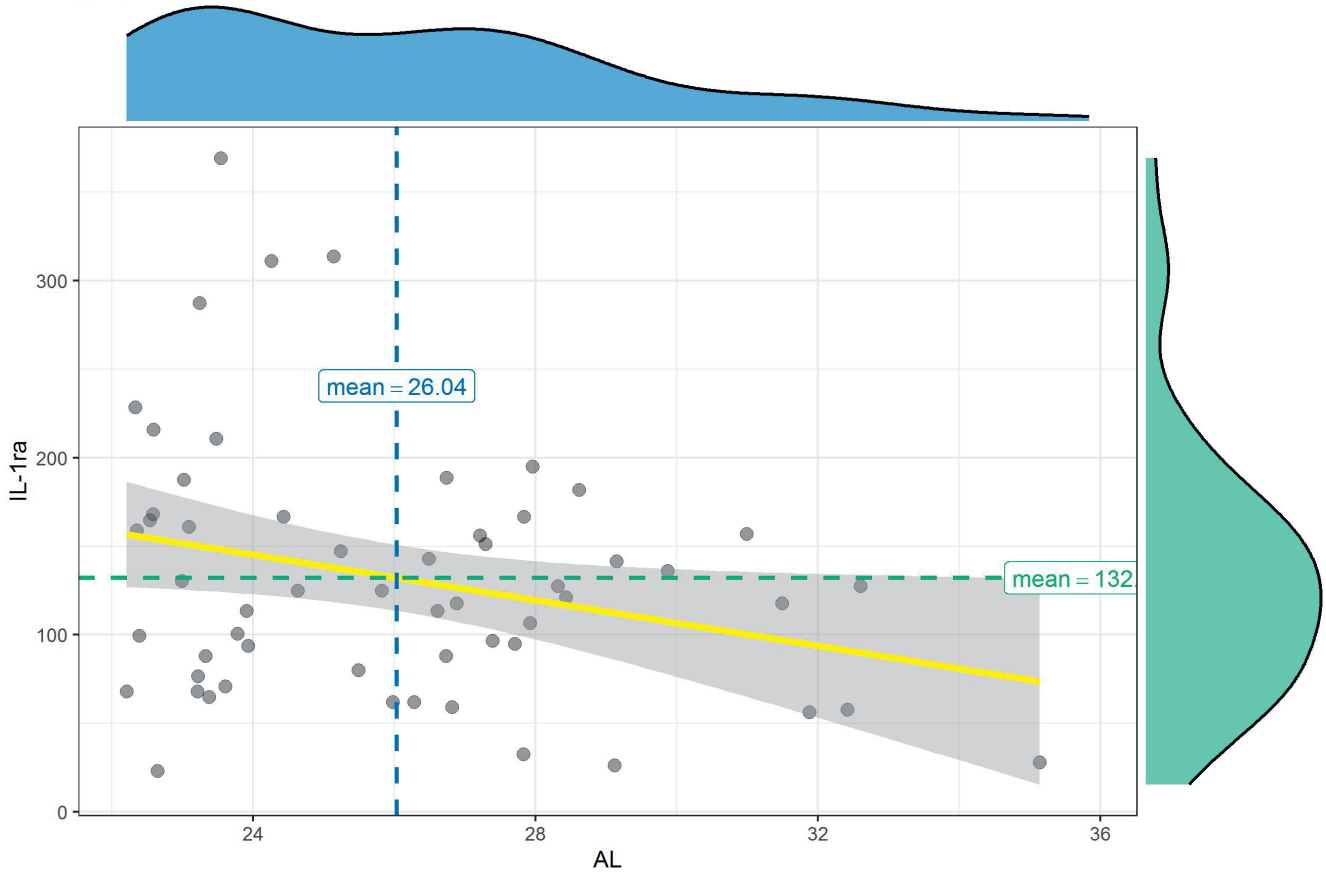

Fig. 8. Correlation between interleukin 1 receptor antagonist (IL-1ra) level and the axial length (AL)

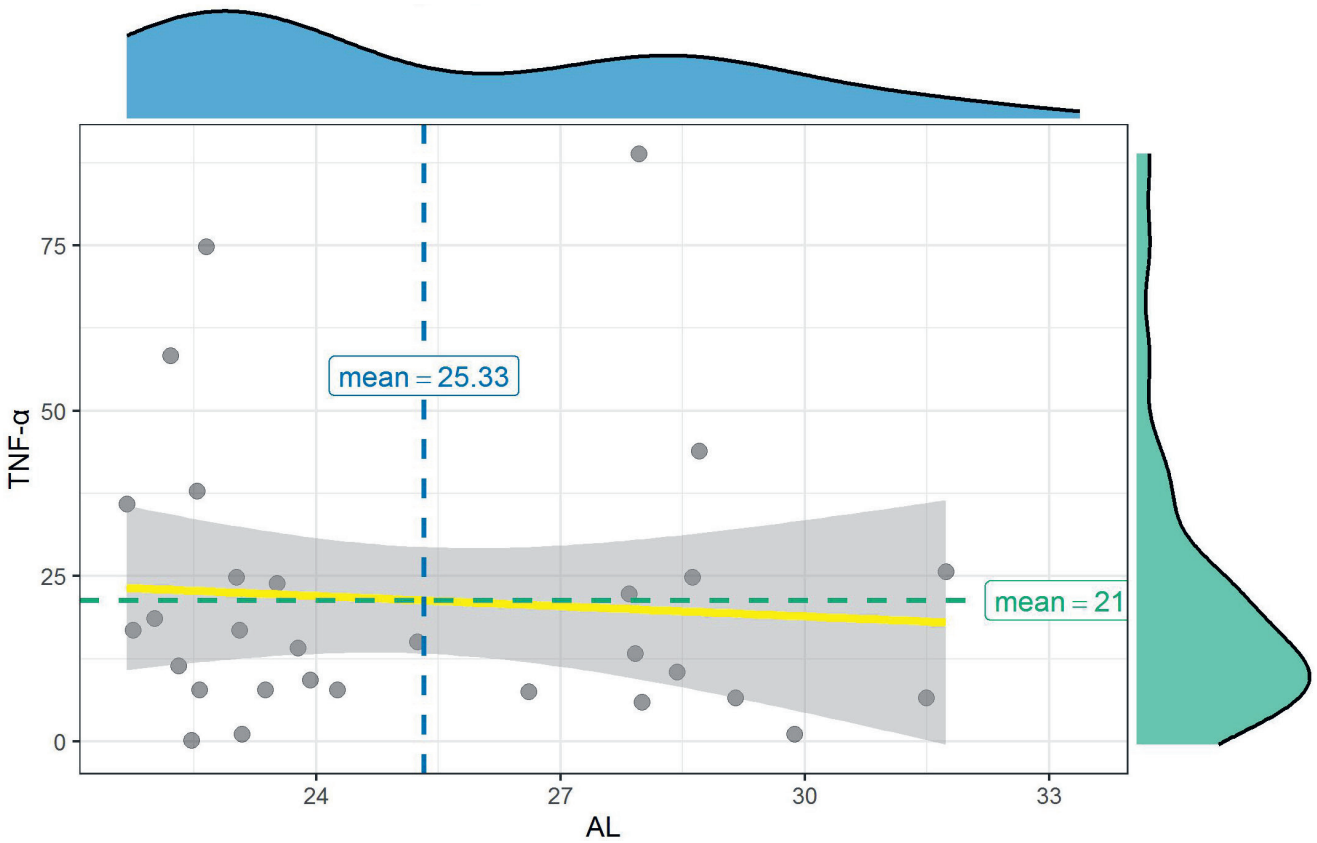

Fig. 9. Correlation between tumor necrosis factor alpha (TNF-α) level and the axial length (AL)

Discussion

In 2012, Bostrom et al. identified an exercise-induced hormone irisin,[6] which is synthesized in several tissues of different species.[16] Irisin[6] is secreted into the circulation after proteolytic cleavage from its cellular form, FNDC5. Irisin can be found not only in the skeletal muscles, but also in brain regions, such as Purkinje cells, paraventricular nucleus and cerebrospinal fluid.[17–19] A few studies investigated irisin immunoreactivity in the eye of dwarf hamsters (*Phodopus roborovskii*). In the retina, irisin was found almost in all layers, except outer nuclear layer. Also, irisin immunoreactivity was observed in the cornea.[9] Moreover, irisin immunoreactivity was found in the neural retina of the crested porcupine (*Hystrix cristata*).[20] To our knowledge, this is the only study showing that irisin exists in the human aqueous humor.

We are all aware that PA has many benefits, including reducing the risk of developing heart disease, stroke and diabetes. It has been speculated that lifestyle changes such as reduced PA, reduced time spend outdoors and more close-up work might be the driving force behind the rapid increase in myopia.[5] Confusion has arisen, because some studies have not distinguished between PA and time spent outdoors. As exercise induces myokine, we decided to analyze irisin in the myopia patients' eyes compared with the control group.

It is difficult to collect the vitreous fluid of these patients, so we tried the analysis of the aqueous humor and found that irisin level in high myopia group is significantly higher than in the controls. In addition, the positive relationship has been found between irisin level and AL. Given the positive result of our study, irisin may be a new research direction in the future. It is worth considering that if physical exercise is good for myopia, the level of irisin produced in consequence of the exercise should be reduced in the long AL group rather than increased. The ideal time to test if PA and myopia are related to each other would be in childhood. This approach, however, will be difficult due to ethical considerations and harvest method. Our samples are from elder people, which may create a selection bias. Another limitation is the lack of serum level of irisin from the subjects. Further experiments are needed to clarify the detailed mechanisms underlying the relationship between PA, myopia and irisin.

Many researchers believe that close-up work is an independent risk factor for myopia.[21–24] However, unlike the role of lack of outdoor activities, this viewpoint still needs to be proved in the future. As people's education level improves, reduced time spent outdoors and more close-up work might be the driving force behind the rapid increase in myopia prevalence. The joint effect of the 2 aspects may be one of the reasons for the increasing incidence of myopia. Our research shows that the intraocular irisin

level increases with the growth of the AL. Current animal experiments have confirmed that irisin can be produced by smooth muscle cells. In other words, the ciliary muscle may also be the main source of irisin in the eye. Therefore, we speculate that the ciliary muscle, which is an important effector of the ocular accommodation mechanism, increases its activity after long-term close-up work, resulting in increased production of irisin in the eye. Therefore, the ocular level of myokine irisin in patients with axial myopia is significantly increased.

On the other hand, few studies have tested the possible relationship between the chronic inflammation and myopia progression.[25–27] One study assumed that inflammation promotes the breakdown of the extracellular matrix (ECM) of the sclera and results in axial elongation. They found a strong association between AL and IL-6: the longer the AL, the higher IL-6 in the aqueous humor.[27] Interleukin 6 is released from the lymphocytes and macrophages, as well as from the skeletal muscle cells, and acts both as a pro-inflammatory cytokine and an anti-inflammatory myokine, depending on the stimuli.[28] In our study, there was no significant difference between 2 groups; the same result was achieved in 1 other study with a smaller sample collection.[29]

Interleukin 6 is related to the increased matrix metalloproteinase 2 (MMP-2) production, especially in neurodegenerative and neuroinflammatory states in human pathophysiology.[30] High myopia-related retinal atrophy, either diffuse or patchy, is a type of neurodegenerative change. The location of the retina is an evagination of the brain and also part of the central nervous system (CNS). Recent studies have shown that the thinning of both the retinal nerve fiber layer and choroid, which are the hallmarks of high myopia, were present in AD,[31–33] which is a neuroinflammatory and neurodegenerative disease. Although we were unable to prove that IL-6 was increased in high myopia patients' eyes, we found a decreased BDNF level compared to control group. The BDNF is a critical regulator of neural plasticity, is known as a widely distributed neurotrophine and plays an important role in synaptic function and neuronal survival.[34] Decreased levels of BDNF have been identified in serum, as well as in hippocampal and cortex samples of AD and PD patients.[35–37] Our result demonstrates the same change in high myopia patients' aqueous humor, which also shows the possible connection between myopia and neurodegenerative diseases.

Leukemia inhibitory factor is a member of the IL-6 cytokine family. The basic expression of LIF is low; however, it has been confirmed to be upregulated at the inflammation site and the serum is elevated systemically after septic shock.[38,39] Leukemia inhibitory factor is expressed in the CNS; it is also a protective cytokine during inflammatory stress[40–44] and a potential neuroprotective cytokine.[45] Studies have reported that LIF plays an important role in the process of retinal degeneration protection via JAK-STAT3 and Akt signaling pathways in animal models of retinal ischemia induced by acute ocular hypertension.[46] The result of our study showed that the LIF level in the long AL group was significantly higher than in the control, and LIF was significantly positively correlated with the AL ($r = 0.486$), indicating that this protective factor was connected with axial myopia progression.

Interleukin 8 is a main chemoattractant for neutrophils. It has been shown that intraocular IL-8 level is higher in age-related macular degeneration (AMD), retinitis pigmentosa (RP) and glaucoma patients.[47–51] Until recently, no study has suggested that IL-8 is related to myopia. We were also unable to find any such association in our samples. Interleukin 10 is an anti-inflammatory cytokine that reduces activation of T cells. A previous study has also shown that IL-10 promotes ocular neovascularization (NV) through macrophage response to retina ischemia.[52] No significant difference of IL-10 level between RP, AMD, glaucoma, and cataract patients has been found by Ten Berge et al.[53] The same result has been shown in our study of IL-10 level, which compared high myopia and control group.

Interleukin 1 receptor antagonist is a natural IL-1ra that has a high affinity for IL-1 receptors.[54] Studies have shown that IL-1ra can reduce various inflammatory reactions caused by IL-1, such as arthritis[55] and graft-versus-host response.[56] Previous animal studies have found that after corneal transplantation, IL-1ra inhibits IL-1 in corneal grafts, and a greater dose of IL-1ra is correlated with a lower expression of interleukin 1 receptor I (IL-1RI) and a lighter inflammatory response in corneal grafts.[57] Our study confirmed that the IL-1ra level in the aqueous humor of the long AL group was significantly lower than that in the other group. Moreover, the longer the AL, the lower the IL-1ra level. Based on the negative correlation, we assumed that higher IL-1ra in the control group suppresses a part of the inflammatory response, and therefore slows the progression of axial myopia. Our result is consistent with previous studies and further confirmed the correlation between myopia and inflammation.

Increased TNF-α levels have been reported in glaucoma patients' intraocular fluid, the trabecular meshwork, optic head, and the retina[58,59]; however, we could not detect TNF-α in most of our samples. As a result, we were unable compare the level in our groups. Cytokines act at concentrations from 10–10 mol/L to 10–15 mol/L to stimulate target cell functions, and such a low concentration range aggravates the detection problems, for instance, causing insufficient assay sensitivity. Different laboratory techniques and diverse patients may be a reason.

Limitations

Our samples are from elder people, which may create a selection bias. Another limitation is the lack of serum level of irisin from the subjects. Further experiments are needed to clarify the detailed mechanisms underlying the relationship between PA, myopia and irisin.

Conclusions

Irisin levels in the aqueous humor are elevated in high myopia patients, which opens a new direction to discover the relationship between PA and myopia. We also found BDNF decreased in high myopia patients' eye, which demonstrated the connection between myopia and neurodegenerative diseases, for instance, AD. The mechanisms of how they influence the myopia progression still need to be clarified.

ORCID iDs

Xijuan Wang https://orcid.org/0000-0002-1488-6223
Li Mingwu https://orcid.org/0000-0002-1143-7027
Ruimao Zheng https://orcid.org/0000-0003-4218-7531
Ting Cui https://orcid.org/0000-0002-9022-3421
Jiayin Qin https://orcid.org/0000-0002-3777-5673
Zhijie Su https://orcid.org/0000-0003-4476-5569
Meng Shang https://orcid.org/0000-0002-6962-9064
Yongzhen Bao https://orcid.org/0000-0001-5896-7239

References

1. Liu HH, Xu L, Wang YX, Wang S, You QS, Jonas JB. Prevalence and progression of myopic retinopathy in Chinese adults: The Beijing Eye Study. *Ophthalmology*. 2010;117(9):1763–1768. doi:10.1016/j.ophtha.2010.01.020
2. Hsu WM, Cheng CY, Liu JH, Tsai SY, Chou P. Prevalence and causes of visual impairment in an elderly Chinese population in Taiwan: The Shihpai Eye Study. *Ophthalmology*. 2004;111(1):62–69. doi:10.1016/j.ophtha.2003.05.011
3. Holden BA, Fricke TR, Wilson DA, et al. Global prevalence of myopia and high myopia and temporal trends from 2000 through 2050. *Ophthalmology*. 2016;123(5):1036–1042. doi:10.1016/j.ophtha.2016.01.006
4. Flitcroft DI. The complex interactions of retinal, optical and environmental factors in myopia aetiology. *Prog Retin Eye Res*. 2012;31(6):622–660. doi:10.1016/j.preteyeres.2012.06.004
5. Saw SM, Chua WH, Wu HM, Yap E, Chia KS, Stone RA. Myopia: Gene–environment interaction. *Ann Acad Med Singap*. 2000;29(3):290–297. PMID:10976381
6. Bostrom P, Wu J, Jedrychowski MP, et al. A PGC1-α-dependent myokine that drives brown-fat-like development of white fat and thermogenesis. *Nature*. 2012;481(7382):463–468. doi:10.1038/nature10777
7. Moreno M, Moreno-Navarrete JM, Serrano M, et al. Circulating irisin levels are positively associated with metabolic risk factors in sedentary subjects. *PLoS One*. 2015;10(4):e0124100. doi:10.1371/journal.pone.0124100
8. Fitzgerald ME, Wildsoet CF, Reiner A. Temporal relationship of choroidal blood flow and thickness changes during recovery from form deprivation myopia in chicks. *Exp Eye Res*. 2002;74(5):561–570. doi:10.1006/exer.2002.1142
9. Gur FM, Timurkaan S, Gencer Tarakci B, et al. Identification of immunohistochemical localization of irisin in the dwarf hamster (*Phodopus roborovskii*) tissues. *Anat Histol Embryol*. 2018;47(2):174–179. doi:10.1111/ahe.12345
10. Ahlskog JE. Does vigorous exercise have a neuroprotective effect in Parkinson disease? *Neurology*. 2011;77(3):288–294. doi:10.1212/WNL.0b013e318225ab66
11. Buchman AS, Boyle PA, Yu L, Shah RC, Wilson RS, Bennett DA. Total daily physical activity and the risk of AD and cognitive decline in older adults. *Neurology*. 2012;78(17):1323–1329. doi:10.1212/WNL.0b013e3182535d35
12. Young MF, Valaris S, Wrann CD. A role for FNDC5/irisin in the beneficial effects of exercise on the brain and in neurodegenerative diseases. *Prog Cardiovasc Dis*. 2019;62(2):172–178. doi:10.1016/j.pcad.2019.02.007
13. Takahashi H, Takase H, Terada Y, Mochizuki M, Ohno-Matsui K. Acquired myopia in Vogt–Koyanagi–Harada disease. *Int Ophthalmol*. 2019;39(3):521–531. doi:10.1007/s10792-018-0841-2
14. Bakri SJ, Snyder MR, Reid JM, Pulido JS, Ezzat MK, Singh RJ. Pharmacokinetics of intravitreal ranibizumab (Lucentis). *Ophthalmology*. 2007;114(12):2179–2182. doi:10.1016/j.ophtha.2007.09.012
15. Funatsu H, Yamashita H, Noma H, et al. Aqueous humor levels of cytokines are related to vitreous levels and progression of diabetic retinopathy in diabetic patients. *Graefes Arch Clin Exp Ophthalmol*. 2005;243(1):3–8. doi:10.1007/s00417-004-0950-7
16. Peng J, Deng X, Huang W, et al. Irisin protects against neuronal injury induced by oxygen-glucose deprivation in part depends on the inhibition of ROS-NLRP3 inflammatory signaling pathway. *Mol Immunol*. 2017;91:185–194. doi:10.1016/j.molimm.2017.09.014
17. Dun SL, Lyu RM, Chen YH, Chang JK, Luo JJ, Dun NJ. Irisin-immunoreactivity in neural and non-neural cells of the rodent. *Neuroscience*. 2013;240:155–162. doi:10.1016/j.neuroscience.2013.02.050
18. Martinez Munoz IY, Camarillo Romero EDS, Garduno Garcia JJ. Irisin as a novel metabolic biomarker: Present knowledge and future directions. *Int J Endocrinol*. 2018;2018:7816806. doi:10.1155/2018/7816806
19. Piya MK, Harte AL, Sivakumar K, et al. The identification of irisin in human cerebrospinal fluid: Influence of adiposity, metabolic markers, and gestational diabetes. *Am J Physiol Endocrinol Metab*. 2014;306(5):E512–E518. doi:10.1152/ajpendo.00308.2013
20. Gencer Tarakci B, Girgin A, Timurkaan S, Yalcin MH, Gur FM, Karan M. Immunohistochemical localization of irisin in skin, eye, and thyroid and pineal glands of the crested porcupine (*Hystrix cristata*). *Biotech Histochem*. 2016;91(6):423–427. doi:10.1080/10520295.2016.1183820
21. Ip JM, Saw SM, Rose KA, et al. Role of near work in myopia: Findings in a sample of Australian school children. *Invest Ophthalmol Vis Sci*. 2008;49(7):2903–2910. doi:10.1167/iovs.07-0804
22. Quek TP, Chua CG, Chong CS, et al. Prevalence of refractive errors in teenage high school students in Singapore. *Ophthalmic Physiol Opt*. 2004;24(1):47–55. doi:10.1046/j.1475-1313.2003.00166.x
23. Lin Z, Vasudevan B, Mao GY, et al. The influence of near work on myopic refractive change in urban students in Beijing: A three-year follow-up report. *Graefes Arch Clin Exp Ophthalmol*. 2016;254(11):2247–2255. doi:10.1007/s00417-016-3440-9
24. Huang HM, Chang DS, Wu PC. The association between near work activities and myopia in children: A systematic review and meta-analysis. *PLoS One*. 2015;10(10):e0140419. doi:10.1371/journal.pone.0140419
25. Herbort CP, Papadia M, Neri P. Myopia and inflammation. *J Ophthalmic Vis Res*. 2011;6(4):270–283. PMID:22454750
26. Lin HJ, Wei CC, Chang CY, et al. Role of chronic inflammation in myopia progression: Clinical evidence and experimental validation. *EBioMedicine*. 2016;10:269–281. doi:10.1016/j.ebiom.2016.07.021
27. Yuan J, Wu S, Wang Y, Pan S, Wang P, Cheng L. Inflammatory cytokines in highly myopic eyes. *Sci Rep*. 2019;9:3517. doi:10.1038/s41598-019-39652-x
28. Pedersen BK. The diseasome of physical inactivity and the role of myokines in muscle fat cross talk. *J Physiol*. 2009;587(Pt 23):5559–5568. doi:10.1113/jphysiol.2009.179515
29. Zhu D, Yang DY, Guo YY, et al. Intracameral interleukin 1beta, 6, 8, 10, 12p, tumor necrosis factor alpha and vascular endothelial growth factor and axial length in patients with cataract. *PLoS One*. 2015;10(2):e0117777. doi:10.1371/journal.pone.0117777
30. Pagenstecher A, Stalder AK, Kincaid CL, Shapiro SD, Campbell IL. Differential expression of matrix metalloproteinase and tissue inhibitor of matrix metalloproteinase genes in the mouse central nervous system in normal and inflammatory states. *Am J Pathol*. 1998;152(3):729–741. PMID:9502415
31. Cheung CY, Ong YT, Hilal S, et al. Retinal ganglion cell analysis using high-definition optical coherence tomography in patients with mild cognitive impairment and Alzheimer's disease. *J Alzheimers Dis*. 2015;45(1):45–56. doi:10.3233/JAD-141659
32. Kirbas S, Turkyilmaz K, Anlar O, Tufekci A, Durmus M. Retinal nerve fiber layer thickness in patients with Alzheimer disease. *J Neuroophthalmol*. 2013;33(1):58–61. doi:10.1097/WNO.0b013e318267fd5f
33. Gharbiya M, Trebbastoni A, Parisi F, et al. Choroidal thinning as a new finding in Alzheimer's disease: Evidence from enhanced depth imaging spectral domain optical coherence tomography. *J Alzheimers Dis*. 2014;40(4):907–917. doi:10.3233/JAD-132039
34. Diniz BS, Teixeira AL. Brain-derived neurotrophic factor and Alzheimer's disease: Physiopathology and beyond. *Neuromolecular Med*. 2011;13(4):217–222. doi:10.1007/s12017-011-8154-x

35. Michalski B, Fahnestock M. Pro-brain-derived neurotrophic factor is decreased in parietal cortex in Alzheimer's disease. *Brain Res Mol Brain Res*. 2003;111(1–2):148–154. doi:10.1016/s0169-328x(03)00003-2
36. Arancibia S, Silhol M, Mouliere F, et al. Protective effect of BDNF against beta-amyloid induced neurotoxicity in vitro and in vivo in rats. *Neurobiol Dis*. 2008;31(3):316–326. doi:10.1016/j.nbd.2008.05.012
37. Giampa C, Montagna E, Dato C, Melone MA, Bernardi G, Fusco FR. Systemic delivery of recombinant brain-derived neurotrophic factor (BDNF) in the R6/2 mouse model of Huntington's disease. *PLoS One*. 2013;8(5):e64037. doi:10.1371/journal.pone.0064037
38. Waring PM, Carroll GJ, Kandiah DA, Buirski G, Metcalf D. Increased levels of leukemia inhibitory factor in synovial fluid from patients with rheumatoid arthritis and other inflammatory arthritides. *Arthritis Rheum*. 1993;36(7):911–915. doi:10.1002/art.1780360707
39. Waring P, Wycherley K, Cary D, Nicola N, Metcalf D. Leukemia inhibitory factor levels are elevated in septic shock and various inflammatory body fluids. *J Clin Invest*. 1992;90(5):2031–2037. doi:10.1172/JCI116083
40. Sugiura S, Lahav R, Han J, et al. Leukaemia inhibitory factor is required for normal inflammatory responses to injury in the peripheral and central nervous systems in vivo and is chemotactic for macrophages in vitro. *Eur J Neurosci*. 2000;12(2):457–466. doi:10.1046/j.1460-9568.2000.00922.x
41. Bugga L, Gadient RA, Kwan K, Stewart CL, Patterson PH. Analysis of neuronal and glial phenotypes in brains of mice deficient in leukemia inhibitory factor. *J Neurobiol*. 1998;36(4):509–524. doi:10.1002/(sici)1097-4695(19980915)36:4<509::aid-neu5>3.0.co;2-#
42. Banner LR, Moayeri NN, Patterson PH. Leukemia inhibitory factor is expressed in astrocytes following cortical brain injury. *Exp Neurol*. 1997;147(1):1–9. doi:10.1006/exnr.1997.6536
43. Lemke R, Gadient RA, Schliebs R, Bigl V, Patterson PH. Neuronal expression of leukemia inhibitory factor (LIF) in the rat brain. *Neurosci Lett*. 1996;215(3):205–208. doi:10.1016/0304-3940(96)12986-4
44. Patterson PH. The emerging neuropoietic cytokine family: First CDF/LIF, CNTF and IL-6; Next ONC, MGF, GCSF? *Curr Opin Neurobiol*. 1992;2(1):94–97. doi:10.1016/0959-4388(92)90169-I
45. Heinrich PC, Behrmann I, Haan S, Hermanns HM, Muller-Newen G, Schaper F. Principles of interleukin (IL)-6-type cytokine signaling and its regulation. *Biochem J*. 2003;374(Pt 1):1–20. doi:10.1042/BJ20030407
46. Hu Q, Huang C, Wang Y, Wu R. Expression of leukemia inhibitory factor in the rat retina following acute ocular hypertension. *Mol Med Rep*. 2015;12(5):6577–6583. doi:10.3892/mmr.2015.4287
47. Jonas JB, Tao Y, Neumaier M, Findeisen P. Cytokine concentration in aqueous humour of eyes with exudative age-related macular degeneration. *Acta Ophthalmol*. 2012;90(5):e381–e388. doi:10.1111/j.1755-3768.2012.02414.x
48. Knickelbein JE, Chan CC, Sen HN, Ferris FL, Nussenblatt RB. Inflammatory mechanisms of age-related macular degeneration. *Int Ophthalmol Clin*. 2015;55(3):63–78. doi:10.1097/IIO.0000000000000073
49. Freedman J, Iserovich P. Pro-inflammatory cytokines in glaucomatous aqueous and encysted Molteno implant blebs and their relationship to pressure. *Invest Ophthalmol Vis Sci*. 2013;54(7):4851–4855. doi:10.1167/iovs.13-12274
50. Yoshida N, Ikeda Y, Notomi S, et al. Clinical evidence of sustained chronic inflammatory reaction in retinitis pigmentosa. *Ophthalmology*. 2013;120(1):100–105. doi:10.1016/j.ophtha.2012.07.006
51. Rezar-Dreindl S, Sacu S, Eibenberger K, et al. The intraocular cytokine profile and therapeutic response in persistent neovascular age-related macular degeneration. *Invest Ophthalmol Vis Sci*. 2016;57(10):4144–4150. doi:10.1167/iovs.16-19772
52. Dace DS, Khan AA, Kelly J, Apte RS. Interleukin-10 promotes pathological angiogenesis by regulating macrophage response to hypoxia during development. *PLoS One*. 2008;3(10):e3381. doi:10.1371/journal.pone.0003381
53. Ten Berge JC, Fazil Z, van den Born I, et al. Intraocular cytokine profile and autoimmune reactions in retinitis pigmentosa, age-related macular degeneration, glaucoma and cataract. *Acta Ophthalmol*. 2019;97(2):185–192. doi:10.1111/aos.13899
54. Eisenberg SP, Evans RJ, Arend WP, et al. Primary structure and functional expression from complementary DNA of a human interleukin-1 receptor antagonist. *Nature*. 1990;343(6256):341–346. doi:10.1038/343341a0
55. Garlanda C, Riva F, Bonavita E, Mantovani A. Negative regulatory receptors of the IL-1 family. *Semin Immunol*. 2013;25(6):408–415. doi:10.1016/j.smim.2013.10.019
56. Dana MR, Dai R, Zhu S, Yamada J, Streilein JW. Interleukin-1 receptor antagonist suppresses Langerhans cell activity and promotes ocular immune privilege. *Invest Ophthalmol Vis Sci*. 1998;39(1):70–77. PMID:9430547
57. Zhang WH, Zhai CB, Pan ZQ, Wu YY. Effects of IL-1 receptor antagonist on the level of cytokine in the rat corneal grafts and aqueous humor after corneal transplantation [in Chinese]. *Zhonghua Yan Ke Za Zhi*. 2003;39:587–591. PMID:14766071
58. Taurone S, Ripandelli G, Pacella E, et al. Potential regulatory molecules in the human trabecular meshwork of patients with glaucoma: Immunohistochemical profile of a number of inflammatory cytokines. *Mol Med Rep*. 2015;11(2):1384–1390. doi:10.3892/mmr.2014.2772
59. Khalef N, Labib H, Helmy H, El Hamid MA, Moemen L, Fahmy I. Levels of cytokines in the aqueous humor of eyes with primary open angle glaucoma, pseudoexfoliation glaucoma and cataract. *Electron Physician*. 2017;9(2):3833–3837. doi:10.19082/3833

Is N-terminal pro-brain type natriuretic peptide a useful marker in newborns with heart defects?

Agata Tarkowska[A–D,F], Wanda Furmaga-Jabłońska[A,C,E,F]

Department of Neonate and Infant Pathology, Medical University of Lublin, Poland

A – research concept and design; B – collection and/or assembly of data; C – data analysis and interpretation;
D – writing the article; E – critical revision of the article; F – final approval of the article

Advances in Clinical and Experimental Medicine, ISSN 1899–5276 (print), ISSN 2451–2680 (online) *Adv Clin Exp Med*. 2021;30(9):905–912

Address for correspondence
Agata Tarkowska
agatatarkowska@umlub.pl

Funding sources
None declared

Conflict of interest
None declared

Received on September 27, 2020
Reviewed on November 1, 2020
Accepted on December 17, 2020

Published online on July 30, 2021

Cite as
Tarkowska A, Furmaga-Jabłońska W. Is N-terminal pro-brain type natriuretic peptide a useful marker in newborns with heart defects? *Adv Clin Exp Med*. 2021;30(9):905–912. doi:10.17219/acem/131746

DOI
10.17219/acem/131746

Abstract

Background. Heart diseases are currently a significant cause of morbidity and mortality in newborns. The existing diagnostic methods are often not sufficient or, in many cases, cannot be used. Great advances have been achieved in medical knowledge concerning biomarkers for the diagnosis of circulatory system disorders in adult patients. Among these biomarkers, N-terminal pro-brain type natriuretic peptide (NT-proBNP) plays a main role. However, in the existing literature, there is not enough data concerning the physiological features of this biomarker in newborns and its potential use in neonatal cardiac diagnostics.

Objectives. To evaluate the diagnostic usefulness of NT-proBNP measurements in correlation with other markers of circulatory failure and myocardial damage in newborns with heart defects.

Materials and methods. This study involved 126 newborns. Patients were divided into 2 main groups: group I included infants with congenital heart defects (CHD) and group II (control) included healthy neonates. Newborns with CHD were further divided into 2 subgroups: group Ia with simple shunts and group Ib with combined heart defects. Patients in group I were further divided according to the hemodynamic significance of CHD. The NT-proBNP level was evaluated using the CARDIAC proBNP immunologic test (Cobas h232; Roche Diagnostics, Basel, Switzerland).

Results. The NT-proBNP concentrations were significantly higher in newborns with CHD compared to healthy ones. Newborns with combined heart defects had higher levels of NT-proBNP than newborns with simple shunts. The NT-proBNP concentrations in newborns with CHD correlated with echocardiographic parameters of hemodynamic significance and with left ventricular ejection fraction (LVEF). Additionally, NT-proBNP correlated with clinical symptoms of heart failure (HF; Ross classification, Reithmann's score).

Conclusions. Statistically significant differences in NT-proBNP level between newborns with heart defects and healthy controls were shown. In newborns with heart diseases, significant correlations were found between NT-proBNP level and the type of heart defect (simple shunt or combined defects), the hemodynamic significance of the defect, LVEF, and the clinical intensity of HF.

Key words: congenital heart defects, biomarkers, newborns, NT-proBNP

Background

Congenital heart defects (CHD) continue to represent a significant diagnostic and therapeutic challenge in newborns.[1] Regarding the specificity of hemodynamic changes during the neonatal period, even serious life-threatening defects may initially appear as non-characteristic, oligosymptomatic diseases. The diagnostic methods currently available are often insufficient or cannot be used in infants due to the limited approach.[2]

Regarding the diagnostic procedures for circulatory system disorders in adults, biochemical markers of heart failure (HF) represent an important tool of unquestionable significance. Among them, brain natriuretic peptide (BNP) and its N-terminal prohormone (NT-proBNP) play key roles.[3] The abovementioned biomarkers might prove to be highly useful in neonatal patients as well.[4–6] However, data concerning adult patients cannot be directly applied to pediatric populations. The clinical value of these markers must be evaluated separately for every age group before applying them in practice.[5]

The BNP is a neurohormone of cardiac origin secreted by the ventricular myocardium in response to increased heart wall tension due to volume and pressure overload, enhanced left ventricle (LV) mass, and a decreased shortening and ejection fraction (SF and EF).[4,6] Natriuretic hormones are synthesized as preprohormones, and both BNP and NT-proBNP can be found in serum. Comparative studies show good correlation of the serum concentrations of both of these hormones.[7]

Concentrations of BNP and NT-proBNP depend on ventricle overload and increase together with the degree of LV dysfunction. At the same time, elevated NT-proBNP may indicate a preclinical stage of HF.[8]

Serum NT-proBNP is strictly connected with left ventricular ejection fraction (LVEF) and SF, and thus enables detection of their decreases with high diagnostic sensitivity and specificity.[8] In patients with CHD, NT-proBNP is assumed to depend on pressure and volume overload.[9] As of yet, no other serum biomarkers are known to indicate HF.

The essence of our project was to search for the least invasive, yet the most sensitive and specific, biomarker that will enable a more complete diagnosis of circulatory system conditions in newborns with cardiac problems. No biochemical markers of neonatal circulatory failure are in routine use yet, and the only potential marker currently known is BNF.

Objectives

The aim of this study was to evaluate the diagnostic usefulness of NT-proBNP measurements in correlation with other markers of circulatory failure in newborns with heart defects. We hope that, in the end, the obtained results and conclusions drawn will allow us to state whether the assessed markers are good diagnostic tools for the abovementioned cardiological problems of the neonatal period and whether they should be routinely used for the assessment of circulatory failure in newborns with heart defects.

Materials and methods

Study design

This study was designed to determine whether the concentration of NT-proBNP in the serum of newborns with CHD is statistically significantly higher than in the control group, and whether the concentration of NT-proBNP is significantly related to the following factors: the type and severity of the defect, the stage of HF assessed on the basis of clinical symptoms, and echocardiographic exponents.

Based on the obtained results, an attempt was made to initially assess whether this indicator is sensitive and specific enough to be used for the detection of pre-symptomatic circulatory failure in newborns.

The study group included patients born in the Lublin Voivodeship (a province of Poland) and hospitalized in the Department of Neonate and Infant Pathology (control group) and in the Department of Pediatric Cardiology (patients with CHD) of the University Children's Hospital of Lublin, Poland.

The study included a total of 126 infants divided into 2 main groups: group I (67 patients with CHD) and group II (control group, 59 healthy infants). As some of the patients were preterm infants, we used both chronological and postmenstrual age for the analysis. The characteristics of the included infants are shown in Table 1.

Table 1. Characteristics of the studied group. Number of patients: 126 (69 boys and 57 girls)

Variable	Minimum	Maximum	Mean
Gestational age	25 weeks	42 weeks	38 weeks
Chronological age	6 days	135 days	21 days
Postmenstrual age	34 weeks	46 weeks	41 weeks
Birth weight	585 g	5400 g	3137 g

Patients with a history of perinatal asphyxia or with severe conditions other than CHD were not included in the study.

The study protocol was approved by the Ethics Committee of Medical University of Lublin. All participants' legal guardians have signed the informed consent.

Variables and data sources

All included infants underwent echocardiographic evaluation with LV SF assessment with flow assessment (continuous wave Doppler) and flow visualization using color

Table 2. Characteristics of heart defects in group I

Division of heart defects			Type of defect	Number of patients
Patients with congenital heart defects (group I) n = 67	significant hemodynamic defects (group Ii) n = 38	simple shunts (group Ia) n = 21	ASD+VSD	12
			ASD+VSD+PDA	4
			ASD+PDA	3
			PDA	1
			ASD	1
		combined heart defects (group Ib) n = 17	CAVC	6
			FT4	3
			PS+ASD	2
			CoA+ASD	2
			TA	1
			L-TGA+VSD+PS	1
			DORV+ASD	1
			SA+PS+ASD+PDA	1
	defects without hemodynamic significance (group In) n = 29	simple shunts (group Ia) n = 28	ASD	12
			ASD+PDA	8
			ASD+VSD	5
			ASD+VSD+PDA	3
		combined heart defects (group Ib) n = 1	PS+ASD	1

n – number of patients; ASD – atrial septum defect; VSD – ventricular septum defect; PDA – persistent ductus arteriosus; CoA – aortic coarctation; PS – pulmonary stenosis; DORV – double outlet right ventricle; TA – truncus arteriosus; TGA – transposition of great arteries; SA – aortic stenosis.

Doppler. Echocardiographic examination was performed according to standard protocol with the use of a SEQUOIA C256 device and Acuson 7v3c probe (frequency 3–7 MHz) (Siemens AG, Munich, Germany). The SF was calculated on the basis of the following formula:

$$SF = [(LVDd - LVSd) / LVDd] \times 100\%,$$

where LVSd – LV systolic diameter and LVDd – LV diastolic diameter, both measured in one-dimensional M-mode registration. Newborns from group I were subsequently divided in 2 ways. First, 2 subgroups were formed according to the type of heart defect: group Ia with simple shunts and group IIb with combined heart defects. Group Ia consisted of 49 patients. The following defects were diagnosed in this group: atrial septum defect (ASD, 13 cases), persistent ductus arteriosus (PDA, 1 case), or coexistence of 2 or 3 shunts, 35 cases: (ASD+VSD, 17 cases), (ASD+PA, 11 cases), (ASD+VSD+PDA, 7 cases). Eighteen newborns were assigned to group IIb. The following defects were diagnosed in this group: common atrioventricular canal (CAVC, 6 cases), tetralogy of Fallot (TOF, 3 cases), pulmonary stenosis (PS) with ASD (3 cases), aortic coarctation (CoA, 2 cases), truncus arteriosus (PTA, 1 case), levo-transposition of the great arteries (L-TGA) with PS and VSD (1 case), double outlet right ventricle (DORV) with ASD (1 case), and aortic stenosis (SA) with PS, ASD, and PDA (1 case).

Another subdivision was formed based on echocardiographic parameters of hemodynamic significance: group Ii included patients with hemodynamically significant CHD, while group In included patients presenting with hemodynamically non-significant heart defects. Group Ii consisted of 38 patients and group In consisted of 29 patients.

The results of the echocardiographic assessment are summarized in Table 2.

Additionally, all patients underwent clinical evaluation for the presence and severity of HF signs and symptoms. Both Ross classification for heart failure in children[11,12] and Reithmann's pediatric heart failure score[13] were applied independently for each studied newborn. The comparison of echocardiographic evaluation and clinical HF scoring results is presented in Table 3.

The NT-proBNP concentrations were evaluated with the Roche CARDIAC proBNP immunologic test using a Cobas h232 system (Roche Diagnostics, Basel, Switzerland). The newborns in the control group were considered healthy; however, some might have clinically silent CHD.

Table 3. Comparison of echocardiographic evaluation and clinical heart failure scoring in group I

Hemodynamic significance of CHD (evaluated with ECHO)	The Ross classification score (mean and SD)	The Reithmann classification score (mean and SD)
Significant (n = 38)	1.53 ±1.01	1.34 ±2.22
Nonsignificant (n = 29)	1 ±0	0.11 ±0.42

CHD – congenital heart defect; SD – standard deviation.

To eliminate this potential bias, all patients from the control group underwent echocardiographic evaluation.

The number of relevant patients hospitalized in the departments during the study period determined the sample size.

We examined the association of clinical signs of HF in infants evaluated using 2 different classifications with the results of echocardiographic evaluation and NT-proBNP concentrations.

Statistical analyses

The obtained results, after checking the normality of the distribution, were statistically analyzed using the appropriate tests with STATISTICA v. 9.0 software (StatSoft Inc., Tulsa, USA). The right-handed asymmetry of certain distributions was eliminated by means of logarithmic transformation. Dependency analysis was performed based on Pearson's linear correlation coefficient (r) or Spearman's (R) rank correlation test and t-tests of the significance of the correlation coefficient in the studied groups. The strength of association between 2 nominal variables was evaluated by the use of the Cramer's V coefficient. A p-value less than 0.05 ($p < 0.05$) was considered statistically significant.

Results

The analyses revealed that NT-proBNP levels in newborns with heart pathology were significantly higher than those in healthy infants. In the control group, the percentage of newborns with a NT-proBNP level <1500 pg/mL was significantly higher than in the CHD group ($p = 0.0001$). Moreover, there were no patients with NT-proBNP > 3000 pg/mL in group II. In group I, 37% of patients presented such high levels ($p < 0.0001$; Fig. 1, Table 4).

Among the CHD group, a significant correlation was observed concerning NT-proBNP and the type of heart defect: newborns with combined defects presented with higher NT-proBNP levels than those with simple shunts ($p = 0.0004$; Table 5).

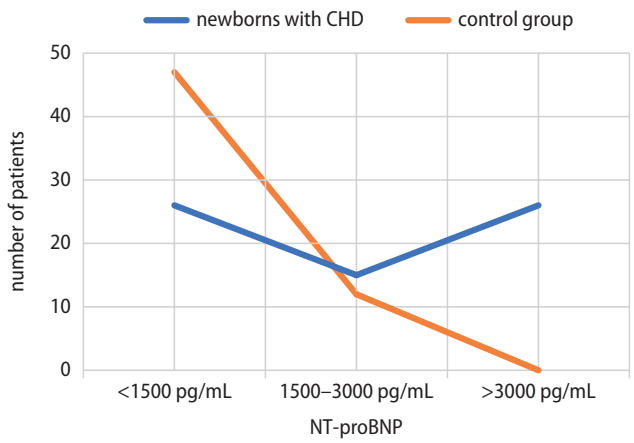

Fig. 1. NT-proBNP concentration ranges in the study groups. CHD – congenital heart defect; NT-pro BNP – N-terminal pro-brain type natriuretic peptide

Table 4. NT-proBNP concentration ranges in studied groups

NT-proBNP [pg/mL]	Newborns with CHD (group I) (n = 67)	Control group (group II) (n = 59)
<1500	26	47
1500–3000	15	12
>3000	26	0

CHD – congenital heart defect; NT-pro BNP – N-terminal pro-brain type natriuretic peptide.

Table 5. NT-proBNP concentration in relationship to the type of heart defect ($p = 0.0004$)

NT-proBNP [pg/mL]	Simple shuts (n = 49)	Combined CHD (n = 18)
<1500	25 (50%)	2 (12%)
1500–3000	13 (27%)	2 (12%)
>3000	11 (23%)	14 (76%)

CHD – congenital heart defect; NT-pro BNP – N-terminal pro-brain type natriuretic peptide.

Table 6. NT-proBNP concentration in relationship to heart defect hemodynamic significance

NT-proBNP (pg/mL)	Significant CHD group Ii (n = 38)	Non-significant CHD group In (n = 29)
<1500	4	23
1500–3000	10	5
>3000	24	1

CHD – congenital heart defect; NT-pro BNP – N-terminal pro-brain type natriuretic peptide.

A significant correlation was also noted between NT-proBNP and CHD hemodynamic significance evaluated with echocardiographic parameters ($p < 0.00001$, Cramer's V coefficient: $V = 0.72$). The percentage of newborns with hemodynamically significant CHD increased with a higher NT-proBNP concentration (Table 6).

Moreover, a strong positive correlation was found between NT-proBNP concentration and severity of HF evaluated using the Ross classification for heart failure in children and Reithmann's pediatric heart failure score. Spearman's rank correlation coefficient for the Ross classification score and serum NT-proBNP was statistically significant ($R = 0.347$, $p = 0.005$). An even stronger positive correlation was observed between Reithmann's heart failure score and NT-pro BNP concentration ($R = 0.448$, $p = 0.0002$). Therefore, the more severe the HF, the higher the NT-proBNP concentration.

Discussion

The BNP and NT-proBNP show high diagnostic accuracy for HF in adults.[14–16] Moreover, they might be used as screening tools as well as markers of response

to treatment and prognosis in asymptomatic adult patients with subclinical heart dysfunction.[15,17,18] According to the literature, BNP and NT-proBNP levels are also elevated in children with heart diseases and can reflect functional efficiency in pediatric chronic HF.[4,10,19,20]

Geiger et al. evaluated 102 pediatric patients aged 0–18 years with CHD and a control group of 65 healthy children. Their study revealed significant differences in NT-proBNP concentrations between children with heart diseases and healthy ones. Additionally, NT-proBNP level is influenced by the presence of clinical symptoms of HF.[20] Similar results were obtained in a study by Mir et al. that aimed to evaluate NT-proBNP serum concentrations in healthy children as well as 31 children aged 1–14 months with clinical signs of HF. The NT-proBNP level was again significantly higher in children with HF than in healthy ones. Moreover, a positive correlation was observed between NT-proBNP level and scoring of clinical HF symptoms. However, the statistical significance depended on the type of pathology (shunts compared to combined defects and cardiomyopathies).[4] A study by Nir et al. confirmed that the mean NT-proBNP serum concentration was higher in patients with hemodynamically significant heart pathologies compared to the control group.[10] Their study compared NT-proBNP concentrations in 55 sick and 58 healthy children aged from 4 months to 15 years. The results were consistent with those of other studies.[4,20] However, the abovementioned studies were conducted in older infants and children, and did not include a neonatal population. Our study revealed that, in newborns with CHD, NT-proBNP serum concentrations were significantly higher than in the control group. Our results are consistent with the data from the literature and confirm the findings of other researchers.[21,22]

Another study concerning newborns with CHD was published by Cantinotti et al.[22] They evaluated BNP in 152 patients with CHD in the 1st month of life (including 6 preterm infants) and 154 healthy neonates as the control group. Patients with CHD showed significantly higher BNP concentrations than healthy ones. Significant differences in BNP concentrations were also observed depending on heart disease characterization: the lowest BNP values were found in patients with right ventricle volume overload, whereas heart defects with LV overload were usually accompanied by higher BNP values. Although some generalizations were possible, BNP did not enable precise distinction between particular heart defects because of the high level of individual variation in concentrations, regardless of pathology type. The conclusion was that BNP could be a cardio-specific marker but is not specific to particular disease entities, which is in accordance with another study.[23] However, our study revealed significant relationships between NT-proBNP and cardiac pathology type in newborns with heart defects. The difference between our results and previous studies probably results from the considerable homogeneity in our patient group. Our study did not include patients with cardiomyopathies or structural disorders other than CHD. This enabled simple division into 2 groups: patients with isolated shunts and patients with combined heart defects. Among newborns with NT-proBNP level >3000 pg/mL, the percentage of patients with combined heart defects was significantly higher than the percentage of newborns with simple shunts. This result may have practical importance, as combined heart defects in newborns usually lead to serious clinical complications and a need for urgent cardiosurgical treatment.

Other researchers have reported elevated serum NT-proBNP levels in children with CHD leading to a left to right shunt.[4,10] In their study, Nir et al. included pediatric patients with heart defects resulting in significant hemodynamic effects.[10] In the studied group, there were 13 patients with a left-to-right shunt. On the basis of this group, the authors revealed that patients with a high pressure leakage (VSD or PDA) presented higher NT-proBNP concentrations than patients with a low-pressure shunt (ASD). Kunii et al. estimated the possibility of using BNP to evaluate leakage significance in a group of 154 children with one of the following abnormalities: VSD, PDA or ASD.[24] The BNP showed a correlation with the Qp:Qs ratio (Qp – pulmonary flow, Qs – systemic flow) for all 3 types of defects. In our study, no correlation was found between left-to-right shunt flow velocity and NT-proBNP concentration in patients with shunts. Similarly, no correlation was found concerning the defect diameter and NT-proBNP concentration. The lack of correlation was probably caused by allocating patients with high and low pressure defects to the same group. The second probable explanation is that some of the defects were hemodynamically insignificant. This explanation seems to be supported by another result – the highly significant correlation between NT-proBNP and hemodynamic significance of the shunt (evaluated on the basis of echocardiographic parameters).

The results of our study may have practical clinical significance, as newborns with inborn heart defects causing serious hemodynamic disturbances typically need urgent cardiologic consultation and treatment. Moreover, serial NT-proBNP measurements in newborns with heart defects may be useful for monitoring hemodynamic disturbances, which quite often increase rapidly in the adaptive period.

In the existing literature, there is limited data concerning the usefulness of the above peptides as markers of cyanotic and other combined heart defects.[25] A study by Hopkins et al. revealed elevated NT-proBNP in 10 adults with cyanotic heart defects (including Eisenmenger's syndrome), despite the lack of increased pressure overload.[26] A study by Koch et al., including 288 children with CHD (33 with TOF) and 152 healthy children in the control group, reported that BNP was not elevated in patients with TOF.[5] The same study showed higher BNP levels in patients with a functional single ventricle compared to healthy children. To date, only a few studies have focused on newborns with severe combined heart defects. Lechner et al.

conducted an interesting study to check if NT-proBNP levels in the cord blood of newborns with CHD were elevated compared to healthy neonates.[27] The study included 60 newborns in which CHD was diagnosed in the prenatal period on the basis of fetal echocardiography. The control group consisted of 200 healthy newborns. All patients from the study group suffered from severe combined heart defects, most of which needed urgent cardiosurgical treatment. However, significant differences in the gestational age and birth weight between the groups were a weak point of the study. On the basis of the NT-proBNP cord blood assay, the authors showed significantly higher concentrations of the marker in newborns with CHD. Additionally, NT-proBNP concentrations in cord blood were significantly higher in patients with a functional single ventricle. Although there were statistically significant differences in NT-proBNP concentrations between healthy newborns and those with CHD, the results in both groups overlapped considerably, which meant that the single cord blood assay did not enable clear identification of sick newborns. The NT-proBNP level was evaluated again in 54 patients between the 3rd and 10th day of life, and NT-proBNP was found to increase compared to cord blood levels in all patients with heart defects.

In our study, clearly elevated NT-proBNP concentrations were observed in newborns with combined heart defects compared to both the control group and newborns with simple shunts. None of the healthy newborns had a NT-proBNP concentration >3000 pg/mL, whereas 26 of the newborns with CHD did.

Both BNP and NT-proBNP have been studied in the context of the identification and evaluation of degree of HF in several pediatric studies.[4,10,20,28–31] Although the studies encompass a small number of patients and include variable heart diseases in children, the results seem to be the same: Regardless of etiology (congenital defect, metabolic disorder, inflammation, ischemia, or primary heart muscle disease), natriuretic peptide concentrations increase in direct proportion to the severity of HF symptoms. In a retrospective study including 36 children with dilated cardiomyopathy, Rusconi et al. evaluated the relationship between HF symptom intensity and NT-proBNP serum concentrations.[32] For each patient, there was a clear relationship between the changes in NT-proBNP and their functional class assessed using New York Heart Association (NYHA)/Ross classification. Similar results were obtained by Mangat et al. in a study of 48 children with HF secondary to left ventricle systolic dysfunction.[31] A progressive increase of NT-proBNP together with an increase in functional NYHA/Ross classification scores was observed.

The abovementioned studies focused on infants and children. However, none of the studies evaluated the correlation between natriuretic peptides and clinical HF scoring in newborns with heart diseases. Furthermore, different researchers used different scales and classification systems to evaluate the severity of HF in infants and children since there is no consensus on which scale best reflects the condition of the circulatory system in pediatric patients.[33] Taking these facts into consideration, in our study, patients were evaluated independently according to 2 different classifications, which seem to be used most often in the existing literature. Each newborn in the study group was evaluated according to the Ross classification score for heart failure in children[11] and the Reithmann's pediatric heart failure score.[13] In order to ensure that both classification systems reliably evaluated heart efficiency, we compared their results with echocardiographic hemodynamic significance evaluation. In the study group, both the Ross classification and Reithmann's score correctly reflected the hemodynamic disturbances established with echocardiographic examination. Subsequently, we evaluated the correlation between NT-proBNP level and HF degree estimated according to each of the 2 classifications. A significant correlation was revealed between NT-proBNP level and HF degree evaluated according to the Ross classification score, and an even stronger significant positive correlation was observed using Reithmann's score. The vNT-proBNP level showed good correlation with clinical parameters of HF in newborns with CHD, similar to other age groups.

According to recently conducted studies, the diagnostic usefulness of BNP and NT-proBNP levels in newborns and infants with CHD might be significant. However, this has not been definitively confirmed, as only a few studies have evaluated natriuretic peptides as cardiovascular markers in this age group. From a theoretical point of view, BNP and NT-proBNP appear promising, especially in the field of neonatal intensive care.[22] The idea of using BNP and NT-proBNP levels as a screening tool to identify newborns with heart defects has received recognition.[21,22,34,35] Parents or legal guardians of newborns showing elevated BNP or NT-proBNP levels would then receive consultation with a cardiologist, and the newborns would undergo additional tests (i.e., echocardiography), in accordance with international guidelines for adult patients.[3]

There are also a few recent studies worth mentioning that have reported a role of NT-proBNP in PDA and bronchopulmonary dysplasia (BPD). Weisz et al. published a broad review on the utility of this biomarker in dealing with PDA in infants; however, they acknowledge that future investigation is still needed.[36] The latest idea is to use NT-proBNP level not only for diagnosis, but also as a predictive marker of therapeutic response in PDA.[37] As for BPD, Xiong et al. published a systematic review concluding that NT-proBNP and BNP levels may be useful for the diagnosis and management of infants with BPD-pulmonary hypertension.[38]

Limitations

The serum concentration of NT-proBNP was determined using the CARDIAC proBNP immunoassay on a Cobas h232 analyzer, and the main limitation of this

study is the relatively narrow measurement range of this device. The device can precisely determine NT-proBNP values only in the range of 60–3000 pg/mL; results outside this range are only shown as <60 pg/mL or >3000 pg/mL. Therefore, it is not possible to determine the mean or median of the results obtained.

Conclusions

There are statistically significant differences in NT-proBNP concentrations in newborns with heart defects compared to healthy subjects. In newborns with heart diseases, NT-proBNP concentration is associated with the type of heart defect (simple shunt or combined defects), hemodynamic significance of the defect, LVEF, and clinical intensity of the disease. Evaluation of NT-proBNP level might be useful as a screening tool for the identification of newborns at risk of a heart disease and for identifying the need for urgent cardiologic consultation. Serial measurements of NT-proBNP level could be useful for monitoring hemodynamic disturbances in newborns with heart diseases. However, future investigations are needed to confirm this.

ORCID iDs

Agata Tarkowska https://orcid.org/0000-0001-9369-4213
Wanda Furmaga-Jabłońska https://orcid.org/0000-0002-6006-7683

References

1. Kawalec W, Kubicka K. Choroby układu krążenia. In: Kubicka K, Kawalec W, eds. Pediatria. Vol. 1. 3rd ed. Warszawa, Poland: PZWL; 2008:270–339.
2. Soongswang J, Durongpisitkul K, Nana A, et al. Cardiac troponin T: A marker in the diagnosis of acute myocarditis in children. *Pediatr Cardiol*. 2005;26(1):45–49. doi:10.1007/s00246-004-0677-6
3. Dickstein K, Cohen-Solal A, Filippatos G, et al; ESC Committee for Practice Guidelines (CPG). ESC Guidelines for the diagnosis and treatment of acute and chronic heart failure 2008: The Task Force for the Diagnosis and Treatment of Acute and Chronic Heart Failure 2008 of the European Society of Cardiology. Developed in collaboration with the Heart Failure Association of the ESC (HFA) and endorsed by the European Society of Intensive Care. *Eur Heart J*. 2008;29(19):2388–2442. doi:10.1093/eurheartj/ehn309
4. Mir TS, Marohn S, Laer S, Eiselt M, Grollomus O, Weil J. Plasma concentrations of N-terminal pro-brain natriuretic peptide in control children from the neonatal to adolescent period and in children with congestive heart failure. *Pediatrics*. 2002;110(6):e76. doi:10.1542/peds.110.6.e76
5. Koch A, Zink S, Singer H. B-type natriuretic peptide in paediatric patients with congenital heart disease. *Eur Heart J*. 2006;27(7):861–866. doi:10.1093/eurheartj/ehi773
6. Jeffires JL, Chang AC. Neurohormonal axis and natriuretic peptides in heart failure. In: Chang AC, Towbin JA, eds. *Heart Failure in Children and Young Adults*. Philadelphia, USA: Elsevier Inc.; 2006:85–95.
7. Bionda C, Bergerot C, Ardail D, et al. Plasma BNP andNT-proBNP assays by automated immunoanalyzers: Analytical and clinical study. *Ann Clin Lab Sci*. 2006;36(3):299–306. PMID:16951271
8. Piechota W. N-końcowy propeptyd natriuretyczny typu B (NT-proBNP) – znaczenie w kardiologii. Warszawa, Poland: Roche Diagnostics Polska; 2005.
9. Cowley CG, Bradley JD, Shaddy RE. B-type natriuretic peptide levels in congenital heart disease. *Pediatr Cardiol*. 2004;25(4):336–340. doi:10.1007/s00246-003-0461-z
10. Nir A, Bar-Oz B, Perles Z, Brooks R, Korach A, Rein AJ. N-terminal pro-B-type natriuretic peptide: Reference plasma levels from birth to adolescence. Elevated levels at birth and in infants and children with heart diseases. *Acta Paediatr*. 2004;93(5):603–607. doi:10.1111/j.1651-2227.2004.tb02984.x
11. Ross RD. Grading the graders of congestive heart failure in children. *J Pediatr*. 2001;138(5):618–620. doi:10.1067/mpd.2001.115707
12. Ross RD, Bollinger RO, Pinsky WW. Grading the severity of congestive heart failure in infants. *Pediatr Cardiol*. 1992;13(2):72–75. doi:10.1007/BF00798207
13. Reithmann C, Reber D, Kozlik-Feldman R, et al. Post-receptor defect of adenyl cyclase in severely failing myocardium from children with congenital heart disease. *Eur J Pharmacol*. 1997;330(1):79–86. doi:10.1016/s0014-2999(97)10131-5
14. Maisel AS, Krishnaswamy P, Nowak RM, et al; Breathing Not Properly Multinational Study Investigators. Rapid measurment of B-type natriuretic peptide in the emergency diagnosis of heart failure. *N Eng J Med*. 2002;347:161–167. doi:10.1056/NEJMoa020233
15. Troughton RW, Frampton CM, Yandle TG, Espiner EA, Nicholls MG, Richards AM. Treatment of heart failure guided by plasma amino-terminal brain natriuretic peptide (N-BNP) concentrations. *Lancet*. 2000;355(9210):1126–1130. doi:10.1016/s0140-6736(00)02060-2
16. Lubien E, DeMaria A, Krishnaswamy P, et al. Utility of B-natriuretic peptide in detecting diastolic dysfunction: Comparison with Doppler velocity recordings. *Circulation*. 2002;105(5):595–601. doi:10.1161/hc0502.103010
17. Redfield MM, Rodeheffer RJ, Jacobsen SJ, Mahoney DW, Bailey KR, Burnett JC Jr. Plasma brain natriuretic peptide to detect preclinical ventricular systolic or diastolic dysfunction: A community-based study. *Circulation*. 2004;109(25):3176–3181. doi:10.1161/01.CIR.0000130845.38133.8F
18. Anand IS, Fisher LD, Chiang YT, et al. Changes in brain natriuretic peptide and norepinephrine over time and mortality and morbidity in the Valsartan Heart Failure Trial (Val-HeFT). *Circulation*. 2004;107(9):1278–1283. doi:10.1161/01.cir.0000054164.99881.00
19. Westerlind A, Wahlander H, Lindstedt G, et al. Clinical signs of heart failure are associated with increased level of natriuretic peptide types B and A in children with congenital heart defects or cardiomyopathy. *Acta Paediatr*. 2004;93(3):340–345. doi:10.1080/08035250410022756
20. Geiger R, Hammerer-Lercher A, Url C, Schweigmann U, et al. NT-proBNP concentrations indicate cardiac disease in pediatric patients. *Int J Cardiol*. 2007;123(1):63–65. doi:10.1016/j.ijcard.2006.11.087
21. Law YM, Hoyer AW, Reller MD, Silberbach M. Accuracy of plasma B-type natriuretic peptide to diagnose significant cardiovascular disease in children: The Better Not Pout children! study. *J Am Coll Cardiol*. 2009;54(15):1467–1475. doi:10.1016/j.jacc.2009.06.020
22. Cantinotti M, Storti S, Ripoli A, et al. Diagnostic accuracy of B-type natriuretic hormone for congenital heart disease in the first month of life. *Clin Chem Lab Med*. 2010;48(9):1333–1338. doi:10.1515/CCLM.2010.251
23. Emdin M, Vittorini S, Passino C, Clerico A. Old and new biomarkers of heart failure. *Eur J Heart Fail*. 2009;11(4):331–335. doi:10.1093/eurjhf/hfp035
24. Kunii Y, Kamada M, Ohtsuki S, et al. Plasma brain natriuretic peptide and the evaluation of volume overload in infants and children with congenital heart disease. *Acta Med Okayama*. 2003;57(4):191–197. doi:10.18926/AMO/32809
25. El-Khuffash A, Molloy EJ. The use of N-terminal-pro-BNP in preterm infants. *Int J Pediatr*. 2009;2009:175216. doi:10.1155/2009/175216
26. Hopkins WE, Chen Z, Fukagawa NK, Hall C, Knot HJ, LeWinter MM. Increased atrial and brain natriuretic peptides in adults with cyanotic congenital heart disease: Enhanced understanding of the relationship between hypoxia and natriuretic peptide secretion. *Circulation*. 2004;109(23):2872–2877. doi:10.1161/01.CIR.0000129305.25115.80
27. Lechner E, Wiesinger-Eidenberger G, Wagner O, et al. Amino terminal proB-type natriuretic peptide levels are elevated in the cord blood of neonates with congenital heart defect. *Pediatr Res*. 2009;66(4):466–469. doi:10.1203/PDR.0b013e3181b3aee4
28. Hammerer-Lercher A, Neubauer E, Muller S, et al. Head-to-head comparison of N-terminal pro-brain natriuretic peptide, brain natriuretic peptide and N-terminal pro-atrial natriuretic peptide in diagnosing left ventricular dysfunction. *Clin Chim Acta*. 2001;310(2):193–197. doi:10.1016/s0009-8981(01)00578-2

29. Cohen S, Springer C, Avital A, et al. Amino-terminal pro-brain-type natriuretic peptide: Heart or lung disease in pediatric respiratory distress? *Pediatrics*. 2005;115(5):1347–1350. doi:10.1542/peds.2004-1429
30. Nir A, Nasser N. Clinical value of NT-ProBNP and BNP in pediatric cardiology. *J Card Fail*. 2005;11(5 Suppl):76–80. doi:10.1016/j.cardfail.2005.04.009
31. Mangat J, Carter C, Riley G, Foo Y, Burch M. The clinical utility of brain natriuretic peptide in paediatric left ventricular failure. *Eur J Heart Fail*. 2009;11(1):48–52. doi:10.1093/eurjhf/hfn001
32. Rusconi PLD, Ratnasamy C, Mas R, Harmon WG, Colan SD, Lipshultz SE. Serial measurements of serum NT-proBNP as markers of left ventricular systolic function and remodeling in children with heart failure. *Am Heart J*. 2010;160(4):776–783. doi:10.1016/j.ahj.2010.07.012
33. Altman CA, Kung G. Clinical recognition of congestive heart failure in children. In: Chang AC, Towbin JA, eds. *Heart Failure in Children and Young Adults*. Philadelphia, USA: Elsevier Inc.; 2006:201–208.
34. Nir A, Lindinger A, Rauh M, et al. NT-pro-B-type natriuretic peptide in infants and children: Reference values based on combined data from four studies. *Pediatr Cardiol*. 2009;30(1):3–8. doi:10.1007/s00246-008-9258-4
35. El-Khuffash A, Molloy EJ. Are B-type natriuretic peptide (BNP) and N-terminal-pro-BNP useful in neonates? *Arch Dis Child Fetal Neonatal Ed*. 2007;92(4):F320–F324. doi:10.1136/adc.2006.106039
36. Weisz DE, McNamara PJ, El-Khuffash A. Cardiac biomarkers and haemodynamically significant patent ductus arteriosus in preterm infants. *Early Hum Dev*. 2017;105:41–47. doi:10.1016/j.earlhumdev.2016.12.007
37. Hu Y, Jin H, Jiang Y, Du J. Prediction of therapeutic response to cyclooxygenase inhibitors in preterm infants with patent ductus arteriosus. *Pediatr Cardiol*. 2018;39(4):647–652. doi:10.1007/s00246-018-1831-x
38. Xiong T, Kulkarni M, Gokulakrishnan G, Shivanna B, Pammi M. Natriuretic peptides in bronchopulmonary dysplasia: A systematic review. *J Perinatol*. 2020;40(4):607–615. doi:10.1038/s41372-019-0588-2

Influence of high tissue-absorbed dose on anti-thyroid antibodies in radioiodine therapy of Graves' disease patients

Maria Henryka Listewnik[A,C,D], Hanna Piwowarska-Bilska[E], Krystyna Jasiakiewicz[B], Bożena Birkenfeld[F]

Department of Nuclear Medicine, Pomeranian Medical University, Szczecin, Poland

A – research concept and design; B – collection and/or assembly of data; C – data analysis and interpretation;
D – writing the article; E – critical revision of the article; F – final approval of the article

Advances in Clinical and Experimental Medicine, ISSN 1899–5276 (print), ISSN 2451–2680 (online) *Adv Clin Exp Med*. 2021;30(9):913–921

Address for correspondence
Maria Henryka Listewnik
E-mail: listrpam@pum.edu.pl

Funding sources
None declared

Conflict of interest
None declared

Received on February 16, 2021
Reviewed on April 7, 2021
Accepted on May 19, 2021

Published online on August 19, 2021

Cite as
Listewnik MH, Piwowarska-Bilska H, Jasiakiewicz K, Birkenfeld B. Influence of high tissue-absorbed dose on anti-thyroid antibodies in radioiodine therapy of Graves' disease patients. *Adv Clin Exp Med*. 2021;30(9):913–921. doi:10.17219/acem/137779

DOI
10.17219/acem/137779

Abstract

Background. The results of radioactive iodine (RAI) treatment for Graves' disease (GD) are related to the choice of diagnostic and dosimetry protocols, the steroid protection used, and the subsequent ^{131}I dose. The effect of a high tissue-absorbed dose on the level of anti-thyroid antibodies (ATA) has been rarely considered.

Objectives. To estimate the effect of the first RAI therapy with a dose of 250 Gy on anti-thyreoperoxidase (anti-TPO) and anti-thyroid-stimulating hormone (TSH) receptor thyrotropin receptor antibody – TRAb levels in GD patients.

Materials and methods. The analysis encompassed 46 consecutive patients with clinical presentation of GD. We examined the serum levels of TSH, free thyroxine (FT4), anti-TPO, TRAb, thyroid volume (ThV), ^{131}I effective half-life (EHL), introduction of steroid protection, levothyroxine dose used in thyroid replacement therapy – TRT, and effectiveness of treatment.

Results. As a result of RAI treatment, hypothyroidism was found in 35 patients (76.1%), euthyroidism in 7 patients (15.2%) and hyperthyroidism in 4 patients (8.7%). After RAI, we observed ThV reduction and increased anti-TPO ($p = 0.001$ and $p = 0.001$, respectively). It was found that a shorter EHL correlated with a higher baseline TRAb concentration and lower final anti-TPO serum concentration ($p = 0.03$ and $p = 0.01$, respectively). Lower final TRAb was found in patients with steroid protection ($p = 0.049$). Intergroup comparison of patients without steroid protection showed significantly higher final anti-TPO concentation ($p = 0.02$). Intergroup comparison of patients with TRT revealed significantly higher final anti-TPO concentration ($p = 0.04$).

Conclusions. The application of a high absorbed dose of 250 Gy in GD resulted in high efficacy of RAI therapy at 1-year follow-up. An increased ATA level and its relationships with EHL and ThV reduction were observed at 1-year follow-up. There is a possible relationship between steroid protection and anti-TPO concentration.

Key words: hypothyroidism, Graves' disease, radioiodine therapy, thyrotropin receptor antibody (TRAb), thyroid peroxidase antibody (TPOAb)

Background

While numerous aspects of radioactive iodine (RAI) treatment, such as its efficacy, its relation to a high absorbed dose, and its impact on clinical outcome and the shrinkage of thyroid volume (ThV) have been described in the literature, there are still some issues to be addressed.[1] In view of a significant reduction of ThV after RAI therapy, one question worth considering is the influence of the therapy on the final level of anti-thyroid antibodies (ATA).[2,3] Another issue to examine is the possible relationship between the level of ATA and radioiodine turnover, specifically the tracer uptake, radioactive iodine uptake – RAIU and thyroidal ^{131}I effective half-life (EHL).[4] The connection of these factors with the use of steroid protection and the potential subsequent dose of thyroid replacement therapy (TRT) due to post-therapeutic hypothyroidism is another issue to be explored.[5]

We believe that knowledge about the final level of ATA in patients treated with RAI due to Graves' disease (GD) is important in their follow-up. It is especially relevant in specific groups of patients, such as those with previous ophthalmopathy, of advanced age, with a history of breast cancer, or women planning a pregnancy.[6] The question is whether the final evaluation of ATA after RAI therapy in patients with GD should be routinely performed.[7] This paper investigates the practical aspects of using pretherapy measurements of ATA levels and the obtained dosimetric data to adjust the applied tissue-absorbed dose in case of rapid turnover. We aim to explore these factors as potentially clinically valuable information.

There are few publications describing baseline results and detailed follow-up data after RAI therapy with dosimetry data and TRT.[8,9] There is also a growing interest in achieving optimal quality of life for patients after RAI.[10,11]

Objectives

The aim of this study was to estimate the effect of first RAI therapy with a dose of 250 Gy on anti-thyreoperoxidase (anti-TPO) and anti-thyroid-stimulating hormone (TSH) receptor (thyrotropin receptor antibody – TRAb) levels in GD patients.

Materials and methods

We present a prospective study based on data collected in 2010. The study included 46 consecutive patients (mean age: 47.4 ±13 years; range: 17–72 years, median (Me) value of 49.5 years with interquartile range Q1–Q3 of 38.0–58.3 years with clinical presentation of GD and an elevated serum concentration of TRAb, admitted to the Department of Nuclear Medicine at Pomeranian Medical University, Szczecin, Poland. They were individually evaluated by a nuclear medicine specialist and received first RAI therapy. The study group comprised of 38 women (82.6%; mean age: 47.1 ±13.4 years, Me: 48.5 (37.25–57.5) years, range: 17–72 years) and 8 men (7.4%; mean age: 48.9 ±11.3 years, Me: 51 (38.5–59.5) years, range: 31–62 years).

Assessment of thyroid function

Thyroid function tests, including TSH level (reference range: 0.4–4 mIU/L), free thyroxine (FT4) level (reference range: 10–25 pmol/L), anti-TPO (reference range: below 60 IU/mL), and TRAb (reference range: below 1.5 IU/L), were performed before and 12 months after RAI therapy. The TSH level was assessed using an immunoradiometric assay, while FT4, anti-TPO and TRAb were assessed with a radioimmunoassay (TSH 1 RIA, FT4 RIA, anti-TPOn RIA, TRAb Human RIA; Thermo Fisher Scientific, Waltham, USA). The laboratory criterion for recognized GD was a TRAb serum concentration level above 1.5 IU/L.

Patient data

The radioimmunoassay was applied as a first-line therapy in 2 (4.3%) patients, as a second-line therapy in 42 patients (91.4%) and as a third-line therapy in 2 patients (4.3%). Anti-thyroid drugs were used in pre-treatment of 44 patients (95.7%). In 10 of them, the withdrawal period was 90–360 days. In the remaining 34 patients, the withdrawal period was 17.4 ±16.9 days (Me: 13 (6–60) days). No significant difference was found for ATA levels before and after RAI treatment (Mann–Whitney test for baseline anti-TPO and TRAb: U = 152, p = 0.63 and U = 161, p = 0.82, respectively; for final anti-TPO and TRAb: U = 160, p = 0.79 and U = 123, p = 0.71, respectively).

Aside from GD, 5 patients (10.9%) had a comorbid autoimmune disease, including 3 (6.5%) with rheumatoid arthritis and lupus erythematosus and 2 (4.4%) with type 2 diabetes.

Prior to RAI therapy, all patients underwent a standard assessment of RAIU after 4 h, 24 h and 48 h, and a thyroid scan with ^{131}I after 24 h. Thyroid volume was estimated at baseline and final assessment using planimetry phantoms. A final thyroid scan with ^{99m}Tc was performed after 10–12 months.

Pretherapeutic thyroid sonography was performed for all patients. A nodular pattern was found in 20 cases (43.5%). In 4 patients (8.7%), a complementary fine-needle aspiration biopsy was performed in selected thyroid lesions and revealed a benign origin.

Eight patients (17.4%) were orally administered 30 mg prednisone to prevent the exacerbation of GD orbitopathy as a routine practice, starting 1 day prior to RAI therapy. The treatment was continued for 56 consecutive days with tapering by 5 mg every 4–5 days according to the in-house protocol.

The inclusion criteria for steroid therapy were as follows: previous history of ophthalmopathy, younger age; and presence of a large-volume goiter. Steroid protection

was not applied if there were comorbidities with contraindications to prednisone.

Adjuvant anti-thyroid drug therapy during follow-up was used for 5 patients (10.9%). Within this group, 2 patients received protective corticosteroid therapy.

The ^{131}I dose was calculated using the Marinelli formula and administered as a single oral dose in an outpatient setting.[12] The radioiodine dose used was calculated according to the following formula[13]:

$$A = 25 \times m \times AD/RAIU \times EHL$$

where: A – ^{131}I therapeutic activity [MBq]; 25 – unit conversion coefficient; m – volume of thyroid gland using planimetry phantoms [mL]; AD – absorbed dose of ^{131}I [Gy]; RAIU – 24-hour ^{131}I uptake [%], and EHL – ^{131}I effective half-life in the thyroid gland [days].

Patients were administered a dose of 463.6 ±188.3 MBq (median: 400.3 (326.7–588.3) MBq, range: 177.6–969.4 MBq). According to the in-house protocol, EHL estimation was based on the difference in RAIU between 24 h and 48 h. The ^{131}I EHL in the thyroid is 6 days. To explain how EHL was established, we provide the following examples: if RAIU at 48 h and 24 h was 53% and 65%, respectively, the difference (53% and 65%) was 12%. In this case, we assessed EHL to be 4.8 days (6 – 1.2). If RAIU at 48 h and 24 h was both 45%, then the difference was 0 (45% – 45%) and EHL was 6 days. For patients with a RAIU of 61% at 48 h and 60% at 24 h, we assessed EHL as 6.1 days (61% – 60%). In practice, 6 days was used as the longest EHL.

A successful outcome of RAI therapy was defined as normal thyroid function or hypothyroidism. Patients with post-therapeutic hypothyroidism were treated with a daily dose of levothyroxine sufficient to normalize TSH serum level as soon as possible. Persistent hyperthyroidism was identified as failure of radioiodine treatment.

No serious complications in thyroid eye disease were observed apart from persistent eye tearing in 3 (6.5%) patients, who underwent corticosteroid therapy.

The study received a waiver of consent from the Bioethical Committee of the Pomeranian Medical University in Szczecin, Poland (decision No. KB-0012/202/06/17). All procedures involving human participants were in accordance with the ethical standards of the institutional and/or national research committee, and with the 1964 Declaration of Helsinki and its later amendments or comparable ethical standards.

Statistical analyses

To evaluate the normality of the distribution of the studied variables, we used the Shapiro–Wilk test. The data are reported as mean ± standard deviation (M ±SD), range (min–max) and, due to skewed distributions, the median value with the interquartile range (Me (Q1–Q3)).

For each categorical variable, the descriptive statistics included the frequency distribution for categorical variables. The direction and strength of association between variables were measured with Spearman's rho. We used the Mann–Whitney U two-tailed test to compare 2 independent groups and the Kruskal–Wallis H two-tailed test to compare 3 groups. Dunn's test of multiple comparisons following the Kruskal–Wallis test was used for post hoc analysis.

Two related matched samples were examined with the Wilcoxon signed-rank test. For categorical variables, we applied Fisher's exact test with degrees of freedom (df). All data were analyzed using STATISTICA v. 13.3 software (StatSoft, Inc, Tulsa, USA). A p-value <0.05 was regarded as statistically significant.

Results

Out of 46 patients, the treatment was successful in 42 patients (91.3%). Normal thyroid function was observed in 7 patients (15.2%) and hypothyroidism occurred in 35 patients (76.1%). Persistent hyperthyroidism was confirmed in 4 patients (8.7%). In the referred group, no significant difference in the mean age between females and males was found (U = 139.5, p = 0.72).

The rate of average reduction of ThV after RAI therapy was 34.9%. In 7 cases (15.2%), no reduction was observed. The age and the therapeutic doses of radioiodine were comparable between patients treated with TRT and those who did not receive TRT (U = 223.5, p = 0.83 and U = 218, p = 0.73, respectively).

The presence of nodules did not affect the rate of hypothyroidism after RAI (df = 1, p = 0.49). It was noted that patients in the group with thyroid nodules were older and their final TRAb levels were higher as compared to those without nodules (53.2 ±11.5 years, Me: 55.5 (46.5–59) years compared to 42.9 ±12.5 years, Me: 43 (34–52) years, U = 142.5, p = 0.008; 19.3 ±16.6 IU/L, Me: 13.3 (4.3–40) IU/L compared to 8.2 ±9.5 IU/L, Me: 3.6 (1.6–12.2) IU/L, U = 116, p = 0.03). In the group with thyroid nodules, the final anti-TPO level was significantly higher than that at baseline (2270.7 ±1130.6 IU/mL, Me: 2896 (2182.3–3000.0) IU/mL compared to 1554.2 ±1213.2 IU/mL, Me: 2741.5 (308.2–3000) IU/mL, Z = 2.29, p = 0.02).

No correlation between baseline ThV and anti-TPO (rho = 0.05, p = 0.74) or TRAb concentration (rho = –0.07, p = 0.63) was observed. At final evaluation, there was no correlation between post-therapeutic ThV and anti-TPO (rho = 0.11, p = 0.48) or TRAb concentration (rho = –0.19, p = 0.26).

After RAI therapy, an increase in anti-TPO and a decrease in ThV level were found, but there were no significant differences for TRAb. A significant reduction of ThV after therapy was confirmed (Table 1).

The moderate positive correlation between the fold change of final to baseline anti-TPO and the fold change of final to baseline TRAb were both statistically significant (Fig. 1).

Table 1. Biochemical parameters and thyroid volume (ThV) measurements at baseline and final assessment. The data are reported as mean ± standard deviation (M ±SD), range (min–max) and median with interquartile range (Me (Q1–Q3))

Parameter	Baseline assessment	Final assessment	Z-value	p-value
TSH [mIU/L]	0.3 ±0.5 (0.001–2.3) 0.1 (0.02–0.2)	6.0 ±14.9 (0.001–86.7) 1.5 (0.5–6.4)	5.1	<0.001
FT4 [pmol/L]	27.2 ±15.7 (8.4–66.1) 20.5 (15.5–38.3)	16.5 ±4.8 (8–25) 17.8 (12.2–18.8)	1.7	0.09
TRAb [IU/L]	9.1 ±9.8 (1.6–40) 5.3 (3.6–9.8)	13.2 ±14.1 (0.2–40) 6.5 (2.2–21.9)	0.9	0.34
Anti-TPO [IU/mL]	1455.4 ±1258.3 (11.3–3000) 939.5 (209.1–3000)	1984 ±1259.1 (8.4–3000) 2790.4 (432.2–3000)	2.5	<0.001
ThV [mL]	26 ±10.5 (10–77) 23.5 (19.8–32)	15.1 ±5.7 (8–31) 13 (10–20)	4.8	<0.001

TSH – thyroid-stimulating hormone; FT4 – free thyroxine; TRAb – thyrotropin receptor antibody; Anti-TPO – anti-thyreoperoxidase; ThV – thyroid volume.

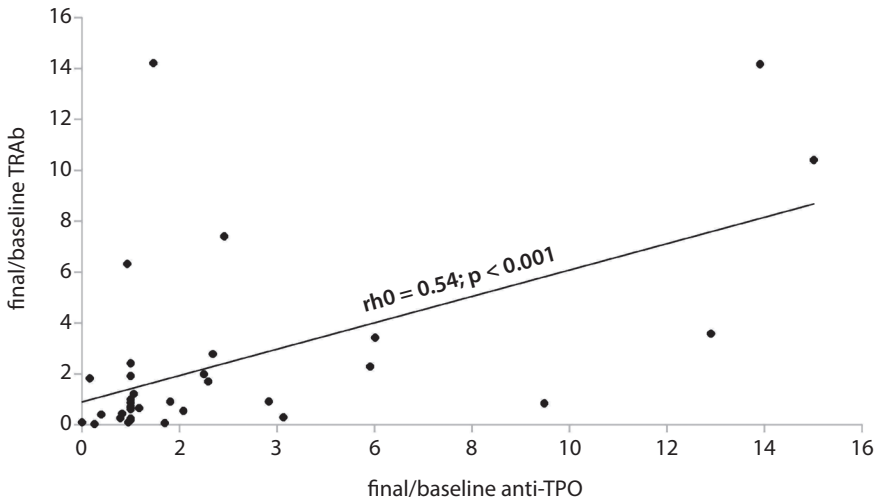

Fig. 1. Correlation between the fold change of anti-thyreoperoxidase (anti-TPO) and thyrotropin receptor antibody (TRAb) levels

Dosimetry considerations

There was a statistically significant but weak correlation between baseline TRAb levels and 4 h, 24 h and 48 h RAIU (rho = 0.38, p = 0.01; rho = 0.36, p = 0.01; and rho = 0.3, p = 0.04, respectively). No relationship between baseline anti-TPO levels and RAIU was found.

We found a weak correlation between EHL and baseline TRAb, and between EHL and final anti-TPO (Fig. 2).

The total value for EHL was 5.71 ±0.38 (4.8–6) days. The results of EHL assessment were categorized into 3 groups (A, B, C) based on the difference between 48 h and 24 h RAIU (range from –12 to 0).

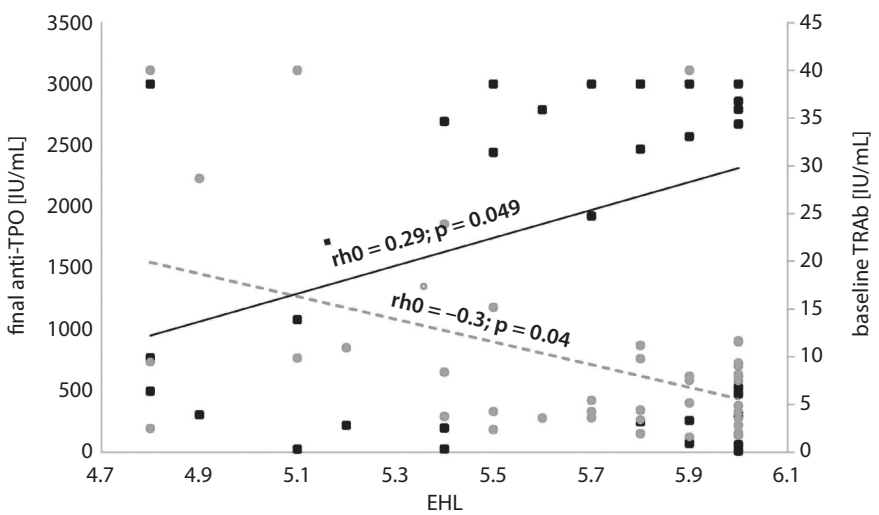

Fig. 2. Correlation between thyroidal turnover expressed as effective half-life (EHL) and final anti-thyreoperoxidase (anti-TPO) and baseline thyrotropin receptor antibody (TRAb)

Table 2A. Anti-thyroid antibodies (ATA), ThV and radioactive iodine uptake (RAIU) prior to radioactive iodine (RAI) therapy ranked according to effective half-life (EHL). The data are reported as mean ± standard deviation (M ±SD), range (min–max) and median with interquartile range (Me (Q1–Q3))

Parameter	Group A (n = 10) 48 h and 24 h RAIU difference range from –12 to –6				Group B (n = 17) 48 h and 24 h RAIU difference range from –5 to –1				Group C (n = 19) 48 h and 24 h RAIU difference range 0			
	baseline	final	Z-value	p-value	baseline	final	Z-value	p-value	baseline	final	Z-value	p-value
TRAb [IU/L]	17.7 ±14.3 (2.5–40) 10.4 (8.4–28.7)	14.9 ±16.1 (0.3–40) 8.3 (2.4–29)	1.2	0.24	7.7 ±9.1 (1.6–40) 4.4 (3.6–7.9)	11.9 ±12.3 (1.6–40) 6.2 (3.6–16.3)	0.8	0.41	5.7 ±3.3 (1.7–11.7) 4.2 (2.8–8.1)	13.8 ±15.8 (0.2–40) 5.7 (1.3–29.6)	1.4	0.16
Anti-TPO [IU/mL]	828.2 ±964.1 (11.3–3000) 493.8 (119.9–1373.1)	880 ±1090 (22.2–3000) 399.4 (196.4–1078.6)	0.06	0.95	1617.9 ±1350.1 (38.8–3000) 1806.1 (232.5–3000)	2339.3 ±1067.9 (70.3–3000) 3000 (2441.5–3000)	2.2	0.03	1640.2 ±1262.4 (28.7–3000) 1159.6 (391.2–3000)	2247.2 ±1219.1 (8.4–3000) 3000 (525–3000)	1.5	0.14
ThV [mL]	27.1 ±5.5 (22–38) 25.5 (23–28)	14.3 ±6.9 (8–27) 12 (10–15)	2.7	0.008	28.3 ±14.6 (17–77) 22 (20–35)	14.6 ±6.7 (8–31) 12 (10–18)	3.3	<0.001	23.6 ±9 (10–36) 22 (15–32)	16 ±5.1 (10–25) 15 (12–20)	2.2	0.03
RAIU 4 h [%]	55.9 ±16.9 (16–77) 58 (49–68)				36.8 ±18.2 (13–73) 36 (20–42)				27.3 ±14.2 (13–56) 21 (15–37)			
RAIU 24 h [%]	66.4 ±9.9 (42–76) 68.5 (65–72)				54.6 ±18.6 (18–83) 52 (45–71)				45.3 ±12.5 (25–69) 45 (36–55)			
RAIU 48 h [%]	57.3 ±9.2 (36–66) 60 (53–65)				52.1 ±18 (16–81) 51 (44–67)				45.9 ±12.7 (25–69) 45 (37–58)			

TRAb – thyrotropin receptor antibody; Anti-TPO – anti-thyreoperoxidase; ThV – thyroid volume; RAIU – radioactive iodine uptake.

Table 2B. Anti-thyroid antibodies (ATA), ThV and radioactive iodine uptake (RAIU) prior to radioactive iodine (RAI) therapy ranked according to effective half-life (EHL). The data are reported as mean ± standard deviation (M ±SD), range (min–max) and median with interquartile range (Me (Q1–Q3))

Parameter	$p\text{-value}_{baseline\ \&\ final}$							
	U_{AB}	$p\text{-value}_{A\ vs\ B}$	U_{AC}	$p\text{-value}_{A\ vs\ C}$	U_{BC}	$p\text{-value}_{B\ vs\ C}$	H	$p\text{-value}_{A\ vs\ B\ vs\ C}$
TRAb [IU/L]	42 & 65.5	0.03 (0.08)* & 0.89	39 & 55.5	0.009 (0.03)* & 0.78	151.5 & 117.5	0.75 & 0.71	7.1 & 0.2	0.03 & 0.92
Anti-TPO [IU/mL]	57.5 & 33.5	0.17 & 0.008 (0.04)*	57 & 41.5	0.09 & 0.01 (0.03)*	151 & 153.5	0.75 & 0.8	3.3 & 8.7	0.19 & 0.01
ThV [mL]	66.5 & 58.5	0.36 & 0.78	70.5 & 55.5	0.27 & 0.26	129 & 189.5	0.32 & 0.25	2.1 & 2	0.36 & 0.37
RAIU 4 h [%]	32.5	0.007 (0.049)*	22.0	<0.001 (<0.001)*	113.5	0.13	13.1	0.002
RAIU 24 h [%]	52	0.1	17.5	<0.001 (0.002)*	103.5	0.07	12.4	0.002
RAIU 48 h [%]	66	0.36	42.5	0.01	122.5	0.22	5.4	0.07

TRAb – thyrotropin receptor antibody; Anti-TPO – anti-thyreoperoxidase; ThV - thyroid volume; RAIU – radioactive iodine uptake; * Dunn's multiple comparison test.

For groups A, B and C, EHL was established as 5.09 ±0.26 (4.8–5.4) days, 5.75 ±0.15 (5.5–5.9) days and 6 (6–6) days, respectively (Table 2A, Table 2B).

The categorization presented above had no impact on the final outcome (df = 2, p = 0.25). There were statistically significant differences between all groups for baseline TRAb (H = 7.1, p = 0.03). More specifically, the significant difference was found between group A and C, with higher baseline TRAb level for group A (p = 0.03).

There were statistically significant differences between all groups for final anti-TPO level (H = 8.7, p = 0.01). In this case, the significant difference was found between groups A and B and between groups A and C, group with the lowest final anti-TPO level for group A (p = 0.04 and p = 0.03, respectively). The implementation of steroid protection or lack of it in all 3 EHL groups had no impact on the final assessment of (RAI) therapy (whether the patients were cured or not) (df = 2, p = 0.61).

Steroid protection

No differences in hypothyroidism frequency after RAI therapy were observed between patients who did (n = 8) or did not (n = 38) receive steroid protection (df = 1, p = 0.66), as assessed with Fisher's exact test. Patients with steroid protection were younger and their baseline volume and administered therapeutic activity of ^{131}I were higher, but their final TRAb was lower, compared to patients without glucocorticoids. Patients without glucocorticoids showed a significantly higher final anti-TPO serum concentration in the intragroup comparison (Table 3).

Thyroid replacement therapy

Out of 35 patients (76.1%) with hypothyroidism, thyroid replacement therapy (TRT) was used in 31 (67.4%) cases. The daily average dose of levothyroxine was 85.7 ±36.2 µg (Me: 75 (62.5–112) µg) with a range of 25–200 µg.

Both groups showed significant differences in ThV before and after RAI. Final ThV was higher for patients without TRT. Comparing baseline to final data in patients with TRT, the serum concentration of anti-TPO increased. For TRAb, no differences were observed. In our study, neither baseline nor final concentrations of ATA were different between patients, irrespective of TRT (Table 4).

Discussion

The presented analysis of data on RAI therapy using a high tissue-absorbed dose of 250 Gy for 46 consecutive patients with GD, previously pretreated with an anti-thyroid drug indicates the need to monitor antibody levels after RAI therapy.

The study group was homogeneous in terms of both the applied absorbed dose and ATA baseline and final measurements. Although the study comprised a relatively small group of patients, many topical issues have been raised. We considered the influence of RAI on ATA with respect to ThV reduction, the usage of steroid protection, and TRT due to post-therapeutic hypothyroidism.

An absorbed dose of 250 Gy is regarded as ablative and can be increased up to 350 Gy according to the European Association of Nuclear Medicine (EANM) guidelines.[14] It should be noted that some publications give the final administered ^{131}I activity value rather than the absorbed dose.[15–20] Common usage of Gy (grays) to express the absorbed dose to thyroid tissue would be helpful for comparing treatment effects and analyzing the influence of particular factors.[21]

In our patient group, where RAI was generally a second-line therapy, 67.4% of patients had TRT at 1-year follow-up. We found no differences in baseline TRAb concentration between patients with or without subsequent TRT.

A recent long-term study by Sjölin et al. was based on a group of 1186 patients with hyperthyroidism, of whom 324 (27.3%) had received RAI as first-line treatment, most often with an absorbed dose of 120 Gy.[11] In the RAI therapy group, 83% of patients had hypothyroidism and 77.3% received TRT at 8 ±0.9 years follow-up. Lack of dosimetry details and different choices regarding treatment make comparison impossible, but the rates of patients with TRT are slightly different, as we had 76.1% patients with hypothyroidism and 67.4% patients under TRT. However, longer follow-up could increase the rate of hypothyroidism. The rate percentage of patients with TRT (not only the total rate of hypothyroidism) is rarely taken into consideration in the literature.

The results presented in the current study are different from those of previous research, especially in terms of the rate of persistent hyperthyroidism. Aung et al. reported that 17% of patients had persistent hyperthyroidism 1 year after RAI therapy.[16] Fanning et al. reported that 20.7% of patients required further treatment.[19] In our group, 8.7% of patients had persistent hyperthyroidism 1 year after RAI. The achieved low failure rate proves the efficacy of RAI treatment with the use of ablative doses.

The mean patient age of 47.4 (17–72) years in our paper is almost identical to that reported in a meta-analysis by Törring et al. – a mean age of 47 (35–57) years.[10] An older age might be an independent factor for an increased level of antibodies, especially anti-TPO.[22]

In our group of patients, 20 (43.5%) had nodular changes. Some authors have described the co-existence of thyroid nodules in GD and ATA in patients treated with RAI. Stoynova et al. reported a similar frequency of thyroid nodularity regardless of the TRAb level in a group previously treated with anti-thyroid drugs.[23] In our group, a significant difference in TRAb levels after RAI was noted.

Mekova and Boyanov found an increased concentration of anti-TPO in 71.4% of patients without nodules among patients with newly diagnosed GD.[24] In contrast to their

Table 3. Selected parameters (biochemical data, ThV, age of patients, and applied RAI activity) categorized according to the application of steroid protection. The data are reported as mean ± standard deviation (M ±SD), range (min–max) and median with interquartile range (Me (Q1–Q3))

Parameter	Encorton (+) n = 8				Encorton (–) n = 38				Encorton (+)/Encorton (–)			
	baseline	final	Z-value	p-value	baseline	final	Z-value	p-value	$U_{baseline}$	$p\text{-value}_{baseline}$	U_{final}	$p\text{-value}_{final}$
TSH [mIU/L]	0.2 ±0.5 (0.001–1.6) 0.05 (0.02–0.07)	8.8 ±18.6 (0.09–54.4) 2.1 (0.8–5)	2.1	0.04	0.3 ±0.5 (0.001–2.3) 0.08 (0.02–0.3)	6 ±14.3 (0.001–86.7) 1.5 (0.5–6.4)	4.7	<0.001	121	0.38	142	0.79
FT4 [pmol/L]	30 ±14.8 (18.5–54.8) 24.5 (19.9–38.8)	15.6 ±4.7 (8.6–18.8) 17.5 (13–18.2)	1.8	0.07	26.6 ±16 (8.4–66.1) 18.6 (15.1–36.6)	16.8 ±5 (8–25) 18 (12.6–19)	0.71	0.48	104	0.17	20	0.68
TRAb [IU/L]	8.3 ±8.6 (1.9–28.7) 6.3 (3.5–8.1)	7.3 ±14.4 (0.3–40) 1.9 (1.6–3.7)	1.2	0.24	9.2 ±10.2 (1.6–40) 5.1 (3.6–9.9)	14.5 ±14 (0.2–40) 8.3 (3.3–22.6)	1.59	0.11	146	0.88	60	0.049
Anti-TPO [IU/mL]	1611.4 ±1259.9 (178.3–3000) 1329 (525.9–3000)	2289.6 ±1261.5 (196.4–3000) 3000 (1547.5–3000)	1.5	0.14	1422.7 ±1272.5 (11.3–3000) 939.5 (189.2–3000)	1920.4 ±1266.5 (8.4–3000) 2682.9 (473.6–3000)	2.25	0.02	128.5	0.5	120	0.36
ThV [mL]	36.3 ±16.2 (20–77) 35 (27–36.5)	16.1 ±7.6 (11–31) 12 (12–25)	2.4	0.02	23.8 ±7.5 (10–40) 22.5 (18–28)	14.8 ±5.4 (8–27) 13 (10–20)	4.1	<0.001	68	0.01	92.5	0.42
Age [years]	38.5 ±11.5 (17–54) 40 (32–46.5)				49.2 ±12.6 (22–72) 52 (40–59)				77.5	0.03		
Dose administered [MBq]	573.5 ±137.3 (462.5–884.3) 512.5 (495.8–612.4)				440.3 ±190.6 (177.6–969.4) 366.3 (303.4–555)				72	0.02		

TSH – thyroid-stimulating hormone; FT4 – free thyroxine; TRAb – thyrotropin receptor antibody; Anti-TPO – anti-thyreoperoxidase; ThV – thyroid volume; RAIU – radioactive iodine uptake.

Table 4. Differences in anti-TPO and TRAb serum concentrations according to the application of thyroid replacement therapy (TRT). The data are reported as mean ± standard deviation (M ±SD), range (min–max) and median with interquartile range (Me (Q1–Q3))

Parameter	Levothyroxine (+) n = 31				Levothyroxine (–) n = 15				Levothyroxine (+)/Levothyroxine (–)			
	baseline	final	Z-value	p-value	baseline	final	Z-value	p-value	$U_{baseline}$	$p\text{-value}_{baseline}$	U_{final}	$p\text{-value}_{final}$
TRAb [IU/L]	9.2 ±10 (1.7–40) 5.2 (3.9–9.5)	10.8 ±12.3 (0.2–40) 5.7 (2.3–13.5)	0.07	0.94	8.8 ±9.7 (1.6–40) 7.5 (2.5–11.5)	18.3 ±16.7 (0.95–40) 16.3 (1.9–40)	1.4	0.16	216	0.71	138	0.29
Anti-TPO [IU/mL]	1269.50 ±1190 (11.3–3000) 754.4 (178.3–3000)	1766.9 ±1312 (8.4–3000) 2467.9 (257.3–3000)	2	0.04	1839.9 ±1349 (28.7–3000) 3000 (316.3–3000)	2434.4 ±1042.7 (59.7–3000) 3000 (2571.2–3000)	1.7	0.08	177	0.2	161	0.1
ThV [mL]	24.2 ±7.6 (10–38) 22 (19–32)	13.6 ±4.7 (8–27) 12 (10–15)	3.9	<0.001	29.7 ±14.4 (15–77) 28 (20–35)	18.1 ±6.7 (8–31) 18 (12–25)	2.7	0.006	182	0.24	105	0.02

TRAb – thyrotropin receptor antibody; Anti-TPO – anti-thyreoperoxidase; ThV – thyroid volume.

results, no differences were found in our study at baseline in nodularity and anti-TPO levels. Additionally, we examined the TRAb level in relation to the anti-TPO level. Similar to Lindgren et al.,[9] a positive correlation between the fold change of anti-TPO and TRAb was found. However, the absorbed dose of 120–300 Gy used by Lindgren et al. makes it difficult to compare the 2 patient groups.

Laurberg et al. also found that TRAb serum concentrations were significantly higher for RAI when compared with medical or surgical therapy, even 5 years after radioiodine therapy.[8] However, Laurberg et al. applied 120 Gy to the thyroid. Similar to Laurberg et al., we observed an increased level of TRAb after 1 year. The question arises whether higher absorbed radioiodine doses, as used in our group, may cause a decrease in ATA to diminish with longer follow-up. This issue is worth investigating in the future. We also underline the importance of ATA in the case of young women planning pregnancy after RAI therapy, who should receive careful surveillance in their follow-up.

Sawicka and Sowiński reported a correlation between ThV and humoral thyroid autoimmunity after RAI therapy in GD patients.[18] The majority of patients (24/36) underwent 2 RAI therapies with 12–18 months of follow-up. The authors found a significant decrease in TRAb levels, whereas our results showed no reduction in TRAb levels after RAI treatment. This difference in results may be attributed to the fact that subsequent RAI therapy may evoke a different immunological response.[2]

In the present paper, TRAb at baseline level correlated with 4 h, 24 h and 48 h RAIU, confirming the immunological origin of GD. This finding proves that RAIU and thyroid scanning still enable a definitive assessment of thyroid physiology.[25] No such correlation was found for baseline anti-TPO. The group of patients with the highest TRAb level and the highest RAIU was characterized by the shortest EHL and the lowest anti-TPO level. In this group, the final anti-TPO level was low and stable after RAI therapy. No significant differences in the TRAb level were observed with regard to steroid protection. Additionally, volume shrinkage was noted in all groups independently of the EHL value. The mechanism of the anti-TPO reaction relies on the access of immune cells to antigens after thyrocyte destruction, whereas TRAb does not trigger such action.[6] We found no explanation for this phenomenon in the literature. We hypothesize that the possible reason for the stable anti-TPO level could be the shortest EHL and the consequent shortest exposition to therapy. That is potentially why the destruction of thyroid cells was limited and, consequently, the level of anti-TPO did not increase.

Our study is not concordant with the data obtained by Aung et al.[16] They showed that one of the reasons for treatment failure was higher TRAb at baseline. However, we found no impact of the baseline TRAb concentration on the success rate.

Additionally, it is known from our everyday practice that patients with the shortest EHL seem to have worse results than those with an average value of EHL.[4] The study showed that, in cases of a high tissue-absorbed dose, no such effect was observed. We also found no impact of the EHL value on the success rate.

Our study also confirmed the finding reported by Jensen et al. that glucocorticoids do not have an impact on the effect of RAI therapy in GD.[26] In our group of patients, those without glucocorticoid protection showed a significantly increased baseline anti-TPO level compared to the final concentration ($Z = 2.25$, $p = 0.02$). Although the volume reaction was similar, glucocorticoids did not attenuate the immunologic reaction in anti-TPO. The reaction was similar to the one noted by Lindgren et al., who did not use glucocorticoids, but observed an increase in anti-TPO.[9]

With regard to TRAb, we found no significant difference in relation to a lack of steroid protection ($Z = 1.59$, $p = 0.11$). Jensen et al., who examined the influence of glucocorticoids, found no changes in the TRAb level in patients with steroid protection.[26] However, it is difficult to compare the 2 datasets due to the shorter protocol time, lower dose of steroid protection and dissimilar dosimetry. Incidentally, our patients tolerated steroid protection very well and their thyroid eye disease did not deteriorate.

Differences in ATA levels after RAI therapy depending on the levothyroxine have not been widely researched in the literature.[3,10,11] While the rate of hypothyroid patients after radioiodine is generally noted, authors do not usually report the fraction of patients treated with TRT. Interestingly, Sjölin et al. underlined that patients undergoing TRT were more likely to report non-recovery (as a subjective perception) than those without TRT.[11] Incidentally, in our group, patients with TRT showed intragroup differences in the anti-TPO level after RAI, compared to baseline. No intergroup differences in anti-TPO and TRAb were found when the final concentrations were compared.

Damage of the thyroid parenchyma reflects the dose of RAI therapy.[27] However, many factors (such as weight and age of patients, drug interactions, etc.) may determine the final dose of TRT needed. This matter requires further investigation.

The publication by Dong et al., which is based on a group of newly diagnosed patients with GD treated with RAI, is the closest to the present study.[3] The patients were divided into 2 groups: those with early and non-early diagnosed post-treatment hypothyroidism. The authors came to the conclusion that serum TRAb and anti-TPO were closely related to the occurrence of early hypothyroidism and played an important role in predicting prognosis after radioiodine treatment in GD.

In nuclear medicine departments, patients are usually followed up for only 1 year. We were concerned about the observed increases in anti-TPO and TRAb levels in GD patients at discharge and decided to analyze this subject. Knowing about elevated TRAb and anti-TPO levels may help endocrinologists with patient management. Patients with increased anti-TPO and TRAb have specific

immunological features that might occur for years. Such patients may require additional testing. Recent research suggests the protective influence of anti-TPO, for example, for extra-thyroidal pathologies in women with breast cancer.[6] Despite the fact that our study was based on a small group of patients, we have identified some trends and further work on the subject is needed.

It would be interesting to design a prospective long-term study encompassing patients treated with RAI due to GD, to assess relationships between ATA and clinical and biochemical data and patient quality of life after RAI.

Limitations

Lack of information on smoking habits before and after RAI. Small number of patients. Any concentration of ATA above 40 IU/L for TRAb and above 3000 IU/mL for anti-TPO was regarded as the maximum concentration on the standard curve.

Conclusions

The application of a high absorbed dose of 250 Gy in patients with GD resulted in high RAI therapy efficacy at 1-year follow-up. An increase ATA and its relationship with EHL and ThV reduction were observed at 1-year follow-up. There is a possible relationship between steroid protection and the anti-TPO concentration.

ORCID iDs

Maria Henryka Listewnik https://orcid.org/0000-0003-2801-1783
Hanna Piwowarska-Bilska https://orcid.org/0000-0003-3617-7687
Krystyna Jasiakiewicz https://orcid.org/0000-0002-2307-2571
Bożena Birkenfeld https://orcid.org/0000-0003-1174-8199

References

1. Chiovato L, Fiore E, Vitti P, et al. Outcome of thyroid function in Graves' patients treated with radioiodine: Role of thyroid-stimulating and thyrotropin-blocking antibodies and of radioiodine-induced thyroid damage. *J Clin Endocrinol Metab*. 1998;83(1):40–46. doi:10.1210/jcem.83.1.4492
2. Du W, Dong Q, Lu X, et al. Iodine-131 therapy alters the immune/inflammatory responses in the thyroids of patients with Graves' disease. *Exp Ther Med*. 2017;13(3):1155–1159. doi:10.3892/etm.2017.4047
3. Dong Q, Liu X, Wang F, et al. Dynamic changes of TRAb and TPOab after radioiodine therapy in Graves' disease. *Acta Endocrinol (Buchar)*. 2017;13(1):72–76. doi:10.4183/aeb.2017.72
4. Zhang R, Zhang G, Wang R, Tan J, He Y, Meng Z. Prediction of thyroidal 131I effective half-life in patients with Graves' disease. *Oncotarget*. 2017;8(46):80934–80940. doi:10.18632/oncotarget.20849
5. Pyzik A, Grywalska E, Matyjaszek-Matuszek B, Roliński J. Immune disorders in Hashimoto's thyroiditis: What do we know so far? *J Immunol Res*. 2015;2015:979167. doi:10.1155/2015/979167
6. Fröhlich E, Wahl R. Thyroid autoimmunity: Role of anti-thyroid antibodies in thyroid and extra-thyroidal diseases. *Front Immunol*. 2017;8:521. doi:10.3389/fimmu.2017.00521
7. Campi I, Vannucchi G, Covelli D, et al. Changes of serum TSH receptor antibodies (TRAB) levels in patients with Graves' disease (GD) submitted to radioiodine therapy (RAI). *Eur Thyroid J*. 2014;3:82. doi:10.1159/000365244
8. Laurberg P, Wallin G, Tallstedt L, Abraham-Nordling M, Lundell G, Tørring O. TSH-receptor autoimmunity in Graves' disease after therapy with anti-thyroid drugs, surgery, or radioiodine: A 5-year prospective randomized study. *Eur J Endocrinol*. 2008;158(1):69–75. doi:10.1530/EJE-07-0450
9. Lindgren O, Asp P, Sundlöv A, et al. The effect of radioiodine treatment on TRAb, anti-TPO, and anti-TG in Graves' disease. *Eur Thyroid J*. 2019;8(2):64–69. doi:10.1159/000495504
10. Törring O, Watt T, Sjölin G, et al. Impaired quality of life after radioiodine therapy compared to antithyroid drugs or surgical treatment for Graves' hyperthyroidism: A long-term follow-up with the thyroid-related patient-reported outcome questionnaire and 36-Item Short Form Health Status Survey. *Thyroid*. 2019;29(3):322–331. doi:10.1089/thy.2018.0315
11. Sjölin G, Holmberg M, Törring O, et al. The long-term outcome of treatment for Graves' hyperthyroidism. *Thyroid*. 2019; doi:10.1089/thy.2019.0085
12. Marinelli L, Quimby E, Hine G. Dosage determination with radioactive isotopes: Practical considerations in therapy and protection. *Am J Roentgenol Radium Ther*. 1948;59(2):260–281. PMID:18905884
13. Szumowski P, Mojsak M, Abdelrazek S, et al. Calculation of therapeutic activity of radioiodine in Graves' disease by means of Marinelli's formula, using technetium. *Endocrine*. 2016;54(3):751–756. doi:10.1007/s12020-016-1074-7
14. Stokkel MPM, Junak DH, Lassmann M, Dietlein M, Luster M. EANM procedure guidelines for therapy of benign thyroid disease. *Eur J Nucl Med Mol Imaging*. 2010;37(11):2218–2228. doi:10.1007/s00259-010-1536-8
15. Czarnywojtek A, Komar-Rychlicka K, Zgorzalewicz-Stachowiak M, et al. Efficacy and safety of radioiodine therapy for mild Graves ophthalmopathy depending on cigarette consumption: A 6-month follow-up. *Pol Arch Med Wew*. 2016;126(10):746–753. doi:10.20452/pamw.3505
16. Aung ET, Zammitt NN, Dover AR, Strachan MWJ, Seckl JR, Gibb FW. Predicting outcomes and complications following radioiodine therapy in Graves' thyrotoxicosis. *Clin Endocrinol (Oxf)*. 2019;90(1):192–199. doi:10.1111/cen.13873
17. Onimode YA, Dairo DM, Ellmann A. Pattern of presentation of Graves' disease and response to radioiodine therapy in South African men. *Pan Afr Med J*. 2018;29:48. doi:10.11604/pamj.2018.29.48.13655
18. Sawicka N, Sowiński J. Correlation between thyroid volume and humoral thyroid autoimmunity after radioiodine therapy in Graves' disease. *Endokrynol Pol*. 2012;63(1):10–13. PMID:22378091
19. Fanning E, Inder WJ, Mackenzie E. Radioiodine treatment for Graves' disease: A 10-year Australian cohort study. *BMC Endocr Disord*. 2018;18(1):94. doi:10.1186/s12902-018-0322-7
20. Sundaresh V, Brito JP, Wang Z, et al. Comparative effectiveness of therapies for Graves' hyperthyroidism: A systematic review and network meta-analysis. *J Clin Endocrinol Metab*. 2013;98(9):3671–3677. doi:10.1210/jc.2013-1954
21. Szumowski P, Abdelrazek S, Kociura Sawicka A, et al. Radioiodine therapy for Graves' disease: Retrospective analysis of efficacy factors. *Endokrynol Pol*. 2015;66(2):126–131. doi:10.5603/EP.2015.0019
22. Vanderpump MP. The epidemiology of thyroid disease. *Br Med Bull*. 2011;99:39–51. doi:10.1093/bmb/ldr030
23. Stoynova MA, Shinkov D, Kovatcheva RD, Stoynova M. Association between some ultrasound parameters and TSH-receptor antibodies. *Endocrinologia*. 2019;24(3):142–146.
24. Mekova R, Boyanov M. Clinical, hormonal, and ultrasound characteristics of patients with newly diagnosed Graves' disease and different thyroid antibody profiles. *Acta Med Bulg*. 2019;46(2):5–12. doi:10.2478/AMB-2019-0011
25. Barbesino G, Tomer Y. Clinical review: Clinical utility of TSH receptor antibodies. *J Clin Endocrinol Metab*. 2013;98(6):2247–2255. doi:10.1210/jc.2012-4309
26. Jensen BE, Bonnema S, Hegedüs L. Glucocorticoids do not influence the effect of radioiodine therapy in Graves' disease. *Eur J Endocrinol*. 2005;153:15–21. doi:10.1530/eje.1.01924
27. Samadi R, Shafiei B, Azizi F, Ghasemi A. Radioactive iodine therapy and glucose tolerance. *Cell J*. 2017;19(2):184–193. doi:10.22074/cellj.2016.4251

Influence of frailty syndrome on patient prognosis after coronary artery bypass grafting

Martyna Kluszczyńska[B–D], Agnieszka Młynarska[A,E,F]

Department of Gerontology and Geriatric Nursing, Faculty of Health Sciences, Medical University of Silesia in Katowice, Poland

A – research concept and design; B – collection and/or assembly of data; C – data analysis and interpretation;
D – writing the article; E – critical revision of the article; F – final approval of the article

Advances in Clinical and Experimental Medicine, ISSN 1899–5276 (print), ISSN 2451–2680 (online) *Adv Clin Exp Med*. 2021;30(9):923–931

Address for correspondence
Martyna Kluszczyńska
E-mail: bednarz.martynaa@gmail.com

Funding sources
None declared

Conflict of interest
None declared

Received on February 17, 2021
Reviewed on April 15, 2021
Accepted on May 17, 2021

Published online on August 19, 2021

Abstract

Background. Frailty syndrome and cardiovascular diseases are closely related because of the shared physiological pathway of chronic, low-intensity inflammation. Frailty syndrome may be an adverse factor in the prognosis of patients with cardiovascular disease (CVD).

Objectives. To assess the influence of frailty syndrome on patient prognosis after coronary artery bypass grafting (CABG).

Materials and methods. The study was conducted at the Clinic of Cardiac Surgery in Katowice and involved 180 patients (56 women, 31.11%) over 60 years of age who qualified for CABG surgery. The Tilburg Frailty Indicator (TFI) was used to assess frailty syndrome and the The World Health Organization Quality of Life Brief Version (WHOQOL-BREF) questionnaire was used to assess quality of life. Statistical analysis was performed using R software.

Results. Frailty syndrome was diagnosed in 42 patients (23.3%), including 24 men and 18 women. More than 1/3 of patients had complications during or after surgery, including 34.6% of patients without frailty syndrome and 28.6% of patients with frailty features. All of the complications occurred in 57 (31.6%) patients. Early complications accounted for 89.5% of all events – 93.3% of which occurred in patients without frailty syndrome and 75% in patients with frailty features ($p = 0.289$).

Conclusions. More than 1/3 of patients experienced complications during or after the CABG procedure. Early postoperative complications accounted for almost all of the adverse events in patients with frailty. However, frailty syndrome was a poor predictor of rehospitalization.

Key words: quality of life, coronary artery bypass grafting, frailty syndrome

Cite as
Kluszczyńska M, Młynarska A. Influence of frailty syndrome on patient prognosis after coronary artery bypass grafting. *Adv Clin Exp Med*. 2021;30(9):923–931. doi:10.17219/acem/137558

DOI
10.17219/acem/137558

Background

The most common group of diseases in elderly patients is cardiovascular system diseases (CVDs). According to data from the National Registry of Cardiac Surgery Procedures (KROK), about 12,000 coronary artery bypass grafting (CABG) procedures were performed in cardiac clinics throughout Poland in 2016.[1]

The classical CABG method uses extracorporeal circulation to provide optimal operating conditions; however, this method may cause complications such as ischemic stroke, myocardial ischemia, deterioration of kidney function, and respiratory failure. Cannulating the myocardium and aorta and clamping the ascending aorta could result in the release of embolic material, potentially endangering the patient's life. Extracorporeal circulation also significantly burdens maintenance of the blood–brain barrier, which can lead to early neurological complications.[2]

Frailty syndrome is characterized by a decrease in immune reserves, resulting from the reduced capacity of various systems and organs, ultimately leading to the collapse of homeostasis, disturbances in organ function, and increased morbidity and mortality in older people. Factors known to contribute to the occurrence of frailty syndrome include old age, visual impairment, impairment of cognitive functions, impaired gait and balance, weakness of the limbs, and the occurrence of comorbidities.[3]

Although frailty syndrome is not synonymous with old age, which is often accompanied by multiple diseases, any bodily dysfunction is a risk factor for frailty syndrome and may lead to disability. Insufficient physiological reserves of the organs increase the likelihood of adverse consequences, such as complications resulting from minor injuries and surgery, which can lead to death.[3–5]

Frailty syndrome and CVD are pathophysiologically closely related because of the common biological pathway of chronic, low-intensity inflammation. A diagnosis of frailty syndrome among patients who are qualified for CABG may quicken the healing process. Implementing appropriate measures customized to a patient's condition, including comprehensive geriatric and psychological care and rehabilitation, can improve the recovery period and reduce the number of adverse events.[6]

A significant problem in frailty syndrome is the coexistence of other diseases such as diabetes, hypertension, diseases of the genitourinary and digestive systems, and neurological diseases. These comorbidities have a large impact on the treatment process and patient recovery.

Elderly patients with a high surgical risk may experience improvement in their condition and quality of life after the procedure; however, there is always the possibility of complications, such as bleeding, stroke and respiratory or renal failure.[7]

The occurrence of frailty syndrome may be an adverse factor for the prognosis of patients with CVD. Mortality, a prolonged length of hospitalization and difficulties in postoperative wound healing are the most common complications after coronary artery bypass procedures. Appropriate diagnosis and therapy for treating frailty syndrome in elderly patients can influence the therapeutic team's actions and selection of the most beneficial treatment for the patient.[8]

Objectives

The aim of this study was to assess the impact of frailty syndrome on the prognosis of patients after coronary bypass surgery.

Materials and methods

Study design and settings

This observational, prospective, cross-sectional study was conducted at the Clinic of Cardiac Surgery in Katowice, Poland, from November 1, 2018 to January 30, 2020. The patient group consisted of 180 patients, 56 of which were women (31.1%).

The mean patient age was 69.34 years (standard deviation (SD) ±6.16) and the age range 60–84 years. All patients met the requirements for CABG in extracorporeal circulation and had undergone 2 or more bypasses.

Study participants and selection

The inclusion criteria were being over the age of 60, qualifying for CABG, consenting to participate in the study, and having a mental state that enabled contact with the team and understanding the questionnaire items. The exclusion criteria were simultaneous qualification for CABG and another procedure such as valve replacement, active cancer and refusal to participate in the follow-up visit.

Stages of the study

This study was conducted in 2 stages. The first stage consisted of a clinical interview, collection of demographic data, anthropometric measurements, and completion of standardized questionnaires. The second stage, which occurred 6 months ±2 weeks after the procedure, involved a follow-up visit that included a clinical history of the occurrence of any postoperative complications with a breakdown into cardiac and non-cardiac causes, repeated hospitalization, death, or other adverse events. The survey questionnaires were also repeated.

Ethical considerations

The study was approved by the Bioethics Committee of the Medical University of Silesia in Katowice (approval No. KNW/0022/KB/22518) on October 16, 2018.

Before joining the study, participants were informed about the confidentiality of the study, their anonymity, the study goals, and the methodology. Patients were also informed that they had the option to withdraw at any stage of the study. Data collection and analysis were performed based on the ethical principles in the Helsinki Declaration. The research was not funded.

Research instruments

The Tilburg Frailty Indicator (TFI) was used to assess frailty syndrome which, in addition to physical dysfunctions, includes psychological and social determinants. The scale consists of two parts, A and B. The first part concerns sociodemographic information such as age, gender, marital status, education level, and country of origin. The second part consists of 15 questions relating to the occurrence of the main components of frailty. It is divided into 3 domains: physical, psychological and social. The total score range is 0–15 points. Frailty syndrome is recognized as a TFI score ≥5. The tool was developed by Gobbens et al. and is based on the concept of the frailty model.[9,10] Quality of life was assessed using the World Health Organization Quality of Life Brief Version (WHOQOL-BREF) questionnaire for the following domains: physical functioning (domain 1), psychological functioning (domain 2), social relations (domain 3), and environmental functioning (domain 4). The questionnaire comprises of 26 questions that enable the 4 above-mentioned domains to be analyzed, a self-assessment of a patient's health condition and a determination of a patient's perception of their quality of life. Each item in each domain is scored between 1 and 5 points. The maximum score is 20 points. The WHOQOL-BREF also includes items that are analyzed separately: question 1 (WHO1): an individual's general perception of their quality of life; and question 2 (WHO2): an individual's general perception of their own health. The scores for these individual items are in a positive direction (i.e., a higher number of points indicates a higher quality of life).[11]

Statistical analyses

Quantitative variables (i.e., expressed with numbers) were analyzed by calculating the mean, SD, median, quartiles, minimum, and maximum. Qualitative (i.e., non-numerical) variables were analyzed by calculating the number and percentage of each value.

Qualitative variables were compared between groups using the χ^2 test (with Yates's correction for 2 × 2 tables) or Fisher's exact test. The values of quantitative variables were compared between 2 groups using the Mann–Whitney test. The quantitative variables for the 2 repeated measurements were compared using the Wilcoxon test for paired data. The Kaplan–Meier curves were compared using the log-rank (LR) test. A receiver operating characteristic (ROC) curve analysis was used to compare the predictive value for patients with frailty syndrome as well as the occurrence of complications and rehospitalization. Results were considered to be significant at p-value <0.05. All of the presented statistical analyses were performed using R software, v. 4.0 (R Foundation for Statistical Computing, Vienna, Austria).[12]

Results

The mean patient age was 69.34 years. Most patients (74.4%) were married or in a partnership. The majority (61.1%) of patients had a secondary education, and the next largest group consisted of patients with a postsecondary education (29.4%). The mean annual household income was 21.612–25.200 PLN in 47.2% of patients. Although more than 50% of patients had 2 or more diseases, 73.9% of them assessed their lifestyle positively in terms of their health. On the New York Heart Association (NYHA) scale, most of the patients were in the first class of disability. Additional details of patient characteristics are presented in Table 1.

Frailty syndrome was diagnosed in 42 patients (23.3%); 54.8% of patients in this subgroup were men and 42.9% were women. The mean age of women with frailty syndrome was 73.5 ±6.4 years; for men, it was 70.17 ±5.3 years. Most patients (80%) with frailty syndrome were widows or widowers. Almost 75% of patients considered themselves to be healthy (73.9%). The mean overall TFI score was 2.79 ±1.97 for women and 2.15 ±1.91 for men. There were statistically significant differences in the total TFI score and in the social components between the sexes (p = 0.025 and p = 0.002, respectively), with higher scores for women. There were no significant differences in the remaining domains. Table 2 presents the mean score for each subscale of the TFI scale for the overall patient group.

The logistic regression model (Table 3) showed that important independent predictors of frailty syndrome included separation or divorce (the chance of frailty syndrome increased 10.416 times compared to living with a spouse/partner) or widowhood (the chance of frailty syndrome increased 6.678 times compared to living with a spouse/partner) and an unhealthy lifestyle (the chance of frailty syndrome increased 10.982 times compared to having a healthy lifestyle).

Before the procedure, all patients had coexisting diseases. The most frequent diseases were arterial hypertension at 60% (69% of patients with frailty and 57% of patients without frailty syndrome), diabetes mellitus at 30.6% (38.1% of patients without frailty syndrome and 28.5% of patients with frailty syndrome) and gastrointestinal diseases at 15.6% (21.4% of patients without frailty syndrome and 13% of patients with frailty syndrome). No statistically significant differences were observed between the groups.

A follow-up visit took place 6 months after the procedure. Follow-up was performed for 170 of the patients from the previous group (8 (4.4%) did not attend and 2 (1.1%) died). More than 1/3 of patients (34.6% of patients without the frailty

Table 1. Characteristics of the individuals included in the study

Variable		Total group	Women	Men	p-value
Number of subjects		180	56 (31.1%)	124 (68.9%)	–
Age [years]		69.3 ±6.1	71.3	68.4	0.003
Height [cm]		168.4 ±8.9	159.4	172.5	0.000
Body weight [kg]		79.5 ±14.0	73.0	82.4	0.000
Marital status	widow/widower	34 (18.9%)	25 (73.5%)	9 (26.5%)	0.000
	married/unmarried/living with a partner	134 (74.4%)	28 (20.9%)	106 (79.1%)	
	separated/divorced	7 (3.9%)	1 (14.3%)	6 (85.7%)	
	unmarried	5 (2.8%)	2 (40%)	3 (60%)	
Net annual income [PLN]	7.200–10.800	1 (0.6%)	0 (0%)	1 (100%)	0.308
	10.801–14.400	3 (1.8%)	1 (33%)	2 (66.7%)	
	14.401–18.000	9 (5%)	2 (22.2%)	7 (77.8%)	
	18.001–21.600	38 (21.1%)	17 (44.7%)	21 (55.3%)	
	21.601–25.200	85 (47.4%)	22 (25.9%)	63 (74.1%)	
	25.201 or more	44 (24.4%)	14 (31.8%)	30 (68.2%)	
Education	no or primary	12 (6.7%)	5 (41.7%)	7 (58.3%)	0.526
	secondary	110 (61.1%)	36 (32.7%)	79 (71.8%)	
	higher	53 (29.4%)	15 (28.3%)	38 (71.7%)	
NYHA	I	63 (35%)	8 (12.7%)	55 (87.3%)	0.000
	II	69 (38.3%)	26 (37.7%)	43 (62.3%)	
	III	34 (18.9%)	17 (50%)	17 (50%)	
	IV	14 (7.8%)	5 (35.7%)	9 (64.3%)	

BMI – body mass index; NYHA – New York Heart Association classes of heart failure. The p-value of according to Mann–Whitney U test.

Table 2. Mean scores in individual domains of the Tilburg Frailty Indicator

TFI	Range of values	n	Mean	SD	Median	Min	Max	Q1	Q3
General TFI result	0–15	180	2.34	1.95	2	0	8	1	4
Physical components	0–8	180	1.43	1.43	1	0	6	0	2
Psychological components	0–4	180	0.45	0.64	0	0	4	0	1
Social components	0–3	180	0.46	0.69	0	0	3	0	1

TFI – the Tilburg Frailty Indicator; SD – standard deviation; Q1 – first quartile; Q3 – third quartile.

syndrome and 28.6% of patients with frailty features) had complications during or after the procedure. All of the documented complications occurred in 57 (31.6%) respondents. There were no statistically significant differences between the groups (p = 0.1). Early complications accounted for 89.5% of all events, including 93.3% in patients without frailty syndrome and 83.3% in patients with frailty syndrome (p = 0.289). Table 4 presents the different types of complications.

Twenty-three patients (13.5%) were rehospitalized, which included 4 patients with frailty syndrome and 19 healthy people (p = 0.737). Eight patients were rehospitalized for cardiac issues (36.5% of all hospitalizations, including 2 patients with frailty syndrome). There were no statistically significant differences between the occurrence of complications and hospitalization and the gender of the patients. On average, patients were discharged 1 week after the surgery. The complication-free survival rates between patients presenting with and without the symptoms of frailty syndrome showed no statistically significant difference (p = 0.734). The results are presented in Fig. 1.

Similar results were observed for patients in both groups who were not rehospitalized. The p-value of the log-rank test was >0.05, indicating that the survival curves for the 2 groups did not differ significantly (p = 0.472). These data are presented in Fig. 2.

In the subjective evaluation of satisfaction with the procedure and hospitalization, patients without frailty syndrome reported higher satisfaction compared to those with frailty syndrome (78% compared to 65%, p = 0.002). Dissatisfaction and moderate satisfaction were expressed by 35% of patients with frailty syndrome who were surveyed.

Frailty syndrome diagnosed in patients before surgery was not a significant predictor of complications: the area under the ROC curve (AUC) was 0.526. The optimal cut-off score for the TFI before surgery was 2 points. When

Table 3. Logistic regression

Characteristic		OR	95% CI		p-value
Sex	women men	1 0.555	ref. 0.21	1.465	0.234
Marital status	married/unmarried/living with a partner	1	ref.	–	–
	unmarried	1.902	0.155	23.418	0.616
	separated/divorced	10.416	1.7	63.831	0.011 *
	widow/widower	6.678	1.259	35.413	0.026 *
Education	no or primary	1	ref.	–	–
	secondary	1.773	0.346	9.072	0.492
	higher	2.881	0.381	21.79	0.305
Net annual income [PLN]	7.200–10.800	1	ref.	–	–
	10.801–14.400	0.133	0.026	0.693	0.017 *
	14.401–18.000	0.124	0.026	0.591	0.009 *
	18.001–21.600	0.076	0.011	0.529	0.009 *
How do you evaluate your lifestyle in terms of health?	healthy	1	ref.	–	–
	neutral	1.751	0.687	4.458	0.24
	unhealthy	10.982	1.328	90.788	0.026 *
Do you have 2 or more diseases and/or chronic disorders?	no yes	1 1.67	ref. 0.665	– 4.188	– 0.275
Are you satisfied with your home environment?	no yes	1 0.64	ref. 0.167	– 2.456	– 0.515
Age	[years]	1.049	0.972	1.132	0.218
BMI	[kg/m^2]	0.983	0.891	1.084	0.725
Death of a loved one	no yes	1 0.201	ref. 0.033	– 1.223	– 0.082
Diagnosed severe disease	no yes	1 4.216	ref. 0.66	– 26.944	– 0.128

BMI – body mass index; OR – odds ratio; 95% CI – 95% confidence interval.

Table 4. Types of postoperative complications for the patients with frailty syndrome

Type of complication	Patients with frailty syndrome (n of complications = 12)	Patients without frailty syndrome (n of complications = 45)
Death (n = 2)	0 (0%)	2 (4.4%)
Lower limb wound (n = 10)	2 (16.7%)	8 (17.8%)
Chest wound (n = 9)	0 (0%)	9 (20%)
Painfulness (n = 4)	0 (0%)	4 (8.9%)
Neurological (n = 8)	2 (16.7%)	6 (13.3%)
Respiratory (n = 5)	1 (8.3%)	4 (8.9%)
Bleeding, heart tamponade (n = 7)	3 (25%)	4 (8.9%)
Another (n = 12)	4 (33.3%)	8 (17.8%)

it was more than 2 points, complications could be expected. The sensitivity was 41.1% and the specificity was 61.3%. The ROC curve is shown in Fig. 3.

The AUC was 0.487 for TFI before the procedure, which means it was a very weak predictor of the occurrence of rehospitalization. The optimal cutoff point for the TFI before surgery in this case was 3 points.

For patients with more than 3 points, rehospitalization was required. The sensitivity was 78.3% and the specificity was 31.9%. The data are presented in Fig. 4.

After the surgery, there were statistically significant changes in nearly every dimension of the patients' mental and physical health. The physical components of frailty were more intense after CABG (p = 0.007).

In patients with diagnosed frailty syndrome, in addition to deterioration in independence in performing everyday activities, there were significant changes in their quality of life. In all areas of life, as well as in the perception of quality of life, these patients reported lower scores. The data are presented Table 5.

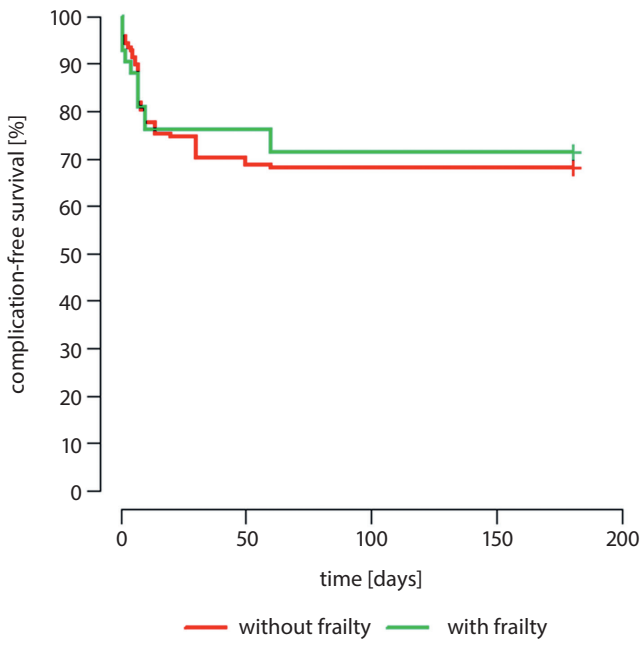

Fig. 1. Complication-free survival for patients with and without frailty syndrome

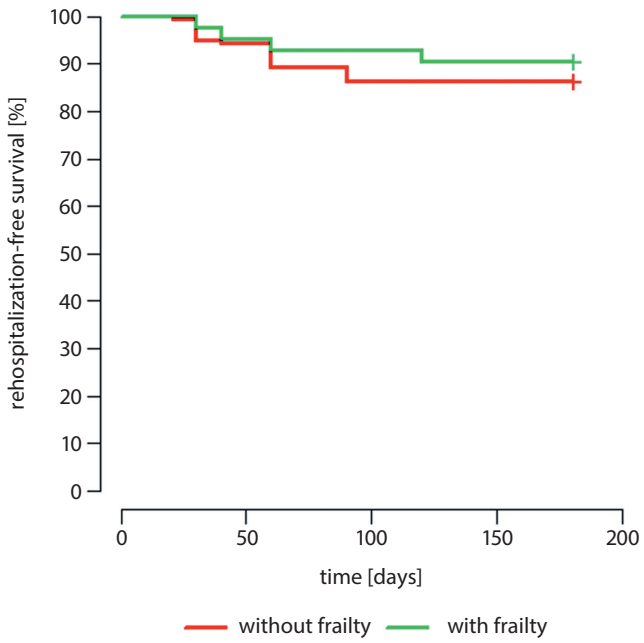

Fig. 2. Hospitalization-free survival of patients with and without frailty syndrome

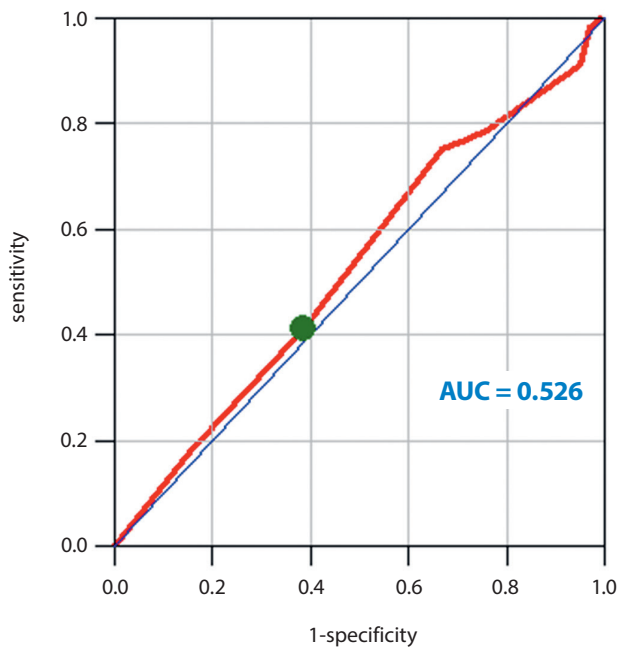

Fig. 3. Receiver operating characteristic (ROC) analysis for complications. AUC – area under the curve.

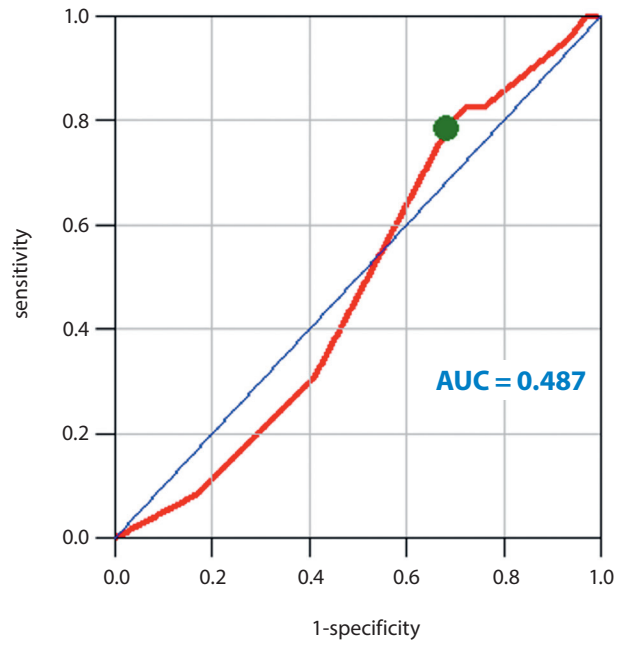

Fig. 4. Receiver operating characteristic (ROC) analysis for rehospitalization. AUC – area under the curve.

Discussion

Frailty syndrome can cause many complications. A meta-analysis conducted by Rockwood et al., which included more than 68,000 individuals, showed that patients with frailty and pre-frailty are at risk for a higher number of falls, frequent hospitalizations, longer stays in the hospital, and more postoperative complications. The authors also demonstrated links between frailty syndrome and imbalance, inferior lower limb muscle control, difficulties in self-service activities, and higher mortality rates. In our research, patients with frailty syndrome did not show prolonged hospital stays. The results revealed that frailty syndrome is a weak predictor of the incidence of hospitalization among this group of patients.[13]

In a three-year prospective cohort study of patients ≥65 years of age undergoing general surgery, the authors drew the following conclusions. In the group of 326 hospitalized patients, frailty syndrome was diagnosed in 38.9% of patients. On admission, frailty patients

Table 5. Comparison of quality of life before and after surgery for patients with frailty syndrome

WHOQoL BREF		Patients with frailty syndrome			Patients without frailty syndrome		
		before surgery	after surgery	Wilcoxon paired test	before surgery	after surgery	Wilcoxon paired test
Perception of quality of life	mean ±SD	3.76 ±0.58	3.71 ±0.61	V = 1 p = 1	3.95 ±0.49	3.87 ±0.56	V = 67.5 p = 0.021
	median	4	4		4	4	
Perception of one's health	mean ±SD	3.45 ±0.77	3.39 ±0.72	V = 27 p = 0.608	3.7 ±0.57	3.56 ±0.7	V = 228.5 p = 0.004
	median	4	3		4	4	
Physical domain	mean ±SD	13.62 ±1.56	13.32 ±1.86	V = 224.5 p = 0.183	14.2 ±1.12	13.86 ±1.41	V = 1626 p < 0.001
	median	14	13		14	14	
Psychological domain	mean ±SD	13 ±1.61	12.32 ±1.97	V = 165 p = 0.005	12.84 ±1.19	12.64 ±1.37	V = 1580 p = 0.01
	median	13	12.5		13	13	
Social domain	mean ±SD	14.36 ±2.08	14 ±2.38	V = 54.5 p = 0.059	14.15 ±1.72	14.14 ±1.85	V = 369.5 p = 0.994
	median	15	15		15	15	
Environmental domain	mean ±SD	15.21 ±1.44	14.76 ±1.63	V = 207.5 p = 0.032	15.09 ±1.25	14.57 ±1.29	V = 1542 p < 0.001
	median	16	14.5		15	14	

WHOQoL BREF – The World Health Organization Quality of Life Brief Version; SD – standard deviation.

received higher American Association of Anesthesiologist (ASA) grades, with grade 1 (ASA I) indicating a healthy patient and grade 4 (ASA IV) indicating a patient with a severe systemic disease that is life-threatening. Hospital complications occurred in 26.7% of patients in this group and the mortality rate was 30%. Patients with frailty syndrome also had higher Failure to Rescue (FTR) results; the higher the rate, the lower the chance of a successful operation. It was determined that frailty syndrome was also a predictor of FTR. The researchers stated that an important element in patient case is the use of indicators to assess frailty syndrome. According to the analysis, frailty syndrome increases the risk of intraoperative complications and patient's death three-fold among elderly patients.[14]

Similar conclusions were drawn by Han et al. in a study of 2278 patients. They assessed the risk of adverse events after surgery with regard to the presence of frailty syndrome features. It was revealed that the risk of postoperative complications was higher in patients with frailty syndrome than in those with no frailty symptoms. Our results are generally consistent with those of Khan and Han: although frailty syndrome did not cause increased mortality or rehospitalization, almost all patients with frailty had early hospital complications.[15]

Birkelbach et al. evaluated the impact of frailty syndrome on the risk of postsurgical complications. Patients were classified according to their frailty using the five-point Fried Frailty Index, where a score of 3 or more points indicates frailty and 2 or fewer points indicates pre-frailty. The occurrence of postoperative complications was evaluated until patients' discharge from the hospital. Of the 1186 participants, almost half (46.9%) were in the pre-frailty group and 11.4% were diagnosed with frailty syndrome. In both groups, there was a higher risk of complications and the postoperative hospital stay was longer compared to patients without frailty. The incidence of adverse events was twice as high in patients with diagnosed frailty syndrome and pre-frailty features. In our research, frailty syndrome was diagnosed in 23% of the patients and the mean TFI score was about 3 points, which suggests that most of the patients were classified as pre-frailty, although we did not test or evaluate this group. There were no statistically significant differences between the groups with and without frailty syndrome and the incidence of postoperative complications.[16]

In their work, Rothenberg et al. examined the effect of frailty syndrome in patients after scheduled surgery after unplanned readmission. Frailty was assessed using Risk Analysis Index (RAI), including physical dysfunctions (renal failure, dyspnea, etc.) and cognitive status. The TFI was also used, which included additional social and psychological domains. They evaluated the data of 417,840 patients using a retrospective cohort design. More than half of patients that were hospitalized (59.2%) after surgery were readmitted to the hospital within 30 days due to complications. Most often, these patients were women or had diagnosed frailty syndrome. When the frailty data were analyzed, the risk of unplanned readmission doubled. The results demonstrated that frailty syndrome is an important risk factor for readmission after a planned outpatient procedure due to complications. Screening for frailty syndrome may affect the development of interventions to reduce unplanned readmissions and treatments. In contrast to our studies, 1/3 of patients had postoperative complications and there were no significant differences between gender groups regarding the occurrence of unplanned events.[17]

This is important because it concerns the same study group as in their own research. After cardiac surgery, patients with frailty syndrome stayed in the intensive care unit (ICU) longer and were more likely to have complications compared to those

without frailty syndrome. On average, the stay in the ICU was prolonged from 28 h to 54 h. There were no significant differences in hospitalizations between the groups of patients with and without frailty syndrome. The average hospital stay was 1 week.[18]

Tran et al. performed four-year follow-up of patients with increased mortality. Frailty syndrome, which was diagnosed in 22% of patients (n = 40,083) at four-year follow-up, was associated with higher postoperative mortality compared to healthy individuals. In this group, there were greater differences in the survival of patients between 40 and 74 years of age than in patients over 85 years of age. In our research, the follow-up visit took place 6 months after the surgery and the mortality rate was very low.[19]

In a Brazilian study, the research on frailty syndrome was included in the holistic nursing care of a patient. Of all of the patients included in this study, 93.6% had memory impairment, 93.6% had physical mobility problems, 82.1% showed general fatigue and weakness, and more than 50% were diagnosed with self-care deficits.[20]

Similar conclusions to our own research were drawn by Uchmanowicz et al. Frailty syndrome was diagnosed in 64.8% of patients with heart diseases who were predisposed to rehospitalization. It was also noted that physical and psychological aspects were important components.[21]

Different conclusions were drawn by Lupon et al. In their study based on 622 patients, 39.9% of whom had diagnosed frailty syndrome, frailty was not a prognostic factor for rehospitalization, but it was for higher mortality in patients with heart failure. In our study, frailty syndrome was not a prognostic factor for mortality or rehospitalization. This could be due to the lower mean age of the patients enrolled in our study compared to those in previous studies by different authors.[22]

Limitations

The population in this study exhibited a relatively low burden of frailty and was relatively young (mean age = 69 years old). The prevalence of frailty syndrome is generally higher in people over the age of 80. This could represent a bias in the present study and may have influenced the findings. This study did not investigate the impact of comorbidities on prognosis.

Conclusions

More than 1/3 of patients had complications during or after the procedure. There were more early postoperative complications in patients with frailty syndrome. There were no statistically significant relationships between the occurrence of complications and hospitalization and the gender of patients. Frailty syndrome was a poor predictor of rehospitalization. Patients without frailty syndrome expressed higher satisfaction in the subjective evaluation of the procedure and hospitalization.

ORCID iDs

Martyna Kluszczyńska https://orcid.org/0000-0002-8216-7490
Agnieszka Młynarska https://orcid.org/0000-0003-4009-0613

References

1. Main cardiac surgery procedures performer in Poland in 2015 (according to the National Registry of Cardiac Surgery Procedures – KROK, Warsaw, Poland 2016). *Pol J Thor Cardiac Surg*. 2016;13(2):185–188. doi:10.5114/kitp.2015.54626
2. Shroyer AL, Grover FL, Hattler B, et al. On-pump versus off-pump coronary artery bypass surgery. *N Engl J Med*. 2009;361(19):1827–1837. doi:10.1056/NEJMoa0902905
3. Gabryś T, Bajorek A, Malinowska-Lipień I. The frailty syndrome: A major health problem of the elderly people. Part I [in Polish]. *Pol Gerontol*. 2015;1:29–33. https://gerontologia.org.pl/wp-content/uploads/2016/07/2015-1_Gerontologia_5.pdf
4. Sacha M, Sacha J. Frailty syndrome: Uni- and multidimensional approach [in Polish]. *Geriatrics*. 2017;1:290–293. https://www.akademiamedycyny.pl/wp-content/uploads/2018/04/Geriatria_4_8.pdf
5. Sobczyńska M, Główczyńska R, Opolski G. Frailty syndrome increases frequency of complications in patients undergoing cardiology procedures and open-heart surgeries [in Polish]. *Folia Cardiologica*. 2017; 12(6):557– 564. doi:10.5603/FC.2017.0106
6. Ferrucci L, Guralnik JM, Studenski S, et al. Designing randomized, controlled trials aimed at preventing or delaying functional decline and disability in frail, older persons: A consensus report. *J Am Geriatr Soc*. 2004;52(4):625–634. doi:10.1111/j.1532-5415.2004.52174.x
7. Szyguła-Jurkiewicz B, Kowalska M, Mościński M. Quality of life as an element of health assessment and treatment effectiveness in patient with cardiovascular diseases [in Polish]. *Folia Cardiologica*. 2011;6(1):62–71. https://journals.viamedica.pl/folia_cardiologica/article/viewFile/23617/18803
8. Życzkowska J, Grądalski T. Frailty: An overview for oncologists [in Polish]. *Onkol Prakt Klin*. 2010;6(2):79–84. https://journals.viamedica.pl/oncology_in_clinical_practice/article/view/9215/7842
9. Gobbens R, van Assen M, Luijkx K, Wijnen-Sponselee MT, Schols JMGA. The Tilburg frailty indicator: Psychometric properties. *J Am Med Dir Assoc*. 2010;11(5):344–355. doi:10.1016/j.jamda.2009.11.003
10. Uchmanowicz I, Jankowska-Polańska B, Łoboz-Rudnicka M, Manulik S, Łoboz-Grudzień K. Gobbens R. Cross-cultural adaptation and reliability testing of the Tilburg Frailty Indicator for optimizing care of Polish patients with frailty syndrome. *Clin Interv Aging*. 2014;9:997–1001. doi:10.2147/CIA.S64853
11. World Health Organization. WHO Quality of Life-BREF (WHOQOL-BREF). https://www.who.int/tools/whoqol. Accessed August 4, 2020.
12. R Core Team. R: A language and environment for statistical computing. Vienna, Austria: R Foundation for Statistical Computing; 2020. https://www.R-project.org/. Accessed January 10, 2020.
13. Rockwood K, Howlett SE, MacKnight C, et al. Prevalence, attributes and outcomes of fitness and frailty in community dwelling older adults: Report from the Canadian study of health and aging. *J Gerontol A Biol Sci Med Sci*. 2004;59(12):1310–1317. doi:10.1093/gerona/59.12.1310
14. Khan M, Jehan F, Zeeshan M, Saljuqi AT, O'Keeffe T, Josepf B. Failure to rescue after emergency general surgery in geriatric patients: Does frailty matter? *J Surg Res*. 2019;233:397–402. doi:10.1016/j.jss.2018.08.033
15. Han B, Li Q, Chen X. Effects of the frailty phenotype on postoperative complications in older surgical patients: A systematic review and metanalysis. *BMC Geriatr*. 2019;19(1):141. doi:10.1186/s12877-019-1153-8
16. Birkelbach O, Mörgeli R, Spies C, et al. Routine frailty assessment predicts postoperative complications in elderly patients across surgical disciplines: A retrospective observational study. *BMC Anesthesiol*. 2019;19(1):204. doi:10.1186/s12871-019-0880-x
17. Rothenberg KA, Stern JR, George EL, Trickey AW, Morris AM, Hall DA. Association of frailty and postoperative complications with unplanned readmissions after elective outpatient surgery. *JAMA Netw Open*. 2019;2(5):e194330. doi:10.1001/jamanetworkopen.2019.4330
18. Niv AD, Holmes SD, Halpin L, Shuman DJ, Miller CE, Lamont D. Effects of frailty in patients undergoing elective cardiac surgery. *J Card Surg*. 2016;31(4):187–194. doi:10.1111/jocs.12699

19. Tran DT, Tu JV, Dupuis JY, Eddeen AB, Sun LY. Association of frailty and long-term survival in patients undergoing coronary artery bypass grafting. *J Am Heart Assoc*. 2018;7(15):e009882. doi:10.1161/JAHA.118.009882
20. Ribeiro IA, Ramos de Lima L, Grou Volpe CR, Funghetto SS, Rehem T, Morato Stival M. Frailty syndrome in the elderly in elderly with chronic diseases in primary care. *Rev Esc Enferm USP*. 2019;53:e03449. doi:10.1590/s1980-220x2018002603449
21. Uchmanowicz I, Lee CS, Vitale C, et al. Frailty and the risk of all-cause mortality and hospitalization in chronic heart failure: A meta-analysis. *ESC Heart Fail*. 2020;21(6):3427–3437. doi:10.1002/ehf2.12827
22. Lupon J, Gonzalez B, Santaeugenia S, et al. Prognostic implication of frailty and depressive symptoms in an outpatient population with heart failure. *Rev Esp Cardiol*. 2008;61(8):835–842. doi:10.1157/13124994

Radiation induces submandibular gland damage by affecting *Cdkn1a* expression and regulating expression of *miR-486a-3p* in a xerostomia mouse model

Wei Wang[B–F], Caizhi Xiao[A,C,E,F], Hong Chen[B,C,E,F], Fangfei Li[B,C,F], Dongqin Xia[B,C,E,F]

Key Laboratory of Biorheological Science and Technology of the Ministry of Education (Chongqing University), Chongqing University Cancer Hospital, China

A – research concept and design; B – collection and/or assembly of data; C – data analysis and interpretation;
D – writing the article; E – critical revision of the article; F – final approval of the article

Advances in Clinical and Experimental Medicine, ISSN 1899–5276 (print), ISSN 2451–2680 (online) *Adv Clin Exp Med*. 2021;30(9):933–939

Address for correspondence
Caizhi Xiao
E-mail: colorzhaodoc@yeah.net

Funding sources
Key projects of science and technology of traditional Chinese medicine (grant No. ZY201701001).

Conflict of interest
None declared

Received on February 26, 2021
Reviewed on March 17, 2021
Accepted on May 7, 2021

Published online on September 6, 2021

Cite as
Wang W, Xiao C, Chen H, Li F, Xia D. Radiation induces submandibular gland damage by affecting *Cdkn1a* expression and regulating expression of *miR-486a-3p* in a xerostomia mouse model. *Adv Clin Exp Med*. 2021;30(9):933–939. doi:10.17219/acem/136457

DOI
10.17219/acem/136457

Abstract

Background. Radiotherapy has been proven to be an effective treatment strategy for inhibiting head-and-neck cancer. However, side effects are common when using high-dosage irradiation, and the mechanism of action of this therapy has not been fully clarified.

Objectives. To discover targeting molecules involved in an electron radiation-induced xerostomia murine model.

Materials and methods. The xerostomia model mice were divided into Gy-3 (n = 5), Gy-7 (n = 5), and Gy-21 (n = 5) groups, and were compared to a negative control (NC) group. Drinking water amount, saliva volume, submandibular gland weight, and body weight were recorded. Real-time polymerase chain reaction (RT-PCR) was performed to amplify gene transcription. Hematoxylin and eosin (H&E) staining was used to identify submandibular gland damage. The dual-luciferase assay was used to observe the interaction between the *Cdkn1a* gene and *miR-486a-3p*.

Results. Electron radiation significantly increased the drinking water amount, and decreased saliva volume and body weight compared to mice without radiation treatment ($p < 0.05$). The H&E staining showed that electron radiation damaged the submandibular gland. Electron radiation also triggered significantly higher transcription of the *Cdkn1a* gene in the submandibular gland of xerostomia mice compared to those without radiation treatment ($p < 0.05$). The dual-luciferase assay demonstrated that *miR-486a-3p* interacted with the *Cdkn1a* gene (miRNA-mRNA).

Conclusions. Radiation was found to induce damage of the submandibular gland and affect *Cdkn1a* expression by regulating the expression of *miR-486a-3p* in a xerostomia murine model. Therefore, modulation of *miR-486a-3p* and the *Cdkn1a* gene in a xerostomia murine model might improve damage of the submandibular gland.

Key words: xerostomia, electron radiation, miRNA-mRNA targeting interaction, *miR-486a-3p*, *Cdkn1a*

Background

Annually worldwide, about 500,000 patients are diagnosed with head-and-neck malignancies, and this tendency is increasing.[1,2] Radiotherapy has proven to be an effective strategy for treating head-and-neck cancer. However, side effects are common when using high-dosage irradiation[3] and include xerostomia (a dry mouth caused by salivary gland damage). Usually, xerostomia influences life quality in patients with head-and-neck malignancy.[4] However, no effective therapeutic regimens have been discovered for xerostomia until now.

In previous studies, plenty of specific mechanisms focusing on dysfunction of salivary glands in xerostomia animal models have been explored, such as necrosis and apoptosis.[5,6] To date, many studies have discovered that extracellular microRNAs (miRNAs) are involved in the pathogenic process of head-and-neck malignancy and the associated radiotherapy resistance.[7,8] Lamichhane et al. reported that circulating miRNAs act as prognostic molecular biomarkers for head-and-neck cancer.[9] Fadhil et al. also proved that miRNAs could act as potential diagnostic biomarkers for human head-and-neck cancer.[10] A previous study also reported that miR-486-5p is involved in the process of neurogenesis and neovascularization.[11] Meanwhile, miR-486-5p is also correlated with pyroptosis or apoptosis, and involved in inflammatory diseases.[12] Moreover, the *Cdkn1a*-encoded p21 molecule can interact with a series of molecules involved in many key biological processes.[13] Thus, we speculated that *Cdkn1a* might interact with miR-486-5p.

Objectives

In this study, we hypothesized that miR-486-5p might participate in the pathogenesis of radiotherapy-induced xerostomia in an animal model. Therefore, this study aimed to discover targeting molecule involved in an electron radiation-induced xerostomia animal model.

Materials and methods

Animals and cells

A total of 20 specific-pathogen-free (SPF) C57BL/6J mice (Ensiweier Biotechnology Co. Ltd., Chongqing, China) were fed with ad libitum food and water, and housed in conditions with a light/dark cycle of 12 h/12 h at 23–25°C.

The Ethical Committee of Chongqing University Cancer Hospital (China) approved this study (approval No. CZLS2021077-A). All of the experiments were conducted in accordance with the Guidance of Care and Use of Laboratory Animals of the National Institutes of Health (NIH).

Xerostomia model generation and grouping

The mice were divided into a normal control (NC) group (n = 5) and an X-ray irradiation injury xerostomia model group (n = 15). Mice in the xerostomia model group were further subdivided into a 3-day electron radiation group (Gy-3 group, n = 5), a 7-day electron radiation group (Gy-7 group, n = 5) and a 21-day electron radiation group (Gy-21 group, n = 5). Mice in the irradiation injury xerostomia model groups were weighed, anesthetized and placed on a linear accelerator in a supine position (with energy of 9 mV and dosage of 3 Gy/min). The submandibular gland of mice was irradiated with a single dose of 18 Gy electron radiation. Mice in the NC group were treated with the same method as the radiation model groups, except for the irradiation.

Measurement of parameters

The drinking water amount was recorded. Saliva was collected and its volume was recorded. The submandibular gland was isolated from xerostomia mice and weighed. The submandibular gland index was calculated using the following formula (Eq. 1):

$$\text{submandibular gland index [mg/g]} = \frac{\text{submandibular gland mass [mg]}}{\text{body weight of mice [g]}}.$$

RT-PCR assay

RNAs were extracted from submandibular gland tissues of xerostomia mice using the MiniBEST Universal RNA Extraction Kit (cat. No. 9767; TaKaRa, Tokyo, Japan) and cDNAs were synthesized with the PrimeScript™ II 1st Strand cDNA Synthesis Kit (cat. No. 6210A; TaKaRa) following the manufacturer's instructions. Transcription of the *Cdkn1a* gene was examined with AceQ® qPCR SYBR Green Master Mix (cat. No. Q111-02; Vazyme, Shanghai, China) using the generated polymerase chain reaction (PCR) primers (Table 1). The gene transcriptional products were analyzed using a Tanon-1600 gel-scanning system (Tanon, Beijing, China) depending on the protocol of the scanning equipment. Finally, the relative gene transcriptions were evaluated using the previously described $2^{-\Delta\Delta ct}$ method.[14]

Table 1. Specific primers for the real-time polymerase chain reaction (RT-PCR) assay

Genes	Sequences (5'-3')
GAPDH – forward	CAGAAGGGGCGGAGATGAT
GAPDH – reverse	AGGCCGGTGCTGAGTATGTC
Cdkn1a – forward	CCCGTGGACAGTGAGCAGTT
Cdkn1a – reverse	GCAGCAGGGCAGAGGAAGTA

Hematoxylin and eosin staining

Submandibular glands were fixed using 4% paraformaldehyde, dehydrated in ethanol at different gradients for transparency, embedded in paraffin, cut into 5-µm thick sections, and then stained with hematoxylin and eosin (H&E) as described by Zhou et al.[15]

Dual-luciferase reporter assay

293T cells were cultured in 24-well plates for 24 h and co-transfected using pmir-Glo-WtCdkn1a+pTK-NC and pmir-Glo-WtCdkn1a+pTK+mmu-miR-486a-3p or pmir-Glo-MuCdkn1a+pTK-NC and pmir-Glo-MuCdkn1a+pTK+mmu-miR-486a-3p. The transfections were carried out using Lipofectamine™ 2000 (Thermo Fisher Scientific, Waltham, USA) as instructed by the manufacturer. About 48 h post-transfection, the dual-luciferase reporter assay system (Promega, Madison, USA) was applied to verify firefly luciferase normalized to Renilla luciferase (ratio).

Statistical analyses

Data are reported as mean ± standard deviation (SD) and analyzed using IBM SPSS Statistics for Windows v. 19.0 software (IBM Corp., Armonk, USA). The Mann–Whitney U test was used to analyze the differences between 2 groups. A value of $p < 0.05$ was considered to be a statistically significant difference.

Results

Electron radiation increased the drinking amounts of xerostomia mice

Electron radiation greatly increased the drinking water amount in xerostomia mice compared to those in the NC group at 0 days (Fig. 1A), 3 days (Fig. 1B), 7 days (Fig. 1C), and 21 days (Fig. 1D) after radiation injury. These results suggest that electron radiation obviously increased the drinking water amount in xerostomia mice.

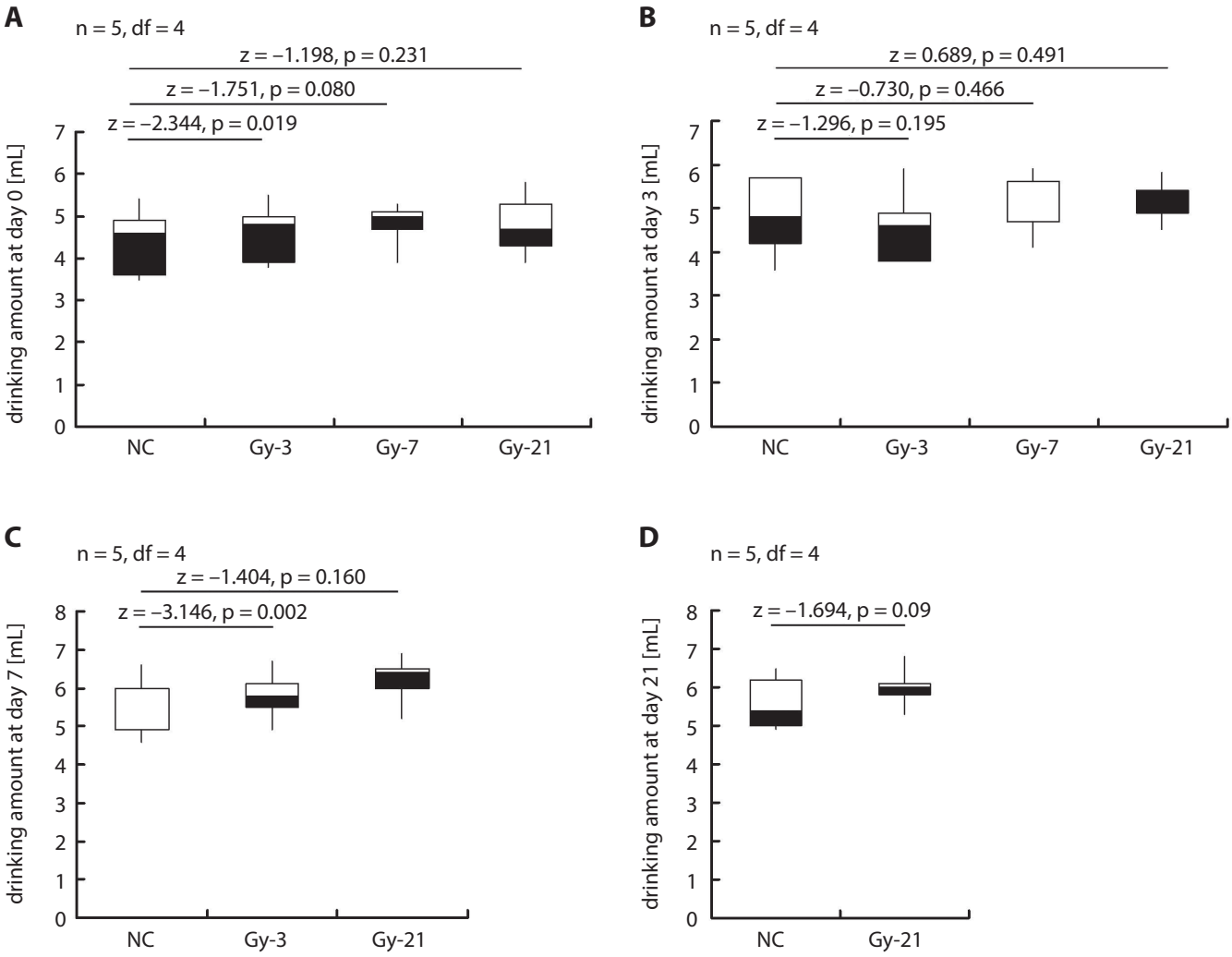

Fig. 1. Effects of electron radiation on drinking water amount (mean ±SD) 0 days (A), 3 days (B), 7 days (C), and 21 days (D) after the radiation treatment (n = 5 for each group). The white and black bar charts represent the negative control (NC) group and Gy-treated groups, respectively. The p-values for comparisons between groups are shown in the images. df – degrees of freedom

Electron radiation reduced the body weight of xerostomia mice

At 3 days (Gy-3 group, Fig. 2A, p = 0.016), 7 days (Gy-7 group, Fig. 2B, p = 0.000) and 21 days (Gy-21 group, Fig. 2C, p = 0.000) after the administration of electron radiation, the body weight of mice was significantly decreased compared to mice in the NC group. These results suggest that electron radiation reduced the body weight of xerostomia mice.

Electron radiation reduced the submandibular gland weight in xerostomia mice

The submandibular gland weight of xerostomia mice in the Gy-3, Gy-7 and Gy-21 groups was significantly reduced compared to the submandibular gland weight of mice in the NC group (Fig. 3A, all p = 0.001) in a time-dependent manner. In addition, the submandibular gland index of xerostomia mice in the Gy-21 group was markedly decreased compared to the index in the NC group (Fig. 3B, p = 0.000). However, there were no obvious changes in the submandibular gland index in the Gy-3 and Gy-7 groups compared with the NC group (Fig. 3B, p = 0.963 and p = 0.357, respectively). Furthermore, the saliva volume of electron radiation-treated mice (Gy-3, Gy-7 and Gy-21 groups) was significantly lower compared to xerostomia mice in the NC group (Fig. 3C, all p = 0.001).

Electron radiation damaged the submandibular gland structure in xerostomia mice

In the NC group, the glands could be seen, the nucleus was close to the base, arranged in an orderly manner, and blood vessels could be seen in the stroma (Fig. 4). In the electron radiation-treated groups, the submandibular gland was atrophied, the number of cells was decreased, the structure of the gland tissue was loose, and the space between glandular lobules was enlarged (Fig. 4).

Electron radiation triggered an increase in *Cdkn1a* gene transcription

The results of the bioinformatics and miRNA/mRNA association analysis (Kyoto Encyclopedia of Genes and Genomes (KEGG) information analysis) (http://www.genome.ad.jp/kegg/) showed that the targeting gene,

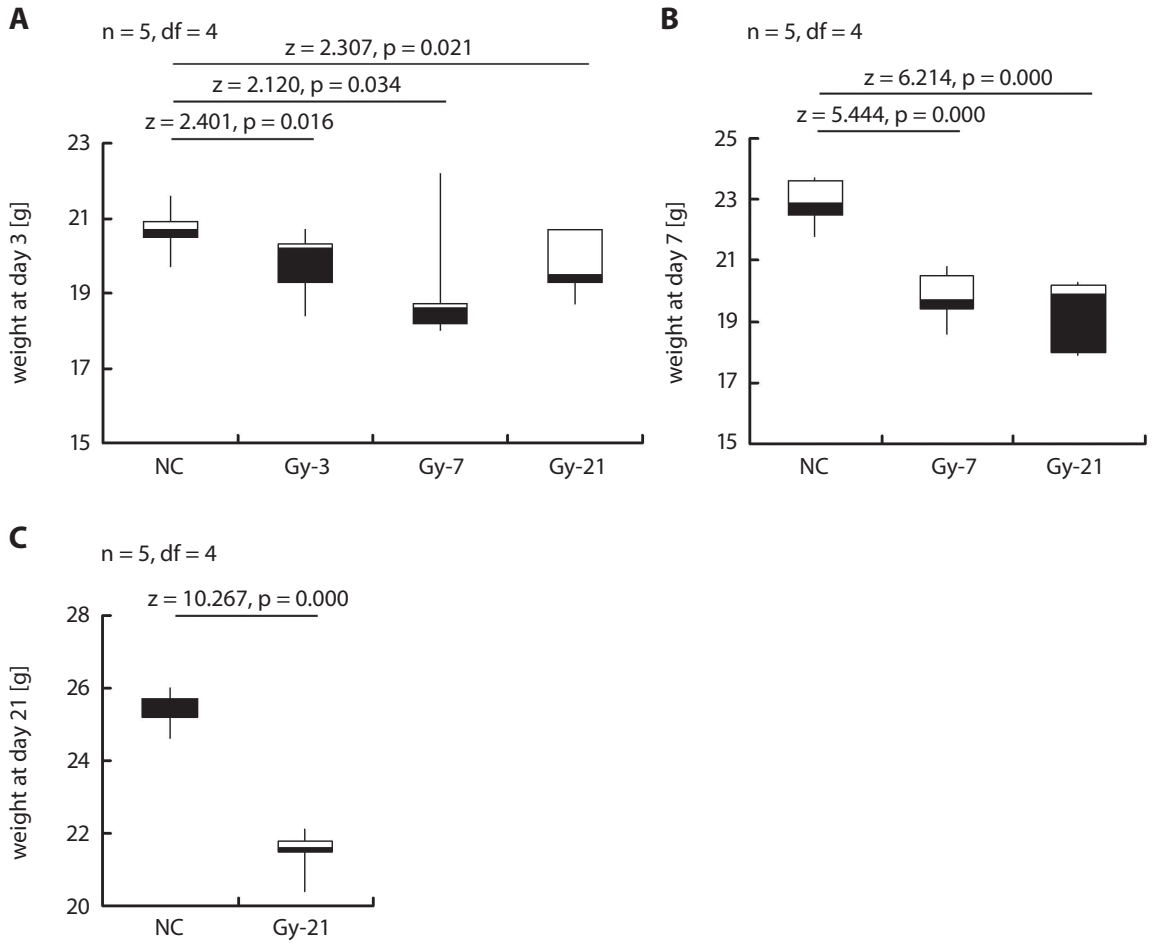

Fig. 2. Electron radiation decreased the body weight (mean ±SD) of xerostomia mice 3 days (A), 7 days (B) and 21 days (C) after the radiation treatment (n = 5 for each group). The white and black bar charts represent the negative control (NC) group and Gy-treated groups, respectively. The p-values for comparisons between groups are shown in the images. df – degrees of freedom

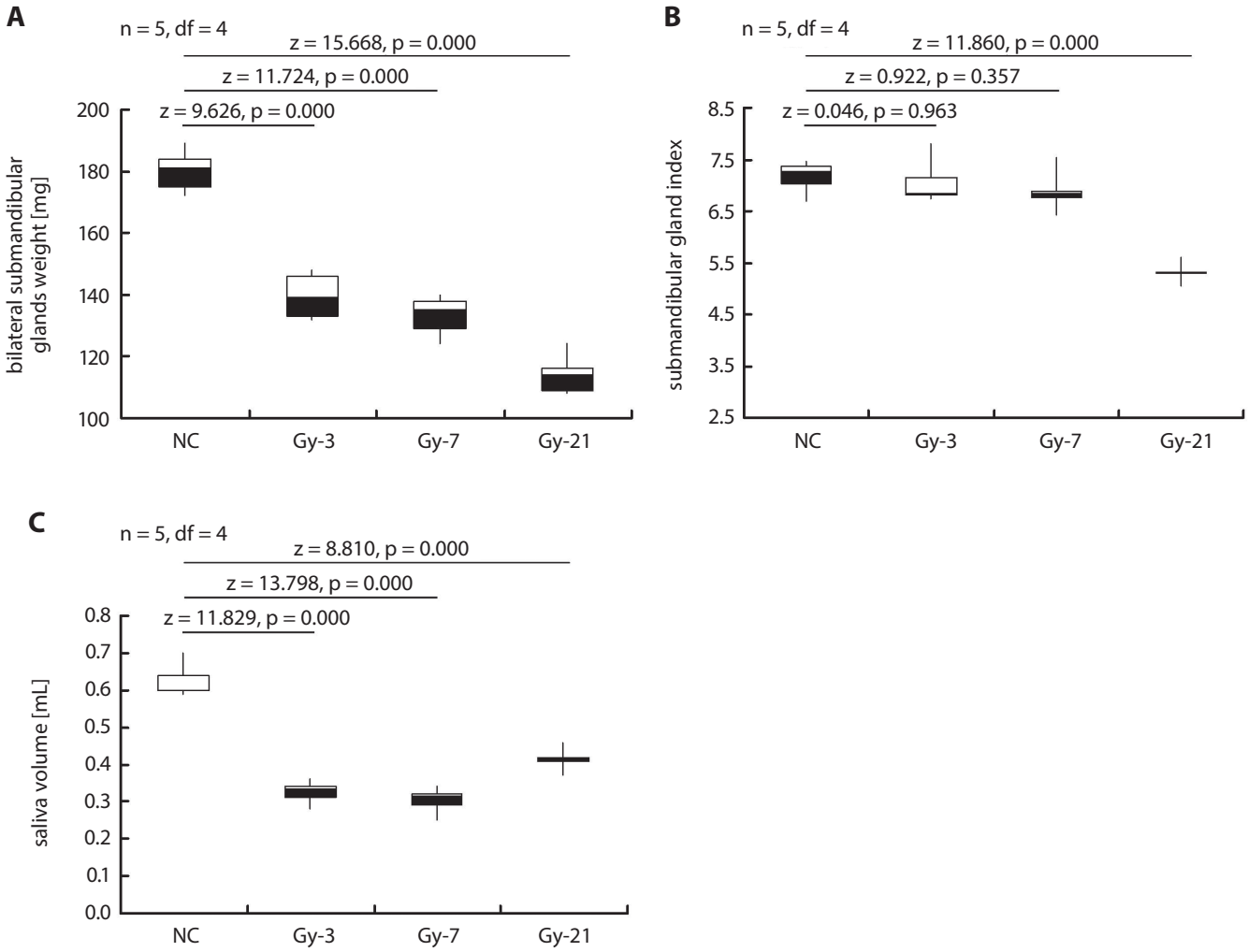

Fig. 3. Effects of electron radiation on the submandibular gland weight (A), submandibular gland index (B), and saliva volume (C) of xerostomia mice (n = 5 for each group). All data are illustrated as mean ±SD. The white and black bar charts represent the negative control (NC) group and Gy-treated groups, respectively. The p-values for comparisons between groups are shown in the images. df – degrees of freedom

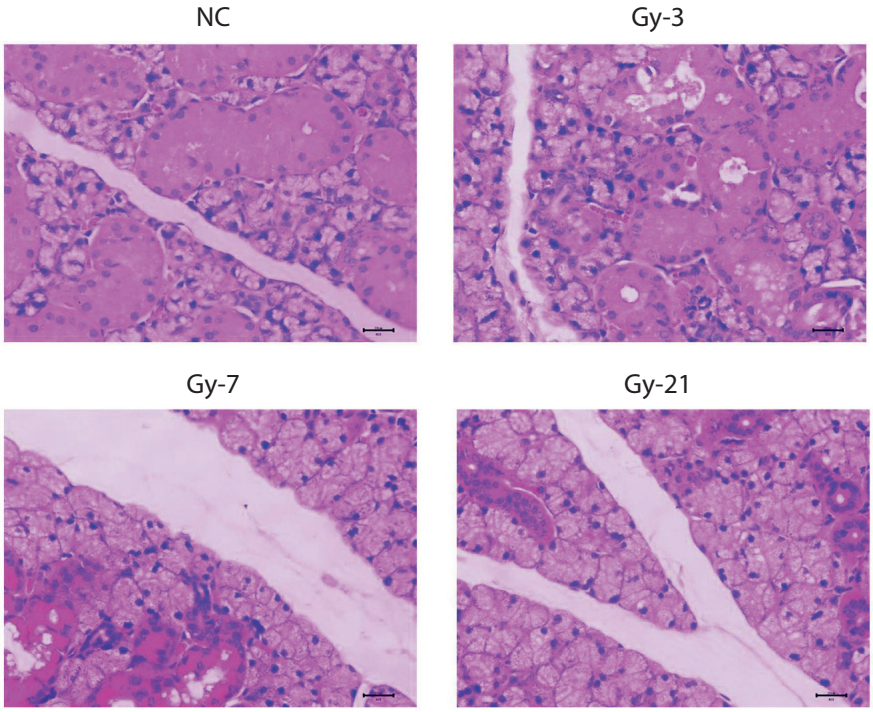

Fig. 4. Electron radiation damaged the structure of the submandibular gland, as determined with hematoxylin and eosin (H&E) staining (n = 5 for each group). NC – negative control

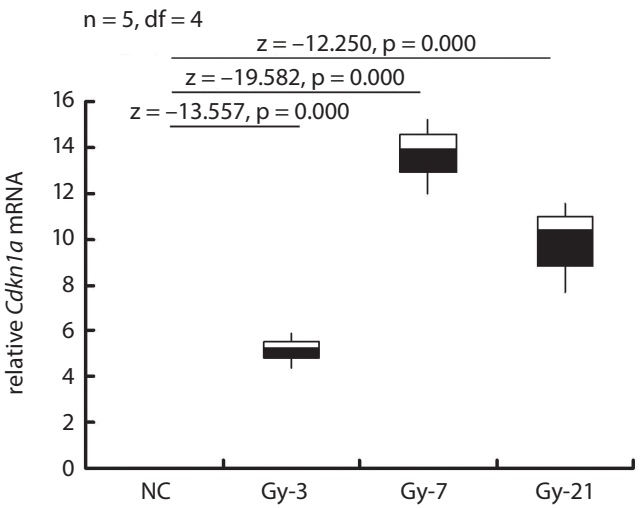

Fig. 5. Electron radiation triggered transcription changes of the *Cdkn1a* gene (n = 5 for each group). All data are illustrated as mean ±SD. The white and black bar charts represent the negative control (NC) group and Gy-treated groups, respectively. The p-values for comparisons between groups are shown in the images. df – degrees of freedom

ENSMUSG00000023067 (*Cdkn1a*), related to xerostomia, was enriched in the p53 signaling pathway. According to the real-time PCR (RT-PCR) findings, *Cdkn1a* gene transcription was significantly increased in mice in the radiation groups compared to mice in the NC group 3 days (p = 0.000), 7 days (p = 0.000) and 21 days (p = 0.000) after the electron radiation treatment (Fig. 5). Therefore, we speculate that *Cdkn1a* might be involved in the pathogenesis of xerostomia.

miR-486a-3p interacted with the *Cdkn1a* gene

As can be observed in Fig. 6, mmu-miR-486a-3p regulated expression of luciferase in 3'-UTR of the *Cdkn1a* gene (p = 0.001). Therefore, mmu-miR-486a-3p effectively regulated the expression of luciferase through binding at 3'-UTR of the *Cdkn1a* gene.

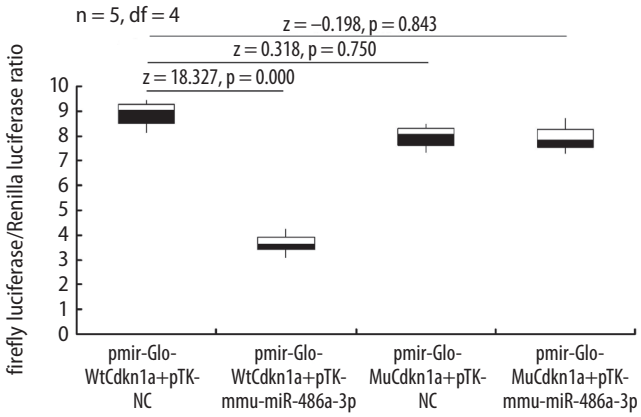

Fig. 6. miR-486a-3p interacted with the *Cdkn1a* gene, as shown using the dual-luciferase assay. The p-values for comparisons between groups are shown in the images. df – degrees of freedom

Discussion

Head-and-neck cancer patients usually suffer from radiotherapy-induced dysfunction of the salivary glands.[16] The submandibular gland secretes about $^{2}/_{3}$ of the amount of unstimulated saliva.[4,17] Therefore, this study mainly focused on investigating the functions of the submandibular gland in xerostomia mice. Previous studies have reported that head-and-neck cancer patients undergoing radiotherapy treatment usually demonstrate decreased salivary secretion and damaged submandibular glands.[18,19] Thus, it is crucial to discover the specific mechanisms for radiation-induced submandibular gland dysfunction and identify the associated molecules.

In this study, we found that electron radiation markedly increased the drinking water amount, decreased saliva volume and body weight, and reduced submandibular gland weight and submandibular gland index of mice compared to those without electron radiation treatment. As shown by these results, the electron radiation-induced symptoms in mice are consistent with those in radiation-treated cancer patients.[20] Based on the H&E staining results, it can be stated that electron radiation damaged the structure of the submandibular gland, resulting in an atrophied gland, decreased cell amounts, loose gland tissues, and enlarged spaces between glandular lobules. We believe that electron radiation might induce the death of cells in the submandibular gland tissues of mice.

According to the KEGG bioinformatics analysis, the *Cdkn1a* gene is highly expressed in submandibular gland tissues. Therefore, it was selected for the dual-luciferase reporter assay to observe the potential interaction with miR-486. As previous studies have documented, plenty of miRNAs have been discovered in the submandibular glands.[21,22] The miR-486 has been proven to participate in the apoptosis process of cells in different disorders. Luo et al. found that *miR-486-5p* promoted apoptosis in an acute lung injury animal model.[23] Fan et al. reported that miR-486 reduction could protect cardiomyocytes against cell injury by inducing apoptosis.[24] The miRNA/mRNA association analysis identified that, taking *Cdkn1a* as the targeting gene, miR-486 demonstrated the most remarkable change. Therefore, we analyzed the relationship between *Cdkn1a* and *miR-486a-3p* and found that *miR-486a-3p* interacts with *Cdkn1a*, which is a typical miRNA–mRNA targeting interaction.[25]

Limitations

Firstly, this study only clarified the interaction between *miR-486a-3p* and *Cdkn1a* in a xerostomia murine model. The downstream molecules involved in the pathological process have not been determined. Secondly, there might be other miRNAs or miRNA–mRNA targeting interactions that participate in the xerostomia process,

which need to be investigated in future studies. Thirdly, this study mainly clarified the miRNA–mRNA targeting interaction between *miR-486a-3p* and the *Cdkn1a* gene. However, the endogenous expression of *miR-486a-3p* and the effects of radiation on *miR-486a-3p* expression have not been determined. Fourthly, this study is only a preliminary investigation of the effects of radiation on xerostomia and proved that *miR-486a-3p* is involved in the effects of radiation. However, whether a deficiency of *miR-486a-3p* could affect *Cdkn1a* expression has not been determined. Lastly, the sample size of this study is small (n = 5 for each group). Therefore, in a follow-up study, we plan to further clarify the specific mechanism for radiation-caused xerostomia in animal models.

Conclusions

Radiation induces damage of the submandibular gland and affects *Cdkn1a* expression by regulating the expression of *miR-486a-3p* in a xerostomia mouse model. Therefore, modulating *miR-486a-3p* and the *Cdkn1a* gene in a xerostomia murine model might reverse damage of the submandibular gland.

ORCID iDs

Wei Wang https://orcid.org/0000-0002-1669-9747
Caizhi Xiao https://orcid.org/0000-0003-0503-7964
Hong Chen https://orcid.org/0000-0003-1403-7157
Fangfei Li https://orcid.org/0000-0003-2710-7089
Dongqin Xia https://orcid.org/0000-0001-6677-1105

References

1. Adesanya MR, Redman RS, Baum BJ, O'Connell BC. Immediate inflammatory responses to adenovirus-mediated gene transfer in rat salivary glands. *Hum Gene Ther*. 1996;7(9):1085–1093. doi:10.1089/hum.1996.7.9-1085
2. Baum BJ, Zheng C, Cotrim AP, et al. Aquaporin-1 gene transfer to correct radiation-induced salivary hypofunction. *Handb Exp Pharmacol*. 2009;190:403–418. doi:10.1007/978-3-540-79885-9_20
3. Emami B, Lyman J, Brown A, et al. Tolerance of normal tissue to therapeutic irradiation. *Int J Radiat Oncol Biol Phys*. 1991;21(1):109–122. doi:10.1016/0360-3016(91)90171-y
4. Limesand KH, Said S, Anderson SM. Suppression of radiation-induced salivary gland dysfunction by IGF-1. *PLoS One*. 2009;4(3):e4663. doi:10.1371/journal.pone.0004663
5. Pucar D, Groves MW, Biddinger P, Figueroa R, Williams HT. Head and neck cancer soft tissue radiation necrosis: Diagnostic challenge. *Clin Nucl Med*. 2019;44(2):e110–e112. doi:10.1097/RLU.0000000000002356
6. Paardekooper GM, Cammelli S, Zeilstra LJ, Coppes RP, Konings AW. Radiation-induced apoptosis in relation to acute impairment of rat salivary gland function. *Int J Radiat Biol*. 1998;73(6):641–648. doi:10.1080/095530098141898
7. Nowicka Z, Stawiski K, Tomasik B, Fendler W. Extracellular miRNAs as biomarkers of head and neck cancer progression and metastasis. *Int J Mol Sci*. 2019;20(19):4799. doi:10.3390/ijms20194799
8. Jing X, Gao Z, Tian L, Liu M. Expressions of miR-122a and miR-3195 in laryngeal cancer and their effects on the proliferation and apoptosis of laryngeal cancer cell Hep-2. *Adv Clin Exp Med*. 2020;29(5):525–534. doi:10.17219/acem/118848
9. Lamichhane SR, Thachil T, Gee H, Milic N. Circulating microRNAs as prognostic molecular biomarkers in human head and neck cancer: A systematic review and meta-analysis. *Dis Markers*. 2019;2019:8632018. doi:10.1155/2019/8632018
10. Fadhil RS, Wei MQ, Nikolarakos D, Good D, Nair RG. Salivary microRNA miR-let-7a-5p and miR-3928 could be used as potential diagnostic bio-markers for head and meck squamous cell carcinoma. *PLoS One*. 2020;15(3):e0221779. doi:10.1371/journal.pone.0221779
11. Dori M, Cavalli D, Lesche M, et al. MicroRNA profiling of mouse cortical prognostors and neurons reveals miR-486-5p as a regulator of neurogenesis. *Development*. 2020;147(9):dev190520. doi:10.1242/dev.190520
12. Zhang C, Gong Y, Li N, et al. Long non-coding RNA Kcnq1to1 promotes cC5b-9-induced podocyte pyroptosis by inhibiting miR-486-3p and upregulating NLRP3. *Am J Physiol Cell Physiol*. 2020;320(3):C355–C364. doi:10.1152/ajpcell.00403.2020
13. Follis AV, Galea CA, Kriwacki RW. Intrinsic protein flexibility in regulation of cell proliferation: Advantages for signaling and opportunities for novel therapeutics. *Adv Exp Med Biol*. 2012;725:27–49. doi:10.1007/978-1-4614-0659-4_3
14. Livak KJ, Schmittgen TD. Analysis of relative gene expression data using real-time quantitative PCR and the $2^{-\Delta\Delta ct}$ method. *Methods*. 2001;25(4):402–408. doi:10.1006/meth.2001.1262
15. Zhou ZH, Shi L, Lang MJ, Chen ZL, Wang YL, He S. Effect of fibroblast growth factor 1 on the proliferating cell nuclear antigen expression in submandibular gland of diabetic mice [in Chinese]. *Zhonghua Kou Qiang Yi Xue Za Zhi*. 2017;52(5):294–299. doi:10.3760/cma.j.issn.1002-0098.2017.05.007
16. Strojan P, Hutcheson KA, Eisbruch A, et al. Treatment of late sequelae after radiotherapy for head and neck cancer. *Cancer Treat Rev*. 2017;59:79–92. doi:10.1016/j.ctrv.2017.07.003
17. de Almeida PDV, Gregio AM, Machado MA, de Lima AA, Azevedo LR. Saliva composition and functions: A comprehensive review. *J Contemp Dent Pract*. 2008;9(3):72–80. PMID:18335122
18. Jensen SB, Vissink A, Limesand KH, Reyland ME. Salivary gland hypofunction and xerostomia in head and neck radiation patients. *J Natl Cancer Inst Monogr*. 2019;2019(53):lgz016. doi:10.1093/jncimonographs/lgz016
19. Almstahl A, Skoogh Andersson J, Alstad T, Fagerberg-Mohlin B, Finizia C. Explorative study on quality of life in relation to salivary secretion rate in head and neck cancer patients treated with radiotherapy up to 2 years post treatment. *Int J Dent Hyg*. 2019;17(1):46–54. doi:10.1111/idh.12363
20. Uchiyama Y, Kreiborg S, Murakami S, Tsujimoto T, Sumida I. Changes in the submandibular gland in patients with head and neck cancer after resection therapy: A preliminary study. *Anticancer Res*. 2017;37(6):3239–3242. doi:10.21873/anticanres.11686
21. Hayashi T, Koyama N, Azuma Y, Kashimata M. Mesenchymal miR-21 regulates branching morphogenesis in murine submandibular gland in vitro. *Dev Biol*. 2011;352(2):299–307. doi:10.1016/j.ydbio.2011.01.030
22. Hayashi T, Koyama N, Gresik EW, Kashimata M. Detection of EGF-dependent microRNAs of the fetal mouse submandibular gland at embryonic day 13. *J Med Invest*. 2009;56(Suppl):250–252. doi:10.2152/jmi.56.250
23. Luo Q, Zhu J, Zhang Q, Xie J, Yi C, Li T. MicroRNA-486-5p promotes acute lung injury via inducing inflammation and apoptosis by targeting OTUD7B. *Inflammation*. 2020;43(3):975–984. doi:10.1007/s10753-020-01183-3
24. Fan J, Shi S, Qiu Y, Zhang Z, Yu L. MicroRNA-486-5p down-regulation protects cardiomyocytes against hypoxia-induced cell injury by targeting IGF-1. *Int J Clin Exp Pathol*. 2019;12(7):2544–2551. PMID:31934081
25. Ma R, Wang C, Wang J, Wang D, Xu J. miRNA–mRNA interaction network in non-small cell lung cancer. *Interdiscip Sci*. 2016;8(3):209–219. doi:10.1007/s12539-015-0117-8

Oxidative and pro-inflammatory lung injury induced by desflurane inhalation in rats and the protective effect of rutin

Mustafa Tosun[1,A,B,D,F], Hasan Olmez[1,A,B,E], Edhem Unver[1,C,E], Yusuf Kemal Arslan[2,C], Ferda Keskin Cimen[3,B,C], Adalet Ozcicek[4,C,E], Mehmet Aktas[5,B,C], Halis Suleyman[6,A,E,F]

[1] Department of Chest Diseases, Faculty of Medicine, Erzincan Binali Yıldırım University, Turkey
[2] Department of Biostatistics, Faculty of Medicine, Erzincan Binali Yıldırım University, Turkey
[3] Department of Pathology, Faculty of Medicine, Erzincan Binali Yıldırım University, Turkey
[4] Department of Internal Medicine, Faculty of Medicine, Erzincan Binali Yıldırım University, Turkey
[5] Department of Biochemistry, Faculty of Medicine, Erzincan Binali Yıldırım University, Turkey
[6] Department of Pharmacology, Faculty of Medicine, Erzincan Binali Yıldırım University, Turkey

A – research concept and design; B – collection and/or assembly of data; C – data analysis and interpretation; D – writing the article; E – critical revision of the article; F – final approval of the article

Advances in Clinical and Experimental Medicine, ISSN 1899–5276 (print), ISSN 2451–2680 (online) *Adv Clin Exp Med*. 2021;30(9):941–948

Address for correspondence
Mustafa Tosun
E-mail: dr.mustafatosun@hotmail.com

Funding sources
None declared

Conflict of interest
None declared

Received on September 26, 2020
Reviewed on March 22, 2021
Accepted on April 27, 2021

Published online on August 19, 2021

Cite as
Tosun M, Olmez M, Unver E, et al. Oxidative and pro-inflammatory lung injury induced by desflurane inhalation in rats and the protective effect of rutin. *Adv Clin Exp Med*. 2021;30(9):941–948. doi:10.17219/acem/136194

DOI
10.17219/acem/136194

Abstract

Background. Desflurane is a mainstay of general inhaled anesthetics with a methyl ethyl ether structure and is widely used in clinical practice. It has been reported to induce inflammation and lipid peroxidation in rat pulmonary parenchyma, to increase alveolar macrophages, and to cause peribronchial infiltration and edema. Rutin, a flavonoid vitamin P1, is known to have biological properties including acting as an antioxidant, an anti-inflammatory, and an inhibitor of bronchoalveolar polymorphonuclear leukocyte (PNL) infiltration.

Objectives. The aim of this study is to examine the effects of rutin on desflurane-induced pulmonary injury using biochemical and histopathological methods.

Materials and methods. The rats were divided into 3 groups (n = 6 each): healthy control (HC), rutin+desflurane-treated (DRT) and desflurane-only (DSF). Briefly, 50 mg/kg of rutin was given orally to the DRT group and an equal volume of normal saline was given to the DSF and HC groups. After 1 h, anesthesia was induced and maintained in the DRT and DSF groups for 2 h. After the rats had been sacrificed, the lungs were removed. Malondialdehyde (MDA), total glutathione (GSH), tumor necrosis factor alpha (TNF-α), and nuclear factor kappa B (NF-κB) levels were measured in the excised lung tissue. The removed tissues were also fixed in 10% formalin, and the obtained sections were stained with hematoxylin and eosin (H&E) and evaluated under light microscopy. The biochemical and histopathological results of the DRT group were compared with those obtained from the DSF and HC groups.

Results. Desflurane increased MDA, TNF-α and NF-κB, and decreased GSH in lung tissue. The PNL infiltration, alveolar macrophages, hemorrhage, alveolar damage, and edema were observed in the lung tissue of the DSF group. Rutin was histopathologically shown to protect lung tissue from oxidative stress by preventing an increase in oxidant parameters and a decrease in antioxidants.

Conclusions. The results suggest that rutin may be useful in the treatment of desflurane-associated lung injury.

Key words: oxidative stress, desflurane, lung injury, rutin

Background

Desflurane is one of the modern inhaled anesthetic drugs commonly used today that has a methyl ethyl ether structure.[1] This anesthetic gas was first synthesized in the USA in the 1960s and entered into service in 1990.[2] Desflurane has been widely used because of its safety and effectiveness, as well as promoting a rapid recovery and extubation.[1,3] However, like other inhalation anesthetics, desflurane affects respiration.[4] The irritant effect of desflurane on the airways is much more pronounced than sevoflurane and halothane.[5,6] Allaouchiche et al. have evaluated bronchoalveolar and systemic oxidative stress in animals exposed to desflurane. In their study, it was shown that desflurane accelerates the lipid peroxidation (LPO) reaction in bronchoalveolar tissue, increases the production of malondialdehyde (MDA), and induces systemic oxidative stress.[7] It has also been reported that desflurane induces inflammation and LPO in rat pulmonary parenchyma, and causes peribronchial infiltration, alveolar septal infiltration and edema, and increases alveolar macrophages.[8] However, the role of pro-inflammatory cytokines, such as tumor necrosis factor alpha (TNF-α) and nuclear factor kappa B (NF-κB), in desflurane-induced lung toxicity has not yet been examined.

Desflurane has not only been reported to cause lung injury but also severe liver injury resulting in death.[9] Studies have shown that oxidative stress plays an important role in the pathogenesis of the toxic effects of desflurane in the liver.[10] To date, there has not been any research examining the effects of desflurane on glutathione (GSH), which acts as a total antioxidant in lung tissue. However, while desflurane causes MDA to increase in liver tissue, the amount of total GSH decreases.[11] These findings indicate that desflurane may cause oxidative and inflammatory damage in lung tissue. In addition, it can be proposed that agents that have both antioxidant and anti-inflammatory activity can protect the lungs from desflurane toxicity.

In this study, the effects of rutin (3,3,4,5,7-pentahydroxyflavone-3-rhamnoglucoside), a vitamin P_1 flavonoid, on desflurane-induced lung injury were examined.[12] Rutin is known to have various biological properties such as antioxidant, anti-inflammatory, antibacterial, and anti-hyperglycemic activity, cytokine inhibition, bronchoalveolar polymorphonuclear granulocyte infiltration inhibition, and immunomodulation.[13–15] Rutin has also been reported to reduce lipopolysaccharide-induced oxidative acute lung injury.[16] These findings indicate that rutin may be effective in reducing the lung damage induced by desflurane. At present, there are no studies that have examined the effects of rutin on desflurane-induced lung injury.

Objectives

The current study aimed to determine the harmful effects of desflurane on the lung using biochemical and histopathological methods, and to measure the protective effects of rutin, a significant antioxidant.

Materials and methods

Animals

Experimental animals were obtained from the Atatürk University Medical Experimental Application and Research Center. A total of 18 male albino Wistar rats weighing 235–248 g were used in the experiments. All of the animals were kept and fed in groups in the laboratory environment (22°C) before the experiment. Animal experiments were performed according to the National Guidelines for the Use and Care of Laboratory Animals, and were approved by the local animal ethics committee of Atatürk University (Erzurum, Turkey) with a decision No. 5/117, dated April 27, 2018.

This study conformed to the ethical standards laid down in the 1964 Declaration of Helsinki. The manuscript does not contain clinical studies or patient data.

Chemicals

Desflurane (Suprane 100% inhalation steam, 240 mL) was obtained from Eczacıbaşı-Baxter Hospital Supply Industry (Istanbul, Turkey) and rutin was obtained from Solgar (Leonia, USA). Each tablet contained 500 mg of rutin (>94% purity).

Experimental groups

The rats were divided into 3 groups with 6 rats each: 1) healthy control (HC) group, 2) desflurane (DSF), and 3) 50 mg/kg rutin and desflurane (DRT).

Preparation of rutin suspension

In order to administer rutin at a dosage of 50 mg/kg to each animal whose average weight was 241.5 g, the calculated dosage was found to be 12.075 mg (241.5 g × 50/1000 = 12.075 mg). The 12.075 mg rutin dosage was prepared for each animal as a suspension in 0.5 mL of a 0.9% NaCl solution.

Experimental procedure

The anesthesia gas vaporizer was calibrated prior to the experiment. The anesthetic gas was adjusted according to the recommendations of Eger–Johnson and Haelwyn with a minimum alveolar concentration of 1% and a desflurane concentration of 6%.[17] Briefly, 50 mg/kg of rutin was orally administered to the DRT group (n = 6). The DSF (n = 6) and HC (n = 6) groups were treated orally with the same volume of normal saline (0.5 mL 0.9%

NaCl). One hour after rutin and 0.9% NaCl administration to the DRT and DSF groups, anesthesia was induced and maintained for 2 h in a 40 × 40 × 70 cm transparent plastic box. The box was connected to the semi-open anesthesia machine with fixed hoses. At five-minute intervals, preoxygenation was applied to the cages with 100% oxygen. Anesthesia maintenance was provided by a mixture of 2 L of oxygen and 2 L of nitrous oxide with 6% desflurane. Following this, the animals were sacrificed by decapitation and their lungs were removed. Malondialdehyde, GSH, TNF-α, and NF-κB levels were measured in the excised lung tissue, and the tissues were evaluated histopathologically. The biochemical and histopathological results of the DRT group were compared with those obtained from the DSF and HC groups.

Biochemical analyses

Sample preparation

Homogenates were prepared from the lung tissues for biochemical analysis. The GSH and MDA levels in the supernatants obtained from these homogenates were determined using appropriate methods based on the literature. Briefly, 0.2 g was weighed from each tissue sample and removed at this stage of the study. The level of MDA in the lung tissue was determined using 1.15% potassium chloride solution, and the other measurements were carried out with phosphate buffer at pH 7.5. The tissue was homogenized in ice and mixed with an appropriate solution, completed to a total of 2 mL.[17,18] The samples were then centrifuged at 4°C for 10 min at 10,000 rpm. The supernatant portion was used as the analysis sample for MDA, GSH, TNF-α, NF-κB, and protein concentration measurements.

MDA analysis

The MDA measurement was based on a spectrophotometric measurement (at 532 nm) of the absorbance of a pink colored complex formed by thiobarbituric acid (TBA) and MDA at a high temperature (95°C).[18] Briefly, 250 μL of homogenate, 100 μL of 8% sodium dodecyl sulfate (SDS), 750 μL of 20% acetic acid, 750 μL of 0.08% TBA, and 150 μL of distilled water were mixed in Eppendorf tubes and vortexed. The mixture was then incubated at 100°C for 60 min and, once cooled down, 2.5 mL of n-Butanol was added. Spectrophotometric measurements were then made. The resulting red color was read using 3 mL cuvettes whose light path is 1 cm at 532 nm. The MDA level of the samples was determined by taking the dilution coefficients into consideration and using a standard graph derived from previously prepared MDA stock solutions. The stock standard solution with a 200 μmol/L concentration was prepared using standard: 1.1.3.3-tetraethoxypropane. Standard solutions with different concentrations were achieved through serial dilution of the prepared stock standard.

GSH analysis

The DTNB (5,5'-Dithiobis (2-nitrobenzoic acid)), a disulfide chromogen used in the measurement medium, is decreased by compounds with sulfhydryl groups. The resulting yellow color was spectrophotometrically measured at 412 nm.[20] Before measurement, 0.5 mL of meta-phosphoric acid was added to 0.5 mL of the prepared supernatant and centrifuged for 2 min at 2000 rpm for deproteinization. Then, 1500 μL of measuring buffer (200 mM Tris-HCl containing 0.2 mM EDTA, pH = 8.2), 500 μL of supernatant, 100 μL of DTNB, and 7900 μL of methanol were mixed in Eppendorf tubes and vortexed. The mixture was incubated at 37°C for 30 min and then measured with the spectrophotometer. The amount of yellow color was read using 3 mL quartz cuvettes at 412 nm, and the GSH levels in the samples were determined by taking the dilution coefficients into consideration and using a standard graph derived from a GSH stock solution prepared previously.

TNF-α and NF-κB analysis

Tissue-homogenate NF-κB and TNF-α concentrations were measured using rat-specific sandwich enzyme-linked immunosorbent assay kits (Rat Nuclear Factor-kappa B ELISA kit, cat. No: 201-11-0288; SunRed Biological Technology, Shangai, China; and Rat Tumor Necrosis Factor α ELISA kit, cat No: YHB1098Ra, Shanghai LZ, Shanghai, China). Analyses were performed according to the manufacturers' instructions. Briefly, monoclonal antibodies specific for rat NF-κB and TNF-α were coated onto the wells of micro plates. The tissue homogenate, standards, biotinylated monoclonal antibody, and streptavidin-horseradish peroxidase (HRP) were pipetted into these wells and then incubated at 37°C for 60 min. After washing, chromogen reagent A and chromogen reagent B were added, which is acted upon by the bound enzyme to produce a color. The samples were then incubated at 37°C for 10 min and a stop solution was added. The intensity of the colored product is directly proportional to the concentration of rat NF-κB and TNF-α present in the original specimen. At the end of the course, the well plates were read at 450 nm. The concentration of the samples was calculated from formulas derived from standard graphs.

Histopathological examination

The removed tissues were fixed in a 10% formalin solution for 24 h. Four micron-thick sections were obtained from the paraffin blocks using routine techniques and stained with hematoxylin and eosin (H&E). All sections were evaluated using light microscopy (Olympus BX 52; Olympus Corp., Tokyo, Japan) by a pathologist who was not aware of the treatment protocols.

Statistical analyses

The results for continuous variables are presented as means ± standard deviation (SD). The normality of the distributions for continuous variables was confirmed with the Kolmogorov–Smirnov test. For the comparison of groups, one-way analysis of variance (ANOVA) was used. The homogeneity of variances was confirmed with Levene's test, and post hoc Tukey's honest significant difference (HSD) or Games–Howell tests were used according to the homogeneity of the variances. The statistical level of significance for all tests was considered to be 0.05. Statistical analyses were performed using IBM SPSS Statistics for Windows v. 19.0 software (IBM Corp., Armonk, USA).

Results

MDA and GSH analysis

Malondialdehyde levels in the lung tissues were different across the study groups ($F(2, 15) = 292.7$, $p < 0.001$). Levels of MDA in the DSF group were significantly higher than the levels of healthy animals (7.3 ±0.7 µmol/g protein compared to 1.3 ±0.4 µmol/g protein, $p < 0.001$). In the DRT group, MDA levels were similar to the HC animals (1.7 ±0.1 µmol/g protein compared to 1.3 ±0.4 µmol/g protein, $p > 0.05$; Fig. 1). In addition, GSH levels in the lung tissues were statistically different across the study groups ($F(2, 15) = 247.9$, $p < 0.001$). Glutathione levels in the lung tissues of the HC animals were statistically higher than in the DSF rats (5.5 ±0.4 nmol/g compared to 1.5 ± 0.2 nmol/g ($p < 0.001$). Rutin allowed GSH levels to be maintained at 5.2 ±0.4 nmol/g and there was no significant difference between GSH levels in the HC and DRT groups ($p > 0.05$; Fig. 2).

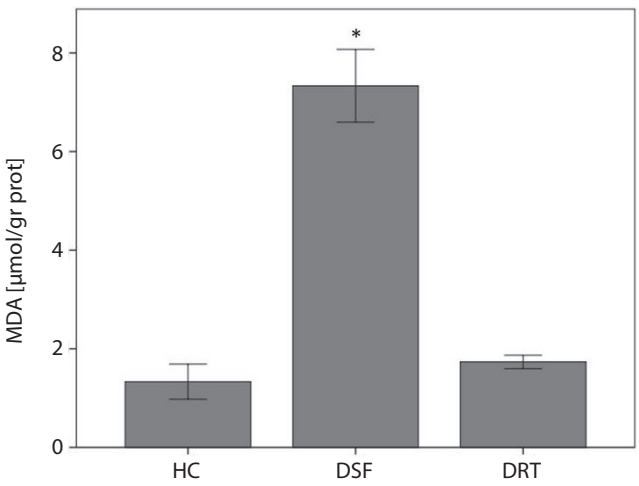

Fig. 1. Malondialdehyde (MDA) levels in the study groups; * $p < 0.001$ when compared with healthy control group (HC). DRT – rutin+desflurane-treated group; DSF – desflurane-only group

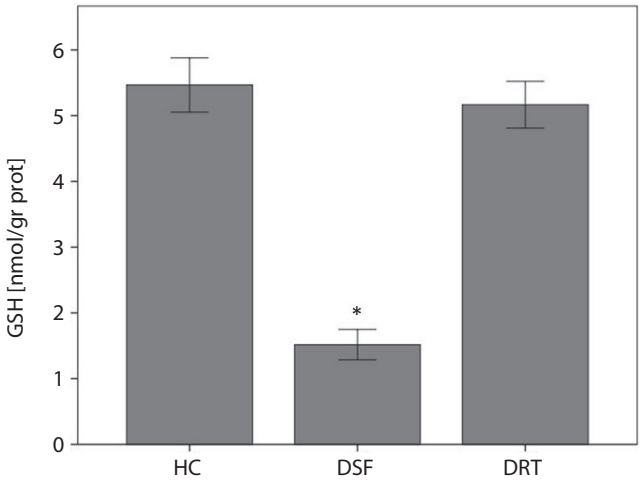

Fig. 2. Glutathione (GSH) levels in the study groups; * $p < 0.001$ when compared with healthy control group (HC). DRT – rutin+desflurane-treated group; DSF – desflurane-only group

TNF-α and NF-κB analysis

The TNF-α and NF-κB levels in the lung tissues were different across the study groups ($F(2, 15) = 250.9$, $p < 0.001$; $F(2, 15) = 554.3$, $p < 0.001$, respectively). The TNF-α and NF-κB levels in the lung tissues of the DSF animals were both significantly higher than in the HC rats (6.7 ±0.6 pg/mL compared to 1.8 ±0.3 pg/mL for TNF-α and 8.8 ±0.5 pg/mL compared to 2.7 ±0.3 pg/mL for NF-κB). However, rutin administration prevented the TNF-α and NF-κB levels increase induced by desflurane ($p > 0.05$; Fig. 3,4). In the DRT group, TNF-α and NF-κB levels were similar to the HC animals (2.2 ±0.2 pg/mL compared to 1.8 ±0.3 pg/mL for TNF-α and 3.0 ±0.3 pg/mL compared to 2.7 ±0.3 pg/mL for NF-κB).

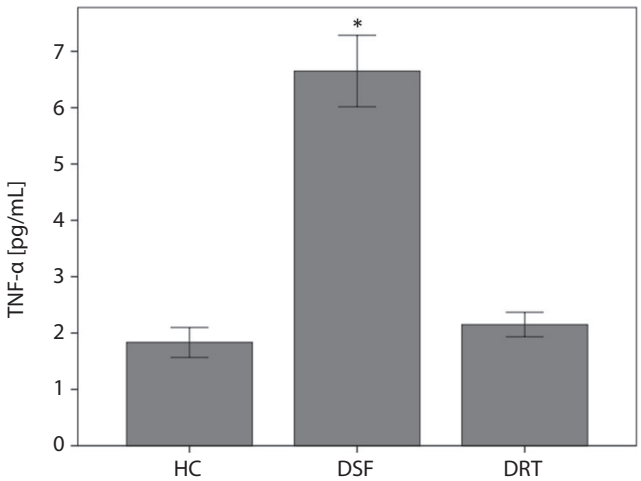

Fig. 3. Tumor necrosis factor alpha (TNF-α) levels in the study groups; * $p < 0.001$ when compared with healthy control group (HC). DRT – rutin+desflurane-treated group; DSF – desflurane-only group

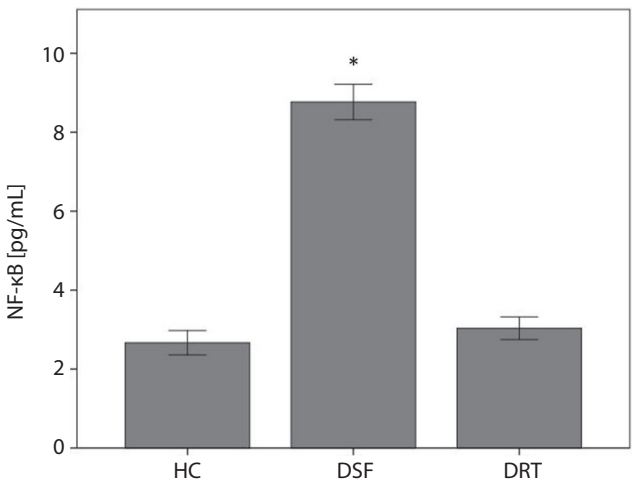

Fig. 4. Nuclear factor kappa B (NF-κB) levels in the study groups; * $p < 0.001$ when compared with healthy control group (HC). DRT – rutin+desflurane-treated group; DSF – desflurane-only group

Histopathological findings

As can be seen in Fig. 5, normal pleural mesothelium, bronchioles pulmonary arterioles and alveolar canals were observed in the lung tissues of healthy animals. On the other hand, polymorphonuclear leucocyte (PNL) infiltration, alveolar macrophages, hemorrhage, alveolar damage, and edema were observed in the lung tissue of the DSF group (Fig. 6). However, no pathological findings were reported in the lung tissue of the DRT group, with the exception of dilated conjunctival blood vessels (Fig. 7).

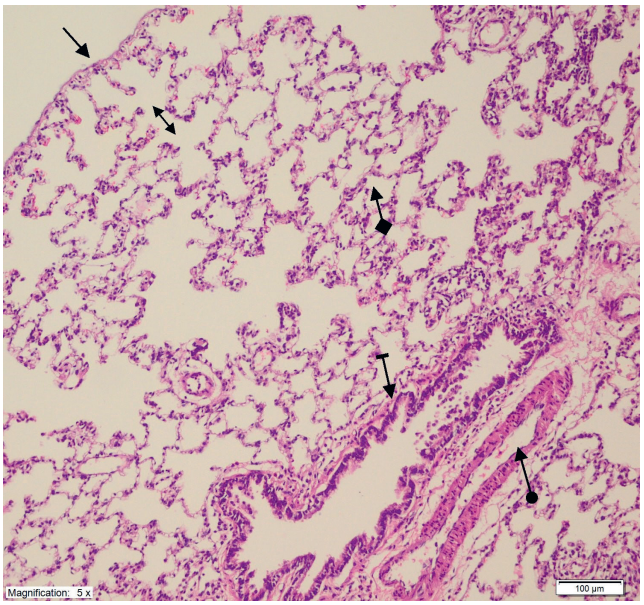

Fig. 5. Histopathological examination of the healthy control group (HC). Normal pleural mesothelium (straight arrow), bronchioles (striped arrow), pulmonary arterioles (round arrow), alveoli (square arrow), and alveolar channels (double arrow) were observed in lung tissues of healthy animals (H&E staining, ×100 magnification)

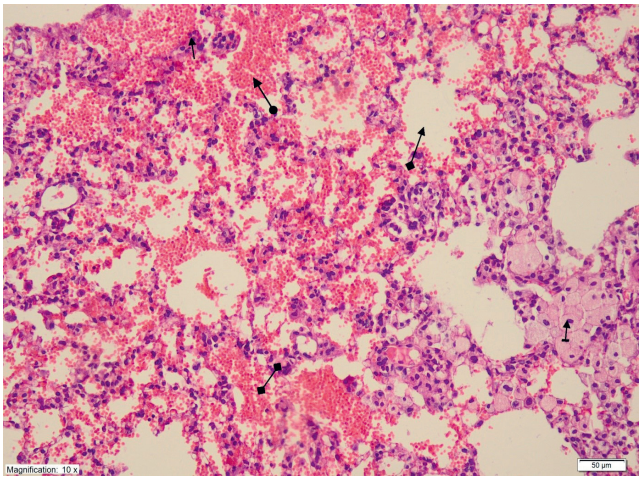

Fig. 6. Histopathological examination of the desflurane-only group (DSF). Polymorphonuclear leucocyte infiltration (straight arrow), alveolar macrophages (straight arrow), hemorrhage (round arrow), alveolar damage (double square arrow), and edema (single square) were observed in the DSF group inhaling desflurane (H&E staining, ×200 magnification)

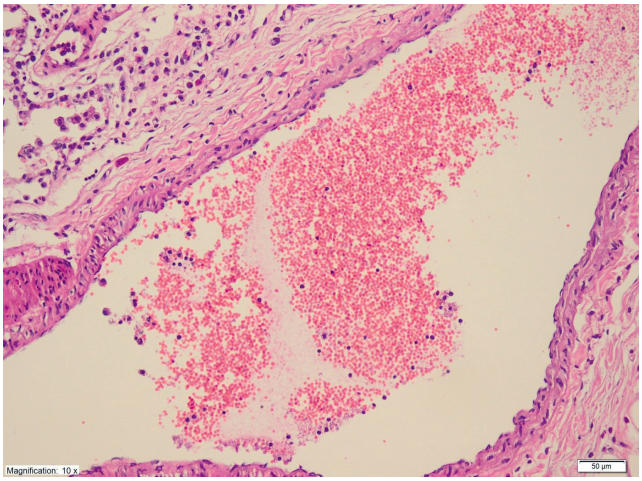

Fig. 7. Histopathological examination of the rutin+desflurane-treated group (DRT). No pathological findings except dilated conjunctival blood vessels were detected in the lung tissue of the DRT group (H&E staining, ×200 magnification)

Discussion

In this study, the effect of rutin on desflurane inhalation induced lung injury in rats was investigated biochemically and histopathologically. The biochemical results showed that, in lung tissues of the DSF animals, the levels of MDA, TNF-α and NF-κB increased, and the level of GSH decreased significantly, compared to HC and DRT groups. Desflurane is a drug that provides rapid awakening when discontinued and shortens the duration of patients' stay in the recovery room. For this reason, it is one of the most commonly used modern inhaled anesthetic agents. However, when desflurane is used alone for induction of anesthesia, it irritates the respiratory tract, increases secretion, and triggers coughing and laryngospasm.[1,2] Desflurane has been compared with other inhaled anesthetics in various

studies and it has been reported that it increases oxidative stress in the lung, and causes inflammation and more lung damage than other anesthetics.[7,21–24] The high MDA and low GSH levels in the lung tissues of the DSF group indicate that the oxidant/antioxidant balance changes in favor of oxidants. Under normal physiological conditions, the oxidant/antioxidant balance is maintained in favor of antioxidants. Any change in this balance in favor of oxidants is called oxidative stress.[25] Reactive oxygen species (ROS) leading to oxidative stress oxidize cell membrane lipids, facilitate the production of toxic products such as MDA from lipids, and exacerbate cellular damage.[26,27] Many studies have reported that desflurane increases MDA levels and plays a role in oxidative stress.[8,28,29] In the current study, MDA levels were similar between the HC group and the DRT group, but significantly elevated in the DSF group. Similar to these results, a recent study conducted by Adefegha et al. reported that rutin suppresses oxidative damage mediated by acute inflammation in rats by its anti-inflammatory activity.[30]

In addition, it has been shown that rutin prevents leakage of polymorphonuclear granulocytes into the bronchoalveolar lavage (BAL) fluid in LPS-induced acute lung injury (ALI).[13,31] Furthermore, rutin has been shown to play a preventive role in the development of acute respiratory distress syndrome (ARDS) by increasing the secretion of pro-inflammatory cytokines and by a concentration-dependent inhibition of LPS-induced inflammatory reactions, including lipid peroxidation.[32] It has also been shown that decreased superoxide dismutase, catalase and glutathione peroxidase caused by LPS, and the activities of antioxidant enzymes, such as oxygenase-1, can be reversed by rutin.[16]

One of the most important non-enzymatic endogenous antioxidants in cellular defense against oxidative damage is GSH. It protects the cell from ROS damage by chemically detoxifying hydrogen peroxide or organic oxides.[33,34] In the current study, it was observed that GSH levels decreased in the desflurane group, whereas they were similar and maintained in the HC and DRT groups. Based on these results, it is likely that rutin, by increasing GSH levels, has preventive effects against oxidative stress.. A high GSH level is accepted as an indicator of normal cell function and viability, whereas a decrease in the GSH level is considered as a weakness of the intracellular defense system and a marker of damage.[35]

Furthermore, in the current study, TNF-α levels in the lung tissues of the DSF animals were found to be higher than that of the HC and DRT groups. The TNF-α, which is the first detectable cytokine in the blood after tissue damage, is a glycoprotein synthesized mainly by monocytes and macrophages that can cause inflammation and tissue damage at high concentrations.[36] Free oxygen radicals induced by TNF-α also cause edema by increasing vascular permeability,[37] and pulmonary edema during septic shock occurs with this mechanism.[38] It has also been reported that TNF-α was elevated in a patient who underwent desflurane anesthesia for ear surgery, and a systemic and intrapulmonary pro-inflammatory response developed.[39] When we evaluated NF-κB levels, it was found that NF-κB levels were increased in the DSF group, and that the HC and DRT groups showed similar levels of TNF-α. Increased NF-κB in the DSF group and similar levels in the HC and DRT groups can be considered an indicator of the anti-inflammatory effects of flavonoids. Studies have also shown that abnormal activation and inhibition of NF-κB plays a role in the pathophysiological processes of many diseases such as metabolic, inflammatory and neurodegenerative diseases, and cancer.[40] Resveratrol, a flavonoid in red wine, also inhibits NF-κB activity. Accordingly, it is thought that resveratrol can reduce the mortality rates of coronary heart diseases and some types of cancer.[41] Lee et al. reported that TNF-α released from endothelial cells stimulated by LPS and subsequently activated NF-κB are suppressed by rutin in a dose-dependent manner, suggesting that rutin may be useful in vascular inflammatory diseases.[42]

In the current study, the biochemical results were also supported by histopathological findings. In a study by Aldemir et al. evaluating the effects of desflurane and isoflurane on the lung histopathologically, the degree of peribronchial inflammatory infiltration and the number of alveolar macrophages were significantly higher in the desflurane group. In addition, alveolar septal infiltration and edema were detected together with high MDA levels.[8] Others have examined changes in the rabits' lungs after human recombinant TNF-α injection, and increased vascular permeability, granulocyte infiltration and edema were found.[37] In this study, PNL infiltration, alveolar macrophages, hemorrhage, alveolar damage, and edema were observed in lung tissues of the DSF group. It is likely that these findings are due to the increase in TNF-α, NF-κB and MDA levels in lung tissue. Many studies have been conducted on the preventive effect of rutin against lung injury caused by LPS.[31,43] Histopathological examination in LPS-induced ALI revealed that rutin prevented PNL infiltration, which is expected to be the dominant cell in BAL fluid, and had a protective effect against ALI.[43] Others have shown that rutin has a preventive effect against ARDS by inhibiting lipid peroxidation.[32] Similar to these studies, no histopathologic findings, except for dilated conjunctival blood vessels, were found in the DRT group in our study. We believe that this is proof of the protective effect of rutin.

Limitations

In order to explain the mechanisms of lung damage caused by desflurane in more detail, total oxidant, total antioxidant and anti-inflammatory cytokine levels should be measured, and the effect of rutin on these parameters should be investigated. In addition, it will be important to examine the molecular histopathology of the tissues.

Conclusions

The results indicate that desflurane inhalation increases MDA, TNF-α and NF-κB, factors associated with inflammation and oxidative stress, and decreases GSH, a strong antioxidant, in lung tissues of rats. Administration of rutin reversed the effects of desflurane on these parameters and eliminated oxidative stress, showing a protective effect on lung tissue. Our experimental results showed that the biochemical and histopathological effects were consistent. We consider that these results will shed light on future studies investigating the protective effect of rutin on the lungs.

ORCID iDs

Mustafa Tosun https://orcid.org/0000-0002-5204-2099
Hasan Olmez https://orcid.org/0000-0003-4153-9953
Edhem Unver https://orcid.org/0000-0002-0322-8102
Yusuf Kemal Arslan https://orcid.org/0000-0003-1308-8569
Ferda Keskin Cimen https://orcid.org/0000-0002-1844-0827
Adalet Ozcicek https://orcid.org/0000-0003-3029-4524
Mehmet Aktas https://orcid.org/0000-0003-1931-8353
Halis Suleyman https://orcid.org/0000-0002-9239-4099

References

1. Jakobsson J. Desflurane: A clinical update of a third-generation inhaled anaesthetic. *Acta Anaesthesiol Scand*. 2012;56(4):420–432. doi:10.1111/j.1399-6576.2011.02600.x
2. Bedi A, Howard Fee JP. Inhalational anaesthesia. *Curr Opin Anaesthesiol*. 2001;14(4):387–392. doi:10.1097/00001503-200108000-00002
3. Meco M, Cirri S, Gallazzi C, Magnani G, Cosseta D. Desflurane preconditioning in coronary artery bypass graft surgery: A double-blinded, randomised and placebo-controlled study. *Eur J Cardiothoracic Surg*. 2007;32(2):319–325. doi:10.1016/j.ejcts.2007.05.005
4. MS Sheller. New volatile anaesthetics: Desflurane-sevoflurane. *Semin Anaesth*. 1992;(11):114–122.
5. Stoelting RK. Pharmacology and physiology in anaesthetic practice. In: *Pharmacology and Physiology in Anaesthetic Practice*. 3rd ed. Philadelphia, USA: Lippincott-Raven Publishers; 1999:47–123.
6. Taylor RH, Lerman J. Induction, maintenance and recovery characteristics of desflurane in infants and children. *Can J Anaesth*. 1992;39(1):6–13. doi:10.1007/BF03008665
7. Allaouchiche B, Debon R, Goudable J, Chassard D, Duflo F. Oxidative stress status during exposure to propofol, sevoflurane and desflurane. *Anesth Analg*. 2001;93(4):981–985. doi:10.1097/00000539-200110000-00036
8. Aldemir T, Turan S, Gomceli I, et al. A comparison of the effects of desflurane and isoflurane on rat pulmonary parenchyme histopathology and malondialdehyde levels. *J Pak Med Assoc*. 2012;62(11):1174–1178. PMID:23866405
9. Lin J, Moore D, Hockey B, et al. Drug-induced hepatotoxicity: Incidence of abnormal liver function tests consistent with volatile anaesthetic hepatitis in trauma patients. *Liver Int*. 2014;34(4):576–582. doi:10.1111/liv.12278
10. Arslan M, Isik B, Kavutcu M, Kurtipek O. Effects of desflurane on oxidant/antioxidant status of female young versus old rat liver tissues. *J Anim Vet Adv*. 2010;9(19):2502–2507. doi:10.3923/javaa.2010.2502.2507
11. Arslan A, Kuyrukluyildiz U, Binici O, et al. Can thiamıne pyrophosphate prevent desflurane induced hepatotoxicıty in rats? *Acta Cir Bras*. 2016;31(3):168–175. doi:10.1590/S0102-865020160030000004
12. Harborne JB. Nature, distribution and function of plant flavonoids. *Prog Clin Biol Res*. 1986;213:15–24. PMID:3520585
13. Ganeshpurkar A, Saluja AK. The pharmacological potential of rutin. *Saudi Pharm J*. 2017;25(2):149–164. doi:10.1016/j.jsps.2016.04.025
14. Singh H, Kaur P, Kaur P, Muthuraman A, Singh G, Kaur M. Investigation of therapeutic potential and molecular mechanism of vitamin P and digoxin in I/R-induced myocardial infarction in rat. *Naunyn Schmiedebergs Arch Pharmacol*. 2015;388(5):565–574. doi:10.1007/s00210-015-1103-8
15. Kamalakkannan N, Prince PSM. Antihyperglycaemic and antioxidant effect of rutin, a polyphenolic flavonoid, in streptozotocin-induced diabetic wistar rats. *Basic Clin Pharmacol Toxicol*. 2006;98(1):97–103. doi:10.1111/j.1742-7843.2006.pto_241.x
16. Yeh CH, Yang JJ, Yang ML, Li YC, Kuan YH. Rutin decreases lipopolysaccharide-induced acute lung injury via inhibition of oxidative stress and the MAPK–NF-κB pathway. *Free Radic Biol Med*. 2014;69:249–257. doi:10.1016/j.freeradbiomed.2014.01.028
17. Eger EI, Johnson BH. MAC of I-653 in rats, including a test of the effect of body temperature and anesthetic duration. *Anesth Analg*. 1987;66(10):974-976. doi:10.1213/00000539-198710000-00009
18. Ohkawa H, Ohishi N, Yagi K. Assay for lipid peroxides in animal tissues by thiobarbituric acid reaction. *Anal Biochem*. 1979;95(2):351–358. doi:10.1016/0003-2697(79)90738-3
19. Weydert CJ, Cullen JJ. Measurement of superoxide dismutase, catalase and glutathione peroxidase in cultured cells and tissue. *Nat Protoc*. 2010;5(1):51–66. doi:10.1038/nprot.2009.197
20. Sedlak J, Lindsay RH. Estimation of total, protein-bound, and nonprotein sulfhydryl groups in tissue with Ellman's reagent. *Anal Biochem*. 1968;25(1):192–205. doi:10.1016/0003-2697(68)90092-4
21. Musacchio E, Rizzoli V, Bianchi M, Bindoli A, Galzigna L. Antioxidant action of propofol on liver microsomes, mitochondria and brain synaptosomes in the rat. *Pharmacol Toxicol*. 1991;69(1):75–77. doi:10.1111/j.1600-0773.1991.tb00414.x
22. Murphy PG, Myers DS, Davies MJ, Webster NR, Jones JG. The antioxidant potential of propofol (2,6-diisopropylphenol). *Br J Anaesth*. 1992;68(6):613–618. doi:10.1093/bja/68.6.613
23. Acat C, Erol A, Topal A, Reisli R, Reisli İ, Otelcioğlu Ş. Bronkoalveolar Lavaj (Bal) Sıvısındaki Nötrofillerin Kemotaktik Fonksiyonları Üzerine Sevofluran, Desfluran ve Propofol Anestezisinin Etkileri. *Türk Anest Rean Der*. 2007;35(6):413–419.
24. Strosing KM, Faller S, Gyllenram V, et al. Inhaled anesthetics exert different protective properties in a mouse model of ventilator-induced lung injury. *Anesth Analg*. 2016;123(1):143–151. doi:10.1213/ANE.0000000000001296
25. Kisaoglu A, Borekci B, Yapca OE, Bilen H, Suleyman H. Tissue damage and oxidant/antioxidant balance. *Eurasian J Med*. 2013;45(1):47–49. doi:10.5152/eajm.2013.08
26. Kanner J, German JB, Kinsella JE, Hultin HO. Initiation of lipid peroxidation in biological systems. *Crit Rev Food Sci Nutr*. 1987;25(4):317–364. doi:10.1080/10408398709527457
27. Dalle-Donne I, Rossi R, Giustarini D, Milzani A, Colombo R. Protein carbonyl groups as biomarkers of oxidative stress. *Clin Chim Acta*. 2003;329(1-2):23–38. doi:10.1016/s0009-8981(03)00003-2
28. Turkan H, Aydin A, Sayal A, Eken A, Akay C, Karahalil B. Oxidative and antioxidative effects of desflurane and sevoflurane on rat tissue in vivo. *Arh Hig Rada Toksikol*. 2011;62(2):113–119. doi:10.2478/10004-1254-62-2011-2096
29. Koksal GM, Sayilgan C, Aydin S, Uzun H, Oz H. The effects of sevoflurane and desflurane on lipid peroxidation during laparoscopic cholecystectomy. *Eur J Anaesthesiol*. 2004;21(3):217–220. doi:10.1017/s0265021504003102
30. Adefegha SA, Leal DBR, De Oliveira JS, Manzoni AG, Bremm JM. Modulation of reactive oxygen species production, apoptosis and cell cycle in pleural exudate cells of carrageenan-induced acute inflammation in ratsby rutin. *Food Funct*. 2017;8(12):4459–4468. doi:10.1039/C7FO01008G
31. Chen WY, Huang YC, Yang ML, et al. Protective effect of rutin on LPS-induced acute lung injury via down-regulation of MIP-2 expression and MMP-9 activation through inhibition of Akt phosphorylation. *Int Immunopharmacol*. 2014;22(2):409–413. doi:10.1016/j.intimp.2014.07.026
32. Ortolani O, Conti A, De Gaudio AR, Masoni M, Novelli G. Protective effects of N-acetylcysteine and rutin on the lipid peroxidation of the lung epithelium during the adult respiratory distress syndrome. *Shock*. 2000;13(1):14–18. doi:10.1097/00024382-200013010-00003
33. Meister A, Anderson ME. Glutathione. *Annu Rev Biochem*. 1983;52(1):711–760. doi:10.1146/annurev.bi.52.070183.003431
34. Akbari M, Ostadmohammadi V, Lankarani K, et al. The effects of vitamin D supplementation on biomarkers of inflammation and oxidative stress among women with polycystic ovary syndrome: A systematic review and meta-analysis of randomized controlled trials. *Horm Metab Res*. 2018;50(04):271–279. doi:10.1055/s-0044-101355

35. Santa T. Recent advances in analysis of glutathione in biological samples by high-performance liquid chromatography: A brief overview. *Drug Discov Ther*. 2013;7(5):172–177. PMID:24270380
36. Vilcek J. First demonstration of the role of TNF in the pathogenesis of disease. *J Immunol*. 2014;181(1):5–6. doi:10.4049/jimmunol.181.1.5
37. Goldblum SE, Hennig B, Jay M, Yoneda K, McClain CJ. Tumor necrosis factor α-induced pulmonary vascular endothelial injury. *Infect Immun*. 1989;57(4):1218–1226. doi:10.1128/iai.57.4.1218-1226.1989
38. Maury CP, Teppo AM. Circulating tumour necrosis factor-alpha (cachectin) in myocardial infarction. *J Intern Med*. 1989;225(5):333–336. doi:10.1111/j.1365-2796.1989.tb00090.x
39. Koksal GM, Sayilgan C, Gungor G, et al. Effects of sevoflurane and desflurane on cytokine response during tympanoplasty surgery. *Acta Anaesthesiol Scand*. 2005;49(6):835–839. doi:10.1111/j.1399-6576.2005.00677.x
40. Camandola S, Mattson MP. NF-kappa B as a therapeutic target in neurodegenerative diseases. *Expert Opin Ther Targets*. 2007;11(2):123–132. doi:10.1517/14728222.11.2.123
41. Yamamoto Y, Gaynor RB. Therapeutic potential of inhibition of the NF-κB pathway in the treatment of inflammation and cancer. *J Clin Invest*. 2001;107(2):135–142. doi:10.1172/JCI11914
42. Lee W, Yoo H, Kim JA, et al. Barrier protective effects of piperlongumine in LPS-induced inflammation in vitro and in vivo. *Food Chem Toxicol*. 2013;58(9):149–157. doi:10.1016/j.fct.2013.04.027
43. Yeh CH, Yang JJ, Yang ML, Li YC, Kuan YH. Rutin decreases lipopolysaccharide-induced acute lung injury via inhibition of oxidative stress and the MAPK-NF-κB pathway. *Free Radic Biol Med*. 2014;69:249–257. doi:10.1016/j.freeradbiomed.2014.01.028

Comparison of a manual walking platform and the CatWalk gait analysis system in a rat osteoarthritis model

Halil Kara[1,A], Ceyhun Çağlar[2,B,D], Mehmet Asiltürk[2,C,D], Siyami Karahan[3,E], Mahmut Uğurlu[4,F]

[1] Pharmacology Department, Ankara Yıldırım Beyazıt University, Turkey
[2] Orthopaedics and Traumatology Department, Ankara City Hospital, Turkey
[3] Veterinary Histology and Embryology Department, Kırıkkale University, Turkey
[4] Orthopaedics and Traumatology Department, Ankara Yıldırım Beyazıt University, Turkey

A – research concept and design; B – collection and/or assembly of data; C – data analysis and interpretation;
D – writing the article; E – critical revision of the article; F – final approval of the article

Advances in Clinical and Experimental Medicine, ISSN 1899–5276 (print), ISSN 2451–2680 (online) *Adv Clin Exp Med*. 2021;30(9):949–956

Address for correspondence
Ceyhun Çağlar
E-mail: ceyhun.caglar@hotmail.com

Funding sources
None declared

Conflict of interest
None declared

Received on March 10, 2021
Reviewed on May 2, 2021
Accepted on May 17, 2021

Published online on August 12, 2021

Abstract

Background. Effects of osteoarthritis (OA) are observed in experimental animal models using different gait analysis systems.

Objectives. The aim of this study was to determine whether the Noldus CatWalk XT v. 10.9 gait analysis system (CatWalk) device can be used effectively in a chemically induced rat OA model and to reveal the strengths and weaknesses of the system compared to manual gait analysis.

Materials and methods. Ten Wistar rats were run on a manual walking platform as well as on the CatWalk and the basal values were recorded. For OA induction, monosodium iodoacetate (MIA) was injected into the left knee of all rats under anesthesia. After a period of 4 weeks for OA development, the rats were again run on both the manual and CatWalk gait platforms. For manual gait analysis, the stride length, paw print width and paw print length were measured on both knees. In addition to these parameters, the average run speed, run duration, maximum contact intensity, paw print area, mean stance, and swing speed were measured on the left knee (affected knee) using the CatWalk device.

Results. Significant differences were observed in the stride width ($p = 0.0272$), left stride length ($p = 0.0344$), and left paw print length ($p = 0.0233$) recorded before and after OA via the manual walking platform. For CatWalk, a significant difference was detected in the left knee's average run speed ($p = 0.0010$), maximum contact intensity ($p = 0.0155$), paw print length ($p = 0.0058$), paw print width ($p = 0.0324$), and swing speed ($p = 0.0066$) based on data obtained before and after OA.

Conclusions. The CatWalk gait analysis system is suitable for the evaluation of OA rat models and related interventions. It also provides additional parameters compared to the manual system and minimizes human-related variation.

Key words: CatWalk, osteoarthritis, rat model, gait analysis, monosodium iodoacetate

Cite as
Kara H, Çağlar C, Asiltürk M, Karahan S, Uğurlu M. Comparison of a manual walking platform and the CatWalk gait analysis system in a rat osteoarthritis model. *Adv Clin Exp Med*. 2021;30(9):949–956. doi:10.17219/acem/137536

DOI
10.17219/acem/137536

Background

Animal models, especially those involving rodents, play an important role in drug development studies. For instance, molecules are used in preclinical studies involving animals to assess their effects on a specific disease to minimize the associated risks for humans before clinical studies.[1] In this context, gait analysis in animal models that respond to a specific treatment and behavioral models are highly important.[2]

Osteoarthritis (OA) is the most frequently seen form of arthritis and its prevalence increases with age.[3] Old age and obesity are particularly significant risk factors for OA.[4,5] Although OA most frequently affects the knee joints, it can be seen in any joint in the body, including hip, waist and finger joints.[6] The main symptoms include joint pain, joint stiffness and swelling.[7] Currently, clinicians consider OA as a failure of the entire joint structure, such that OA not only affects articular cartilage but also affects the subchondral bone, ligaments, joint capsule, synovial membrane, and periarticular muscles. By another definition, OA starts as a result of the mechanical failure of the joint, during which the joint makes an effort to repair the defect area and fix the abnormal joint biomechanics.[8] For OA treatment, pharmacological, non-pharmacological and surgical options are available. However, none of the available treatments provide an absolute solution for OA. Thus, there have been continuous efforts to reveal the complete pathobiology of OA and develop better treatment options. The response of animal models to OA treatments is measured using various kinds of in vivo techniques and through postmortem evaluations.

In previous studies, various chemicals have been used for the induction of OA in animals.[9] In the present study, monosodium iodoacetate (MIA) is used. Intraarticular injection of MIA is one of the animal models of chemically induced OA. As a metabolic inhibitor, MIA causes disruption of glycolysis in cells by inhibiting the glyceraldehyde-3-phosphate dehydrogenase enzyme.[10] Subsequently, this leads to an increase in oxidative stress in the environment that induces loss of chondrocytes, resulting in reduction of cartilage thickness and osteolysis.[11–13] This mechanism of action governs the basis of MIA-induced OA. These changes bring about histological and morphological modifications in the joint cartilage similar to the prognosis of OA patients.[14,15] Many studies have been conducted using MIA-induced OA rat models.[16–19]

There are several methods of rodent spatiotemporal gait analysis, and these systems have significant advantages compared to the main inkpad methods used earlier. Unfortunately, the system array and reporting of multiple parameters frequently make gait analysis more difficult. The CatWalk XT v. 10.9 gait analysis system (CatWalk; Noldus Company, Wageningen, the Netherlands) is a gait analysis device suitable for rodents, especially rats and mice. The data obtained by walking a rat on a platform are automatically saved.

Objectives

The purpose of this study is to evaluate the gait analysis patterns of rats before and after onset of OA induced by MIA. Using the values before induction of OA, the rat model was evaluated in terms of how the gait parameters changed after OA induction using the CatWalk device, which is one of the most powerful gait analysis systems available for rats and mice. In addition, data collected using the CatWalk software were compared to those obtained manually on graph paper. Evaluation of this rat model of OA will provide a basis for future OA studies involving gait analysis.

Materials and methods

Animals

Our research was approved by the Research Ethics Committee for Animal Experiments of Kırıkkale University, Turkey. The study was carried out with 10 male conventional Wistar rats weighing approx. 300 ±31.3 g and aged 12–24 weeks. The rats were kept in individual cages and fed ad libitum. A pellet diet was used for food and refined tap water was provided in an autoclavable Makrolon bottle. Sawdust was used as the bedding material and cleaned 4 times per week. The rat holding room was maintained at 23°C with 60% humidity and a 12 h/12 h light/dark cycle. The air was completely replaced 15 times per hour. Prior to the gait procedures and injections, food was restricted for 24 h and water was restricted for 6 h. Rats were regularly run on the CatWalk platform prior to the study and were thus adapted to the device. The animals were numbered by marking their tails.

Knee osteoarthritis pain model

Anesthesia was achieved by injection of 100 mg/kg intramuscular ketamine (Alfamine®; Egevet, Izmir, Turkey; 100 mg/mL) and 8 mg/kg intramuscular xylazine (Alfazyne®; Egevet; 2%) through a 30-gauge needle. Under general anesthesia, the left knees of the rats were shaved and 0.2 mg of MIA (Sigma-Aldrich, St. Louis, USA) in 10 µL of sterile saline was injected. The solution was injected through the patellar ligament using a 27-gauge needle with the leg flexed at a 90° angle at the knee. After surgery, we waited 4 weeks for the formation of chemically induced OA.

Gait analysis

We selected 2 different systems for gait analysis. The 1st gait analysis system was a manual walking platform. Analysis with a manual platform involves the movement of the animal along a single inkpad followed by the measurement

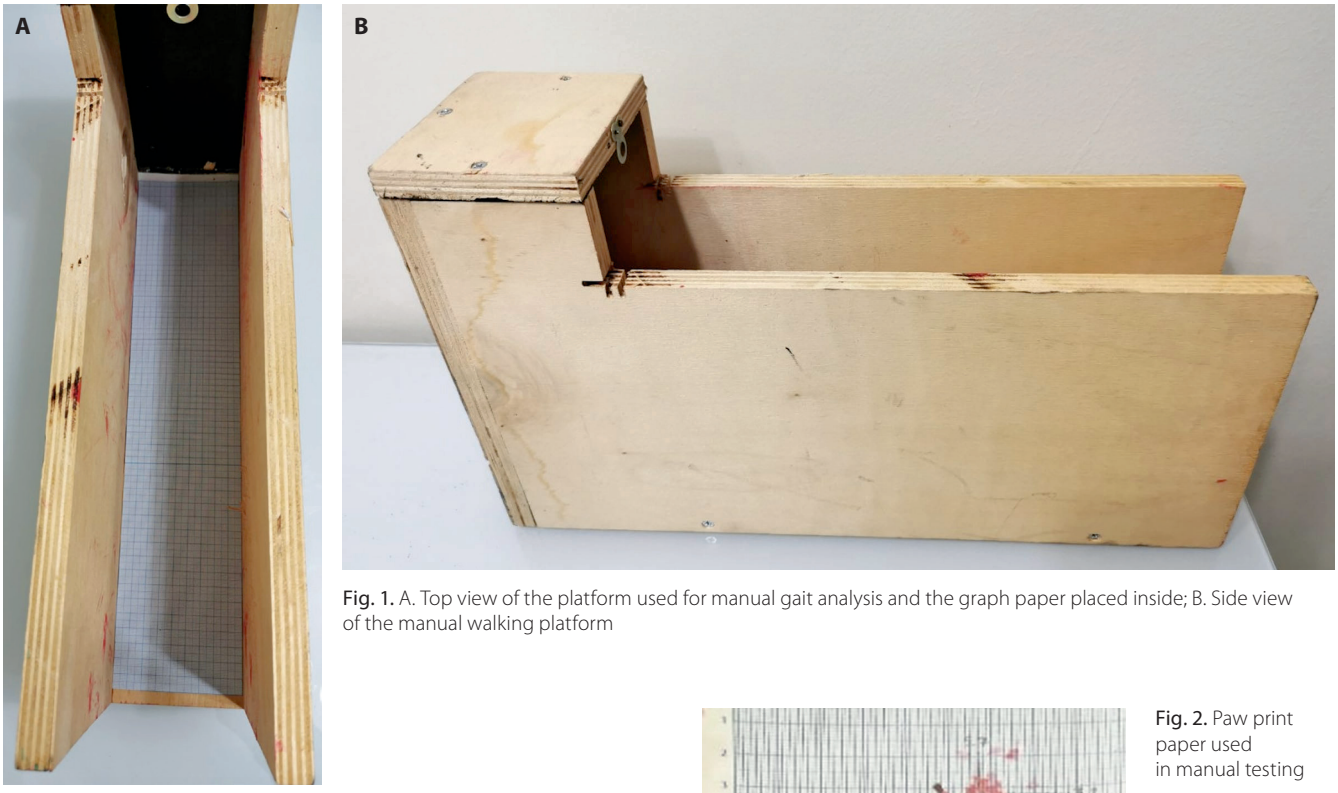

Fig. 1. A. Top view of the platform used for manual gait analysis and the graph paper placed inside; B. Side view of the manual walking platform

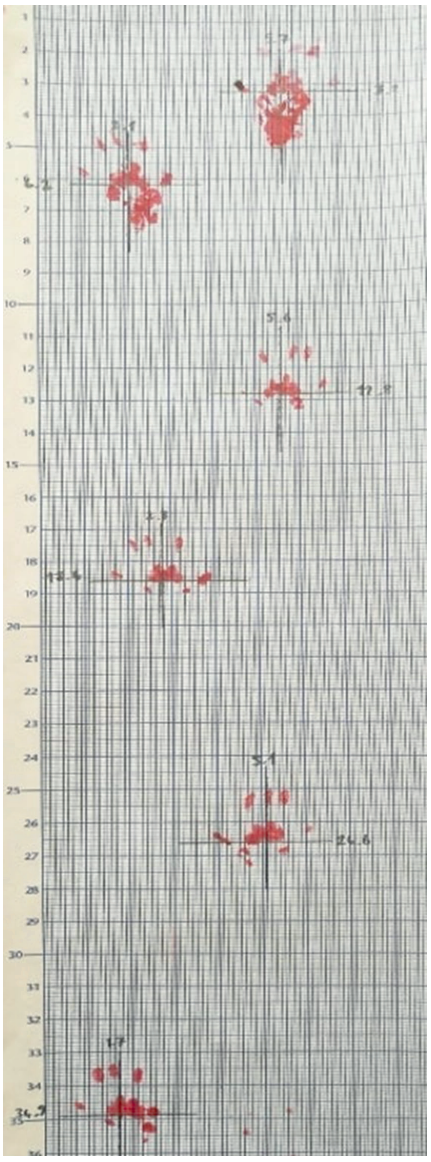

Fig. 2. Paw print paper used in manual testing

of the pattern of the ink prints on graph paper. Bait was placed at the end of the manual walking platform to encourage the rats. The rats walked in a dark room until they were accustomed to the manual walking platform (Fig. 1A,B). Once the rats were completely used to the platform and started walking, their hind paws were painted with ink. The rats were walked on graph paper and the values were recorded. The main data, such as stride length, stride width, paw print length, paw print width, and paw print area, are then measured from this paper. Variables such as the angle between the paws may also be assessed, but it should be kept in mind that these are not independent measurements and are derived from step length and width.[20,21] Of note, the amount of ink is inconsistent between steps and trials and, therefore, the paw print areas are highly variable. Thus, modern high-speed videography has a higher probability of enabling robust analysis of spatial parameters.

The present study also used the CatWalk device for analysis using a machine learning-based approach. CatWalk is a gait analysis system for mice and rats that allows voluntary diagonal passage toward a target box over a glass surface in a darkened room, with the animals allowed to walk freely.[22] A light from a lamp is aimed through the glass surface. When an animal's paw touches the glass surface, the light beams are reflected downward. The entire run is recorded with a video camera. When the rat walks, the paw prints are automatically captured, recorded and analyzed.[23] This system has been explained in detail elsewhere.[24] The animals walked on graph paper on the manual walking platform (Fig. 2) and the CatWalk device (Fig. 3A,B) in sequence before injection. All base

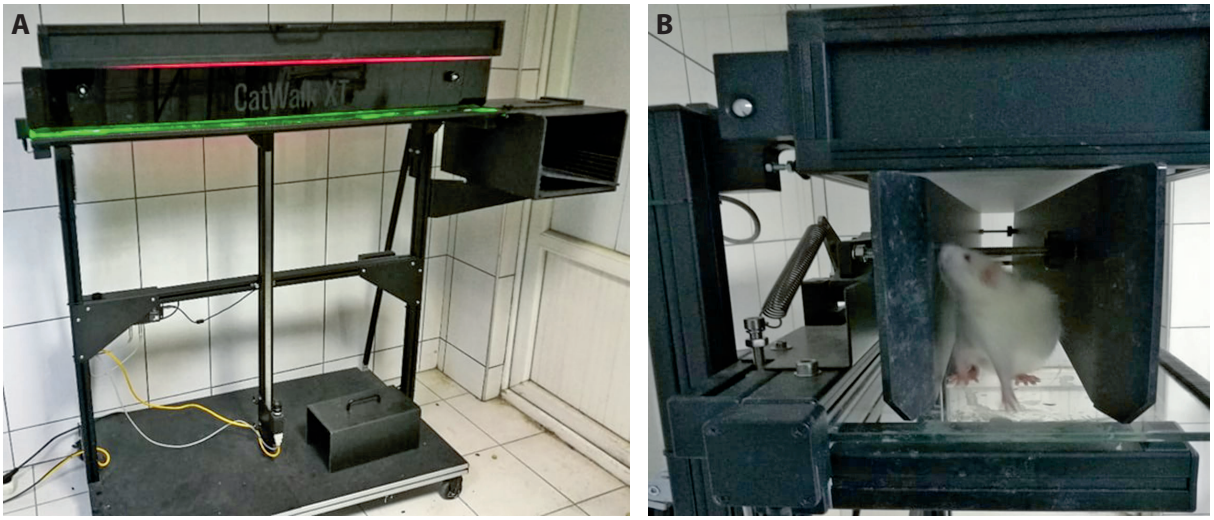

Fig. 3. A. The CatWalk hardware for gait analysis used for rats; B. A rat walking on the CatWalk platform

values were recorded for both platforms after this first walk. At this stage, the rats were administered MIA as mentioned above and 4 weeks were allowed for the formation of OA.

Four weeks after induction of OA, the animals were forced to walk again on the manual walking platform as well as the walking platform of the CatWalk device. Data collected both manually and via the CatWalk system before and after OA induction were categorized and analyzed. Data collected before and after OA induction were compared, and data collected manually and via CatWalk were analyzed for the presence of correlations.

With the analysis conducted using the CatWalk device, several parameters such as pre-treatment walking velocity, usage of the treated knee, comparisons with the other knees, run duration and average run speed, maximum contact area and intensity, stride length, paw print length, paw print width, paw print area, mean stance, and swing speed were analyzed by recording both baseline and OA values.

Histological analysis

All animals were euthanized by cervical dislocation after the second walk. The complete knee joint was collected. The joint samples were fixed in 10% phosphate-buffered formalin and then decalcified in 5% formic acid. Decalcification was confirmed by radiography. Sections were then processed with routine histological techniques. The joints in paraffin blocks were cut to a thickness of 7 µm and finally stained with toluidine blue (Fig. 4A,B) which enabled the researchers to evaluate loss of glycosaminoglycans in addition to morphology. The samples were then examined under a light microscope. The most severely affected regions of the joints were scored using the modified scoring system shown in Table 1. A total score for left knee joints was obtained and used in statistical analyses. Histological score data were expressed as median (minimum–maximum) scores.

Table 1. Rat osteoarthritis scoring system (0–25)[25]

Morphology (0–7)
0 = normal 1 = slight surface erosion or flaking of superficial zone 2 = erosion no deeper than superficial zone 3 = erosion into middle zone with or without fissuring 4 = erosion into deep zone with or without fissuring 5 = erosion into calcified zone 6 = erosion into the subchondral bone (eburnation) 7 = fibrous tissue on eburnated areas
Tidemark (0–2)
0 = normal 1 = touched by blood vessels 2 = crossed by blood vessels
Doubling of tidemark
0 = normal (a basophilic line) 1 = doubled
Glycosaminoglycan loss (0–5)
0 = normal 1 = increased in all layers of articular cartilage 2 = significantly decreased or no deeper than superficial zone 3 = significantly decreased or absent, no deeper than middle zone 4 = significantly decreased or absent, no deeper than tidemark 5 = no staining at all
Chondrocyte morphology (0–5)
0 = normal 1 = enlarged cells close to the surface of articular cartilage 2 = hypercellular with or without small clones 3 = noticeable hypocellularity with or without clones 4 = significant hypocellularity with or without clones 5 = severe hypocellularity
Osteophyte formation (0–2)
0 = none 1 = extensive mix tissue formation and remodeling at joint margin 2 = osteophyte
Synovitis (0–4)
0 = normal (1- to 3-cell-thick synovium and few mononuclear cells in subintima) 1 = slight increase in number of synoviocytes and mononuclear cells 2 = mononuclear cell infiltration and hyperemic blood vessels 3 = hyperplastic synovium 4 = extensive hyperplasia with pannus formation

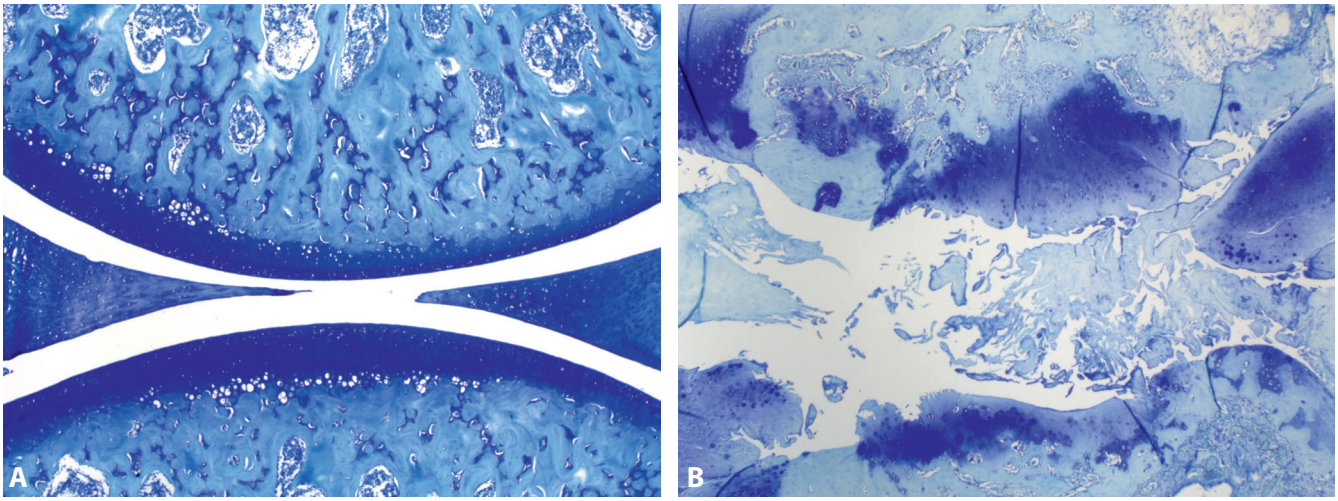

Fig. 4. A. Microscopic view of a cross-section of a toluidine-stained knee joint of a rat before the induction of osteoarthritis; B. Microscopic view of a cross-section of a toluidine-stained knee joint of a rat after the induction of osteoarthritis. Note the severe cartilage damage in the femorotibial joint

Table 2. Values of the rats' left (affected) and right (unaffected) knees measured from manual walking platform plotting paper

Parameter	Base values, median (min–max)	After OA values, median (min–max)	p-value*
Stride width [cm]	3.35 (3.00–4.10)	4.20 (3.90–4.70)	0.0272
Right stride length [cm]	11.10 (9.70–12.30)	12.85 (11.20–14.10)	0.3288
Left stride length [cm]	11.90 (10.20–14.0)	10.35 (9.30–12.90)	0.0344
Right paw print width [cm]	0.85 (0.70–1.0)	1.25 (1.0–1.40)	0.4267
Left paw print width [cm]	1.05 (0.90–1.20)	0.90 (0.70–0.90)	0.1241
Right paw print length [cm]	0.95 (0.80–1.20)	1.25 (1.0–1.5)	0.2230
Left paw print length [cm]	1.30 (1.30–1.40)	1.10 (1.0–1.10)	0.0233

* Wilcoxon rank-sum test; n (number of rats): 10; df (degrees of freedom): 9; $p < 0.05$ statistically significant; OA – osteoarthritis

Statistical analyses

Data are presented as median (minimum–maximum) values. The Wilcoxon rank-sum test, which is a non-parametric test, was used to assess whether or not there was a significant difference between both the base and after OA values of distance and histological OA scores between control and MIA-injected knees. The analyses were carried out using IBM SPSS Statistics for Windows v. 21 (IBM Corp., Armonk, USA). A value of $p < 0.05$ was accepted as significant in all statistical test.

Results

In histological sections, MIA-injected knees exhibited signs of OA. Surface erosion, fibrillation, clone formation, eburnation, tidemark invasion, and synovitis were common findings. The OA scoring system used for the rats in this study is shown in Table 1. While the average OA score in the MIA-injected knee was 21.4 (18–25), the OA score in the control knee was 0.7 (0–3). The OA scores in the MIA-injected knees were significantly higher compared to those in the control knees ($p < 0.05$).

Seven parameters were evaluated with the manual walking platform. The calculated values are shown in Table 2. After induction of OA, the) stride length of the left (affected) knee and the left paw print width and length values decreased; at the same time, the stride length of the right (unaffected) knee, right paw print width and length, and stride width increased. Among the data recorded from the manual walking platform, the values of stride width, left stride length and left paw print length were statistically significant.

The CatWalk software provided data for 9 different parameters. As the injections were administered to the left knee in all animals, values pertaining to the left hind limb were prioritized for analysis. The recorded values from the CatWalk device are shown in Table 3. After induction of OA, the run duration and mean stance values of the left knee increased; at the same time, the average run speed, maximum contact intensity, paw print length, paw print width, paw print area, stride length, and swing speed of the same knee decreased. Among the data recorded with the CatWalk device, the average run speed, maximum contact intensity, paw print length, paw print width, and swing speed values were statistically significant.

Table 3. Values of the left (affected) knee of rats obtained base and post OA parameters in CatWalk gait analysis system

Parameter	Base values, median (min–max)	After OA values, median (min–max)	p-value*
[1]Run duration [s]	2.55 (1.75–3.38)	3.00 (2.45–4.10)	0.1077
[2]Run average speed [cm/s]	35.25 (29.85–41.15)	32.28 (25.78–38.46)	0.0010
[3]Mean stance [s]	0.15 (0.11–0.20)	0.21 (0.14–0.27)	0.4054
[4]Maximal contact intensity [%]	97.00 (92.50–100.00)	75.00 (68.50–81.00)	0.0155
[5]Paw print length [cm]	1.00 (0.88–1.17)	0.75 (0.62–0.85)	0.0058
[6]Paw print width [cm]	0.90 (0.82–0.95)	0.70 (0.60–0.75)	0.0324
[7]Paw print area [cm^2]	0.40 (0.35–0.48)	0.32 (0.25–0.40)	0.3895
[8]Stride length [cm]	9.80 (8.92–10.47)	8.95 (8.20–9.45)	0.3333
[9]Swing speed [cm/s]	148.40 (119.10–176.20)	95.30 (72.40–102.70)	0.0066

Data are presented as median (min–max); * Wilcoxon rank-sum test; n (number of rats): 10; df (degrees of freedom): 9; $p < 0.05$ statistically significant; OA –osteoarthritis. 1. The time in which the rat crosses the walking platform. 2. The speed of the rat on the walking platform. 3. The contact time of the paw on the plate while walking. 4. The degree of contact with the glass plate. 5. The length that the paw occupied when it touched the walkway. 6. The width that the paw occupied when it touched the walkway. 7. The space that the paw occupied when it touched the walkway. 8. The distance between steps of the same paw. 9. The speed of a paw while it was in the air.

Discussion

There are many different systems that can be used for automatic gait analysis.[26] These include DigiGait, TreadScan, the open-source Experimental Dynamic Gait Arena for Rodents, and CatWalk. In a study by Xu et al., the DigiGait and CatWalk gait analysis systems were compared and the advantages of each were reported.[27] Five different automatic gait analysis systems were compared in a study by Jacobs et al., who mentioned that these devices play an important role in rodent OA models.[28] In the present study, we compared manual platform data analysis and automated CatWalk gait data analysis.

The CatWalk gait analysis system allows simultaneous analysis of several factors by recording the steps of rats walking on a band, categorizing these steps and creating dozens of parameters.[29] Data regarding all of the parameters, which are collected by the software, were statistically analyzed in this study. Upon the detection of significant differences, data were compared between groups. The CatWalk device can provide many more types of data, and the software is fast and easy to use. In this sense, it was observed that the CatWalk device has clear advantages over the manual platform method in terms of gait analysis. In addition to the parameters measured by classical methods, CatWalk can evaluate parameters that we think are important for OA within the walking analysis system.[30]

The MIA administration is an important method for chemical induction of OA.[16] Other methods of chemical OA described in the literature include anterior cruciate ligament transection, destabilization of the medial meniscus and the use of collagenase.[31] For example, Adães et al. used collagenase to create a rat model of OA,[32] while Jacobs et al. used surgical medial meniscus and anterior cruciate ligament transection to create a similar OA model.[33] Most importantly, the MIA OA model progresses with a pathology similar to that of degenerative OA.[13,34,35] Thus, we preferred the MIA model for OA induction. Signs of OA were observed in the left hind limbs of all rats following MIA administration in our study.

In the analysis, the first marked evidence was the presence of differences between data collected prior to and after OA induction. Such differences were obtained from both the CatWalk and the manual platform. Therefore, the parameters used in the CatWalk gait analysis system can be considered to detect gait changes in the MIA-induced rat OA model, a successful and well-established OA model documented in the literature.[36]

In the measurements after OA induction, it was observed that the rats deliberately avoided putting weight on their left hind limbs and possibly felt pain.[37] The average run speed and swing speed decreased and, secondarily to this, the run duration and main stance increased. Moreover, the decrease in the length, width, and area of the paw prints and stride length after OA induction suggest that the rats stepped on the platform less widely to reduce the pressure on the foot of the affected limb. This hypothesis is also supported by decreases in the maximum contact density values. Whereas paw print measurements on the manual walking platform are performed manually with the help of a ruler, paw print measurements in the CatWalk system are automatically analyzed and provided by the software. Thus, the CatWalk system is more convenient and more objective than the manual walking platform. Gabriel et al. used the CatWalk software to assess acute inflammatory pain model rats and reported that they obtained objective and detailed data.[38] In another study, rats with complete Freund's adjuvant-induced monoarthritis were analyzed using CatWalk software and clearer and non-biased results were also obtained.[39] All of these results support that the parameters used by the CatWalk software are valuable for monitoring in vivo OA progression as well as responses to any intervention in OA.

Limitations

Our study has some limitations. First, the measurements from the manual walking platforms were obtained using a completely hand-held manner and may thus contain intra-observer and inter-observer measurement errors. One disadvantage of the CatWalk gait analysis system is that only rats and mice can be used. Also, rodents need a certain amount of time to adjust to the walking platform. Since the study was carried out in a dark room, the rodents behaved shyly in the environment and required a period of serious acclimatization.

Conclusions

In conclusion, the CatWalk gait analysis system is a useful, reliable and convenient method for monitoring gait changes in rat knee OA models. The CatWalk gait analysis system and its associated parameters, such as stride length, paw print width, paw print length, average run speed, run duration, maximum contact intensity, paw print area, mean stance, and swing speed, are appropriate for the evaluation of rat knee OA models.

ORCID iDs

Halil Kara https://orcid.org/0000-0002-7557-7897
Ceyhun Çağlar https://orcid.org/0000-0003-4286-7852
Mehmet Asiltürk https://orcid.org/0000-0002-1069-8743
Siyami Karahan https://orcid.org/0000-0002-2744-1717
Mahmut Uğurlu https://orcid.org/0000-0001-9968-5393

References

1. Cardillo TM, Govindan SV, Sharkey RM, et al. Humanized anti Trop-2 IgG-SN-38 conjugate for effective treatment of diverse epithelial cancers: Preclinical studies in human cancer xenograft models and monkeys. *Clin Cancer Res*. 2011;17(10):3157–3169. doi:10.1158/1078-0432.CCR-10-2939
2. Berryman ER, Harris RL, Moalli M, et al. Digigait quantitation of gait dynamics in rat rheumatoid arthritis model. *J Musculoskelet Neuronal Interact*. 2009;9(2):89–98. PMID:19516084
3. Huang Y, Liu X, Xu X, et al. Intra-articular injections of platelet-rich plasma, hyaluronic acid or corticosteroids for knee osteoarthritis: A prospective randomized controlled study. *Orthopade*. 2019;48(3):239–247. doi:10.1007/s00132-018-03659-5
4. Litwic A, Edwards MH, Dennison EM, et al. Epidemiology and burden of osteoarthritis. *Br Med Bull*. 2013;105:185–199. doi:10.1093/bmb/lds038
5. Allen KD, Golightly YM. State of the evidence. *Curr Opin Rheumatol*. 2015;27(3):276–283. doi:10.1097/BOR.0000000000000161
6. Rafanan BS, Valdecañas BF, Lim BP, et al. Consensus recommendations for managing osteoarthritic pain with topical NSAIDs in Asia-Pacific. *Pain Manag*. 2018;8(2):115–128. doi:10.2217/pmt-2017-0047
7. Zhang Y, Jordan JM. Epidemiology of osteoarthritis. *Clin Geriatr Med*. 2010;26(3):355–369. doi:10.1016/j.cger.2010.03.001
8. Arnstein PM. Evolution of topical NSAIDs in the guidelines for treatment of osteoarthritis in elderly patients. *Drugs Aging*. 2012;29(7):523–531. doi:10.2165/11631550-000000000-00000
9. Bendele AM. Animal models of osteoarthritis. *J Musculoskelet Neuronal Interact*. 2001;1(4):363–376. PMID:15758487
10. Guzman R, Evans M, Bove S, et al. Mono-iodoacetate-induced histologic changes in subchondral bone and articular cartilage of rat femorotibial joints: An animal model of osteoarthritis. *Toxicol Pathol*. 2003;31(6):619–624. doi:10.1080/01926230390241800
11. Pomonis JD, Boulet JM, Gottshall SL, et al. Development and pharmacological characterization of a rat model of osteoarthritis pain. *Pain*. 2005;114(3):339–346. doi:10.1016/j.pain.2004.11.008
12. Mannelli LDC, Bani D, Bencini A, et al. Therapeutic effects of the superoxide dismutase mimetic compound MnIIMe2DO2A on experimental articular pain in rats. *Mediators Inflamm*. 2013;2013:905360. doi:10.1155/2013/905360
13. Kobayashi K, Imaizumi R, Sumichika H, et al. Sodium iodoacetate-induced experimental osteoarthritis and associated pain model in rats. *J Vet Med Sci*. 2003;65(11):1195–1199. doi:10.1292/jvms.65.1195
14. van der Kraan PM, Vitters EL, van de Putte LB, et al. Development of osteoarthritic lesions in mice by "metabolic" and "mechanical" alterations in the knee joints. *Am J Pathol*. 1989;135(6):1001–1014. PMID:2556924
15. Abdel-Rahman RF, Abd-Elsalam RM, Amer MS, et al. Manjarix attenuated pain and joint swelling in a rat model of monosodium iodoacetate-induced osteoarthritis. *Food Funct*. 2020;11(9):7960–7972. doi:10.1039/d0fo01297a
16. Miyagi M, Ishikawa T, Kamoda H, et al. Efficacy of nerve growth factor antibody in a knee osteoarthritis pain model in mice. *BMC Musculoskelet Disord*. 2017;18(1):428. doi:10.1186/s12891-017-1792-x
17. Ishikawa G, Koya Y, Tanaka H, et al. Long-term analgesic effect of a single dose of anti-NGF antibody on pain during motion without notable suppression of joint edema and lesion in a rat model of osteoarthritis. *Osteoarthritis Cartilage*. 2015;23(6):925–932. doi:10.1016/j.joca.2015.02.002
18. Lakes EH, Allen KD. Quadrupedal rodent gait compensations in a low dose monoiodoacetate model of osteoarthritis. *Gait Posture*. 2018;63:73–79. doi:10.1016/j.gaitpost.2018.04.023
19. Sa L, Wei X, Huang Q, et al. Contribution of salidroside to the relieve of symptom and sign in the early acute stage of osteoarthritis in rat model. *J Ethnopharmacol*. 2020;259:112883. doi:10.1016/j.jep.2020.112883
20. de Medinaceli L, Freed WJ, Wyatt RJ. An index of the functional condition of rat sciatic nerve based on measurements made from walking tracks. *Exp Neurol*. 1982;77(3):634–643. doi:10.1016/0014-4886(82)90234-5
21. Varejão AS, Cabrita AM, Geuna S, et al. Toe out angle: A functional index for the evaluation of sciatic nerve recovery in the rat model. *Exp Neurol*. 2003;183(2):695–699. doi:10.1016/s0014-4886(03)00208-5
22. Bernardes D, Oliveira ALR. Comprehensive catwalk gait analysis in a chronic model of multiple sclerosis subjected to treadmill exercise training. *BMC Neurol*. 2017;17(1):160. doi:10.1186/s12883-017-0941-z
23. Herold S, Kumar P, Jung K, et al. CatWalk gait analysis in a rat model of multiple sclerosis. *BMC Neurosci*. 2016;17(1):78. doi:10.1186/s12868-016-0317-0
24. Hamers FP, Lankhorst AJ, van Laar TJV, et al. Automated quantitative gait analysis during overground locomotion in the rat: Its application to spinal cord contusion and transection injuries. *J Neurotrauma*. 2001;18(2):187–201. doi:10.1089/08977150150502613
25. Karahan S, Kincaid SA, Kammermann JR, et al. Evaluation of the rat stifle joint after transection of the cranial cruciate ligament and partial medial meniscectomy. *Comp Med*. 2001;51(6):504–512. PMID:11924812
26. Lakes EH, Allen KD. Gait analysis methods for rodent models of arthritic disorders: Reviews and recommendations. *Osteoarthritis Cartilage*. 2016;24(11):1837–1849. doi:10.1016/j.joca.2016.03.008
27. Xu Y, Tian NX, Bai QY, et al. Gait assessment of pain and analgesics: Comparison of the DigiGait™ and CatWalk™ gait imaging systems. *Neurosci Bull*. 2019;35(3):401–418. doi:10.1007/s12264-018-00331-y
28. Jacobs BY, Kloefkorn HE, Allen KD. Gait analysis methods for rodent models of osteoarthritis. *Curr Pain Headache Rep*. 2014;18(10):456. doi:10.1007/s11916-014-0456-x
29. Jacquez B, Choi H, Bird CW, et al. Characterization of motor function in mice developmentally exposed to ethanol using the Catwalk system: Comparison with the triple horizontal bar and rotarod tests. *Behav Brain Res*. 2021;396:112885. doi:10.1016/j.bbr.2020.112885
30. Chen H, Du J, Zhang Y, et al. Establishing a reliable gait evaluation method for rodent studies. *J Neurosci Methods*. 2017;283:92–100. doi:10.1016/j.jneumeth.2017.03.017
31. Gerwin N, Bendele AM, Glasson S, et al. The OARSI histopathology initiative: Recommendations for histological assessments of osteoarthritis in the rat. *Osteoarthritis Cartilage*. 2010;18(Suppl 3):24–34. doi:10.1016/j.joca.2010.05.030

32. Adães S, Mendonça M, Santos TN, et al. Intra-articular injection of collagenase in the knee of rats as an alternative model to study nociception associated with osteoarthritis. *Arthritis Res Ther.* 2014;16(1):R10. doi:10.1186/ar4436
33. Jacobs BY, Dunnigan K, Pires-Fernandes M, et al. Unique spatiotemporal and dynamic gait compensations in the rat monoiodoacetate injection and medial meniscus transection models of knee osteoarthritis. *Osteoarthritis Cartilage*. 2017;25(5):750–758. doi:10.1016/j.joca.2016.12.012
34. Fonsi M, El Amrani AI, Gervais F, et al. Intra-articular hyaluronic acid and chondroitin sulfate: Pharmacokinetic investigation in osteoarthritic rat models. *Curr Ther Clin Exp*. 2019;92:100573. doi:10.1016/j.curtheres.2019.100573
35. Park MH, Jung JC, Hill S, et al. FlexPro MD®, a combination of krill oil, astaxanthin and hyaluronic acid, reduces pain behavior and inhibits inflammatory response in monosodium iodoacetate-induced osteoarthritis in rats. *Nutrients*. 2020;12(4):956. doi:10.3390/nu12040956
36. Tschon M, Salamanna F, Martini L, et al. Boosting the intra-articular efficacy of low dose corticosteroid through a biopolymeric matrix: An in vivo model of osteoarthritis. *Cells*. 2020;9(7):1571. doi:10.3390/cells9071571
37. Zhang W, Moskowitz RW, Nuki G, et al. OARSI recommendations for the management of hip and knee osteoarthritis. Part II: OARSI evidence-based, expert consensus guidelines. *Osteoarthritis Cartilage*. 2008;16(2):137–162. doi:10.1016/j.joca.2007.12.013
38. Gabriel AF, Marcus MA, Honig WM, et al. The CatWalk method: A detailed analysis of behavioral changes after acute inflammatory pain in the rat. *J Neurosci Methods*. 2007;163(1):9–16. doi:10.1016/j.jneumeth.2007.02.003.
39. Parvathy SS, Masocha W. Gait analysis of C57BL/6 mice with complete Freund's adjuvant-induced arthritis using the CatWalk system. *BMC Musculoskelet Disord*. 2013;14:14. doi:10.1186/1471-2474-14-14.

MYBL2 in synergy with *CDC20* promotes the proliferation and inhibits apoptosis of gastric cancer cells

Qianxi Deng[1,A,F], Linju Wu[2,B,D], Yiming Li[1,C,E], Long Zou[1,B,E]

[1] Department of Gastroenterology, The Third Hospital of Mianyang, Sichuan Mental Health Center, China
[2] Department of Anesthesiology, The Third Hospital of Mianyang, Sichuan Mental Health Center, China

A – research concept and design; B – collection and/or assembly of data; C – data analysis and interpretation;
D – writing the article; E – critical revision of the article; F – final approval of the article

Advances in Clinical and Experimental Medicine, ISSN 1899–5276 (print), ISSN 2451–2680 (online) *Adv Clin Exp Med*. 2021;30(9):957–966

Address for correspondence
Qianxi Deng
E-mail: dengqianxi12@163.com

Funding sources
None declared

Conflict of interest
None declared

Received on December 30, 2020
Reviewed on March 9, 2021
Accepted on April 20, 2021

Published online on August 6, 2021

Abstract

Background. Gastric cancer (GC) is a common malignant tumor with a high morbidity and mortality worldwide. It has been reported that V-Myb avian myeloblastosis viral oncogene homolog-like 2 (*MYBL2*) could be a promising prognostic biomarker for GC. However, the specific role of *MYBL2* in GC progression remains unclear.

Objectives. To examine the role of *MYBL2* in GC progression and investigate the underlying mechanisms.

Materials and methods. The mRNA levels of target genes were detected using quantitative real-time polymerase chain reaction (RT-qPCR) and protein expression was measured with western blot analysis. Cell Counting Kit-8 (CCK-8) and colony formation assays were employed to inspect HGC-27 cell proliferation, and cellular apoptosis was determined with TUNEL staining. Finally, the interaction of *MYBL2* and cell division cycle 20 (*CDC20*) was verified with immunoprecipitation.

Results. *MYBL2* was confirmed to be overexpressed in GC cells. *MYBL2* knockdown inhibited HGC-27 cell proliferation and promoted cellular apoptosis, and these effects were reversed by *CDC20* overexpression. Interestingly, *MYBL2* interacted with *CDC20* and regulated its expression. *MYBL2* knockdown also inhibited activation of the Wnt/β-catenin signaling pathway, while *CDC20* overexpression showed the opposite effect.

Conclusions. In summary, the synergy between *MYBL2* and *CDC20* induced the proliferation of GC cells and inhibited cell apoptosis; these effects may have involved the Wnt/β-catenin signaling pathway. Thus, *MYBL2* may be a promising target for GC treatment.

Key words: apoptosis, gastric cancer, proliferation, cell division cycle 20 (*CDC20*), V-Myb avian myeloblastosis viral oncogene homolog-like 2 (*MYBL2*)

Cite as
Deng Q, Wu L, Li Y, Zou L. *MYBL2* in synergy with *CDC20* promotes the proliferation and inhibits apoptosis of gastric cancer cells. *Adv Clin Exp Med*. 2021;30(9):957–966. doi:10.17219/acem/135938

DOI
10.17219/acem/135938

Background

Gastric cancer (GC) is the 5th most common malignant tumor and the associated mortality rate is 3rd globally.[1,2] There are more than one million new GC cases diagnosed worldwide each year and this disease has become a major burden on human health.[3] Since patients with early GC have no obvious symptoms, the majority are already at an advanced stage at the time of diagnosis.[4,5] While great progress has been achieved through the development of new diagnostic methods and treatment strategies, the five-year survival rate in advanced patients has not exceeded 15%.[6] Due to the complex molecular mechanisms involved in the onset and development of GC, the specifics of GC pathogenesis are still unclear. Hence, it is important to explore novel and effective biomarkers for the diagnosis, treatment and prognosis of GC.

V-Myb avian myeloblastosis viral oncogene homolog-like 2 (*MYBL2*) is a member of the MYB family of transcription factors and is involved in the regulation of infinite replicative potential, evasion from apoptosis, tissue infiltration, and metastasis.[7] Expression of *MYBL2* is ubiquitous and can be observed in almost every proliferating cell.[8] Overexpression of this gene is also associated with a poor prognosis in multiple cancers.[7] Upregulation of *MYBL2*, a key downstream effect of Akt/FoxM1 signaling, facilitates the progression of glioma.[9] Recently, *MYBL2* overexpression has been also observed in malignant tumors including colorectal cancer,[10] acute myeloid leukemia[11] and breast cancer,[12] suggesting that this gene plays an essential role in tumor cell growth and carcinogenesis. A search of the CCLE database (https://portals.broadinstitute.org/ccle) suggests that *MYBL2* is generally upregulated in numerous tumor cell lines. Interestingly, it has been reported that *MYBL2* is relevant to cancer cell differentiation and lymph node metastasis. Studies have shown that its expression is negatively correlated with the survival rate of GC patients, suggesting that this gene could be a promising prognostic biomarker for gastric adenocarcinoma.[6] However, the specific role of *MYBL2* in the occurrence and progression of GC remains unclear.

Cell division cycle 20 (*CDC20*), a gene first discovered in yeast, plays an essential role in the progress of cell cycle.[13] *CDC20* is an indispensable developmental gene as its inhibition in mice leads to chromosome condensation and embryonic death, partly due to abnormal mitosis.[14] *CDC20* ablation can also effectively inhibit the invasiveness of mouse skin tumors, mainly due to increased apoptosis.[15] In addition, a retrospective study identified *CDC20* expression as a useful biomarker for the prognosis of pancreatic cancer.[16] This gene has also been studied in a great diversity of other tumors.[17]

Objectives

The results cited above suggest that *MYBL2* is very promising as a biomarker for the prognosis of GC. Thus, the aim of this study is to verify the role of *MYBL2* in GC progression, and more importantly, to investigate the underlying mechanisms.

Materials and methods

Cell culture and transfection

Human GC cell lines, including MKN-45, MKN-74, AGS and HGC-27, and a normal gastric GES-1 cell line were purchased from the Type Culture Collection of the Chinese Academy of Sciences (Shanghai, China). All of these cell lines were cultured in RPMI-1640 medium (Gibco, Thermo Fisher Scientific, Waltham, USA) containing 10% fetal bovine serum (FBS; Thermo Fisher Scientific), 100 U/mL of penicillin-G, and 100 μg/mL of streptomycin. The cells were maintained in a 37°C humidified atmosphere with 5% CO_2.

Small interfering (si)-*MYBL2* (si-MYBL2-1 5′-CCAAGAGCACACCTGTTAA-3′; si-MYBL2-2 5′-CCAGAAACATGCTGCGTTT-3′), and the scramble siRNA (si-NC, 5′-ACGTGACACGTTCGGAGAATT-3′) as a negative control (NC), were obtained from Shanghai GenePharma Co., Ltd. (Shanghai, China). The si-*MYBL2* (50 nM) and si-NC (50 nM) were transfected into HGC-27 cells (5×10^5 cells/well) using Lipofectamine 2000 (Invitrogen, Carlsbad, USA) according to the manufacturer's instructions. In addition, *CDC20* transcript cDNA was inserted into the pCDNA3.1 by Lederer Biological Technology (Guangdong, China), and then transfected into HGC-27 cells (20 μg) to achieve *CDC20* overexpression (Ov-*CDC20*). An empty vector without *CDC20* sequence was used as the negative control (OV-NC).

RT-qPCR

Total RNA from HGC-27 cells was extracted using TRIzol® reagent (Invitrogen; Thermo Fisher Scientific) following the manufacturer's protocol. Complementary DNA (cDNA) was synthesized using a Reverse Transcription kit (Thermo Fisher Scientific) according to manufacturer's instructions. Real-time quantitative polymerase chain reaction (RT-qPCR) was performed using Roche SYBR Green PCR kits (Roche Diagnostics, Basel, Switzerland) and carried out using the Opticon Real-Time PCR Detection System (ABI 7500; Life Technologies, Carlsbad, USA). The *GAPDH* gene was used as an internal gene for normalization. The cycling conditions were as follows: 1 cycle of 95°C for 2 min and 40 cycles of 95°C for 15 s, with a final extension at 60°C for 60 s. The relative mRNA quantity was calculated using the $2^{-\Delta\Delta Cq}$ method.[18] The primer sequences were as follows: *MYBL2* forward, 5'-AAAACAGTGAGGAGGAAC-3' and reverse, 5'-CAGGGAGGTCAAATTTAC-3'; *CDC20* forward, 5'-GGCACCAGTGATCGACACATTCGCAT-3' and reverse, 5'-GCCATAGCCTCAGGGTCTCATCTGCT-3'; and *GAPDH* forward, 5'-CTGGGCTACACTGAGCACC-3' and reverse, 5'-AAGTGGTCGTTGAGGGCAATG-3'.

Western blot analysis

The cells were washed with cold phosphate-buffered saline (PBS) and then lysed in a lysis buffer supplemented with phenylmethylsulfonyl fluoride (1 mM), trypsin (10 μg/mL), aprotinin (10 μg/mL), and leupeptin (10 μg/mL). A bicinchoninic acid (BCA) protein assay was used to quantify the protein concentration. Proteins (25 μg/lane) were separated in a 10% sodium dodecyl sulphate-polyacrylamide gel electrophoresis (SDS-PAGE) gel and then transferred onto polyvinylidene difluoride PVDF membranes. The membranes were then blocked with skim milk for 2 h at room temperature and subsequently incubated with primary antibodies against *MYBL2* (#PA5-79713; 1:1000), PCNA (#13-3900; 1:1000), Ki-67 (#14-5698-82; 1:1000), Bcl-2 (#MA5-11757; 1:1000), Bax (#33-6400; 1:1000), cleaved caspase-3 (#ab2302; 1:500; Abcam, Cambridge, UK), caspase-3 (#MA5-11521; 1:1000), *CDC20* (#PA5-63103; 1:1000), c-Myc (#MA1-980; 1:1000), β-catenin (#MA1-301; 1:1000), p-GSK-3β (#MA5-14873; 1:500), and GSK-3β (#39-9500; 1:1000) at 37°C overnight. *GAPDH* (#39-8600; 1:1000) was used as a loading control. After washing with PBS 3 times, the polyvinylidene difluoride (PVDF) membranes were incubated with horseradish peroxidase (HRP)-goat anti-rabbit secondary antibody (#G-21234; 1:50000; Invitrogen) for 2 h at room temperature, and the intensities of the bands were analyzed using ImageJ software v. 1.6 (National Institutes of Health, Bethesda, USA). Antibodies that are not branded were obtained from Thermo Fisher Scientific.

CCK-8 assay

A Cell Counting Kit-8 (CCK-8) assay (Beyotime Institute of Biotechnology, Haimen, China) was used to investigate the effects of *MYBL2* knockdown and *CDC20* overexpression on the viability of HGC-27 cells. Cells were seeded in 3 independent 96-well plates (5×10^3 cells/well) and incubated for 24 and 48 h at 37°C. Following this, CCK-8 reagent (10 μL) was added into each well and the plates were subsequently incubated at 37°C for another 2 h. The absorbance at 450 nm was detected using an enzyme-linked immunosorbent assay (ELISA) plate reader (Bio-Rad, Hercules, USA).

Colony formation assay

The colony formation assay was performed to detect the effect of *MYBL2* knockdown and *CDC20* overexpression on cell proliferation. After transfection, cells (1×10^3/well) were seeded in a 35-mm petri dish and incubated for 10 days at 37°C to form colonies. Subsequently, HGC-27 cells were fixed with 4% paraformaldehyde for 5 min and stained with 0.1% crystal violet solution for 20 min at room temperature. The number of colonies (diameters >0.5 mm) within a field was counted using a digital camera (Nikon Corp., Tokyo, Japan).

TUNEL staining

HGC-27 cells (1×10^5 cells/mL) were seeded in six-well plates and then fixed in 4% paraformaldehyde for 5 min at room temperature. After permeabilization with 0.1% Triton X-100 (Sigma-Aldrich, Merck KGaA, St. Louis, USA) for 5 min, HGC-27 cells were stained according to the protocol of the ApopTag Fluorescein In Situ Apoptosis Detection kit (Chemicon International Inc., Temecula, USA). Nuclei were labeled with 4′,6-diamidino-2-phenylindole (DAPI) and quantified under a fluorescence microscope at ×200 magnification (Leica Microsystems GmbH, Wetzlar, Germany).

Immunoprecipitation

Cells were collected and lysed with immunoprecipitation (IP) lysis buffer containing protease inhibitors. After centrifugation at 12,000 × g at 4°C, *MYBL2* antibody (1 μg) was added into the supernatant and the samples were placed on a rotating platform overnight at 4°C. Subsequently, 50 μL of SureBeads™ protein G magnetic beads (No. 1614023; Bio-Rad) were added into the above mixture at 4°C with gentle rotation for 4 h. The pellets were dissolved in 60 μL ×1 electrophoresis sample buffer and boiled for 5 min. Samples (30 μL) were analyzed using western blot analysis as outlined above.

Statistical analyses

Data are presented as the mean ± standard error of mean (SEM) of at least 3 experiments. Statistical analyses was performed using SPSS v. 17.0 software (SPSS Inc., Chicago, USA). Analysis of variance (ANOVA) followed by Bonferroni's post hoc test were used to determine the differences in the means among multiple groups. P-value <0.05 was considered to indicate a statistically significant difference.

Results

MYBL2 is highly expressed in GC cells

A search of the CCLE database suggested that *MYBL2* is generally upregulated in numerous tumor cell lines, including GC cell lines (Fig. 1A). To explore the effect of *MYBL2* on GC progression, the mRNA and protein expression of *MYBL2* were detected using RT-qPCR and western blot analysis, respectively. The mRNA and protein expression of *MYBL2* is significantly upregulated in GC cell lines, including MKN-45, MKN-74, AGS, and HGC-27, compared to the GES-1 cell line, suggesting that *MYBL2* may play an oncogenic role in the onset and development of GC (Fig. 1B,C).

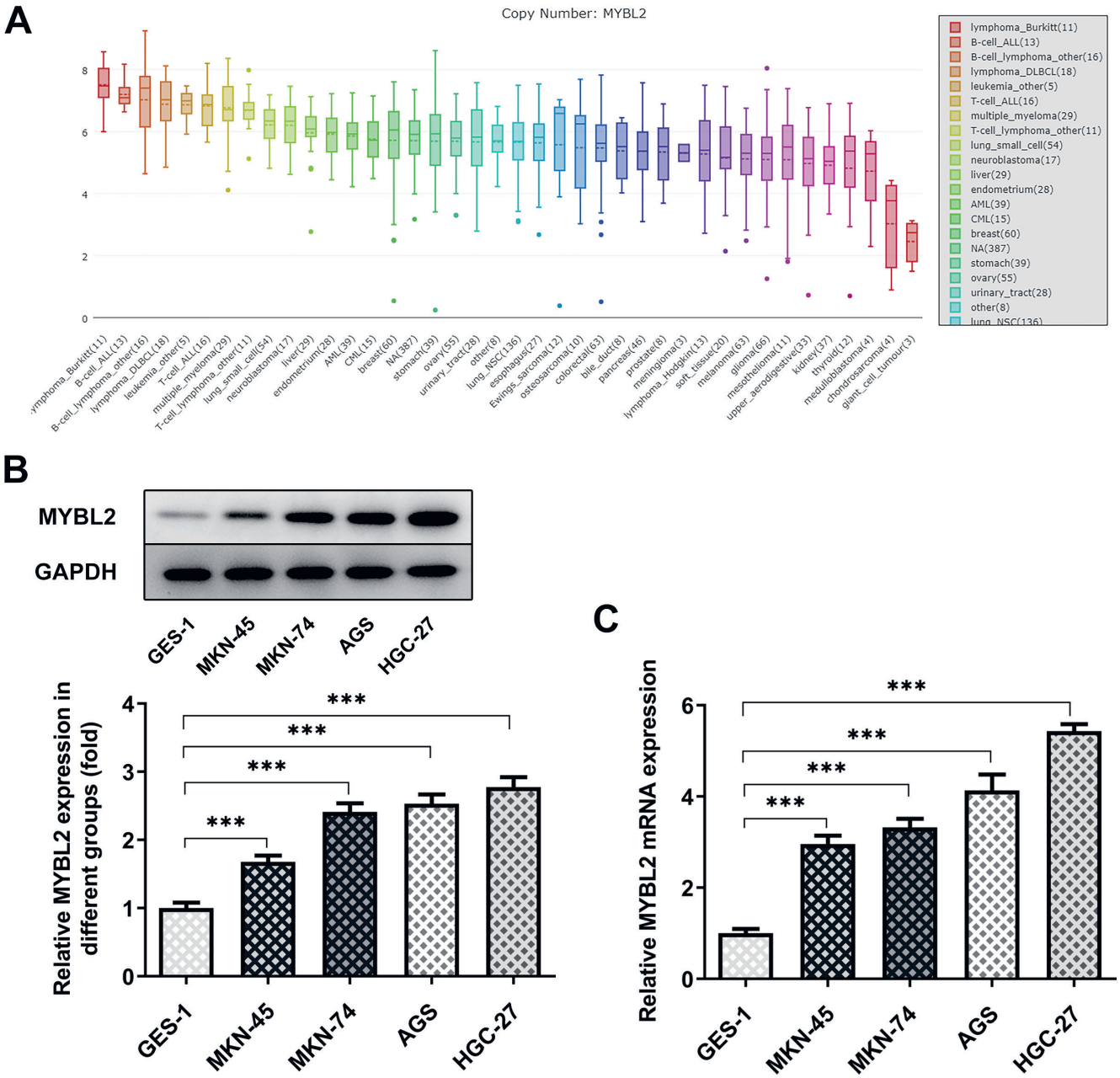

Fig. 1. *MYBL2* is highly expressed in gastric cancer (GC) cells. A. The *MYBL2* expression in multiple cancer cell lines in the CCLE database; B. The MYBL2 protein expression was determined with western blot analysis and quantification; C. The *MYBL2* mRNA level was analyzed with quantitative real-time polymerase chain reaction (RT-qPCR). Error bars represent the mean ±standard error of mean (SEM) from 3 independent experiments

***$p < 0.001$.

MYBL2 silencing inhibits HGC-27 cell growth

To examine the specific effect of *MYBL2* on GC progression, cell growth was analyzed with CCK-8 and colony formation assays. The si-*MYBL2* was used to achieve *MYBL2* knockdown. As shown in Fig. 2A, si-*MYBL2* caused a significant reduction in the *MYBL2* mRNA level, especially in the si-MYBL2-1 group. Hence, si-MYBL2-1 was selected for the subsequent experiments. Moreover, the results of the CCK-8 assay showed that viability was significantly depressed by *MYBL2* knockdown at the indicated time (24 h and 48 h), as compared to the control (Fig. 2B). The results of the western blot analysis demonstrated that the expression levels of proliferative markers, including proliferating cell nuclear antigen (PCNA) and Ki-67, were decreased in HGC-27 cells from the si-*MYBL2* group (Fig. 2C,D). Finally, the results of the colony formation assay showed that *MYBL2* silencing remarkably suppressed the proliferation of HGC-27 cells (Fig. 2E). These results indicate that *MYBL2* silencing inhibits HGC-27 cell growth.

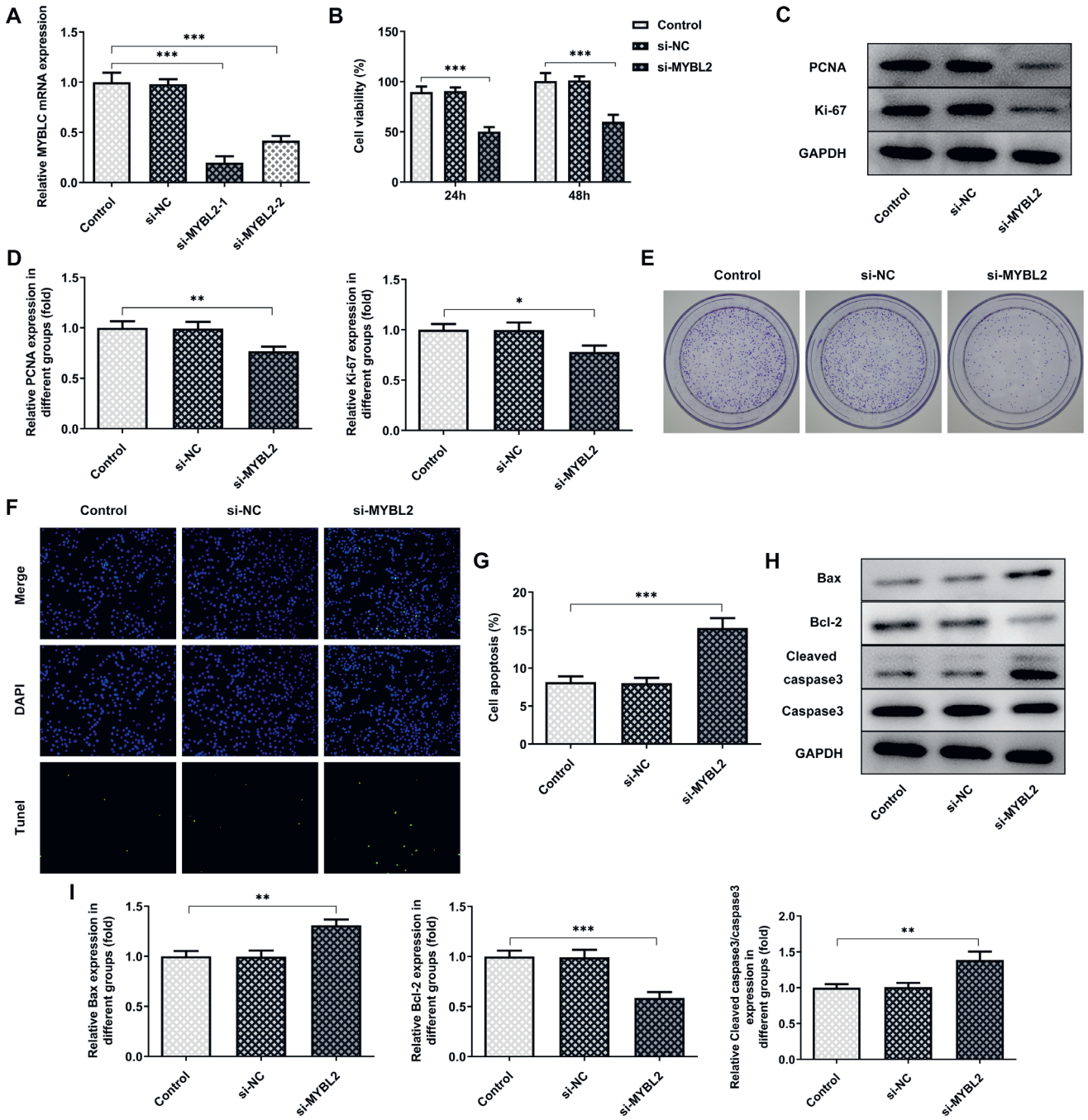

Fig. 2. *MYBL2* silencing inhibits cells growth and promotes cell apoptosis of HGC-27 cells. A. The *MYBL2* mRNA level was analyzed with quantitative real-time polymerase chain reaction (RT-qPCR); B. The HGC-27 cell viability was detected using the Cell Counting Kit-8 (CCK-8) assay; C and D. The proliferating cell nuclear antigen (PCNA) and Ki-67 protein expressions were determined with western blot analysis and quantification; E. HGC-27 cell proliferation was analyzed using colony formation assay; F and G. The HGC-27 cell apoptosis was determined with TUNEL staining; H and I. Bax, Bcl-2, cleaved caspase-3, and caspase-3 protein expressions were determined using western blot analysis and quantification. Error bars represent the mean ±standard error of mean (SEM) from 3 independent experiments

*p < 0.05; **p < 0.01; ***p < 0.001.

MYBL2 silencing promotes the apoptosis of HGC-27 cells

Apoptosis was analyzed by TUNEL staining to detect the specific effect of *MYBL2* on GC progression. The HGC-27 cell apoptosis rate in the si-MYBL2-1 group was higher than that in the control group (Fig. 2F,G). Additionally, the expression levels of Bax (pro-apoptotic), Bcl-2 (anti-apoptotic) and cleaved caspase-3/caspase-3 were assessed using western blot analysis. *MYBL2* silencing led to the loss of Bcl-2 and upregulation of Bax and cleaved caspase-3 (Fig. 2H,I). These results imply that *MYBL2* silencing promotes the apoptosis of HGC-27 cells.

MYBL2 interacts with *CDC20* and regulates its expression

To investigate the underlying mechanism of *MYBL2* in GC progression, studies were carried out to explore its downstream targets. Based on the LinkedOmics website (www.linkedomics.org), the correlation between the *MYBL2* and *CDC20* in GC was analyzed. It was found that *MYBL2* expression is positively correlated with most genes (Fig. 3A,B), and is highly correlated with *CDC20* ($p < 0.0001$; Fig. 3C). Furthermore, the co-expression of *MYBL2* and *CDC20* in the Gene Expression Omnibus (GEO) database was analyzed using COEXPEDIA (https://www.coexpedia.org/), as shown in Fig. 3D.

The role of *CDC20* in GC progression and its expression in GC cells was assessed by RT-qPCR and western blot analysis. The mRNA and protein expression levels of *CDC20* were significantly increased in GC cell lines, including MKN-45, MKN-74, AGS, and HGC-27, as compared to the GES-1 cell line (Fig. 3E,F). Moreover, *MYBL2* knockdown inhibited protein and mRNA expression of *CDC20* (Fig. 3G,H). Consistently with the search results outlined above, the IP assay showed that endogenous *CDC20* and *MYBL2* formed a complex in HGC-27 cells (Fig. 3I). Collectively, these results suggest that *MYBL2* interacts with *CDC20* in vitro.

MYBL2 knockdown inhibits the proliferation and promotes apoptosis of HGC-27 cells through the regulation of *CDC20* expression

To confirm the mechanism by which *MYBL2* regulates GC cell growth, the biological significance of the interaction between *MYBL2* and *CDC20* was examined. First, an Ov-*CDC20* plasmid was constructed, and its transfection efficiency was confirmed using RT-qPCR and western blot analysis (Fig. 4A,B). The results from the CCK-8 assay demonstrated that *CDC20* overexpression partly abolished the inhibitive effects of *MYBL2* knockdown on HGC-27 cell viability (Fig. 4C) and proliferative markers expressions (Fig. 4D). Consistent with these observations, the results from the colony formation assay showed that *CDC20* overexpression reversed the inhibitive effect of *MYBL2* silencing on HGC-27 cell proliferation (Fig. 4E). Furthermore, the results from TUNEL staining showed that the cell apoptosis rate was significantly decreased in HGC-27 cells co-transfected with si-*MYBL2* and Ov-*CDC20* compared to cells transfected with si-*MYBL2* alone (Fig. 4F,G). The Bcl-2 expression level in HGC-27 cells from the si-*MYBL2*+Ov-*CDC20* group was higher, while the expression levels of Bax and cleaved caspase-3 was lower, than that in si-*MYBL2* group (Fig. 4H,I). These results indicate that *MYBL2* knockdown inhibits the proliferation and promotes the apoptosis of HGC-27 cells through the regulation of *CDC20* expression.

Effects of *MYBL2* on the Wnt/β-catenin signaling pathway

To further clarify the underlying mechanisms of *MYBL2* in GC progression, the effects of *MYBL2* on the Wnt/β-catenin signaling pathway were analyzed. As shown in Fig. 5, *MYBL2* knockdown led to a reduction in the expression of β-catenin, p-GSK-3β and mc-Myc, which was reversed by *CDC20* overexpression. These results suggest that *MYBL2* knockdown induces inactivation of Wnt/β-catenin signaling pathway.

Discussion

Gastric cancer is a common malignant tumor with a high morbidity and mortality globally. Nowadays, due to risk factors such as changes in diet and lifestyle, the incidence of GC is increasing.[19] It is a disease that is highly heterogeneous in terms of molecular and cellular phenotype, and is diagnosed histologically through endoscopic biopsy. Endoscopic resection is mainly used for early-stage GC, and surgery is mainly used for advanced GC.[1] Despite the advances that have been achieved in diagnosis and therapy, the outcome for GC patients remains poor. There are great limitations in the understanding of the etiology of GC, which involves a multifaceted process and complex molecular mechanisms. Hence, it is important to explore promising targets for GC treatment.

The MYB family of proteins contains numerous subtypes with diverse functions, the majority of which act as transcription factors and have different numbers of MYB domain repeats. This latter feature endows these proteins with the ability to bind DNA.[20] Rapidly accumulating evidence now suggests that the MYB family regulates the cell cycle to maintain DNA replication, cell survival and proliferation.[9,21,22] It has also been reported that *MYBL2* expression is significantly increased in numerous cancer tissues as compared to adjacent tissue, and is negatively associated with the survival rate of cancer patients.[7] In addition, *MYBL2* downregulation inhibits the proliferation and DNA replication of gallbladder cancer cells in vitro,[23] which is consistent with the current findings. Specifically, in the current study, it was observed that *MYBL2* is overexpressed in GC cell lines (MKN-45, MKN-74, AGS, and HGC-27) compared to a normal gastric cell line (GES-1). Hence, *MYBL2* may be an oncogene in GC progression. To confirm the role of *MYBL2* in GC progression, *MYBL2* downregulation was induced by the transfection of si-*MYBL2*, and the survival and apoptosis of HGC-27 cells were detected using CCK-8, colony formation and TUNEL assays. The results suggested that *MYBL2* downregulation inhibits the proliferation and promotes the apoptosis of HGC-27 cells.

In order to explore the underlying mechanisms by which *MYBL2* regulates GC progression, the molecules that can

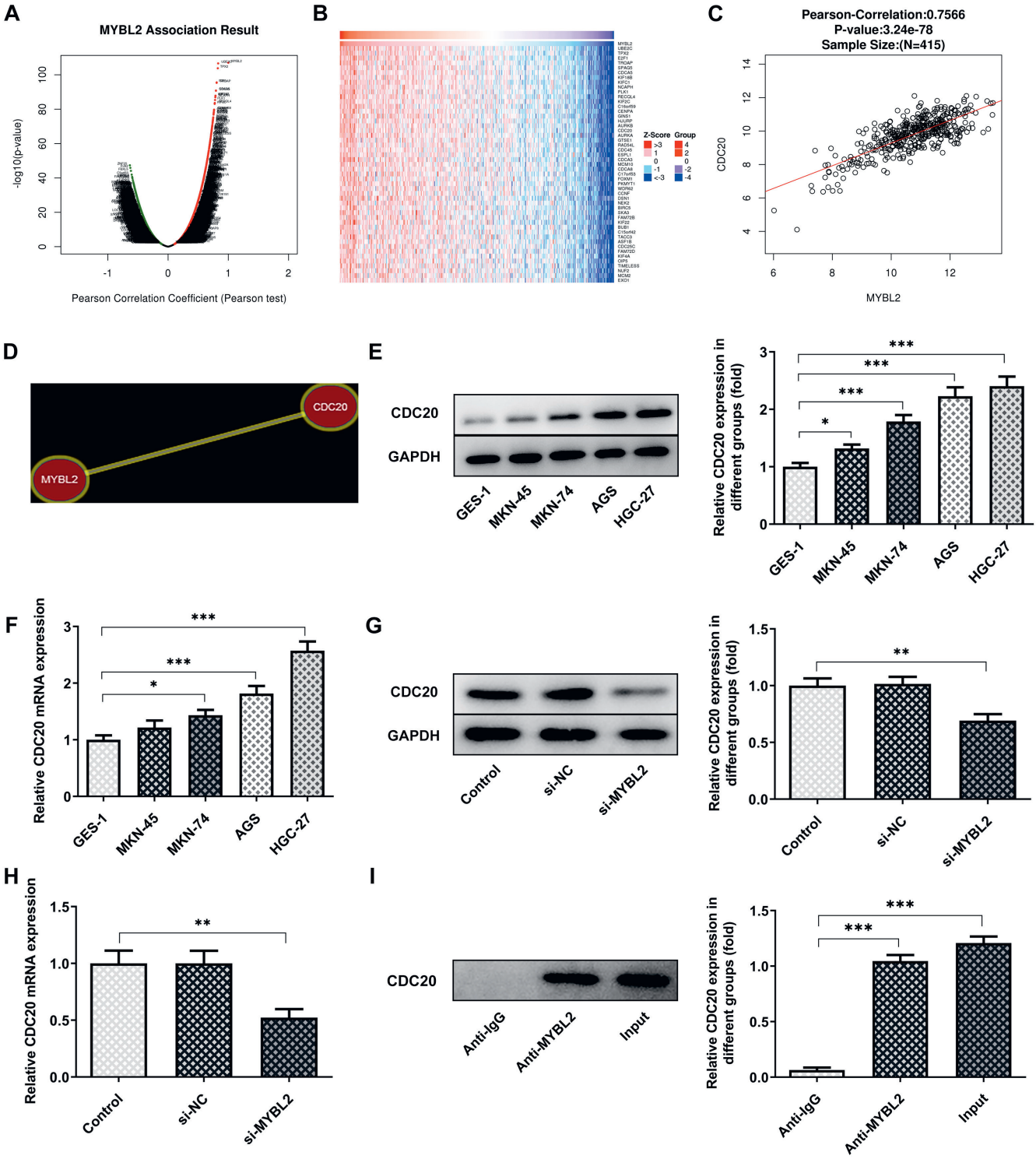

Fig. 3. *MYBL2* interacts with *CDC20* and regulates its expression. A–C. The correlation between *MYBL2* and *CDC20* in gastric cancer (GC) was analyzed using the LinkedOmics website; D. The co-expression of *MYBL2* and *CDC20* in the Gene Expression Omnibus (GEO) database was analyzed using the COEXPEDIA website; E and G. The CDC20 protein expression was determined with western blot analysis and quantification; F and H. The *CDC20* mRNA level was analyzed with quantitative real-time polymerase chain reaction (RT-qPCR); I. The interaction between *MYBL2* and *CDC20* was determined using IP. Error bars represent the mean ±standard error of mean (SEM) from 3 independent experiments

*p < 0.05; **p < 0.01; ***p < 0.001.

interact with this protein were searched on the LinkedOmics and COEXPEDIA websites. The results suggested that *MYBL2* expression is positively correlated with *CDC20*. Consistent with these search results, an IP assay indicated that *MYBL2* interacts with *CDC20* in vitro. It has been reported that *CDC20* possesses regulatory potential at multiple points of the cell cycle and plays a carcinogenic role in various types of tumor.[24] For example, 445 breast

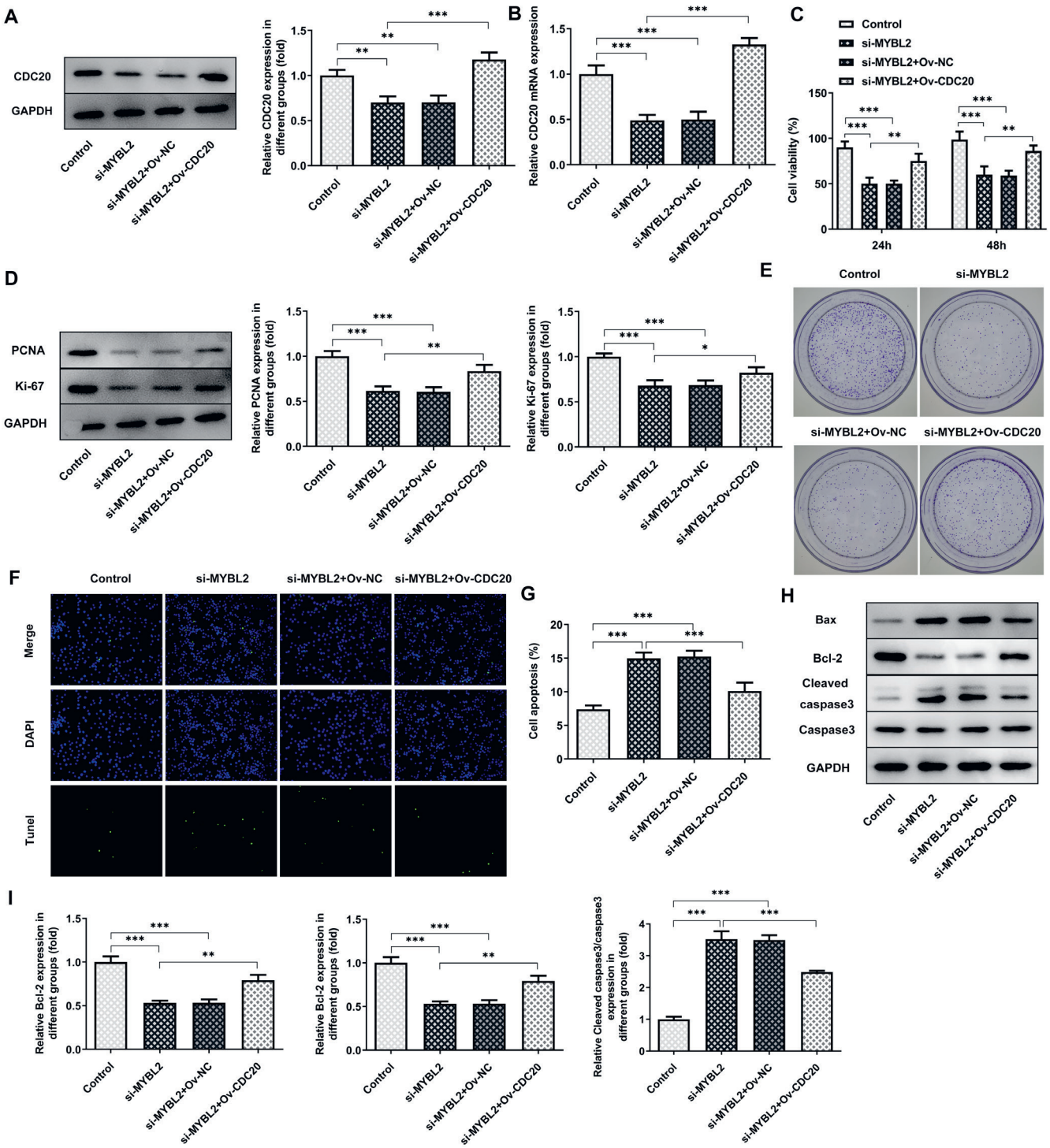

Fig. 4. *MYBL2* knockdown inhibits the proliferation and promotes apoptosis of HGC-27 cells via the regulation of *CDC20* expression. A. The CDC20 protein expression was determined with western blot analysis and quantification; B. The *CDC20* mRNA level was analyzed with quantitative real-time polymerase chain reaction (RT-qPCR); C. HGC-27 cell viability was detected using the Cell Counting Kit-8 (CCK-8); D. The proliferating cell nuclear antigen (PCNA) and Ki-67 protein expressions were determined with western blot analysis and quantification; E. HGC-27 cell proliferation was analyzed with the colony formation assay; F and G. HGC-27 cell apoptosis was determined with TUNEL staining; H and I. Bax, Bcl-2, cleaved caspase-3, and caspase-3, and protein expressions were determined using western blot analysis and quantification. Error bars represent the mean ±standard error of mean (SEM) from 3 independent experiments

**$p < 0.01$; ***$p < 0.001$.

cancer patients were followed up for 20 years to detect the expression of *CDC20*, which verified that *CDC20* is highly expressed in breast cancer patients. In addition, the overexpression of *CDC20* was related to the aggressive course of breast cancer.[25] *CDC20* is also overexpressed in colorectal cancer cell lines and primary cancer tissues. It is worth noting that the expression of *CDC20* is relevant to clinical stage, metastasis and short-term overall survival,

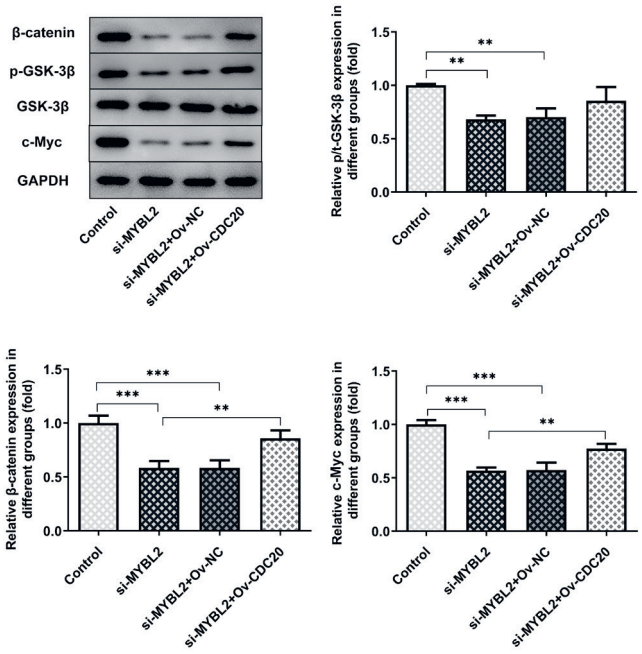

Fig. 5. The effect of *MYBL2* on the Wnt/β-catenin signaling pathway. The protein levels of β-catenin, p-GSK-3β, GSK-3β, and c-Myc were assessed with western blot analysis and quantification. Error bars represent the mean ±standard error of mean (SEM) from 3 independent experiments

**p < 0.01; ***p < 0.001.

which indicates that *CDC20* can be regarded as an independent prognostic biomarker for human colorectal cancer.[26] Importantly, a previous study has demonstrated that *CDC20* expression is significantly increased in GC tumor tissues compared noncancerous tissues, and its overexpression is closely related to aggressive progression and poor prognosis in GC patients.[27] On the basis of the result that *MYBL2* silencing depressed *CDC20* expression, the biological significance of the interaction between *MYBL2* and *CDC20* was subsequently examined. The findings revealed that *CDC20* overexpression partly abolished the effect of *MYBL2* downregulation on HGC-27 cell proliferation and apoptosis, suggesting that *MYBL2* works in synergy with *CDC20* to promote the proliferation and inhibit the apoptosis of GC cells.

The Wnt signal transduction cascade is a key driving factor for a variety of tissue stem cells. The Wnt pathway can participate in and can cause a variety of growth-related pathologies and cancers.[28] In breast, lung and hematopoietic malignancies, activation of the Wnt/β-catenin signaling pathway has been found and it mediates tumor recurrence.[29,30] It has been reported that *CDC20* silencing not only suppresses prostate cancer growth, but also enhances chemosensitivity to docetaxel via inhibition of Wnt/β-catenin signaling.[31] In this study, it was found that *MYBL2* knockdown induced inactivation of the Wnt/β-catenin signaling pathway, while *CDC20* upregulation had the opposite effect. Thus, *MYBL2*, in synergy with *CDC20*, promotes the proliferation and inhibits the apoptosis of GC cells, and these effects may involve the Wnt/β-catenin signaling pathway.

The purpose of this study was to investigate the underlying mechanisms of *MYBL2* in the progression of GC. However, the current experiments were carried out in vitro and thus require further investigation in vivo.

Conclusions

Taken together, the current results indicate that the synergy between *MYBL2* and *CDC20* induces the proliferation of GC cells and inhibits cell apoptosis, and that these processes may involve the Wnt/β-catenin signaling pathway. Thus, *MYBL2*, as a promising target, is of great significance for advancing the treatment of GC.

ORCID iDs

Qianxi Deng https://orcid.org/0000-0002-8901-9191
Linju Wu https://orcid.org/0000-0003-4190-0075
Yiming Li https://orcid.org/0000-0002-0614-8052
Long Zou https://orcid.org/0000-0003-1647-2697

References

1. Smyth EC, Nilsson M, Grabsch HI, van Grieken NC, Lordick F. Gastric cancer. *Lancet*. 2020;396(10251):635–648. doi:10.1016/s0140-6736(20)31288-5
2. Venerito M, Link A, Rokkas T, Malfertheiner P. Gastric cancer: Clinical and epidemiological aspects. *Helicobacter*. 2016;21(Suppl 1):39–44. doi:10.1111/hel.12339
3. Thrift AP, El-Serag HB. Burden of gastric cancer. *Clin Gastroenterol Hepatol*. 2020;18(3):534–542. doi:10.1016/j.cgh.2019.07.045
4. Zong L, Abe M, Seto Y, Ji J. The challenge of screening for early gastric cancer in China. *Lancet*. 2016;388(10060):2606. doi:10.1016/s0140-6736(16)32226-7
5. Yao J, Zhang H, Liu C, Chen S, Qian R, Zhao K. miR-450b-3p inhibited the proliferation of gastric cancer via regulating KLF7. *Cancer Cell Int*. 2020;20:47. doi:10.1186/s12935-020-1133-2
6. Jia Y, Gao Y, Li J, Chang Z, Yan J, Qin Y. Prognostic implications of *MYBL2* in resected Chinese gastric adenocarcinoma patients. *Oncotargets Ther*. 2019;12:1129–1135. doi:10.2147/ott.s188820
7. Musa J, Aynaud MM, Mirabeau O, Delattre O, Gruenewald TG. *MYBL2* (B-Myb): A central regulator of cell proliferation, cell survival and differentiation involved in tumorigenesis. *Cell Death Dis*. 2017;8(6):e2895. doi:10.1038/cddis.2017.244
8. Bayley R, Ward C, Garcia P. *MYBL2* amplification in breast cancer: Molecular mechanisms and therapeutic potential. *Biochim Biophys Acta Rev Cancer*. 2020;1874(2):188407. doi:10.1016/j.bbcan.2020.188407
9. Zhang X, Lv QL, Huang YT, Zhang LH, Zhou HH. Akt/FoxM1 signaling pathway-mediated upregulation of *MYBL2* promotes progression of human glioma. *J Exp Clin Cancer Res*. 2017;36(1):105. doi:10.1186/s13046-017-0573-6
10. Ren F, Wang L, Shen X, et al. *MYBL2* is an independent prognostic marker that has tumor-promoting functions in colorectal cancer. *Am J Cancer Res*. 2015;5(4):1542–1552.
11. Fuster O, Llop M, Dolz S, et al. Adverse prognostic value of *MYBL2* overexpression and association with microRNA-30 family in acute myeloid leukemia patients. *Leuk Res*. 2013;37(12):1690–1696. doi:10.1016/j.leukres.2013.09.015
12. Li X, Zhang X, Wu CC, et al. The role of MYB proto-oncogene like 2 in tamoxifen resistance in breast cancer. *J Mol Histol*. 2021;52(1):21–30. doi:10.1007/s10735-020-09920-6
13. Hartwell LH, Mortimer RK, Culotti J, Culotti M. Genetic control of the cell division cycle in yeast. V. Genetic analysis of cdc mutants. *Genetics*. 1973;74(2):267–286. PMID:17248617

14. Li M, York JP, Zhang P. Loss of *CDC20* causes a securin-dependent metaphase arrest in two-cell mouse embryos. *Mol Cell Biol*. 2007; 27(9):3481–3488. doi:10.1128/mcb.02088-06
15. Manchado E, Guillamot M, de Carcer G, et al. Targeting mitotic exit leads to tumor regression in vivo: Modulation by Cdk1, Mastl, and the PP2A/B55α,δ phosphatase. *Cancer Cell*. 2010;18(6):641–654. doi:10.1016/j.ccr.2010.10.028
16. Chang DZ, Ma Y, Ji B, et al. Increased *CDC20* expression is associated with pancreatic ductal adenocarcinoma differentiation and progression. *J Hematol Oncol*. 2012;5:15. doi:10.1186/1756-8722-5-15
17. Wang L, Zhang J, Wan L, Zhou X, Wang Z, Wei W. Targeting *CDC20* as a novel cancer therapeutic strategy. *Pharmacol Ther*. 2015;151: 141–151. doi:10.1016/j.pharmthera.2015.04.002
18. Ma Y, Kong J, Yan G, et al. NQO1 overexpression is associated with poor prognosis in squamous cell carcinoma of the uterine cervix. *BMC Cancer*. 2014;14:414. doi:10.1186/1471-2407-14-414
19. Yusefi AR, Bagheri Lankarani K, Bastani P, Radinmanesh M, Kavosi Z. Risk factors for gastric cancer: A systematic review. *Asian Pac J Cancer Prev*. 2018;19(3):591–603. doi:10.22034/apjcp.2018.19.3.591
20. Dubos C, Stracke R, Grotewold E, Weisshaar B, Martin C, Lepiniec L. MYB transcription factors in Arabidopsis. *Trends Plant Sci*. 2010;15(10): 573–581. doi:10.1016/j.tplants.2010.06.005
21. Qin H, Li Y, Zhang H, et al. Prognostic implications and oncogenic roles of *MYBL2* protein expression in esophageal squamous-cell carcinoma. *Onco Targets Ther*. 2019;12:1917–1927. doi:10.2147/ott.s190145
22. Wei T, Weiler SME, Toth M, et al. YAP-dependent induction of UHMK1 supports nuclear enrichment of the oncogene *MYBL2* and proliferation in liver cancer cells. *Oncogene*. 2019;38(27):5541–5550. doi:10.1038/s41388-019-0801-y
23. Liang HB, Cao Y, Ma Q, et al. *MYBL2* is a potential prognostic marker that promotes cell proliferation in gallbladder cancer. *Cell Physiol Biochem*. 2017;41(5):2117–2131. doi:10.1159/000475454
24. Chu Z, Zhang X, Li Q, Hu G, Lian CG, Geng S. *CDC20* contributes to the development of human cutaneous squamous cell carcinoma through the Wnt/β-catenin signaling pathway. *Int J Oncol*. 2019;54(5): 1534–1544. doi:10.3892/ijo.2019.4727
25. Karra H, Repo H, Ahonen I, et al. *CDC20* and securin overexpression predict short-term breast cancer survival. *Br J Cancer*. 2014;110(12): 2905–2913. doi:10.1038/bjc.2014.252
26. Wu WJ, Hu KS, Wang DS, et al. *CDC20* overexpression predicts a poor prognosis for patients with colorectal cancer. *J Transl Med*. 2013; 11:142. doi:10.1186/1479-5876-11-142
27. Ding ZY, Wu HR, Zhang JM, Huang GR, Ji DD. Expression characteristics of *CDC20* in gastric cancer and its correlation with poor prognosis. *Int J Clin Exp Pathol*. 2014;7(2):722–727. PMID:24551295
28. Nusse R, Clevers H. Wnt/β-catenin signaling, disease, and emerging therapeutic modalities. *Cell*. 2017;169(6):985–999. doi:10.1016/j.cell.2017.05.016
29. Krishnamurthy N, Kurzrock R. Targeting the Wnt/beta-catenin pathway in cancer: Update on effectors and inhibitors. *Cancer Treat Rev*. 2018;62:50–60. doi:10.1016/j.ctrv.2017.11.002
30. Li Y, Jin K, van Pelt GW, et al. c-Myb enhances breast cancer invasion and metastasis through the Wnt/β-catenin/axin2 pathway. *Cancer Res*. 2016;76(11):3364–3375. doi:10.1158/0008-5472.can-15-2302
31. Li K, Mao Y, Lu L, et al. Silencing of *CDC20* suppresses metastatic castration-resistant prostate cancer growth and enhances chemosensitivity to docetaxel. *Int J Oncol*. 2016;49(4):1679–1685. doi:10.3892/ijo.2016.3671

Extracellular Nampt (eNampt/visfatin/PBEF) directly and indirectly stimulates ACTH and CCL2 protein secretion from isolated rat corticotropes

Piotr Celichowski[1,A,C,D,F], Karol Jopek[1,2,B,C,E], Marta Szyszka[1,B], Paulina Milecka[1,B], Marianna Tyczewska[1,3,B,C,E], Svetlana Sakhanova[4,C,E], Witold Szaflarski[1,E,F], Ludwik Kazimierz Malendowicz[1,C–F], Marcin Ruciński[1,C,E,F]

[1] Department of Histology and Embryology, Poznan University of Medical Sciences, Poland
[2] Regional Blood Center, Poznan University of Medical Sciences, Polska
[3] Department of Anatomy and Histology, University of Zielona Góra, Poland
[4] Scientific-Practical Center, West Kazakhstan Marat Ospanov Medical University, Aktobe, Kazakhstan

A – research concept and design; B – collection and/or assembly of data; C – data analysis and interpretation;
D – writing the article; E – critical revision of the article; F – final approval of the article

Advances in Clinical and Experimental Medicine, ISSN 1899–5276 (print), ISSN 2451–2680 (online) *Adv Clin Exp Med*. 2021;30(9):967–980

Address for correspondence
Piotr Celichowski
E-mail: pcelichowski@ump.edu.pl

Funding sources
The present study was supported by PRELUDIUM (grant No. 2016/21/N/NZ4/00122) from the National Science Centre (Kraków, Poland). Svetlana Sakhanova (WKMOMU) and Witold Szaflarski (PUMS) were supported by the Social Health Insurance Project, Republic of Kazakhstan (Contract No. SHIP-2.3/CS-02).

Conflict of interest
None declared

Received on October 28, 2020
Reviewed on February 26, 2021
Accepted on April 26, 2021

Published online on August 20, 2021

Cite as
Celichowski P, Jopek K, Szyszka M, et al. Extracellular Nampt (eNampt/visfatin/PBEF) directly and indirectly stimulates ACTH and CCL2 protein secretion from isolated rat corticotropes. *Adv Clin Exp Med*. 2021;30(9):967–980. doi:10.17219/acem/136172

DOI
10.17219/acem/136172

Abstract

Background. Nicotinamide phosphoribosyltransferase (Nampt/visfatin/PBEF) acts both as an enzyme in the nicotinamide adenine dinucleotide (NAD) synthesis pathway as well as an extracellular hormone (eNampt). Among its effects, eNampt exerts potent pro-inflammatory effects. We have recently shown that, in rats, eNampt stimulates corticosterone secretion by acting through the pituitary rather than the hypothalamus.

Objectives. To investigate the mechanism of action of eNampt on the secretion of adrenocorticotropic hormone (ACTH) and chemokine (C-C motif) ligand 2 (CCL2), which are cytokines secreted by pituitary neuroendocrine tumors.

Materials and methods. The research was carried out on the AtT-20 murine cell line, primary rat pituitary cell culture, isolated pituitary corticotropes, and in vivo. The effects of the performed experiments were examined using the following methods: gene expression profiling using microarrays, quantitative polymerase chain reaction (qPCR) and enzyme-linked immunosorbent assay (ELISA).

Results. The results suggest that eNampt stimulates ACTH secretion from rat corticotropes both directly and indirectly. Indirect action most likely occurs through interleukin (IL)-6 secreted by folliculostellate cells of the pituitary gland. In isolated ACTH cells of the rat pituitary gland, eNampt stimulates the expression of genes involved in the immune response. Among them, the protein encoded by the *CCL2* gene seems to also be involved in the regulation of corticotropin-releasing hormone (CRH)-dependent metabolism. Unlike rat corticotropes, murine AtT-20 corticotropic cells do not react to either eNampt or Fk866 (the inhibitor of Nampt enzymatic action).

Conclusions. The eNampt stimulates the secretion of ACTH from rat corticotropes indirectly and directly, likely by stimulating IL-6 secretion from folliculostellate cells of the pituitary gland. This effect was not observed in the AtT-20 corticotropic cell cancer cell line.

Key words: ACTH, Nampt, pituitary gland, CCL2, IL-6

Background

Nicotinamide phosphoribosyltransferase (Nampt) is the rate-limiting enzyme for nicotinamide adenine dinucleotide (NAD) salvage synthesis in mammals, thereby influencing NAD-dependent enzymes and constituting a strong endogenous defense system against various stresses. Nampt, apart from its intracellular function (iNampt), is secreted outside the cells where it circulates in the bloodstream as a hormone (eNampt), also called visfatin or pre-B cell colony-enhancing factor (PBEF).[1–3] eNampt is secreted mainly by adipose tissue, but has also been proven to be secreted by many other types of cells.[4] eNampt can be detected in the human bloodstream and other extracellular fluids, where it exerts pro-inflammatory, prochemotactic (promoting migration of the cells), proangiogenic, and insulin-like effects. The exact mechanism of action of eNampt is still unclear.[4] In the literature, there are 3 not necessarily mutually exclusive theories: 1) eNampt binds to toll-like receptor 4 (TLR4), C-C motif chemokin receptor 5 (CCR5) or a yet unidentified receptor; 2) eNampt is enzymatically active in the extracellular matrix; and/or 3) eNampt is carried in the systemic circulation in extracellular vesicles (EV) and liberated upon internalization, enhancing NAD+ biosynthesis.[4–7]

Our earlier studies demonstrated that intraperitoneal (i.p.) administration of eNampt within 1 h significantly increased levels of corticosterone, but not aldosterone and adrenocorticotropic hormone (ACTH), in rat serum.[8] Under experimental conditions, proopiomelanocortin (POMC) mRNA levels in the pituitary glands of the examined rats increased. Moreover, eNampt protein did not affect the secretion of corticotropin-releasing hormone (CRH) from rat hypothalamic explants and inhibited the release of CRH, induced by potassium ions. In anterior pituitary fragments, eNampt did not stimulate ACTH but did increase POMC mRNA expression. The obtained results suggest that the stimulating effect of eNampt protein on corticosterone secretion in rats is dependent on the pituitary gland. However, the mechanism of action of eNampt on changes in the pituitary gland of rats described above remains unexplained.

The anterior lobe of the pituitary gland (adenohypophysis) is a complex structure composed of many different hormone-secreting cells, such as corticotropes, thyrotropes, gonadotropes, somatotropes, lactotropes, a small population of mammosomatotropes, and hormonally nonactive folliculostellate cells, as well, as blood vessels and fibroblasts.[9,10] Under the influence of hypothalamic CRH, the corticotropes of the adenohypophysis secrete ACTH, the main hormone regulating the growth, differentiation and secretory activity of adrenocortical cells.[11] Stimulation of pituitary secretion of ACTH also occurs in response to inflammatory factors, such as interleukin (IL)-1 or tumor necrosis factor alpha (TNF-α).[12] However, these factors do not act directly on corticotropes, but rather exert their biological effect through folliculostellate cells.[13,14] Under the influence of these inflammatory factors, folliculostellate cells secrete a variety of pro- and anti-inflammatory factors, including interleukin(IL)-6.[15,16] There are experiments showing that secreted IL-6 exerts a stimulating effect on ACTH secretion by corticotropes. It is suggested that, due to this mechanism, *CRH* gene silencing in mice does not prevent pituitary secretion of ACTH.[17] It appears that only neutralization of IL-6 with specific antibodies completely inhibits activation of the hypothalamo–pituitary–adrenal (HPA) axis in mice with *CRH* gene knockout.[18,19]

As mentioned above, the stimulating effect of eNampt protein on corticosterone secretion in rats most likely occurs at the pituitary level.[8] In this respect, it should be stressed that pituitary folliculostellate cells, in response to stimulation of CD14 and TLR4 receptors, secrete IL-6.[13,14] It has also been shown that eNampt has the ability to bind to TLR4 receptors.[6] Moreover, there are reports that eNampt protein stimulates IL-6 secretion by human leukocytes.[20] In view of these studies, it seems that the stimulating effect of eNampt on corticotropes may be mediated by pituitary folliculostellate cells. To investigate this hypothesis, we performed several experiments with the AtT-20 murine corticotropic cell line as well as with isolated rat corticotropes. These cells were exposed to eNampt as well as CRH, IL-6 and Fk866 – an inhibitor of Nampt enzymatic action – and their effects were determined using enzyme-linked immunosorbent assay (ELISA), microarray analysis of gene expression and quantitative polymerase chain reaction (qPCR). Considering the fact that pituitary neuroendocrine tumors secrete numerous cytokines, including CCL2,[21] in isolated ACTH cells of the rat pituitary gland exposed to eNampt or ACTH, the expression of various cytokines with particular attention to CCL2 was characterized.

Objectives

To verify the main research hypothesis presented above, we formulated several specific objectives. The 1st objective was to investigate the effect of eNampt on ACTH secretion in the AtT-20 cell line, rat primary pituitary cell culture and isolated corticotropes. The 2nd objective was to determine the effect of eNampt CRH and IL-6 on the transcriptome profiling of isolated rat corticotropes. The last objective was to investigate the effect of eNampt on CCL2 biosynthesis in rat primary pituitary cell culture, isolated corticotropes and a rat in vivo study.

Materials and methods

Reagents

If not stated otherwise, all reagents were obtained from Sigma-Aldrich (Merck KGaA, Darmstadt, Germany) or Avantor Performance Materials Poland S.A. (Gliwice, Poland).

AtT-20 murine cell line

The mouse pituitary corticotrope AtT-20/D16v-F2 tumor cell line was bought from Sigma-Aldrich (94050406). The cells were cultured within Dulbecco's Modified Eagle Medium (DMEM)/F12 (without phenol red) medium supplemented with 10% fetal bovine serum (FBS) and 1× AA solution (Sigma-Aldrich; A5955). The cells were cultured in 96-well plates at ~10,000 cells/well.

Primary rat pituitary cell culture

The 21-day old Wistar rats were obtained from the Animal House of Wielkopolska Centre for Advanced Technologies (Poznań, Poland). The brains of the rats were removed directly after decapitation and the adenohypophyses were isolated using sterile surgical tools and transferred to DMEM/F12 (no phenol red) medium supplemented with 10% FBS and 1× AA solution. Subsequently, the glands were fragmented with scissors and treated with 0.9 mg/mL collagenase I (collagenase type I; Sigma-Aldrich) in phosphate-buffered saline (PBS) solution for 20 min at 37°C. Subsequently, the cells were centrifuged (1000 × g for 7 min), suspended in 15 mM ethylenediaminetetraacetic acid (EDTA) (Sigma-Aldrich) in phosphate-buffered saline (PBS) solution, and incubated for 10 min at 37°C. After such treatment, the cells were filtered with a Corning® 70-µm cell strainer nylon membrane (Sigma-Aldrich ref. No. 431751). The cells were then centrifuged (1000 × g for 7 min) and resuspended in DMEM/F12 with 1× AA solution, 10% FBS and 0.05 µg/L fibroblast growth factor (FGF) solution (Thermo Fisher Scientific, Waltham, USA; cat. No. 1263344C). The described procedure delivered the isolated rat pituitary cells, of which ~60% were alive. The living cells percentage was estimated using a Countess II FL Automated Cell Counter (Thermo Fisher Scientific; cat. No. A27974) in the presence of trypan blue. The cells were cultured in 96-well plates at ~10,000 cells/well.

Isolation of corticotropes

After 2 days of isolated rat pituitary cell culture, the cells were treated with 1× trypsin solution (Sigma-Aldrich; 59427C) and collected from culture plates. The corticotropic cells were separated from culture using CELLection™ Biotin Binder Kit (Thermo Fisher Scientific – Invitrogen; lot: 11533D). For cell separation, the anti CRHR1 antibody was used (Alomone Labs, Jerusalem, Israel; ACR050AN0150) with secondary biotin-labeled antibody (Abcam, Cambridge, UK; anti-IgG ab6720). After separation, the cells were cultured with DMEM/F12 with 1× AA solution, 10% FBS and 0.05 µg/L FGF. The cells were cultured in 96-well plates at ~10,000 cells/well.

Animals

As an additional observation, we measured CCL2 levels in animal blood plasma obtained from experiments described in our previous publication.[8] Briefly, experiments were performed on 15 adult (3–4 months old, 250–300 g body weight) male rats. The eNampt protein was administered by ip. injection at a dose of 4 µg/100 g, while ACTH (Cortrosyn®; Organon Pharmaceuticals, Merck KGaA, Darmstadt, Germany) was given at a dose of 2.5 µg/100 g. Rats in the control group were administered 0.2 mL physiological saline. Each group (control, eNampt and ACTH) consisted of 5 animals. Rats were decapitated 1 h after injection. Trunk blood was collected on EDTA (150 mM, pH 8, 300 µL/5 mL) and centrifuged at 1000 × g for 10 min at 4°C. The serum was collected in fresh tubes and stored at –20°C until analysis. The study protocol was approved by the independent Local Ethics Committee for Animal Studies in Poznań (protocol No. 75/2016).

Hormone administration

If not stated otherwise, the studied substances were administered in medium at final concentrations of 10^{-8} M for Nampt (BioVendor R&D Products, Brno, Czech Republic), 10^{-6} µM for CRH (CRH Ferring®; Ferring Pharmaceuticals, Saint-Prex, Switzerland) and 50 pg/mL of IL-6 (Sino Biological, Beijing, China). The culture media were collected 24 h after administration of the tested substances and frozen at –20°C. The cells were subsequently subjected to RNA isolation.

Hormone level detection

The culture media were analyzed using ELISA to determine the concentration of ACTH (Phoenix Europe GmbH, Karlsruhe, Germany; cat. No. EK-001-21), IL-6 (Invitrogen; BM5625) and CCL2 – MCP1 (CCL2) Rat ELISA Kit (Abcam; ab100778). All determinations were performed according to the manufacturers' protocols.

RNA isolation

After incubation, the cells were washed with PBS. Total RNA was extracted from 96-well plates using 100 µL of TRIzol Reagent (Thermo Fisher Scientific; cat. No. 15596026). Further isolation was carried out according to the protocol and reagent proportions stated in the manufacturer's protocol. The amount of total mRNA was determined by optical density at 260 nm and its purity was estimated by the 260/280 nm absorption ratio (>1.8; NanoDrop ND-1000 spectrophotometer; Thermo Fisher Scientific).

Microarray assay

The microarray study was carried out as described elsewhere.[22–24] A 5 ng/sample of total RNA from isolated corticotropic cells was subjected to microarray analysis. The microarray procedure was performed using GeneChip™ WT Pico Kit (Thermo Fisher Scientific; cat. No. 902622) and GeneChip™ Hybridization, Wash and Stain Kit (Thermo

Fisher Scientific; cat. No. 900720). Biotin-labeled fragments of cDNA were hybridized to the GeneChip™ Rat Gene 2.1 ST Array Strip (Thermo Fisher Scientific; cat. No. 902126, 48°C/20 h). Next, the microarrays were washed and stained according to the technical protocol using the Affymetrix GeneAtlas™ Fluidics Station. Subsequently, the array strips were scanned using the Imaging Station of GeneAtlas System. Preliminary analysis of the scanned chips was performed using Affymetrix GeneAtlas™ Operating Software. The quality of gene expression data was checked according to quality control criteria provided by the software. The obtained CEL files were imported into downstream data analysis software. All of the presented analyses and graphs were performed using Bioconductor and the R programming language (R Foundation for Statistical Computing, Vienna, Austria). For analysis we used following bioconductor packages pd.ragene.2.1.st (3.14.1) (a), limma (3.48.1) (b) and arrayQualityMetrics (3.48.0) (c). Each CEL file was merged with a description file. In order to correct the background, and normalize and summarize results, we used the robust multiarray averaging (RMA) algorithm.

Statistical significance of the analyzed genes was assessed with moderated t-statistics using the empirical Bayes method. The obtained p-values were corrected for multiple comparisons using the Benjamini–Hochberg false discovery rate (1995). The selection of significantly changed gene expression was based on p-values <0.05, a false discovery ratio <20% and an expression fold change higher than 2.

Finally, interactions between differentially expressed genes and their protein products were investigated using STRING10 software (Search Tool for the Retrieval of Interacting Genes; https://string-db.org/).[25] The list of gene names was used as a query for an interaction prediction. The search criteria were based on the co-occurrences of genes/proteins in scientific texts (text mining), co-expression and experimentally observed interactions. The results of such analyses generated a gene/protein interaction network, where the intensity of the edges reflects the strength of the interaction score.

RT-qPCR

The reverse transcription (RT) was performed using the Transcriptor First Strand cDNA Synthesis Kit (Roche Diagnostics, Basel, Switzerland; cat. No. 04379012001). It was performed according to the manufacturer's protocol. The primers used for qPCR (Table 1) were designed by Primer 3 software v. 0.4.0 (Whitehead Institute for Biomedical Research, Cambridge, USA) and purchased from the Laboratory of DNA Sequencing and Oligonucleotide Synthesis, Institute of Biochemistry and Biophysics, Polish Academy of Sciences (Warszawa, Poland). The qPCR was performed using a CFX96 Deep Well Real-Time System (Bio-Rad, Hercules, USA).

Using the aforementioned primers, a SYBR Green detection system was applied, as described previously.[8,23,26–28] Every 20 µL of reaction mixture contained 2 µL template cDNA (standard or control), 0.5 µM specific primers and a previously determined optimum concentration of $MgCl_2$ (3.5 µM per reaction). LightCycler FastStart DNA Master SYBR-Green I mix (Roche Applied Science, Penzberg, Germany) was used. The qPCR program included a 10-min denaturation step at 95°C to activate the Taq DNA polymerase, followed by 45 cycles of a three-step amplification program: denaturation at 95°C for 10 s; annealing at 56°C for 5 s; and extension at 72°C for 10 s. The specificity of the reaction products was checked by determination of the melting points (0.1°C/s transition rate). The gene expression was normalized to the *HPRT* and *B2M* genes using the Pfaffl ratio method.[29]

Statistical analyses

Statistical analyses of the microarray experiments are described above. For the ELISA assay and qPCR analysis, we used the Kruskal–Wallis test with Dunnett's post hoc test for comparison of multiple experimental groups and the Wilcoxon test for comparison of 2 groups.

Table 1. The quantitative polymerase chain reaction (qPCR) starters sequences

Gene	Forward	Reverse	Accession	Product size
CCL2	ATGCAGTTAATGCCCCACTC	TTCCTTATTGGGGTCAGCAC	NM_031530.1	167
C3	TGCTTCATGCATCAGTCACA	TTTAGGGCGTTTCTGCACTT	NM_016994.2	233
Cp	CAGTTGCTCCAACGTTACCA	TTCCGACAAACAATCAATGG	NM_001270961.1	172
Sod2	AAGGAGCAAGGTCGCTTACA	GGGCTTCACTTCTTGCAAAC	NM_017051.2	215
Lcn2	TCACCCTGTACGGAAGAACC	CAGGTGATTCTCTGGCAACA	NM_130741.1	237
Tlr4	CCCTGGTGTTGGATTTTACG	TCGTTTCTCACCCAGTCCTC	NM_019178.1	223
Cd14	GGCTGGAGCACGTACCTAAA	GAGCAAAGCCAAAGTTCCTG	NM_021744.1	236
Pomc	CATGACGTACTTCCGGGGAT	TCACCACGGAAAGCAACCTG	XM_017594033	192
IL-6	TGATGGATGCTTCCAAACTG	GAGCATTGGAAGTTGGGGTA	NM_012589.2	230
Nampt	TGATCCCAACAAAAGGTCGAA	CCCACTCACACAAAAGCCTA	NM_177928	238
B2m	CTTGCAGAGTTAAACACGTCA	CTTGATTACATGTCTCGGTC	NM_012512.2	70
Hprt	ATAGAAATAGTGATAGGTCCA	TCTGCATTGTTTTACCAGT	XM_008773659	177

Results

AtT-20 cells

When planning our research, we intended to perform experiments on the AtT-20 cell line. However, for these cells, 24-h eNampt exposure at concentrations of 10^{-10} M to 10^{-7} M did not change the basal secretion of ACTH (Fig. 1). Similarly, 24-h exposure of AtT-20 cells to the iNampt inhibitor Fk866 did not affect the basal output of corticotrophin. It is interesting that the combined addition of Fk866 and CRH to the incubation medium reduced ACTH secretion by the examined cells (Fig. 2).

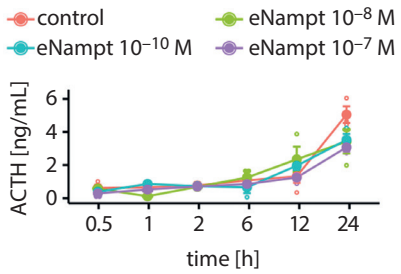

Fig. 1. The concentration of adrenocorticotropic hormone (ACTH) [pg/mL] in the incubation medium of cultured murine AtT-20 cells exposed to different concentrations of eNampt (10,000 cells/well). Each circle indicates an individual measurement. Data are presented as mean ± standard error of the mean (SEM)

Isolated rat corticotropes

Since the experiments with AtT-20 mouse cancer cells did not show any effect of eNampt on ACTH secretion, we decided to change the experimental model to use rat pituitary cells. In this case, we used 2 models: primary rat pituitary cell culture and isolated rat corticotropes. It appeared that eNampt, CRH and IL-6 stimulated ACTH output by cultured isolated rat corticotropes. Although eNampt stimulated IL-6 production in primary rat pituitary cell culture, no such effect was observed in cultured isolated rat corticotropes (Fig. 3).

Gene expression profiling using microarrays

In the 2nd series of experiments, we performed microarray analysis on isolated rat corticotropes cultured for 24 h in the presence of CRH, eNampt or IL-6. As shown in Fig. 4, under these conditions, the expression level of only a small number of genes was upregulated: CRH upregulated

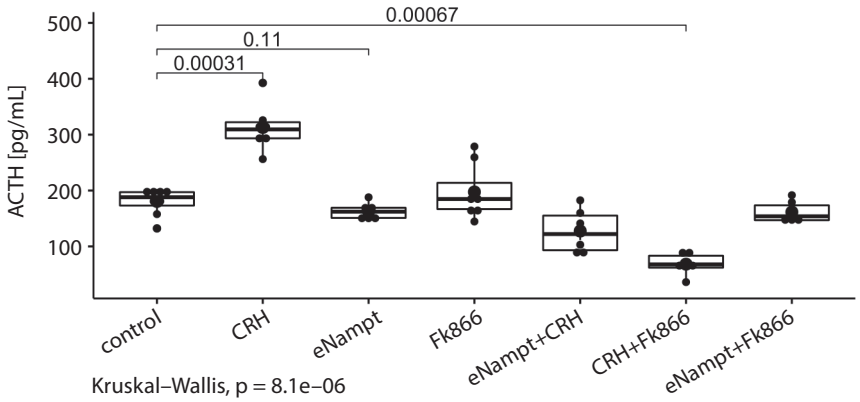

Fig. 2. The concentration of adrenocorticotropic hormone (ACTH) [pg/mL] in the incubation medium of cultured murine AtT-20 cells exposed for 24 h to corticotropin-releasing hormone (CRH), eNampt, Fk866, and their combinations. The figure shows the median and quartiles. Each symbol indicates an individual measurement (10,000 cells/well). Significant differences were observed between the control and CRH groups (p = 0.00031) as well as between the control and CRH+Fk866 groups (p = 0.00067). No significant differences between other experimental groups were observed

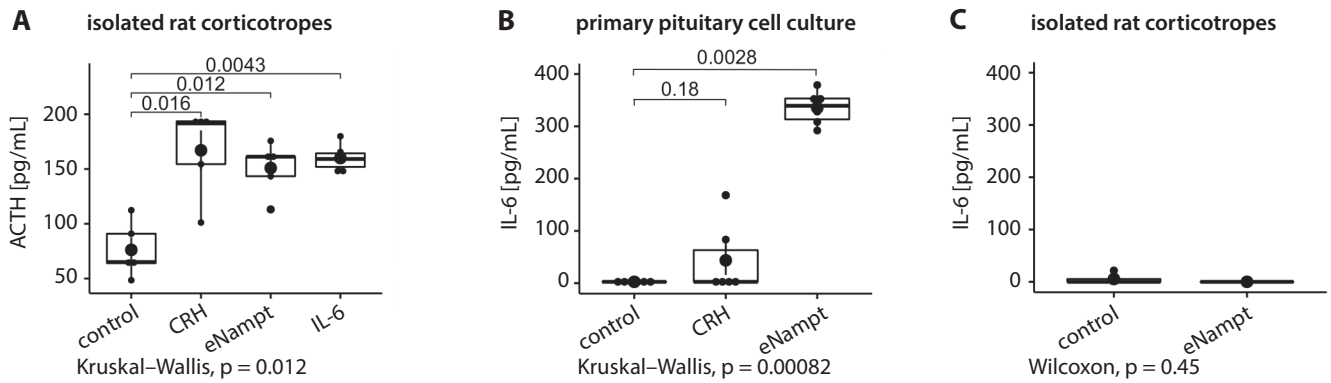

Fig. 3. The response of primary pituitary cell cultures to eNampt, CRH and IL-6. The data are presented as median and quartiles. A. All 3 studied compounds stimulated adrenocorticotropic hormone (ACTH) production of isolated rat corticotropes. Significant differences were observed between the control and corticotropin-releasing hormone (CRH) groups (p = 0.016); control and eNampt groups (p = 0.012); and control and IL-6 groups (p = 0.0043); B. eNampt stimulated IL-6 production in primary rat pituitary cell culture. A significant difference was observed between the control and eNampt groups (p = 0.0028). There was no significant difference between the control and CRH groups (p = 0.18); C. eNampt did not stimulate IL-6 secretion in isolated rat corticotropes culture (p = 0.45)

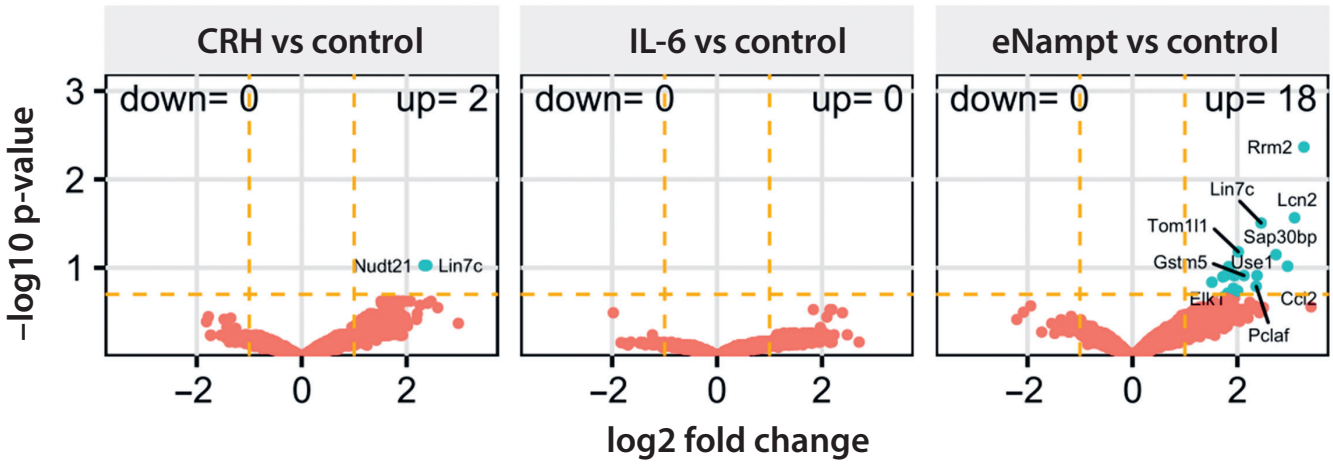

Fig. 4. Volcano plot. Each dot represents 1 gene. Genes with a fold ratio >2 and false discovery rate below 20% are marked in cyan. The names of the 10 most upregulated and downregulated genes are show in the figure

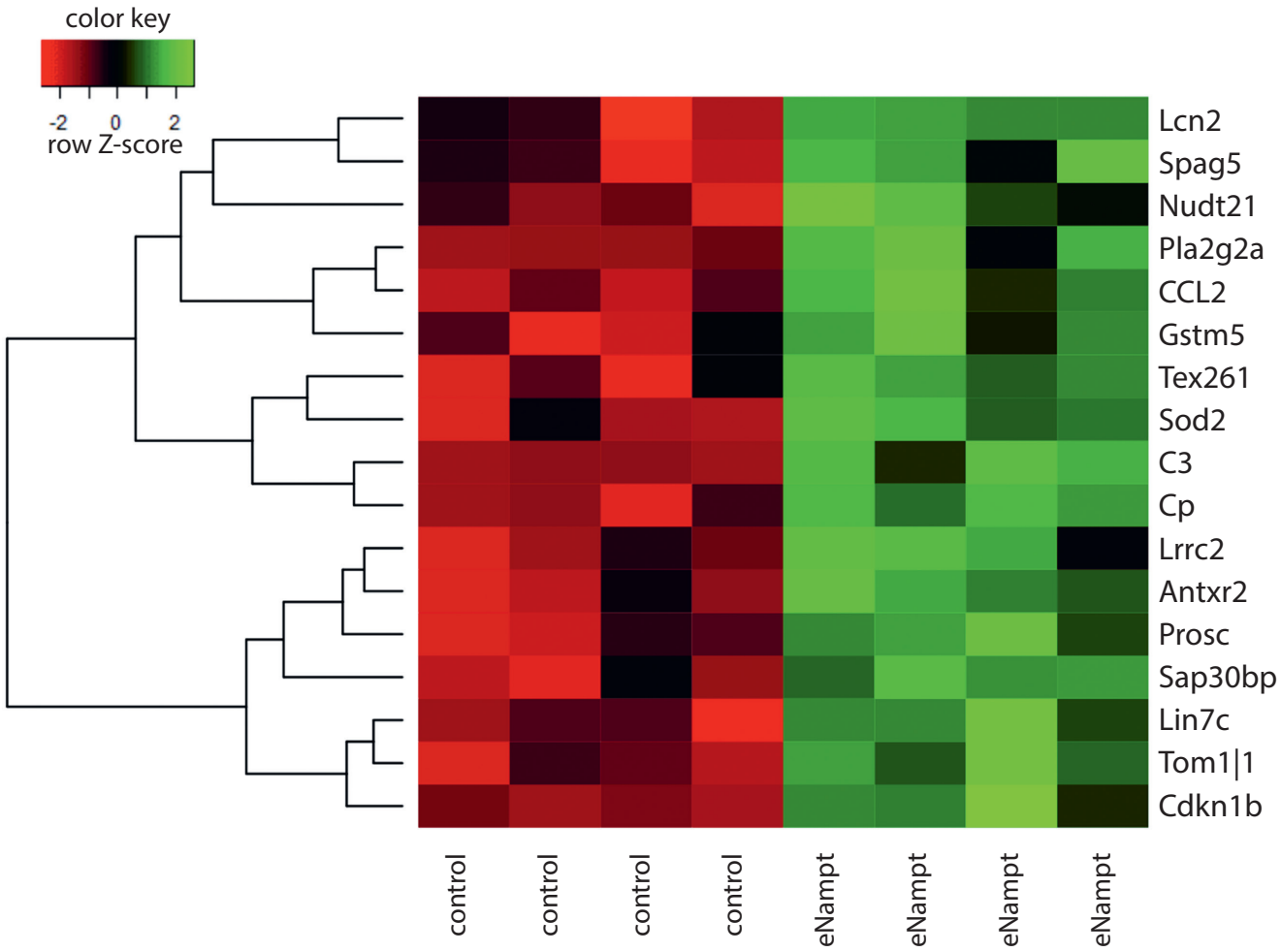

Fig. 5. Heatmap presenting the differences in gene expression between control and eNampt-treated isolated corticotropic cells. Gene expression is presented as a color gradient where red symbolizes the lowest expression level and green symbolizes the highest expression level. This gradient is presented separately for each gene. The histogram on the left shows the clusterization pattern. The genes with the most similar expression patterns are grouped together

2 genes, eNampt upregulated 18 genes and IL-6 did not affect the expression of any of the genes studied.

The results obtained for the microarray analysis were validated with the qPCR method. Only corticotropes treated with eNampt were subjected to these studies. The results of this analysis are presented as heatmap graphs. As Fig. 5 shows, the results of gene expression level determination with qPCR of isolated corticotropes

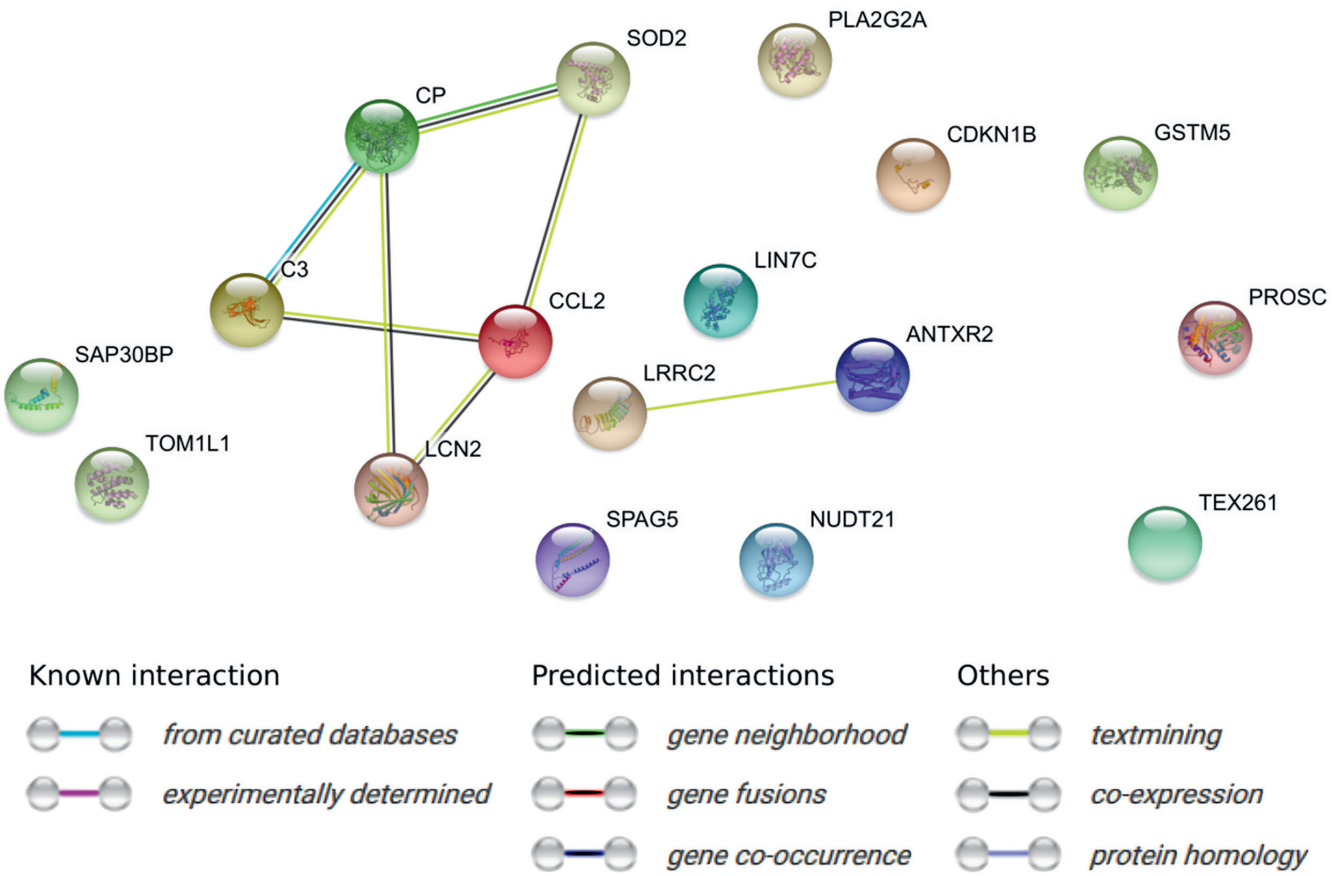

Fig. 6. STRING-generated interaction network with differently expressed genes of the eNampt-treated isolated corticotropes. The color of the edges reflects the type of interaction

cultured in the presence of eNampt are consistent with the results obtained using microarray analysis.

These genes were then subjected to analysis with STRING-db software via its browser API. The STRING-generated interaction network provides information about molecular interactions formed between the protein products of the studied genes (Fig. 6). The STRING analysis showed that genes such as *CCL2* (chemokine (C-C motif) ligand 2), *Sod2* (superoxide dismutase 2), *LCN2* (lipocalin-2), *C3* (complement component 3), and *CP* (ceruloplasmin) are functionally connected. They were mostly shown to be co-expressed. Most of these genes seem to be involved in inflammatory processes.

In the next stage of the study, we compared the expression levels of selected genes in primary rat pituitary cell culture, with those observed in cultured isolated rat corticotropes. Cultured cells were exposed for 24 h to CRH, eNampt or IL-6, and the expression levels of the studied genes were evaluated using qPCR. For these studies, we chose genes for which the level of expression changed significantly after exposure to eNampt. As presented in Fig. 7, in the primary rat pituitary cell culture, the influence of the investigated substances on the expression level of the studied genes was negligible. In both experimental models, eNampt did not change the expression level of the *Nampt* and *IL-6* genes. Similarly, no effect was observed for the genes *Cd14* (cluster of differentiation 14) and *Tlr4* (toll-like receptor 4) (results not shown). In contrast, in isolated corticotropes, eNampt increased the expression levels of the *Sod2*, *LCN2*, *CCL2,* and *C3* genes. In the employed experimental models, CRH increased the expression level of the *POMC* (proopiomelanocortin) gene only in isolated corticotropes, whereas exposure of the tested cells to IL-6 did not change the expression level of any of the studied genes (in both experimental models).

CCL2 protein secretion in vivo and in vitro

In our study, both the microarray and qPCR analysis data indicated that, under the applied experimental conditions and after cell exposure to eNampt, the *CCL2* gene expression level increased significantly. In this regard, the literature shows that CCL2 protein is secreted from human mammary epithelial cells after eNampt stimulation.[30,31] Moreover, CCL2 is secreted by pituitary neuroendocrine tumors.[21] Based on the literature data, we decided to investigate CCL2 protein secretion both in vivo and in vitro. As shown in Fig. 8, 60 min after the injection of eNampt, the level of CCL2 protein in rat blood serum increased significantly, while administration of CRH did not change the CCL2 protein level.

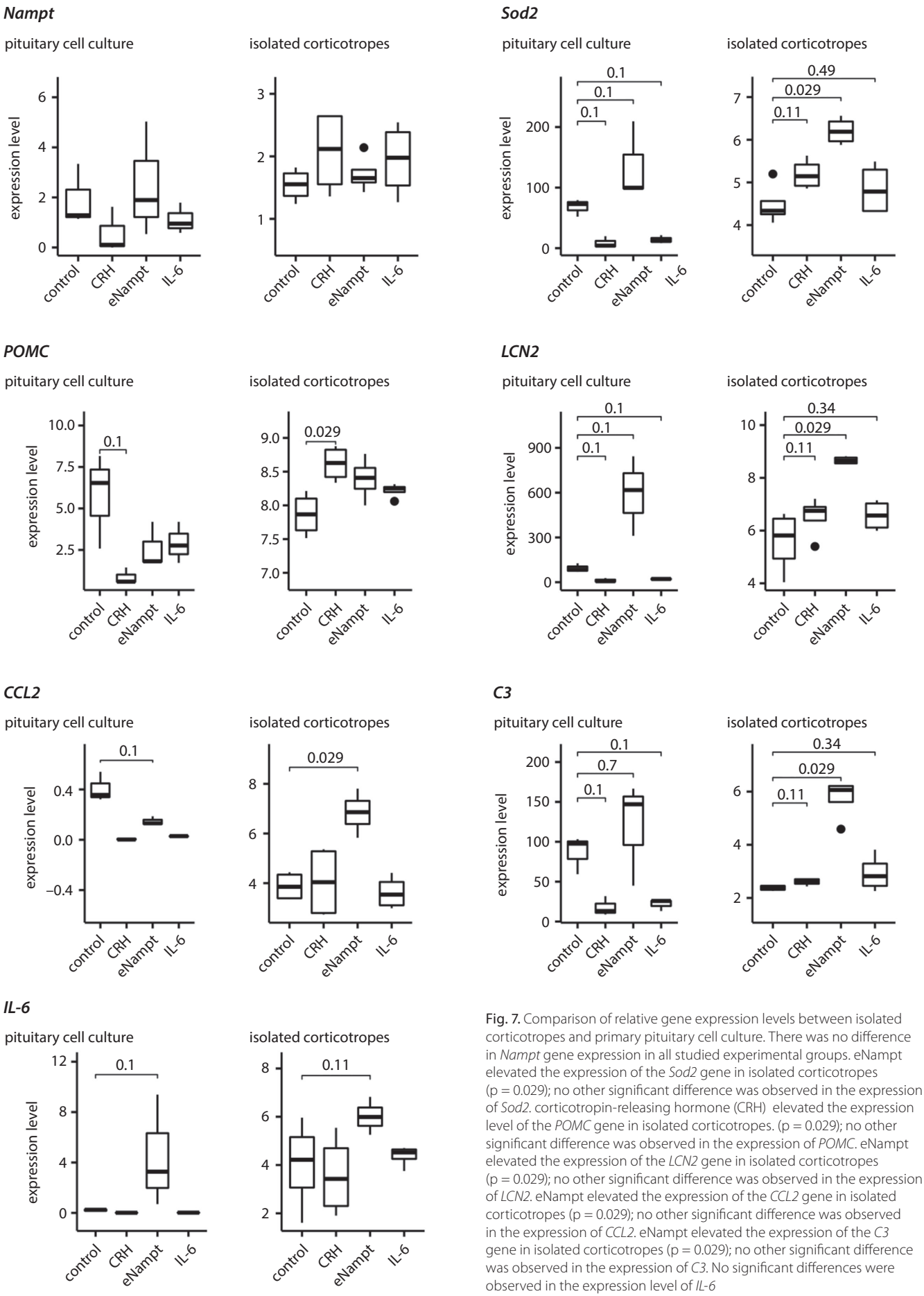

Fig. 7. Comparison of relative gene expression levels between isolated corticotropes and primary pituitary cell culture. There was no difference in *Nampt* gene expression in all studied experimental groups. eNampt elevated the expression of the *Sod2* gene in isolated corticotropes ($p = 0.029$); no other significant difference was observed in the expression of *Sod2*. corticotropin-releasing hormone (CRH) elevated the expression level of the *POMC* gene in isolated corticotropes. ($p = 0.029$); no other significant difference was observed in the expression of *POMC*. eNampt elevated the expression of the *LCN2* gene in isolated corticotropes ($p = 0.029$); no other significant difference was observed in the expression of *LCN2*. eNampt elevated the expression of the *CCL2* gene in isolated corticotropes ($p = 0.029$); no other significant difference was observed in the expression of *CCL2*. eNampt elevated the expression of the *C3* gene in isolated corticotropes ($p = 0.029$); no other significant difference was observed in the expression of *C3*. No significant differences were observed in the expression level of *IL-6*

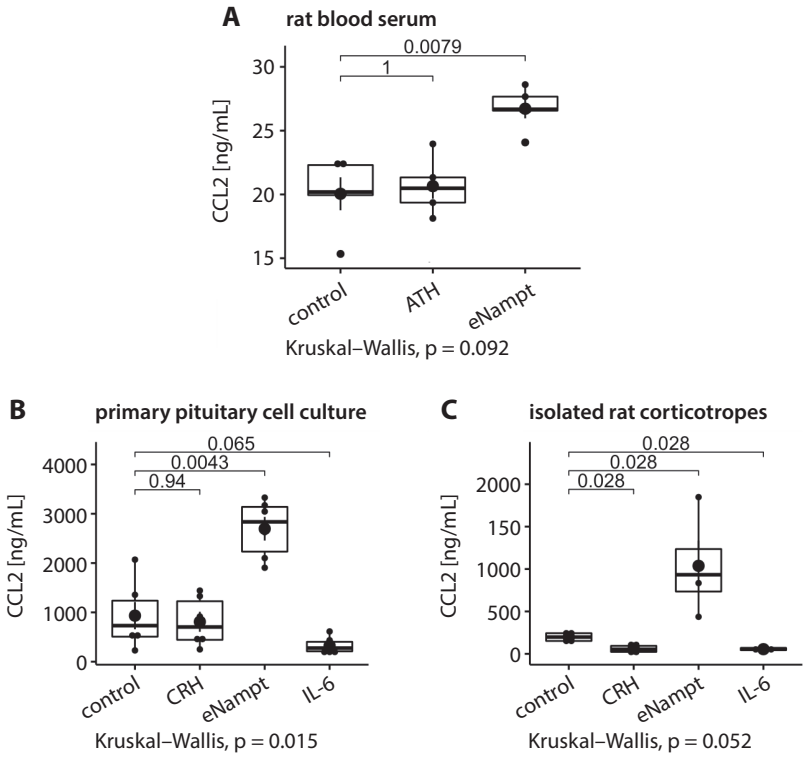

Fig. 8. CCL2 levels measured in rat blood serum, culture medium of primary pituitary cell culture and rat isolated corticotropes. A. Intraperitoneal administration of eNampt elevated CCL2 levels in rat serum (p = 0.0092); B. eNampt administration increased secretion of CCL2 in primary pituitary cell culture (p = 0.0043); C. CRH and IL-6 decreased secretion of CCL2 in isolated rat corticotropes (p = 0.028 and p = 0.028, respectively), while eNampt elevated secretion level by these cells (p = 0.028)

eNampt also increased the CCL2 protein concentration in the incubation medium of the primary pituitary cell culture and cultured isolated corticotropes. It is interesting that, in case of the isolated corticotrope culture, both CRH and IL-6 decreased the secretion of the analyzed protein.

Discussion

It is well known that ACTH secreted by corticotropic cells of the anterior pituitary lobe plays an essential role in the regulation of differentiation, growth, and function of the adrenal cortex. In turn, secretion of ACTH depends on the hypothalamic hormone CRH.[32–35]

As we showed in an earlier publication, one of the factors regulating pituitary secretion of ACTH is eNampt.[8] Our in vitro experiments showed that in the anterior pituitary lobe fragments, eNampt increases *POMC* gene expression and ACTH secretion into the incubation medium. However, the mechanism of eNampt action on pituitary ACTH cells is not known. Therefore, the aim of the present study was to explain the mechanism of action of eNampt on the secretory function of rat corticotropic cells.

Initially, we planned to perform the projected studies in the AtT-20 mouse pituitary tumor cell line, which secretes a huge amount of ACTH. However, under a wide range of eNampt concentrations, these cells did not change the level of secretion of ACTH in response to eNampt, nor did they react to CRH and Fk866 added to the medium. The lack of reaction of AtT-20 cells to the applied compounds forced us to use another experimental models. These experimental models included primary rat pituitary cell culture and cultured isolated rat corticotropes. In the primary rat pituitary cell culture, all of the cells of the anterior pituitary lobe are present, which likely retains the ability for possible functional interactions of all gland cells. Such interactions take place in the pituitary, and the pituitary folliculostellate cells play an essential role in this process.[9]

The classical pathway of HPA axis activation, i.e., via CRH secreted by the hypothalamus, is not the only pathway leading to ACTH secretion. ACTH might also be secreted after IL-6 stimulation, which is secreted by folliculostellate cells.[9,12,15–19,36] In this respect, it should be noted that eNampt also stimulates the secretion of IL-6 in isolated human leukocytes.[20] Moreover, *Nampt* gene expression positively correlates with serum levels of IL-6 and CRP.[37]

Based on these observations, we decided to check whether eNampt affects the secretion of ACTH by the paracrine route through IL-6 secreted by pituitary folliculostellate cells. To test this hypothesis, we isolated corticotropic cells from the primary pituitary cell culture and compared the effects of eNampt and IL-6 on ACTH secretion in both experimental systems. It appeared that both eNampt and IL-6 increased ACTH secretion by isolated rat corticotropes. It also appeared that eNampt increased the secretion of IL-6 in primary pituitary cell culture, but did not show such an effect in the case of isolated rat pituitary ACTH cells. These results suggest that eNampt may have an indirect effect (via IL-6) on ACTH secretion by isolated rat corticotropes. However, we have also shown that eNampt can directly stimulate corticotropin secretion from the examined cells. These observations suggest that

the stimulating effect of IL-6 on the secretion of ACTH by rat corticotropes may occur both directly and indirectly, mediated by the studied interleukin.

The lack of influence of eNampt on ACTH secretion in the case of the AtT-20 mouse pituitary tumor cell line is noteworthy, yet there was a clear stimulating effect on corticotropin secretion by isolated rat corticotropes. Differences in the effect of eNampt on normal and tumor cells were also observed in our previous studies.[38] In these studies, in primary culture, eNampt did not affect the rate of proliferation of rat adrenocortical cells, but it did stimulate proliferation of the H295R adrenocortical cancer cell line. It is difficult to explain the causes of the different effects of eNampt on normal and neoplastic cells.

It is well known that Nampt is a protein essential for the life of cells and organisms. For example, whole body deletion of the *Nampt* gene results in embryonic lethality, and muscle-specific Nampt deficient mice exhibit progressive muscle degeneration.[39,40] Moreover, retina-specific Nampt deficient mice exhibit severe vision loss.[41,42] In humans and mice, the level of eNampt in circulation decreases significantly with age. On the other hand, increasing the eNampt level in the blood of aged mice by adipose tissue-specific overexpression of Nampt increases NAD+ levels in multiple tissues, thereby enhancing their functions and extending the lifespan in female mice.[5] However, beyond its physiological function, Nampt has been indicated as one of the most important factors in cancer malignances.[43–45] Its expression was found to be higher in tumor cells than in normal cells.[43,46–55] It should be noted that eNampt serum concentrations in various types of cancer are usually elevated,[4,56–63] and at least part of the circulating protein is derived from the tumor itself.[64]

In this regard, it can be suggested that in the case of AtT-20 cells where the level of Nampt is most likely to be elevated (maximal stimulation), eNampt added to the culture may no longer increase ACTH secretion. The AtT-20 cell line is characterized by autonomous ACTH secretion; therefore, it might be difficult to further increase its ACTH secretion. Moreover, various factors, such as an inhibitor of the Jak2 signaling pathway (Lapatinib),[65] somatostatin analog (SOM230)[66] and DNA replication inhibitor (Aphidiloclin),[67] have been proven to decrease ACTH secretion of this cell line. It is also surprising and incomprehensible to note that Fk866 added to the AtT-20 cell culture also did not change ACTH secretion by these cells.

It is also worth mentioning that eNampt has been proven to promote stemness and dedifferentiation of cancer cells, which is critical for tumor initiation, progression, therapy resistance, and metastasis.[45,68–72] Moreover, previous studies strongly suggest that the effects of eNampt, as a cytokine, are independent of iNampt enzymatic activity.[45,70–73] Since eNampt has a strong and dedifferentiating effect on cancer cells, it is possible that the molecular mechanism of eNampt-induced secretion of ACTH was lost or altered in AtT-20. However, the reasons behind the observed differences between AtT-20 and primary corticotropes remain unknown and require further study.

In the next stage of the study, we attempted to explain the changes in gene expression levels that accompany the actions of CRH, eNampt and IL-6 on isolated rat corticotropes. We used microarray analysis for this purpose, which revealed changes in the expression level of only a few genes of the studied corticotropes, among which there were no Pomc and Nampt genes. It should be noted that, under the applied conditions, all examined substances increased ACTH secretion of isolated corticotropes. In our previous work,[8] we reported that 2 h of exposure to eNampt stimulated *POMC* and *Nampt* gene expression levels in isolated rat pituitary explants. It seems that after 24 h of culture, the expression levels of these genes were already normalized.

However, under these experimental conditions, 17 genes still showed elevated expression levels after administration of eNampt (24-h exposure). In further research, we focused on these genes. This group includes genes such as *CCL2* (chemokine (C-C motif) ligand 2), *Sod2* (superoxide dismutase 2), *LCN2* (lipocalin-2), *C3* (complement component 3), and *CP* (ceruloplasmin). This group of genes is functionally connected and the proteins they encode take part in the immune response. For example, CCL2 recruits monocytes, memory T cells, and dendritic cells to the sites of inflammation evoked by either tissue injury or infection.[74,75] Sod2 protein plays an antiapoptotic role against oxidative stress, ionizing radiation and inflammatory cytokines.[76] LCN2 is involved in innate immunity by sequestrating iron, thus limiting bacterial growth,[77] and C3 plays a central role in the complement system and contributes to innate immunity.

It should be noted that eNampt affects inflammatory processes and it is commonly recognized as a pro-inflammatory cytokine.[4,78–81] Therefore, among the genes that are controlled by eNampt in isolated corticotropes, the stimulation of *CCL2* gene expression seems interesting.

Previous data indicate that pituitary neuroendocrine tumors secrete numerous cytokines, including CCL2.[21] Since we observed an elevated *CCL2* gene expression level in isolated rat corticotropes after eNampt exposure, we decided to measured level of secreted CCL2 protein in the in vitro model as well as in rat serum from an in vivo experiment described earlier.[8] It appears that, in all cases (in vivo as well as in vitro), eNampt leads to an increase in CCL2 protein secretion. This observation indicates that part of the CCL2 protein found in rat serum originates from pituitary ACTH cells.

CCL2 is implicated in the pathogenesis of several diseases characterized by monocytic infiltrates, such as psoriasis, rheumatoid arthritis and atherosclerosis,[82] as well as various diseases of the central nervous system (CNS) characterized by neuronal degeneration.[83–89] Moreover, gene and protein expression of CCL2 is significantly

increased in the blood and tumors of renal cell carcinoma patients.[90] Some studies have indicated that CCL2 protein is also involved in regulating metabolism. CCL2 impairs insulin signaling in skeletal muscle cells and significantly reduces insulin-stimulated glucose uptake in myocytes.[91] In parallel, the CCL2 protein regulates liver and muscle metabolism and mitochondrial biogenesis, and participates directly or indirectly in the progression of obesity-related metabolic complications or aging.[92,93]

In light of these observations, it seems reasonable to suggest that stimulated eNampt secretion of CCL2 protein by isolated rat corticotropes is not only related to the regulation of immune response, but may also be related to the regulation of metabolism.[94] This is further suggested by the inhibition of CCL2 protein secretion by CRH, which we observed in isolated ACTH cells. It is well documented that the synthesis and secretion of CRH are regulated by various neuropeptides that regulate, among others, feeding and appetite, thus regulating metabolism.[95–100] Therefore, the results obtained suggest that crosstalk between CRH and CCL2 may be involved in regulating metabolism.

Limitations

A main limitation of this study is the lack of experiments involving isolated folliculostellate cells. The rat pituitary primary cell culture model used in the current study contained many different cell types derived from the pituitary gland. Therefore, it is possible that the observed eNampt-dependent stimulation of IL-6 secretion may occur via other cell types than folliculostellate cells. Unfortunately, to the best of our knowledge, folliculostellate cells do not possess any specific surface marker that would allow their isolation and thus the establishment of a specific cell culture model.

The results of our findings suggest that eNampt is involved in the stimulation of ACTH, IL-6 and CCL2 secretion, but do not clarify the molecular mechanism of eNampt action. Regarding IL-6 secretion, it is known that eNampt binds to the TLR4 receptor of human cell lines. It is also known that eNampt administration results in IL-6 secretion from human lymphocytes. In the present study, we did not examine whether a similar mechanism occurs in folliculostellate cells or primary corticotropes. This aspect requires further studies.

Conclusions

The results of this study suggest that eNampt stimulates ACTH secretion from rat corticotropes both directly and indirectly. Indirect action most likely occurs through IL-6 secreted by folliculostellate cells of the pituitary gland. In isolated ACTH cells of the rat pituitary gland, eNampt stimulates the expression of genes involved in the immune response. Among them, the protein encoded by the *CCL2* gene seems to also be involved in the regulation of CRH-dependent metabolism. Unlike rat corticotropes, murine AtT-20 corticotropic cells do not react to either eNampt or Fk866 (the inhibitor of Nampt enzymatic action).

ORCID iDs

Piotr Celichowski https://orcid.org/0000-0001-8211-7664
Karol Jopek https://orcid.org/0000-0002-7399-0303
Marta Szyszka https://orcid.org/0000-0003-0150-3665
Paulina Milecka https://orcid.org/0000-0002-1969-954X
Marianna Tyczewska https://orcid.org/0000-0003-0623-9496
Svetlana Sakhanova https://orcid.org/0000-0001-9786-6326
Witold Szaflarski https://orcid.org/0000-0001-5059-268X
Ludwik Malendowicz https://orcid.org/0000-0001-6155-8460
Marcin Ruciński https://orcid.org/0000-0002-2525-5777

References

1. Samal B, Sun Y, Stearns G, Xie C, Suggs S, McNiece I. Cloning and characterization of the cDNA encoding a novel human pre-B-cell colony-enhancing factor. *Mol Cell Biol*. 1994;14(2):1431–1437. doi:10.1128/mcb.14.2.1431-1437.1994
2. Araki T, Sasaki Y, Milbrandt J. Increased nuclear NAD biosynthesis and SIRT1 activation prevent axonal degeneration. *Science*. 2004;305(5686):1010–1013. doi:10.1126/science.1098014
3. Revollo JR, Grimm AA, Imai S. The NAD biosynthesis pathway mediated by nicotinamide phosphoribosyltransferase regulates Sir2 activity in mammalian cells. *J Biol Chem*. 2004;279(49):50754–50763. doi:10.1074/jbc.M408388200
4. Carbone F, Liberale L, Bonaventura A, et al. Regulation and function of extracellular nicotinamide phosphoribosyltransferase/visfatin. *Compr Physiol*. 2017;7(2):603–621. doi:10.1002/cphy.c160029
5. Yoshida M, Satoh A, Lin JB, et al. Extracellular vesicle-contained eNAMPT delays aging and extends lifespan in mice. *Cell Metabol*. 2019;30(2):329–342.e5. doi:10.1016/j.cmet.2019.05.015
6. Camp SM, Ceco E, Evenoski CL, et al. Unique Toll-like receptor 4 activation by NAMPT/PBEF induces NFkappaB signaling and inflammatory lung injury. *Sci Rep*. 2015;5:13135. doi:10.1038/srep13135
7. Torretta S, Colombo G, Travelli C, et al. The cytokine nicotinamide phosphoribosyltransferase (eNAMPT; PBEF; visfatin) acts as a natural antagonist of C-C chemokine receptor type 5 (CCR5). *Cells*. 2020;9(2). doi:10.3390/cells9020496
8. Celichowski P, Jopek K, Milecka P, et al. Nicotinamide phosphoribosyltransferase and the hypothalamic–pituitary–adrenal axis of the rat. *Mol Med Rep*. 2018;17(4):6163–6173. doi:10.3892/mmr.2018.8569
9. Denef C. Paracrinicity: The story of 30 years of cellular pituitary crosstalk. *J Neuroendocrinol*. 2008;20(1):1–70. doi:10.1111/j.1365-2826.2007.01616.x
10. Griffin JE, Ojeda SR. *Textbook of Endocrine Physiology*. 5th ed. Oxford, UK: Oxford University Press; 2004:431.
11. Keller-Wood M, Wood CE, McCartney J, Jesse NM, Perrone D. A role for mineralocorticoid receptors in the physiology of the ovine fetus: Effects on ACTH and lung liquid composition. *Pediatr Res*. 2011;69(6):491–496. doi:10.1203/PDR.0b013e318217f4cf
12. Beishuizen A, Thijs LG. Endotoxin and the hypothalamo–pituitary–adrenal (HPA) axis. *J Endotoxin Res*. 2003;9(1):3–24. doi:10.1179/096805103125001298
13. Bilezikjian LM, Leal AM, Blount AL, Corrigan AZ, Turnbull AV, Vale WW. Rat anterior pituitary folliculostellate cells are targets of interleukin-1beta and a major source of intrapituitary follistatin. *Endocrinology*. 2003;144(2):732–740. doi:10.1210/en.2002-220703
14. Lohrer P, Gloddek J, Nagashima AC, et al. Lipopolysaccharide directly stimulates the intrapituitary interleukin-6 production by folliculostellate cells via specific receptors and the p38alpha mitogen-activated protein kinase/nuclear factor-kappaB pathway. *Endocrinology*. 2000;141(12):4457–4465. doi:10.1210/endo.141.12.7811
15. Vankelecom H, Carmeliet P, Van Damme J, Billiau A, Denef C. Production of interleukin-6 by folliculo-stellate cells of the anterior pituitary gland in a histiotypic cell aggregate culture system. *Neuroendocrinology*. 1989;49(1):102–106. doi:10.1159/000125097

16. Vankelecom H, Matthys P, Van Damme J, Heremans H, Billiau A, Denef C. Immunocytochemical evidence that S-100-positive cells of the mouse anterior pituitary contain interleukin-6 immunoreactivity. *J Histochem Cytochem*. 1993;41(2):151–156. doi:10.1177/41.2.8419456
17. Turnbull AV, Smith GW, Lee S, Vale WW, Lee KF, Rivier C. CRF type I receptor-deficient mice exhibit a pronounced pituitary-adrenal response to local inflammation. *Endocrinology*. 1999;140(2):1013–1017. doi:10.1210/endo.140.2.6675
18. Silverman MN, Miller AH, Biron CA, Pearce BD. Characterization of an interleukin-6- and adrenocorticotropin-dependent, immune-to-adrenal pathway during viral infection. *Endocrinology*. 2004;145(8):3580–3589. doi:10.1210/en.2003-1421
19. Venihaki M, Dikkes P, Carrigan A, Karalis KP. Corticotropin-releasing hormone regulates IL-6 expression during inflammation. *J Clin Investig*. 2001;108(8):1159–1166. doi:10.1172/JCI12869
20. Moschen AR, Kaser A, Enrich B, et al. Visfatin, an adipocytokine with proinflammatory and immunomodulating properties. *J Immunol*. 2007;178(3):1748–1758. doi:10.4049/jimmunol.178.3.1748
21. Marques P, Barry S, Carlsen E, et al. Chemokines modulate the tumour microenvironment in pituitary neuroendocrine tumours. *Acta Neuropathol Commun*. 2019;7(1):172. doi:10.1186/s40478-019-0830-3
22. Szyszka M, Paschke L, Tyczewska M, et al. Analysis of transcriptome, selected intracellular signaling pathways, proliferation and apoptosis of LNCaP cells exposed to high leptin concentrations. *Int J Mol Sci*. 2019;20(21):5412. doi:10.3390/ijms20215412
23. Jopek K, Celichowski P, Szyszka M, et al. Transcriptome profile of rat adrenal evoked by gonadectomy and testosterone or estradiol replacement. *Front Endocrinol*. 2017;8:26. doi:10.3389/fendo.2017.00026
24. Jopek K, Tyczewska M, Ramanjaneya M, et al. Effect of ACTH and hCG on the expression of gonadotropin-inducible ovarian transcription factor 1 (Giot1) gene in the rat adrenal gland. *Int J Mol Sci*. 2018;19(8):2285. doi:10.3390/ijms19082285
25. von Mering C, Jensen LJ, Snel B, et al. STRING: Known and predicted protein-protein associations, integrated and transferred across organisms. *Nucleic Acids Res*. 2005;33(Database issue):D433–D437. doi:10.1093/nar/gki005
26. Tyczewska M, Rucinski M, Ziolkowska A, et al. Enucleation-induced rat adrenal gland regeneration: Expression profile of selected genes involved in control of adrenocortical cell proliferation. *Int J Endocrinol*. 2014;2014:130359. doi:10.1155/2014/130359
27. Rucinski M, Albertin G, Spinazzi R, Ziolkowska A, Nussdorfer GG, Malendowicz LK. Cerebellin in the rat adrenal gland: Gene expression and effects of CER and [des-Ser1]CER on the secretion and growth of cultured adrenocortical cells. *Int J Mol Med*. 2005;15(3):411–415. PMID:15702230
28. Rucinski M, Tortorella C, Ziolkowska A, Nowak M, Nussdorfer GG, Malendowicz LK. Steroidogenic acute regulatory protein gene expression, steroid-hormone secretion and proliferative activity of adrenocortical cells in the presence of proteasome inhibitors: In vivo studies on the regenerating rat adrenal cortex. *Int J Mol Med*. 2008;21(5):593–597. PMID:18425351
29. Pfaffl MW. A new mathematical model for relative quantification in real-time RT-PCR. *Nucleic Acids Res*. 2001;29(9):e45. doi:10.1093/nar/29.9.e45
30. Adya R, Tan BK, Chen J, Randeva HS. Pre-B cell colony enhancing factor (PBEF)/visfatin induces secretion of MCP-1 in human endothelial cells: Role in visfatin-induced angiogenesis. *Atherosclerosis*. 2009;205(1):113–119. doi:10.1016/j.atherosclerosis.2008.11.024
31. Bae YH, Bae MK, Kim SR, Lee JH, Wee HJ, Bae SK. Upregulation of fibroblast growth factor-2 by visfatin that promotes endothelial angiogenesis. *Biochem Biophys Res Commun*. 2009;379(2):206–211. doi:10.1016/j.bbrc.2008.12.042
32. Nussdorfer GG. Cytophysiology of the adrenal cortex. *Int Rev Cytol*. 1986;98:1–405. PMID:3512469
33. Gallo-Payet N, Martinez A, Lacroix A. ACTH action in the adrenal cortex: From molecular biology to pathophysiology. *Front Endocrinol*. 2017;8:101. doi:10.3389/fendo.2017.00101
34. Keller-Wood M. Hypothalamic–pituitary–adrenal axis: Feedback control. *Comprehensive Physiol*. 2015;5(3):1161–1182. doi:10.1002/cphy.c140065
35. Gallo-Payet N, Payet MD. Mechanism of action of ACTH: Beyond cAMP. *Microsc Res Tech*. 2003;61(3):275–287. doi:10.1002/jemt.10337
36. Givalois L, Dornand J, Mekaouche M, et al. Temporal cascade of plasma level surges in ACTH, corticosterone, and cytokines in endotoxin-challenged rats. *Am J Physiol*. 1994;267(1 Pt 2):R164–R170. doi:10.1152/ajpregu.1994.267.1.R164
37. Oki K, Yamane K, Kamei N, Nojima H, Kohno N. Circulating visfatin level is correlated with inflammation, but not with insulin resistance. *Clin Endocrinol*. 2007;67(5):796–800. doi:10.1111/j.1365-2265.2007.02966.x
38. Celichowski P, Jopek, K, Milecka, P, et al. Nampt (visfatin) influence on proliferative activity of normal rat adrenocortical cells and human adrenal corticocarcinoma NCI-H295R cells. *Med J Cell Biol*. 2018;6(2):33–38. doi:10.2478/acb-2018-0007
39. Revollo JR, Korner A, Mills KF, et al. Nampt/PBEF/visfatin regulates insulin secretion in beta cells as a systemic NAD biosynthetic enzyme. *Cell Metabol*. 2007;6(5):363–375. doi:10.1016/j.cmet.2007.09.003
40. Frederick DW, Loro E, Liu L, et al. Loss of NAD homeostasis leads to progressive and reversible degeneration of skeletal muscle. *Cell Metabol*. 2016;24(2):269–282. doi:10.1016/j.cmet.2016.07.005
41. Lin JB, Kubota S, Ban N, et al. NAMPT-mediated NAD(+) biosynthesis is essential for vision in mice. *Cell Rep*. 2016;17(1):69–85. doi:10.1016/j.celrep.2016.08.073
42. Yaku K, Okabe K, Nakagawa T. NAD metabolism: Implications in aging and longevity. *Ageing Res Rev*. 2018;47:1–17. doi:10.1016/j.arr.2018.05.006
43. Chen H, Wang S, Zhang H, Nice EC, Huang C. Nicotinamide phosphoribosyltransferase (Nampt) in carcinogenesis: New clinical opportunities. *Exp Rev Anticancer Ther*. 2016;16(8):827–838. doi:10.1080/14737140.2016.1190649
44. Nakajima N, Nobusawa S, Nakata S, et al. BRAF V600E, TERT promoter mutations and CDKN2A/B homozygous deletions are frequent in epithelioid glioblastomas: A histological and molecular analysis focusing on intratumoral heterogeneity. *Brain Pathol*. 2018;28(5):663–673. doi:10.1111/bpa.12572
45. Navas LE, Carnero A. NAD(+) metabolism, stemness, the immune response, and cancer. *Signal Transduct Target Ther*. 2021;6(1):2. doi:10.1038/s41392-020-00354-w
46. Shackelford RE, Mayhall K, Maxwell NM, Kandil E, Coppola D. Nicotinamide phosphoribosyltransferase in malignancy: A review. *Genes Cancer*. 2013;4(11–12):447–456. doi:10.1177/1947601913507576
47. Nergiz Avcioglu S, Altinkaya SO, Kucuk M, Yuksel H, Omurlu IK, Yanik S. Visfatin concentrations in patients with endometrial cancer. *Gynecol Endocrinol*. 2015;31(3):202–207. doi:10.3109/09513590.2014.975687
48. Zhao Y, Hu Q, Cheng F, et al. SoNar, a highly responsive NAD+/NADH sensor, allows high-throughput metabolic screening of anti-tumor agents. *Cell Metabol*. 2015;21(5):777–789. doi:10.1016/j.cmet.2015.04.009
49. Bi TQ, Che XM. Nampt/PBEF/visfatin and cancer. *Cancer Biol Ther*. 2010;10(2):119–125. doi:10.4161/cbt.10.2.12581
50. Shackelford RE, Bui MM, Coppola D, Hakam A. Over-expression of nicotinamide phosphoribosyltransferase in ovarian cancers. *Int J Clin Exp Pathol*. 2010;3(5):522–527.
51. Buldak RJ, Buldak L, Polaniak R, et al. Visfatin affects redox adaptative responses and proliferation in Me45 human malignant melanoma cells: An in vitro study. *Oncol Rep*. 2013;29(2):771–778. doi:10.3892/or.2012.2175
52. Olesen UH, Petersen JG, Garten A, et al. Target enzyme mutations are the molecular basis for resistance towards pharmacological inhibition of nicotinamide phosphoribosyltransferase. *BMC Cancer*. 2010;10:677. doi:10.1186/1471-2407-10-677
53. Guo J, Lam LT, Longenecker KL, et al. Identification of novel resistance mechanisms to NAMPT inhibition via the de novo NAD(+) biosynthesis pathway and NAMPT mutation. *Biochem Biophys Res Commun*. 2017;491(3):681–686. doi:10.1016/j.bbrc.2017.07.143
54. Sawicka-Gutaj N, Waligorska-Stachura J, Andrusiewicz M, et al. Nicotinamide phosphorybosiltransferase overexpression in thyroid malignancies and its correlation with tumor stage and with survivin/survivin DEx3 expression. *Tumour Biol*. 2015;36(10):7859–7863. doi:10.1007/s13277-015-3506-z
55. Zhang H, Zhang N, Liu Y, et al. Epigenetic regulation of NAMPT by NAMPT-AS drives metastatic progression in triple-negative breast cancer. *Cancer Res*. 2019;79(13):3347–3359. doi:10.1158/0008-5472.CAN-18-3418

56. Garten A, Schuster S, Penke M, Gorski T, de Giorgis T, Kiess W. Physiological and pathophysiological roles of NAMPT and NAD metabolism. *Nat Rev Endocrinol*. 2015;11(9):535–546. doi:10.1038/nrendo.2015.117
57. Wang G, Tian W, Liu Y, et al. Visfatin triggers the cell motility of non-small cell lung cancer via up-regulation of matrix metalloproteinases. *Basic Clin Pharmacol Toxicol*. 2016;119(6):548–554. doi:10.1111/bcpt.12623
58. Fazeli MS, Dashti H, Akbarzadeh S, et al. Circulating levels of novel adipocytokines in patients with colorectal cancer. *Cytokine*. 2013;62(1):81–85. doi:10.1016/j.cyto.2013.02.012
59. Nakajima TE, Yamada Y, Hamano T, et al. Adipocytokine levels in gastric cancer patients: Resistin and visfatin as biomarkers of gastric cancer. *J Gastroenterol*. 2009;44(7):685–690. doi:10.1007/s00535-009-0063-5
60. Tsai YD, Wang CP, Chen CY, et al. Elevated plasma level of visfatin/pre-b cell colony-enhancing factor in male oral squamous cell carcinoma patients. *Med Oral Patol Oral Cir Bucal*. 2013;18(2):e180–e186. doi:10.4317/medoral.18574
61. Reddy PS, Umesh S, Thota B, et al. PBEF1/NAmPRTase/visfatin: A potential malignant astrocytoma/glioblastoma serum marker with prognostic value. *Cancer Biol Ther*. 2008;7(5):663–668. doi:10.4161/cbt.7.5.5663
62. Soncini D, Caffa I, Zoppoli G, et al. Nicotinamide phosphoribosyltransferase promotes epithelial-to-mesenchymal transition as a soluble factor independent of its enzymatic activity. *J Biol Chem*. 2014;289(49):34189–34204. doi:10.1074/jbc.M114.594721
63. Tian W, Zhu Y, Wang Y, et al. Visfatin, a potential biomarker and prognostic factor for endometrial cancer. *Gynecol Oncol*. 2013;129(3):505–512. doi:10.1016/j.ygyno.2013.02.022
64. Grolla AA, Torretta S, Gnemmi I, et al. Nicotinamide phosphoribosyltransferase (NAMPT/PBEF/visfatin) is a tumoural cytokine released from melanoma. *Pigment Cell Melanoma Res*. 2015;28(6):718–729. doi:10.1111/pcmr.12420
65. Asari Y, Kageyama K, Nakada Y, et al. Inhibitory effects of a selective Jak2 inhibitor on adrenocorticotropic hormone production and proliferation of corticotroph tumor AtT20 cells. *Oncotargets Ther*. 2017;10:4329–4338. doi:10.2147/OTT.S141345
66. Murasawa S, Kageyama K, Sugiyama A, et al. Inhibitory effects of SOM230 on adrenocorticotropic hormone production and corticotroph tumor cell proliferation in vitro and in vivo. *Mol Cell Endocrinol*. 014;394(1–2):37–46. doi:10.1016/j.mce.2014.07.001
67. Kageyama K, Sugiyama A, Murasawa S, et al. Aphidicolin inhibits cell proliferation via the p53-GADD45beta pathway in AtT-20 cells. *Endocrine J*. 2015;62(7):645–654. doi:10.1507/endocrj.EJ15-0084
68. Carnero A, Garcia-Mayea Y, Mir C, Lorente J, Rubio IT, Me LL. The cancer stem-cell signaling network and resistance to therapy. *Cancer Treatment Rev*. 2016;49:25–36. doi:10.1016/j.ctrv.2016.07.001
69. Carnero A, Lleonart M. The hypoxic microenvironment: A determinant of cancer stem cell evolution. *Bioessays*. 2016;38(Suppl 1):S65–S74. doi:10.1002/bies.201670911
70. Lucena-Cacace A, Otero-Albiol D, Jimenez-Garcia MP, Munoz-Galvan S, Carnero A. NAMPT is a potent oncogene in colon cancer progression that modulates cancer stem cell properties and resistance to therapy through Sirt1 and PARP. *Clin Cancer Res*. 2018;24(5):1202–1215. doi:10.1158/1078-0432.CCR-17-2575
71. Lucena-Cacace A, Otero-Albiol D, Jimenez-Garcia MP, Peinado-Serrano J, Carnero A. NAMPT overexpression induces cancer stemness and defines a novel tumor signature for glioma prognosis. *Oncotarget*. 2017;8(59):99514–99530. doi:10.18632/oncotarget.20577
72. Lucena-Cacace A, Umeda M, Navas LE, Carnero A. NAMPT as a dedifferentiation-inducer gene: NAD(+) as core axis for glioma cancer stem-like cells maintenance. *Front Oncol*. 2019;9:292. doi:10.3389/fonc.2019.00292
73. Li Y, Zhang Y, Dorweiler B, et al. Extracellular Nampt promotes macrophage survival via a nonenzymatic interleukin-6/STAT3 signaling mechanism. *J Biol Chem*. 2008;283(50):34833–34843. doi:10.1074/jbc.M805866200
74. Carr MW, Roth SJ, Luther E, Rose SS, Springer TA. Monocyte chemoattractant protein 1 acts as a T-lymphocyte chemoattractant. *Proc Natl Acad Sci U S A*. 1994;91(9):3652–3656. doi:10.1073/pnas.91.9.3652
75. Xu LL, Warren MK, Rose WL, Gong W, Wang JM. Human recombinant monocyte chemotactic protein and other C-C chemokines bind and induce directional migration of dendritic cells in vitro. *J Leukocyte Biol*. 1996;60(3):365–371. doi:10.1002/jlb.60.3.365
76. Becuwe P, Ennen M, Klotz R, Barbieux C, Grandemange S. Manganese superoxide dismutase in breast cancer: From molecular mechanisms of gene regulation to biological and clinical significance. *Free Radic Biol Med*. 2014;77:139–151. doi:10.1016/j.freeradbiomed.2014.08.026
77. Yang J, Goetz D, Li JY, et al. An iron delivery pathway mediated by a lipocalin. *Mol Cell*. 2002;10(5):1045–1056. doi:10.1016/s1097-2765(02)00710-4
78. Chyl-Surdacka KM, Bartosinska J, Kowal M, Przepiorka-Kosinska J, Krasowska D, Chodorowska G. Assessment of visfatin concentrations in the serum of male psoriatic patients in relation to metabolic abnormalities. *Adv Clin Exp Med*. 2020;29(1):79–84. doi:10.17219/acem/111820
79. Al-Suhaimi EA, Shehzad A. Leptin, resistin and visfatin: The missing link between endocrine metabolic disorders and immunity. *Eur J Med Res*. 2013;18:12. doi:10.1186/2047-783X-18-12
80. Hognogi LD, Simiti LV. The cardiovascular impact of visfatin: An inflammation predictor biomarker in metabolic syndrome. *Clujul Med*. 2016;89(3):322–326. doi:10.15386/cjmed-591
81. Martinez-Morcillo FJ, Canton-Sandoval J, Martinez-Menchon T, et al. Non-canonical roles of NAMPT and PARP in inflammation. *Dev Comp Immunol*. 2020;2021:103881. doi:10.1016/j.dci.2020.103881
82. Xia M, Sui Z. Recent developments in CCR2 antagonists. *Exp Opin Ther Pat*. 2009;19(3):295–303. doi:10.1517/13543770902755129
83. Gerard C, Rollins BJ. Chemokines and disease. *Nat Immunol*. 2001;2(2):108–115. doi:10.1038/84209
84. Foresti ML, Arisi GM, Katki K, Montanez A, Sanchez RM, Shapiro LA. Chemokine CCL2 and its receptor CCR2 are increased in the hippocampus following pilocarpine-induced status epilepticus. *J Neuroinflamm*. 2009;6:40. doi:10.1186/1742-2094-6-40
85. Fabene PF, Bramanti P, Constantin G. The emerging role for chemokines in epilepsy. *J Neuroimmunol*. 2010;224(1–2):22–27. doi:10.1016/j.jneuroim.2010.05.016
86. Kim JS, Gautam SC, Chopp M, et al. Expression of monocyte chemoattractant protein-1 and macrophage inflammatory protein-1 after focal cerebral ischemia in the rat. *J Neuroimmunol*. 1995;56(2):127–134. doi:10.1016/0165-5728(94)00138-e
87. Hickman SE, El Khoury J. Mechanisms of mononuclear phagocyte recruitment in Alzheimer's disease. *CNS Neurol Dis Drug Targets*. 2010;9(2):168–173. doi:10.2174/187152710791011982
88. Ransohoff RM, Hamilton TA, Tani M, et al. Astrocyte expression of mRNA encoding cytokines IP-10 and JE/MCP-1 in experimental autoimmune encephalomyelitis. *FASEB J*. 1993;7(6):592–600. doi:10.1096/fasebj.7.6.8472896
89. Semple BD, Bye N, Rancan M, Ziebell JM, Morganti-Kossmann MC. Role of CCL2 (MCP-1) in traumatic brain injury (TBI): Evidence from severe TBI patients and CCL2−/− mice. *J Cereb Blood Flow Metabol*. 2010;30(4):769–782. doi:10.1038/jcbfm.2009.262
90. Guan X, Liu Z, Zhang J, Jin X. Myeloid-derived suppressor cell accumulation in renal cell carcinoma is correlated with CCL2, IL-17 and IL-18 expression in blood and tumors. *Adv Clin Exp Med*. 2018;27(7):947–953. doi:10.17219/acem/70065
91. Sell H, Dietze-Schroeder D, Kaiser U, Eckel J. Monocyte chemotactic protein-1 is a potential player in the negative cross-talk between adipose tissue and skeletal muscle. *Endocrinology*. 2006;147(5):2458–2467. doi:10.1210/en.2005-0969
92. Luciano-Mateo F, Cabre N, Fernandez-Arroyo S, et al. Chemokine C-C motif ligand 2 overexpression drives tissue-specific metabolic responses in the liver and muscle of mice. *Sci Rep*. 2020;10(1):11954. doi:10.1038/s41598-020-68769-7
93. Ishii M, Araki S, Goto M, Yamamoto Y, Kusuhara K. CCL2 level is elevated with metabolic syndrome and CXCL10 level is correlated with visceral fat area in obese children. *Endocrine J*. 2016;63(9):795–804. doi:10.1507/endocrj.EJ15-0731
94. Le Thuc O, Cansell C, Bourourou M, et al. Central CCL2 signaling onto MCH neurons mediates metabolic and behavioral adaptation to inflammation. *EMBO Rep*. 2016;17(12):1738–1752. doi:10.15252/embr.201541499
95. Kalra SP, Dube MG, Pu S, Xu B, Horvath TL, Kalra PS. Interacting appetite-regulating pathways in the hypothalamic regulation of body weight. *Endocrine Rev*. 1999;20(1):68–100. doi:10.1210/edrv.20.1.0357
96. Hillebrand JJ, de Wied D, Adan RA. Neuropeptides, food intake and body weight regulation: A hypothalamic focus. *Peptides*. 2002;23(12):2283–2306. doi:10.1016/s0196-9781(02)00269-3

97. Leibowitz SF, Wortley KE. Hypothalamic control of energy balance: Different peptides, different functions. *Peptides*. 2004;25(3):473–504. doi:10.1016/j.peptides.2004.02.006
98. Bloom S. Hormonal regulation of appetite. *Obesity Rev*. 2007;8(Suppl 1): 63–65. doi:10.1111/j.1467-789X.2007.00320.x
99. Schulz C, Paulus K, Lobmann R, Dallman M, Lehnert H. Endogenous ACTH, not only alpha-melanocyte-stimulating hormone, reduces food intake mediated by hypothalamic mechanisms. *Am J Physiol Endocrinol Metabol*. 2010;298(2):E237–E244. doi:10.1152/ajpendo.00408.2009
100. Wortley KE, Chang GQ, Davydova Z, Fried SK, Leibowitz SF. Cocaine- and amphetamine-regulated transcript in the arcuate nucleus stimulates lipid metabolism to control body fat accrual on a high-fat diet. *Regul Pept*. 2004;117(2):89–99. doi:10.1016/j.regpep.2003.08.005

Research letter

What factors affect the length of hospitalization in patients with erysipelas? A 10-year retrospective study of patients hospitalized in Lower Silesia, Poland

Magdalena Łyko[1,B–D], Mateusz Kaczmarek[1,B,D], Polina Nekrasova[1,B,D], Anita Hryncewicz-Gwóźdź[2,E], Joanna Maj[2,E], Alina Jankowska-Konsur[2,A,C,D,F]

[1] Student Research Group of Experimental Dermatology, Department of Dermatology, Venereology and Allergology, Wroclaw Medical University, Poland
[2] Department of Dermatology, Venereology and Allergology, Wroclaw Medical University, Poland

A – research concept and design; B – collection and/or assembly of data; C – data analysis and interpretation; D – writing the article; E – critical revision of the article; F – final approval of the article

Advances in Clinical and Experimental Medicine, ISSN 1899–5276 (print), ISSN 2451–2680 (online) *Adv Clin Exp Med*. 2021;30(9):981–985

Address for correspondence
Anita Hryncewicz-Gwóźdź
E-mail: anhryn@gmail.com

Funding sources
None declared

Conflict of interest
None declared

Received on November 9, 2020
Reviewed on November 16, 2020
Accepted on May 10, 2021

Published online on August 18, 2021

Cite as
Łyko M, Kaczmarek M, Nekrasova P, Hryncewicz-Gwóźdź A, Maj J, Jankowska-Konsur A. What factors affect the length of hospitalization in patients with erysipelas? A 10-year retrospective study of patients hospitalized in Lower Silesia, Poland. *Adv Clin Exp Med*. 2021;30(9):981–985. doi:10.17219/acem/136504

DOI
10.17219/acem/136504

Abstract

Background. Erysipelas is an acute skin infection caused by group A and G streptococci. This infection is associated with many comorbidities and often requires hospitalization.

Objectives. The aim of this study was to identify the factors related to the length of hospitalization in patients with erysipelas.

Materials and methods. This retrospective study included 153 admissions of 135 patients (63 women and 72 men) hospitalized due to erysipelas from January 2010 to December 2019. Clinical symptoms, test results, comorbidities, and antibiotic treatments were taken into consideration as factors affecting the length of hospital stay.

Results. The median length of hospitalization was 10 days (interquartile range (IQR) = 7–14). Women spent less time in the ward, but the difference was not significant. Features such as tinea pedis (15.5 days, IQR = 13.5–20; $p = 0.002$), anemia (11 days, IQR = 9–15; $p = 0.02$), chills (12 days, IQR = 9–15; $p = 0.03$), elevated serum C-reactive protein (CRP) level over 100 mg/L (11 days, IQR = 8–17; $p = 0.02$), and leukocytosis (11 days, IQR = 8–15, $p = 0.005$) were identified as prolonged hospitalization factors. Moreover, patients with erysipelas localized to the legs ($p = 0.01$) and with a gangrenous variant of erysipelas ($p = 0.03$) were hospitalized longer. The first-choice antibiotic was not significant in terms of prolonged hospitalization. Patients treated with clindamycin during hospitalization, regardless of whether it was a first-line or subsequent antibiotic, stayed in the ward significantly longer ($p = 0.005$).

Conclusions. Patients suffering from erysipelas with the features identified above, have a higher risk of a prolonged stay in the hospital. Significantly increased inflammatory factors, anemia and tinea pedis contributed to prolonged hospitalization.

Key words: therapy, hospitalization, antibiotics, erysipelas, clindamycin

Background

Erysipelas is an acute infection of the dermis and the subcutaneous tissues, most commonly localized to the lower limbs and the face.[1–3] This infection mainly affects adults and older people, has a repetitive nature, and is associated with certain comorbidities, including tinea pedis and diabetes.[1–4] The acute infection is primarily caused by group A (*Streptococcus pyogenes*) and group G β-hemolytic streptococci.[1–7] Diagnosis is usually made based on clinical features including local erythema with a clearly demarcated margin that is associated with pain and edema, as well as general symptoms (fever, chills, nausea, and malaise).[1–4,7–9] Guidelines for the management of skin and soft tissue infections are typically based on expert opinion and pathophysiological considerations. However, antibiotic therapy for erysipelas is most often empirical and depends on the clinical experience of the treating physician.[10–13] Erysipelas is a common cause of hospitalization, including prolonged and repetitive hospitalizations that generate high costs for the healthcare system.

Objectives

This study aimed to identify the factors affecting the length of hospitalization in patients admitted to the dermatology department due to erysipelas.

Materials and methods

Study design

The study was based on an analysis of clinical data from patients hospitalized due to erysipelas in the department of dermatology. Patients admitted for erysipelas treatment from January 2010 to December 2019 were enrolled in the study. Data analyses included identified risk factors for erysipelas development, inflammatory parameters measured upon admission to the hospital (C-reactive protein (CRP), procalcitonin, erythrocyte sedimentation rate (ESR), leukocytosis), the results of microbiological swabs, and applied antibiotic treatments. The obtained data were compared in order to examine their impact on the length of hospitalization (Table 1).

Setting and participants

The study was conducted in the Department of Dermatology, Venereology and Allergology at Wroclaw Medical University. Patients admitted for erysipelas treatment during the period of time from January 1, 2010 to December 31, 2019 were identified in the hospital electronic database using the International Classification of Diseases, 10th revision (ICD-10) code A46 (erysipelas). In the analyzed period, 153 hospitalizations were identified. This corresponded to 135 patients (63 women and 72 men, mean age 61.2 ±16.8 years) who were included in the study. The number of admissions exceeded the number of patients due to repeated hospitalizations of patients with relapses. The demographics and clinical characteristics of the study population are summarized in Table 1.

Statistical analyses

Statistical analyses were performed using STATISTICA v. 13 software (StatSoft Inc., Tulsa, USA). The quantitative variables were described using median, range, interquartile range (IQR), and means ± standard deviations (SD). The relationships between the length of hospitalization and the factors were examined using the Mann–Whitney U test. To compare more than 2 groups the Kruskal–Wallis one-way analysis of variance (ANOVA) was used. Values of $p < 0.05$ were considered statistically significant.

Results

The median length of hospitalization was 10 (IQR = 7–14) days. Regarding sex, the median length of hospitalization in women was slightly shorter than in men, but the difference was not significant (9 days, IQR = 7–14 compared to 10 days, IQR = 7–14, respectively; $p > 0.05$). Neither age nor the number of episodes were associated with prolonged stay in the hospital.

Patients suffering from tinea pedis stayed in the hospital significantly longer than those without this condition (15.5 days, IQR = 13.5–20 compared to 9 days, IQR = 7–14, respectively; $p = 0.002$). In addition, anemia was associated with prolonged hospitalization ($p = 0.03$; Table 2). Diabetes mellitus, venous insufficiency, cardiac diseases, hypercholesterolemia, malignancy, and post-lymphadenectomy status did not influence the length of the hospitalization (Table 2).

Chills at the time of admission were associated with significantly longer hospitalization ($p = 0.02$). Moreover, patients with lymphadenopathy stayed in the hospital longer than those without lymphadenopathy, but the difference did not reach statistical significance (17 days compared to 9.5 days, respectively; $p = 0.06$; Table 2).

The hospitalization duration varied with the clinical subtype of erysipelas ($p = 0.009$). The post hoc tests revealed that patients with a gangrenous variant of erysipelas stayed in the hospital significantly longer than patients with an erythematous subtype ($p = 0.03$; Table 2). Furthermore, patients with disease localized to the lower extremities were hospitalized significantly longer than patients with erysipelas on other parts of the body ($p = 0.01$; Table 2).

During hospitalization, a cutaneous swab was taken from 16 patients. A positive culture result was associated

Table 1. Demographic and clinical characteristics of the patients

Variable	Number of patients (%)
Sex	
Female	63 (46.7%)
Male	72 (53.3%)
Age	
<20 years	1 (0.7%)
21–30 years	5 (3.7%)
31–40 years	12 (8.9%)
41–50 years	15 (11.1%)
51–60 years	32 (23.7%)
61–70 years	31 (23.0%)
71–80 years	24 (17.8%)
>80 years	15 (11.1%)
Localization of erysipelas	
Face	16 (10.5%)
Upper extremity	3 (2.0%)
Trunk	9 (5.9%)
Lower extremity	121 (79.1%)
More than 1 part of the body	4 (2.6%)
Subtype	
Erythematous	108 (70.6%)
Bullous	26 (17.0%)
Hemorrhagic	8 (5.2%)
Gangrenous	3 (2.0%)
Bullo-hemorrhagic	8 (5.2%)
General symptoms	
Fever	100 (65.4%)
Chills	32 (20.9%)
Weakness	42 (27.5%)
Nausea	9 (5.9%)
Lymphadenopathy	11 (7.2%)
Comorbidities	
Tinea pedis	8 (5.2%)
Diabetes mellitus	40 (26.1%)
Hypertension	79 (51.6%)
Hypercholesterolemia	19 (12.4%)
Chronic venous insufficiency of lower legs	30 (19.6%)
Anemia	54 (35.3%)
Cardiac disease	50 (32.7%)
Malignancy	22 (14.4%)
Post-lymphadenectomy status	10 (6.5%)
Chronic renal disease	14 (9.2%)
Obesity	19 (12.4%)
Antibiotic therapy before admission	
Yes	67 (43.8%)
No	86 (56.2%)

Table 2. Length of hospitalization according to different variables. Localization in the lower extremities, erysipelas gangrenous, the presence of chills, tinea pedis, anemia, positive swab culture, elevated CRP, and leukocytosis were determined as factors associated with prolonged hospitalization

Variable	The median length of stay in the hospital (IQR)	p-value	
Sex			
Female	9 (7–14)	0.8	
Male	10 (7–14)		
Localization of erysipelas			
Face	7 (6–8.5)	**0.01**	
Upper extremity	7 (6–18)		
Trunk	9 (7–10)		
Lower extremity	11 (7–15)		
More than 1 part of the body	10 (7–14)		
Subtype			
Erythematous	9 (6.5–12.5)	0.009*	**0.03****
Bullous	11.5 (8–19)		
Hemorrhagic	13.5 (9.5–15)		
Gangrenous	25 (19–28)		
Bullous-hemorrhagic	14 (10–20)		
General symptoms			
Fever No fever	9 (7–14) 10 (7–14)	0.9	
Chills No chills	12 (9–15) 9 (7–14)	**0.02**	
Malaise No malaise	9.5 (8–15) 10 (7–14)	0.3	
Nausea No nausea	9 (9–15) 10 (7–14)	0.5	
Lymphadenopathy No lymphadenopathy	17 (7–21) 9.5 (7–14)	0.06	
Comorbidities			
Tinea pedis	15.5 (13.5–20)	**0.002**	
Diabetes mellitus	10 (7–13.5)	0.9	
Hypertension	10 (7–15)	0.1	
Hypercholesterolemia	10 (7–14)	0.9	
Chronic venous insufficiency	11 (7–14)	0.7	
Anemia	11 (9–15)	**0.03**	
Cardiac disease	10 (7–14)	0.9	
Malignancy	9 (5–10)	0.07	
Post-lymphadenectomy status	10 (9–11)	0.9	
Chronic renal disease obesity	9.5 (7–11)	0.5	
Obesity	11 (8–15)	0.3	
Laboratory tests			
Positive swab culture	17.5 (9.5–21)	**0.007**	
Elevated ERS	10 (7–15)	0.3	
Elevated CRP (>100 mg/L)	11 (8–17)	**0.02**	
Leukocytosis	11 (8–15)	**0.005**	
Elevated procalcitonin	13 (7–15)	0.97	

IQR – interquartile range; ERS – erythrocyte sedimentation rate; CRP – C-reactive protein; * p-value obtained with the Kruskal–Wallis test; ** p-value obtained with post hoc test. Values in bold are statistically significant.

with longer hospitalization (17.5 days, IQR = 9.5–21; p = 0.007). Regarding markers of inflammation on admission, 87 (56.9%) patients had leukocytosis (median 10.89×10^3 cells/μL, IQR = 8.3–14.3; range $3.04–37.8 \times 10^3$ cells/μL), 140 (91.5%) had elevated serum CRP levels (median 82.9 mg/L, IQR = 35.5–158.8; range 0.4–530.0 mg/L), 112 (73.2%) had increased ESR (median 67 mm/h, IQR = 35–86; range 4–125 mm/h), and 73 (47.7%) had elevated procalcitonin values (median 0.2 ng/mL, IQR = 0.07–0.83; range 0.01–14.7 ng/mL). Patients with leukocytosis were hospitalized significantly longer than patients with a normal white blood cell range (p = 0.005), and an elevated CRP level over 100 mg/L significantly increased the length of stay in the ward (p = 0.02; Table 2).

Before the admission, 67 (43.8%) patients used an oral antibiotic treatment. Antibiotic therapy before hospitalization did not affect the length of stay (p = 0.8; Table 2). As the first-line treatment during hospitalization, the most commonly chosen antibiotic was clindamycin (n = 41; 26.8%), followed by amoxicillin with clavulanic acid (n = 34; 22.2%). Twenty-six (17.0%) patients were treated with cephalosporins, 23 (15.0%) with penicillin, and 20 (13.1%) with lincomycin. Eight (5.2%) were treated with combination antibiotic therapy since day 1. There were no statistically significant differences between the length of stay and the first-line antimicrobial therapy (p = 0.1). However, patients treated with clindamycin during their hospitalization, regardless of whether it was a first-line or subsequent antibiotic, spent significantly more time in the ward than patients treated with other antimicrobial medications (p = 0.005).

Discussion

Prolonged hospitalization of patients with erysipelas is a significant financial burden for the healthcare system. Higher costs are associated with additional tests and examinations, long antibiotic therapy courses, and a delay in patient's return to activities and work.

The current results did not demonstrate the superiority of any of the antibiotics in terms of hospitalization time. However, it was observed that patients treated with clindamycin were hospitalized longer than patients treated with other antibiotics. Brindle et al.[14] analyzed 43 studies with 5999 patients to examine the optimum antibiotic treatment for erysipelas and cellulitis. This review also did not determine an advantage for using any group of antibiotics or antibiotic combination therapy. The German guidelines recommend intravenous treatment with crystalline penicillin G for 7–10 days. In the case of penicillin allergy, treatment with clindamycin for 7–10 days is recommended.[13] Since the bacterial sensitivity to a particular antibiotic may change over time and the treatment is often empirical, knowledge of the most common local pathogens causing erysipelas may help in choosing the right therapeutic option.

In the current research, it was observed that tinea pedis is one of the factors associated with a prolonged stay in the hospital. Pavlotski et al.[15] also identified tinea pedis as a contributing factor for recurrent episodes of erysipelas. Moreover, obesity, venous insufficiency, and lymphedema were mentioned as recurrence risk factors.[15] A recent publication by Korecka et al.[16] also found tinea pedis as an important risk factor for the disease, not only for the first episode, but also for recurrent erysipelas.

Another factor identified in the current study that significantly affected prolonged stay in the ward was anemia. While there is less evidence in the literature to support the association between these variables, the relationship may be due to a lower oxygen supply, ischemia and more severe erysipelas caused by a low hemoglobin concentration.

Roda et al.[17] found that positive culture results, CRP and leukocytosis were characteristics associated with a prolonged stay in the hospital. In the current study, it was also observed that these factors were associated with longer hospitalization. Other factors affecting prolonged hospitalization were advanced age, previous episodes of erysipelas/cellulitis, and the presence of complications.[17]

It was also found that localization to the lower extremities and increased levels of inflammatory markers were risk factors for a prolonged hospital stay. These findings are in line with other studies.[18] In contrast, correlations between the length of hospitalization and fever on admission, abscesses, obesity, diabetes mellitus, and thrombosis, that have been reported in other studies, were not observed here.[18]

Limitations

We realize that our research carries the risk of bias. The main limitation of the present study is the possible exclusion of potential confounding factors for prolonged hospitalization, such as the adverse social context or the occurrence of other complications not directly related to erysipelas. Another limitation is the possible misclassification of a certain number of cases. Most cases were classified as erysipelas on clinical grounds only and this condition cannot always be clearly distinguished from cellulitis. Due to these limitations, further prospective research should be carried out to verify our conclusions.

Conclusions

Erysipelas is an infectious disease that, due to its severe course, often requires hospitalization. Prolonged hospitalization is a burden for the healthcare system and an additional risk for patients. Here, we revealed that some factors, such as the clinical features of the disease, laboratory test results, and the choice of treatment, have an impact on the length of hospitalization of patients with erysipelas. In clinical practice, patients with the above risk factors should receive special care.

ORCID iDs

Magdalena Łyko https://orcid.org/0000-0001-9622-1593
Mateusz Kaczmarek https://orcid.org/0000-0003-2711-6452
Polina Nekrasova https://orcid.org/0000-0002-8795-6894
Anita Hryncewicz-Gwóźdź https://orcid.org/0000-0002-1601-471X
Joanna Maj https://orcid.org/0000-0001-8300-8208
Alina Jankowska-Konsur https://orcid.org/0000-0003-4944-5388

References

1. Blaeckberg A, Trell K, Rasmussen M. Erysipelas: A large retrospective study of aetiology and clinical presentation. *BMC Infect Dis*. 2015;15:402. doi:10.1186/s12879-015-1134-2
2. Celestin R, Brown J, Kihiczak G, Schwartz RA. Erysipelas: A common potentially dangerous infection. *Acta Dermatovenerol Alp Pannonica Adriat*. 2007;16(3):123–127. PMID:17994173
3. Eriksson B, Jorup-Roenstroem C, Karkkonen K, Sjoeblom AC, Holm SE. Erysipelas: Clinical and bacteriologic spectrum and serological aspects. *Clin Infect Dis*. 1996;23(5):1091–1098. doi:10.1093/clinids/23.5.1091
4. Socan K, Socan M. Trends in the epidemiology of erysipelas in Slovenia. *Acta Dermatovenerol Alp Pannonica Adriat*. 2018;27(1):1–4. PMID: 29589637
5. Bernard P, Bedane C, Mounier M, Denis F, Catanzano G, Bonnetblanc JM. Streptococcal cause of erysipelas and cellulitis in adults: A microbiologic study using a direct immunofluorescence technique. *Arch Dermatol*. 1989;125(6):779–782. PMID:2658843
6. Trell K, Rignér S, Wierzbicka M, Nilson B, Rasmussen M. Colonization of β-hemolytic streptococci in patients with erysipelas: A prospective study. *Eur J Clin Microbiol Infect Dis*. 2019;38(10):1901–1906. doi:10.1007/s10096-019-03625-9
7. Brishkoska-Boshkovski V, Dimitrovska I, Kondova-Topuzovska I. Clinical presentation and laboratory characteristics in acute and recurrent erysipelas. *Open Access Maced J Med Sci*. 2019;7:771–774. doi:10.3889/oamjms.2019.213
8. Bonnetblanc JM, Bedane C. Erysipelas: Recognition and management. *Am J Clin Dermatol*. 2003;4(3):157–163. doi:10.2165/00128071-200304030-00002
9. Inghammar M, Rasmussen M, Linder A. Recurrent erysipelas: Risk factors and clinical presentation. *BMC Infect Dis*. 2014;14:270. doi:10.1186/1471-2334-14-270
10. Eron LJ, Lipsky BA, Low DE, et al. Managing skin and soft tissue infections: Expert panel recommendations on key decision points. *J Antimicrob Chemother*. 2003;52(Suppl 1):i3–i17. doi:10.1093/jac/dkg466
11. Stevens DL, Bisno AL, Chambers HF, et al; Infectious Diseases Society of America. Practice guidelines for the diagnosis and management of skin and soft tissue infections: 2014 update by the Infectious Diseases Society of America [published correction appears in: *Clin Infect Dis*. 2015;60:1448. Dosage error in article text]. *Clin Infect Dis*. 2014;59(2): e10–e52. doi:10.1093/cid/ciu444
12. Kwak YG, Choi SH, Kim T, et al. Clinical guidelines for the antibiotic treatment for community-acquired skin and soft tissue infection. *Infect Chemother*. 2017;49(4):301–325. doi:10.3947/ic.2017.49.4.301
13. Sunderkoetter C, Becker K, Eckmann C, Graninger W, Kujath P, Schoefer H. Calculated initial parenteral treatment of bacterial infections: Skin and soft tissue infections. *GMS Infect Dis*. 2020;8:Doc11. doi:10.3205/id000055
14. Brindle R, Williams OM, Barton E, Featherstone P. Assessment of antibiotic treatment of cellulitis and erysipelas: A systematic review and meta-analysis. *JAMA Dermatol*. 2019;155(9):1033–1040. doi:10.1001/jamadermatol.2019.0884
15. Pavlotsky F, Amrani S, Trau H. Recurrent erysipelas: Risk factors. *J Dtsch Dermatol Ges*. 2004;2(2):89–95. doi:10.1046/j.1439-0353.2004.03028.x
16. Korecka K, Mikiel D, Banaszak A, Neneman A. Fungal infections of the feet in patients with erysipelas of the lower limb: Is it a significant clinical problem? *Infection*. 2021 [online ahead of print]. doi:10.1007/s15010-021-01582-0
17. Roda A, Pinto AM, Filipe AR, Travassos AR, Freitas JP, Filipe P. Clinical and laboratory factors associated with prolonged hospital stay among patients with cellulitis/erysipelas [in Spanish]. *Acta Med Port*. 2019;32:448–452. doi:10.20344/amp.10735
18. Kozłowska D, Myśliwiec H, Kiluk P, Baran A, Milewska AJ, Flisiak I. Clinical and epidemiological assessment of patients hospitalized for primary and recurrent erysipelas. *Przegl Epidemiol*. 2016;70(4):575–584. PMID:28221013